

RD-A153 753

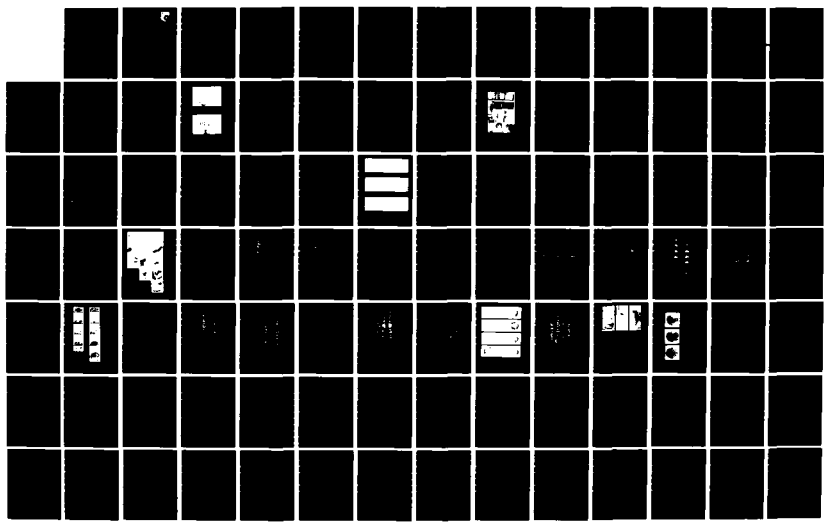
MULTI-DUCTED INLET COMBUSTOR RESEARCH AND DEVELOPMENT
(U) UNIVERSAL ENERGY SYSTEMS INC DAYTON OH G D STREBY
MAR 85 AFWAL-TR-85-2004 F33615-81-C-2674

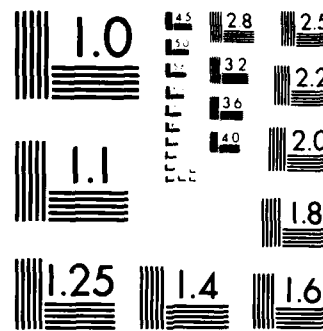
1/3

UNCLASSIFIED

F/G 21/5

NL





MICROCOPY RESOLUTION TEST CHART
NATIONAL BUREAU OF STANDARDS 1954

AD-A153 753

AFWAL-TR-85-2004



MULTI-DUCTED INLET COMBUSTOR RESEARCH AND DEVELOPMENT

Universal Energy Systems, Inc.
4401 Dayton-Xenia Road
Dayton, Ohio 45432

March 1985

Final Report for the Period 31 August 1981 to 31 August 1984

Approved for public release; distribution unlimited.

DTIC FILE COPY

AERO PROPULSION LABORATORY
AIR FORCE WRIGHT AERONAUTICAL LABORATORIES
AIR FORCE SYSTEMS COMMAND
WRIGHT-PATTERSON AIR FORCE BASE, OHIO 45433

NOTICE

When Government drawings, specifications, or other data are used for any purpose other than in connection with a definitely related Government procurement operation, the United States Government thereby incurs no responsibility nor any obligation whatsoever, and the fact that the government may have formulated, furnished, or in any way supplied the said drawings, specifications, or other data, is not to be regarded by implication or otherwise as in any manner licensing the holder or any other person or corporation, or conveying any rights or permission to manufacture, use, or sell any patented invention that may in any way be related thereto.

This report has been reviewed by the Office of Public Affairs (ASD/PA) and is releasable to the National Technical Information Service (NTIS). At NTIS, it will be available to the general public, including foreign nations.

This technical report has been reviewed and is approved for publication.

Kenneth G. Schwartzkopf
KENNETH G. SCHWARTZKOPF
Project Engineer

Frank D. Stull
FRANK D. STULL
Chief, Ramjet Technology Branch
Ramjet Engine Division

FOR THE COMMANDER:

William G. Beecroft
WILLIAM G. BEECROFT
Deputy Director
Ramjet Engine Division
Aero Propulsion Laboratory

"If your address has changed, if you wish to be removed from our mailing list, or if the addressee is no longer employed by your organization please notify AFWAL/PORT, WPAFB, OH 45433 to help us maintain a current mailing list."

Copies of this report should not be returned unless return is required by security considerations, contractual obligations, or notice on a specific document.

UNCLASSIFIED

SECURITY CLASSIFICATION OF THIS PAGE (When Data Entered)

REPORT DOCUMENTATION PAGE		READ INSTRUCTIONS BEFORE COMPLETING FORM
1. REPORT NUMBER AFWAL-TR-85-2004	2. GOVT ACCESSION NO.	3. RECIPIENT'S CATALOG NUMBER
4. TITLE (and Subtitle) MULTI-DUCTED INLET COMBUSTOR RESEARCH AND DEVELOPMENT		5. TYPE OF REPORT & PERIOD COVERED FINAL REPORT 31 August 1981-31 August 1984
7. AUTHOR(s) Gary D. Streby Project Engineer		6. PERFORMING ORG. REPORT NUMBER
9. PERFORMING ORGANIZATION NAME AND ADDRESS Universal Energy Systems, Inc. 4401 Dayton-Xenia Road Dayton, Ohio 45432		10. PROGRAM ELEMENT, PROJECT, TASK AREA & WORK UNIT NUMBERS 2308S110
11. CONTROLLING OFFICE NAME AND ADDRESS Aero Propulsion Laboratory (AFWAL/PORT) Air Force Wright Aeronautical Laboratories (AFSC) Wright-Patterson Air Force Base, Ohio 45433		12. REPORT DATE March 1985
14. MONITORING AGENCY NAME & ADDRESS (if different from Controlling Office)		13. NUMBER OF PAGES 195
16. DISTRIBUTION STATEMENT (of this Report) Approved for Public Release; Distribution Unlimited.		15. SECURITY CLASS. (of this report) Unclassified
17. DISTRIBUTION STATEMENT (of the abstract entered in Block 20, if different from Report)		
18. SUPPLEMENTARY NOTES		
19. KEY WORDS (Continue on reverse side if necessary and identify by block number) Multi-Ducted Inlet Ramjet Combustors Hydrodynamic Simulation Flow Visualization Internal Fluid Flow Fields Residence Times Dispersion Characteristics		
20. ABSTRACT (Continue on reverse side if necessary and identify by block number) Hydrodynamic simulations were conducted of dual inlet side dump combustor configurations to obtain flow visualization and residence time data using the Water Tunnel test rig facility of the Ramjet Technology Branch AFWAL/PORT Wright-Patterson AFB, Ohio. Tests were conducted for inlet duct angles of 30, 45 and 60 degrees for variations in the combustor dome plate height from 0.0 to 6.0 inches, for total combustor fluid flow rates of 200, 300 and 400 gallons per minute, for nozzle area to combustor area ratios of 0.20, 0.29		

UNCLASSIFIED

SECURITY CLASSIFICATION OF THIS PAGE(When Data Entered)

and 0.39, and for combustor lengths of 20.13, 39.0 and 53.25 inches. The inlet duct Reynolds Numbers for each total flow rate tested were 125,640 for 200 gallons per minute, 188,400 for 300 gallons per minute, and 251,300 for 400 gallons per minute. Also reported on are specialized research efforts conducted to support advanced combustor studies.

UNCLASSIFIED

SECURITY CLASSIFICATION OF THIS PAGE(When Data Entered)

PREFACE

This final report describes the research and development efforts conducted by Universal Energy Systems, Inc., on Project and Task 23085110, Ducted Rocket Flowfield Characterization, Contract No. F33615-81-C-2074. These efforts were in support of the research and development programs of the Ramjet Technology Branch (AFWAL/PORT) of the Aero Propulsion Laboratory, Wright-Patterson Air Force Base, Ohio.

The research and development reported herein was performed during the period 31 August 1981 through 31 August 1984, under the direction of the author, Mr. Gary D. Streby, Project Engineer. This report was released in November 1984.

This final report details the research and development studies that were accomplished during the performance of this contract and presents the results obtained in utilizing hydrodynamic simulation to obtain fluid flow characteristics of multi-ducted inlet side dump combustor configurations. Also included in this report is a summary of engineering and technical support efforts that were provided to other test rigs of the Ramjet Technology Branch by Universal Energy Systems, Inc., in conjunction with the research and development effort.

Previously submitted annual interim technical reports titled "Multi-Ducted Inlet Combustor Research and Development", AFWAL-TR-82-2101 (Project and Task Number 2308S101) and "Multi-Ducted Inlet Combustor Research and Development" AFWAL-TR-83-2081 (Project and Task Number 2308S110), detail the previous two years efforts of the thirty-six month research program respectively.

Accession For	
NTIS GRA&I <input checked="" type="checkbox"/>	
DTIC TAB <input type="checkbox"/>	
Unannounced <input type="checkbox"/>	
Justification	
By _____	
Distribution/ _____	
Availability Codes _____	
ONE	Avail and/or Dist Special
QUALITY INSPECTED 1	
A-1	

TABLE OF CONTENTS

<u>SECTION</u>	<u>PAGE</u>
I INTRODUCTION	1
II SUMMARY OF SPECIALIZED STUDIES AND IMPROVEMENTS.	2
2.1 Burner Thrust Stand Test Rig.	2
2.2 Cold Flow Channel Test Rig.	3
2.3 Water Tunnel Test Rig	5
III WATER TUNNEL TEST FACILITY	7
IV MULTI-DUCTED INLET COMBUSTOR CONFIGURATION	11
V RESIDENCE TIME MEASUREMENT INSTRUMENTATION	14
VI TEST PROGRAM	17
6.1 Flow Visualization Studies.	17
6.2 Injection Probe	18
6.3 Residence Time Studies.	23
6.4 Specialized Studies	23
VII DATA PRESENTATION AND DISCUSSION	25
7.1 Flow Visualization Data	25
7.2 Residence Time Measurement Technique and Results.	55
VIII CONCLUSIONS AND RECOMMENDATIONS.	75
8.1 Conclusions	75
8.2 Recommendations	77
Appendices	
A Holography Diagnostic Techniques for Ramjet Flows.	78
B Analytical Characterization of Flowfield in Ducted-Rocket Combustor Geometrics	105
C AFWAL/PORT Water Tunnel Residence Time Test Data	178
D Data Reduction and Analysis Equations.	180
References	195

LIST OF ILLUSTRATIONS

<u>FIGURE</u>		<u>PAGE</u>
1	Photographs of Catalytic Flame Holders	4
2	AFWAL/PORT Water Tunnel Facility Schematic	8
3	AFWAL/PORT Water Tunnel Test Rig	9
4	Dual Inlet Side Dump Combustor Configuration	12
5	Laser/Optical Detection System Diagram	15
6	Block Diagram of Water Tunnel Instrumentation System	16
7	Dye Tracer Injection Probe Designs	20
8	Photographs of Dye Injection in Inlet Duct	21
9	Concentration-Time Function Curve for Dye Injection	22
10	Flow Visualization Sketches - 30 Degree Inlets	27
11	Flow Visualization Sketches - 45 Degree Inlets	28
12	Flow Visualization Sketches - 60 Degree Inlets	29
13	Photographs of Combustor Flow Patterns at Various Longitudinal Stations	31
14	Relative Vortex Center Versus Longitudinal Station	32
15	Flow Visualization Sketches for Various Combustor Lengths for 45 Degree Configuration	33
16	Flow Visualization Sketches for Various Combustor Lengths for 45 Degree Configuration	34
17	Flow Visualization Sketches for Various Combustor Lengths for 45 Degree Inlet Configuration	35
18	Test Setup for Viewing Radial Flow Patterns	37
19	Radial Flow Pattern Sketches of the 60 Degree Inlet Configuration	38
20	Effect of Combustor Centerline Divider on Flow Patterns for 30 Degree Configuration	40
21	Effect of Combustor Centerline Divider on Flow Patterns for 45 Degree Configuration	41
22	Effects of Combustor Centerline Divider on Flow Patterns for 60 Degree Configuration	42

LIST OF ILLUSTRATIONS (CONTINUED)

<u>SECTION</u>	<u>PAGE</u>
23 Photographs of Combustor Flow Patterns with Divide Installed	44
24 Inlet Turning Vane Configuration	45
25 Effect of Inlet Turning Vanes on Combustor Flow Patterns for 45 Degree Configuration	46
26 Effect of Gas Generator Port Location on Combustor Flow Patterns for 30 Degree Configuration	49
27 Effect of Gas Generator Port Location on Combustor Flow Patterns for 45 Degree Configuration	50
28 Photographs of Gas Generator Flow for Various Port Locations for 45 Degree Configuration - 300 GPM	51
29 Effect of Gas Generator Flow on Combustor Flow Patterns for 45 Degree Configuration	52
30 Photographs of Combustor Side View Flow Patterns for Gas Generator Flows	53
31 Photographs of 45 Degree Inlet Configuration Flow Patterns Showing Effects of Gas Generator Flows	54
32 Dual Inlet Side Dump Combustor Residence Times	61
33 Residence Times Versus Inlet Reynolds Numbers	62
34 Ratio of Apparent Stagnation Volume to Total Combustor Volume Versus Dome Plate Position	66
35 Effects of Combustor Lengths on Residence Times	67
36 Effect of Nozzle Area to Combustor Area Ratios on Residence Times	69
37 Gas Generator and Inlet Flow Residence Times Versus Dome Plate Position	70
38 Dispersion Coefficient Versus Dome Plate Position	72
39 Residence Time Versus Variance Delta	74

LIST OF ILLUSTRATIONS (CONTINUED)

APPENDIX A

<u>FIGURE</u>	<u>PAGE</u>
1 Holocamera Installation in AFAPL Ramjet Facility	86
2 Atomization Study	87
3 Crossflow Fuel Atomization	93
4 Fuel Atomization Study - Orifice Injector	95
5 Fuel Atomization Study - Pentil Injector	96
6 Droplet Size Analysis - Orifice Injector	97
7 Droplet Velocity Analysis - Orifice Injector	99
8 Droplet Size Analysis - Combustion Study	101
9 Determining Particle Size Distribution from the Holographically Recorded Fourier Transform	104

APPENDIX B

1 Water Tunnel Combustor Configuration	135
2 General Flow Pattern Is Cross-Sectional Phase	136
3 Flow Pattern In The Vertical (r-z) Plane (Light Source Place Paralled To Duct Axis)	137
4 Location Of Injection Ports and a Typical Finite - Difference Grid	138
5 Finite - Diference Grid For -2 Inch Dome Position	139
6 Flowfield In (r-θ) Plane For $\alpha = 45^\circ$, $H = 2$ Inches	141
7 Flowfield In (r-z) Plane For $\alpha = 45^\circ$, $H = 2$ Inches	145
8 Finite Difference Gride For The 0 Inch Dome Position	149
9 Flowfield In (r-θ) Plane For $\alpha = 45^\circ$, $H = 0$ Inches	151
10 Flowfield In (r-z) Plane for $\alpha = 45^\circ$, $H = 0$ Inches	155
11 Flowfield In (r-θ) Plane For $\alpha = 60^\circ$, $H = 2$ Inches	159
12 Flowfield In (r-z) Plane For $\alpha = 60^\circ$, $H = 2$ Inches	163

LIST OF ILLUSTRATIONS (CONCLUDED)

APPENDIX B

<u>FIGURE</u>	<u>PAGE</u>
13 Flowfield In (r-θ) Plane For $\alpha = 60^\circ$, H = 0 Inches	167
14 Flowfield In (r-z) Plane For $\alpha = 60^\circ$, H = 0 Inches	171

APPENDIX D

1 Dye Calibration Curve	182
2 Concentration - Time Function Distribution Plot	185

LIST OF TABLES

<u>TABLE</u>	<u>PAGE</u>
1 Sketch Matrix	19
2 Inlet Duct Reynolds Numbers	24
3 Residence Time Measurement Test Matrix	57
4 Combustor Volumes for Various Test Configurations	58
5 Fluid Flow Rates for Various Total Flows	58
6 Calculated Residence Times	59
APPENDIX A	
1 Text Matrix	90
APPENDIX B	
1 Finite - Difference Grid Used In Computations	140
2 Finite - Difference Grid Used In Computations	150

LIST OF SYMBOLS

A	area
D	diameter
D/uL	reactor dispersion no. (dimensionless group)
GPM	gallons per minute
Ht	dome height
in.	inch
Re	Reynold Number
sec.	second
T	time
U	velocity
V	volume
W	fluid flow rate
α	inlet angle
β	radial angle about combustor axis
η	kinematic viscosity
δ	variance delta
$^{\circ}F$	degrees fahrenheit

Subscript

C	combustor
CAL	calculated
H	hydraulic
I	inlet
N	nozzle
T	residence time

SECTION V RESIDENCE TIME MEASUREMENT INSTRUMENTATION

The AFWAL/PORT Water Tunnel test rig instrumentation was improved and modified by UES in an effort to upgrade the capabilities of the facility and enable research studies to be conducted of the multi-ducted inlet side dump combustor configuration. A laser/optical detection system was installed which make possible the detection of minute concentrations of injected dye at various points within the combustor configuration. Sampling, reduction, and analysis of dye concentration data were obtained with a Mod Comp MODACS III computer data acquisition system which was installed and placed into operation by UES. Figure 5 shows a diagram of the laser/optical detection system depicting the relationship of the various components to the test configuration. Figure 5 is a block diagram of the instrumentation system utilized in the residence time testing phase of the research program.

section through specially designed dome plates and regulated in proportion to the total tunnel flow. The design of gas generator section allowed for visual and photographic observation of internal fluid flow patterns during operation.

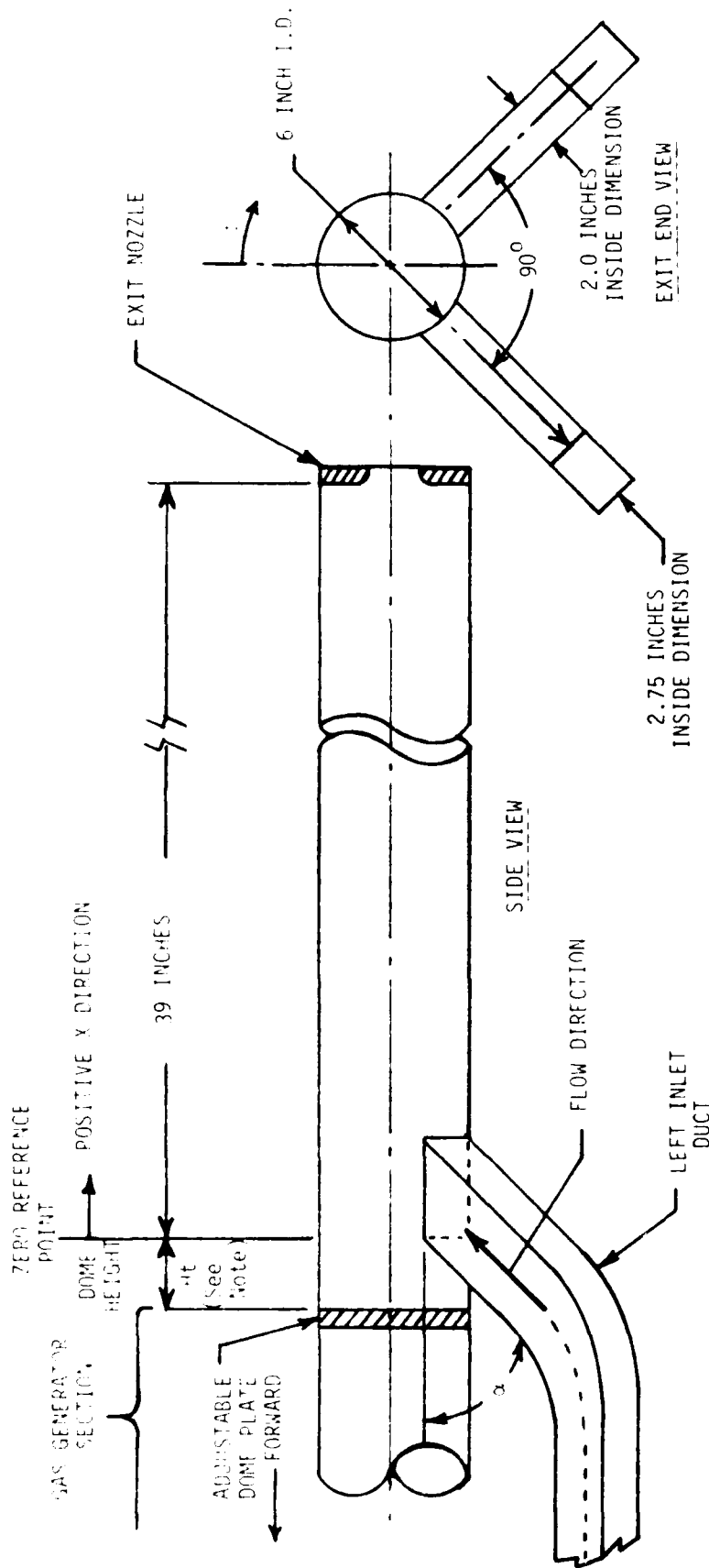


Figure 4. Dual Inlet Side Dump Combustor Configuration

SECTION IV

MULTI-DUCTED INLET COMBUSTOR CONFIGURATION

The test configuration under investigation in this research program was the dual inlet side dump combustor. The test configuration was made up of two rectangular inlet ducts, a combustor section, a gas generator section, and an exhaust nozzle. A schematic diagram showing physical dimensions of the test configuration is presented in Figure 4.

Test hardware was available that allowed the two inlet ducts to intersect the combustor at inlet angles of 30, 45, or 50 degrees. Test data reported herein were obtained for all three test configurations. The centerline of the inlet ducts intersect the combustor section at the same axial station and are located radially at 90 degrees to each other. The internal dimensions of the inlet ducts measure 2.0 by 2.75 inches. The upstream edge of the inlet ducts was taken as the combustor longitudinal zero reference point. Longitudinal measurements downstream of the zero reference point are positive and are negative upstream of the zero reference point, refer to Figure 4.

The combustor section was a cylinder with a 5.0 inch inside diameter and measured 39.0 inches in length from the combustor longitudinal zero reference point to the exit nozzle. The combustor dome plate was located at the upstream end of the combustor section and could be positioned axially from the zero reference point to approximately 10.0 inches forward of the inlet ducts. Various configurations of the dome plate were available to simulate gas generator flows or fuel injection techniques. Flow visualization and residence time data results reported herein are for both the solid flat dome plate and for dome plates with gas generator flows. The exit nozzle of the combustor was removable to allow different nozzle exit area to combustor area ratios to be tested. Nozzle exit area to the combustor area ratios of 0.20, 0.29, and 0.39 were available for test purposes.

The gas generator section of the multi-ducted inlet side dump combustor configuration was designed to simulate gas generator flow or fuel injection. Water flow could be introduced into the combustor

source output is adjustable up to 65,000 lumens at 1000 volts D.C. The mercury lamp generates an intense source of radiant energy which is focused to a narrow plane beam. The narrow light beam (light sheet) is used to illuminate injected air bubbles which describe internal flow patterns. Various lamp fixtures are available to position the light plane perpendicular or parallel to the combustor axis and at positions along the combustor axis.

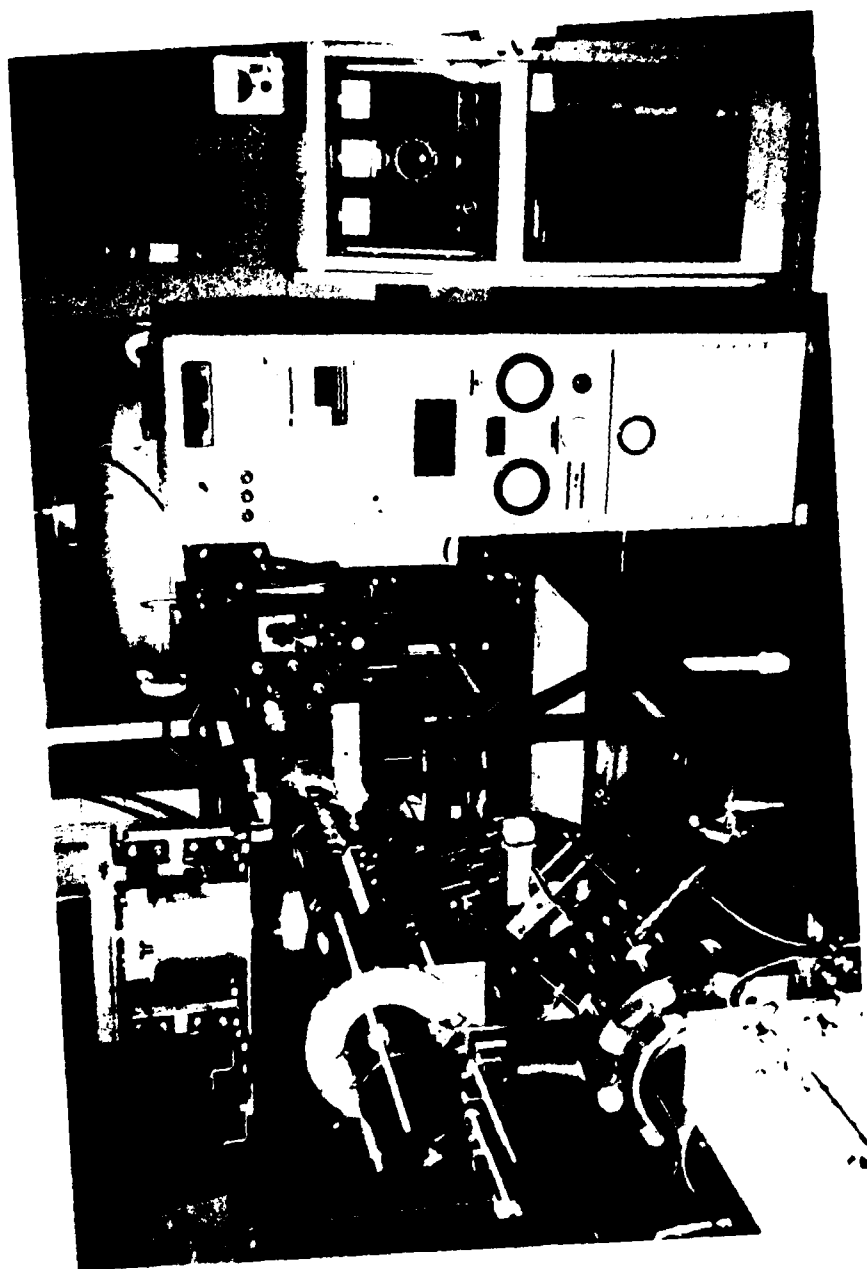


Figure 3. AFWAL/PORT Water Tunnel Test Rig

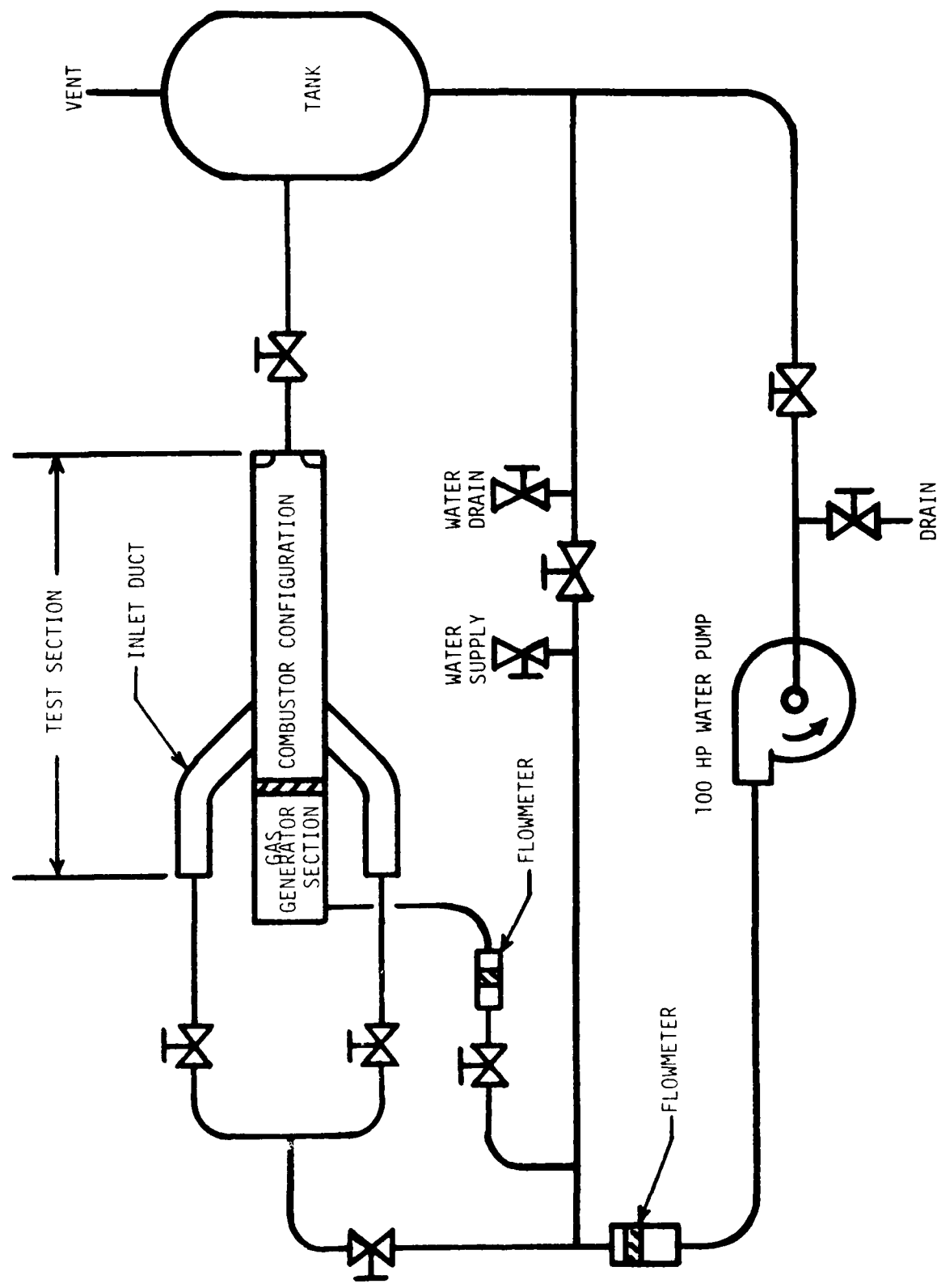


Figure 2. AFWAL/PORT Water Tunnel Facility Schematic

SECTION III

WATER TUNNEL TEST FACILITY

The Ramjet Technology Branch's Water Tunnel test rig facility is a closed loop water tunnel for the simulation of internal fluid flow dynamics of ramjet combustor configurations. The Water Tunnel is located in Building 18E, Room 23, Wright-Patterson AFB, Ohio and is capable of circulating up to 1500 gallons of water per minute. A schematic diagram of the Water Tunnel test rig, components, and system arrangement is presented in Figure 2. Figure 3 is a photograph of the facility. All piping in the Water Tunnel system is of PVC plastic and the test section is constructed of clear plexiglas. The clear plexiglas test section allows for complete observation of flows in the test configuration. The Water Tunnel test rig is capable of testing full scale single and multi-ducted inlet ramjet combustor configurations over an inlet duct Reynolds number range of 0.4 to 4.0 million per foot. Simulations of associated combustor flows such as gas generators and fuel injectors are also possible. Support systems to the Water Tunnel test rig include an air/dye injection system, a laser/optical detection system, and a high intensity light source.

The air/dye injection system is capable of injecting air bubbles or colored dye into combustor configurations for flow visualization or for residence time measurements. Injections are made through a variety of specialized probes or test ports and can be controlled manually or by a precision timer control. Pulse durations as short as 0.01 second are possible. Dye injections are made through a vernier metering valve to allow for accurate control of the quantity of injected dye.

The laser/optical detector system consists of a Spectra Physics 0.05 watt Argon laser, two RCA 6655A photomultiplier detector tubes, and various beam splitting and alignment optics. This system is utilized for the detection and measurement of injected dye concentrations to obtain concentration time histories for residence time determinations.

The high intensity light source consists of a high voltage D.C. power supply which powers a high intensity mercury lamp. The light

- Procurement and installation of Mod Comp MODACS III computer system.
- Procurement and installation of Honeywell 1858 Visicorder.
- Procurement of Lafayette 16mm Data Analyzer for analysis of high speed movies.
- Design and fabrication of data acquisition instrumentation, optical, and signal conditioning systems.
- Improvement of High Intensity Light Source fixture.
- Designed and installed Water Tunnel modification to simulate combustor gas generator flows.

- Completed fabrication of gas columns and molecular sieves for gas sampling experimentation.
- Completed modifications of the Ion Mass Spectrometer test equipment.

2.3 WATER TUNNEL TEST RIG

2.3.1 3-D Computer Code Development

Engineering support was provided for the development of a three dimensional computer code for use in the analysis of multi-ducted inlet side dump combustor configurations. The services of Dr. Pratap Vanka of Argonne National Laboratories were obtained to perform computer simulation studies. Dr. Vanka developed computer code modifications to describe the internal flow fields and flow characteristics of dual inlet side dump combustor configurations. Dr. Vanka also presented informal lectures to UES and AFWAL/PORT personnel to discuss analytical characterization methods and their use. The results of Dr. Vanka's work (2) is presented in Appendix B.

2.3.2 Math Modelling Support

The services of Dr. F. Eastep and Dr. J. Scott, of the University of Dayton, were obtained to conduct a literature survey of related technical studies and math modelling techniques that could be applied to the Water Tunnel investigations. Their investigation revealed the different aspects of fluid flow within the multi-ducted inlet side dump combustor configuration and the applicability of various modelling techniques. In addition, several definitions of residence time were detailed which were subsequently utilized in Water Tunnel studies.

2.3.3 Data Acquisition and Computational Improvements

During the performance of the research and development effort, equipment and capabilities of the AFWAL/PORT Water Tunnel test rig were upgraded and improved. These improvements were necessary to achieve reliable and accurate results in the study of internal fluid flow characteristics of combustor designs using hydrodynamic simulation. These improvements provided for; the measurement of minute dye concentrations within the moving combustor fluid; the acquisition, storage, and analysis of test data; and the improvement of flow visualization capabilities of the Water Tunnel test rig. Following is a list of the major Water Tunnel improvements that were accomplished.

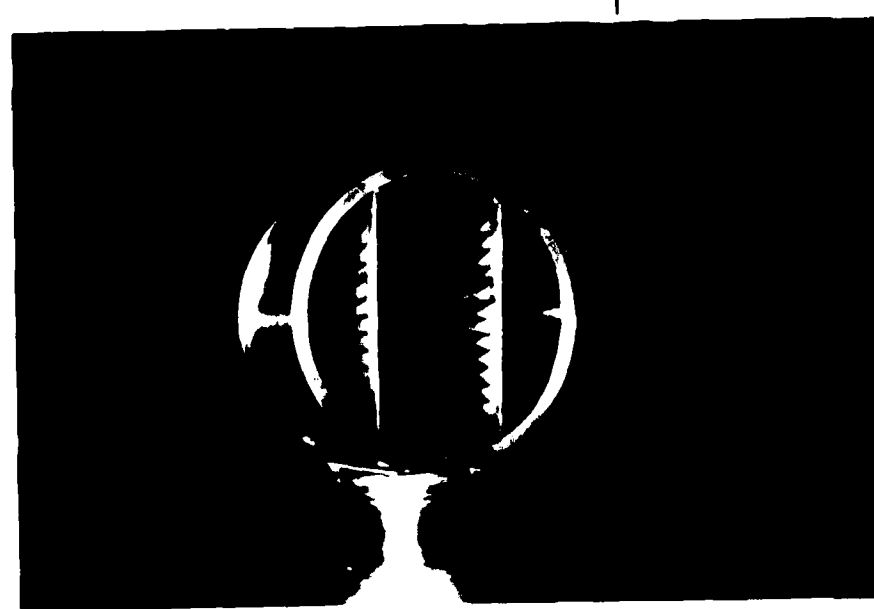


Figure 1. Photographs of Catalytic Flame Holders

2.1.3 WWVB Time Code System

UES personnel designed the installation of a WWVB time code receiver, generator, and video inserter system into the data acquisition system of the Burner Thrust Stand test rig. The WWVB time code system receives and displays the National Bureau of Standards time code signal to provide an accurate time reference for all video and computer data generated in test operations utilizing the Burner Thrust Stand test rig.

2.1.4 Catalytic Flameholder Investigation

UES supported an investigation into the use of catalytic flameholders in ramjet combustors. UES prepared design drawings and fabricated stainless steel shells for catalytic flameholders designed by Dr. William B. Retallick. A completed catalytic flameholder is shown in Figure 1. The catalytic flameholders were tested and evaluated by AFWAL/PORT.

2.1.5 Ramjet Instability Study

UES obtained the services of Dr. Frederick H. Reardon to prepare a standardized nomenclature for ramjet combustion oscillation studies. A Standardized Nomenclature for Ramjet Pressure Oscillation Studies was prepared and submitted to the 18th JANNAF Combustion Meeting, October 1981.

2.2 COLD FLOW CHANNEL TEST RIG

UES provided specialized technical support to conduct cold flow studies and gas sampling research related to multi-ducted inlet side dump combustor configurations. These efforts were in support of the AFWAL/PORT Cold Flow Channel test rig. A number of systems were upgraded and improvements made in an effort to increase capabilities of the facility. Following are major accomplishments achieved during the UES support effort:

- ° Design, Fabrication, and installation of new test rig control instrumentation.
- ° Completion of oil flow visualization studies of the side dump combustor configuration.
- ° Completion of design and fabrication of new gas sampling probes.
- ° Improved capabilities of the traverse probe drive system.

SECTION II

SUMMARY OF SPECIALIZED STUDIES AND IMPROVEMENTS

Universal Energy Systems, Inc., in addition to conducting advanced combustor research, provided engineering and technical support to the AFWAL/PORT Water Tunnel and other related test rigs of the Ramjet Technology Branch of the Aero Propulsion Laboratory. This support was provided to accomplish test rig modifications and improvements; to maintain specialized test instrumentation; and to conduct unique experimental investigations.

2.1 BURNER THRUST STAND TEST RIG

2.1.1 Holographic Fuel Droplet Study

UES subcontracted the engineering and technical services of Spectron Development Laboratories of Costa Mesa, California to conduct a combustor fuel droplet study utilizing the Burner Thrust Stand test rig located in Building 18C. This study was to examine fuel droplet size distributions and dispersion for various fuel injection methods and for different flow parameters using hot combustor flows. The holographic study was conducted from the 23rd of September to the 21st of October 1982. Laser holograms were made for a number of test conditions and developed on-site for preliminary review. After the testing phase of the program was completed, the holograms were taken to Spectron Laboratories for further analysis. After analysis, a set of selected holograms were furnished to AFWAL/PORT. The results of the holographic study (1) are presented in Appendix A.

2.1.2 Exhaust Nozzle Control System

Efforts were undertaken by UES to modify and upgrade the Burner Thrust Stand test rig. Dynamics Controls, Inc., Dayton, Ohio was subcontracted by UES to design, fabricate, and install an exhaust nozzle control system onto the Burner Thrust Stand. The system was designed to maintain allowable nozzle clearance tolerances during hot combustor operations when thermo movement of the exhaust nozzle occurs. A complete operations manual for the system and detailed design drawings were provided to AFWAL/PORT as part of this support.

SECTION I INTRODUCTION

Future Air Force requirements for supersonic air-breathing tactical missiles will require the development of advanced or improved propulsion systems. These propulsion systems will have to operate at extreme altitudes and high mach numbers, be cost effective, simple in operation, and compact. The propulsion system design which best fits these design parameters is the ramjet combustor. Ramjet combustors operate most efficiently at high mach numbers and altitudes; they work on the ram compression principle requiring no moving parts; and can be designed into small and compact propulsion system packages. In order to realize the full potential of ramjet combustor designs, research and development efforts are necessary to obtain data regarding combustor performance characteristics for variations in design parameters. This information is presently obtained from actual hot combustor testing and from fluid flow simulations.

Universal Energy Systems, Inc. (UES) has completed a 36 month research and development effort to obtain both qualitative and quantitative data pertaining to the internal fluid flow characteristics of the multi-ducted side dump ramjet combustor design. These studies were conducted utilizing the AFWAL/PORT Water Tunnel test rig located in Building 18E, Area B, Wright-Patterson Air Force Base, Ohio. Research and development studies were undertaken to obtain cold flow fluid dynamic characteristics of the dual inlet side dump combustor configuration for variations in basic combustor design parameters. Studies included fluid flow observations using improved flow visualization techniques and the measurement of residence times of combustor flows.

Presented in this report are details of the engineering and technical efforts to improve and upgrade research test rigs of the Ramjet Technology Branch (AFWAL/PORT) and the results of hydrodynamic simulations of ramjet combustor flows using the AFWAL/PORT Water Tunnel test rig. Results obtained include visual and photographic data as well as combustor residence times. Test results are presented in detail with a discussion of unique characteristics that were observed or measured, conclusions arrived at and recommendations for future study.

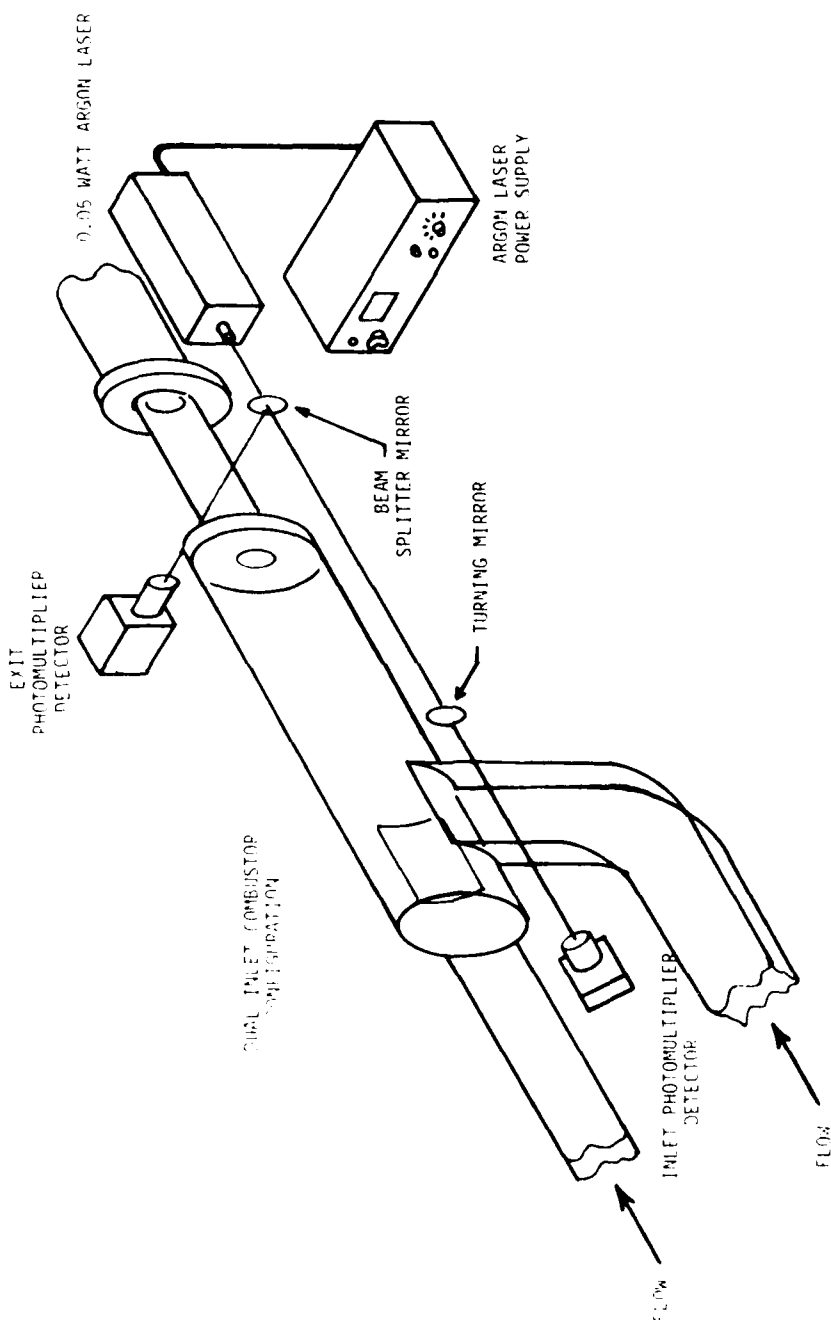


Figure 5. Laser/Optical Detection System Diagram

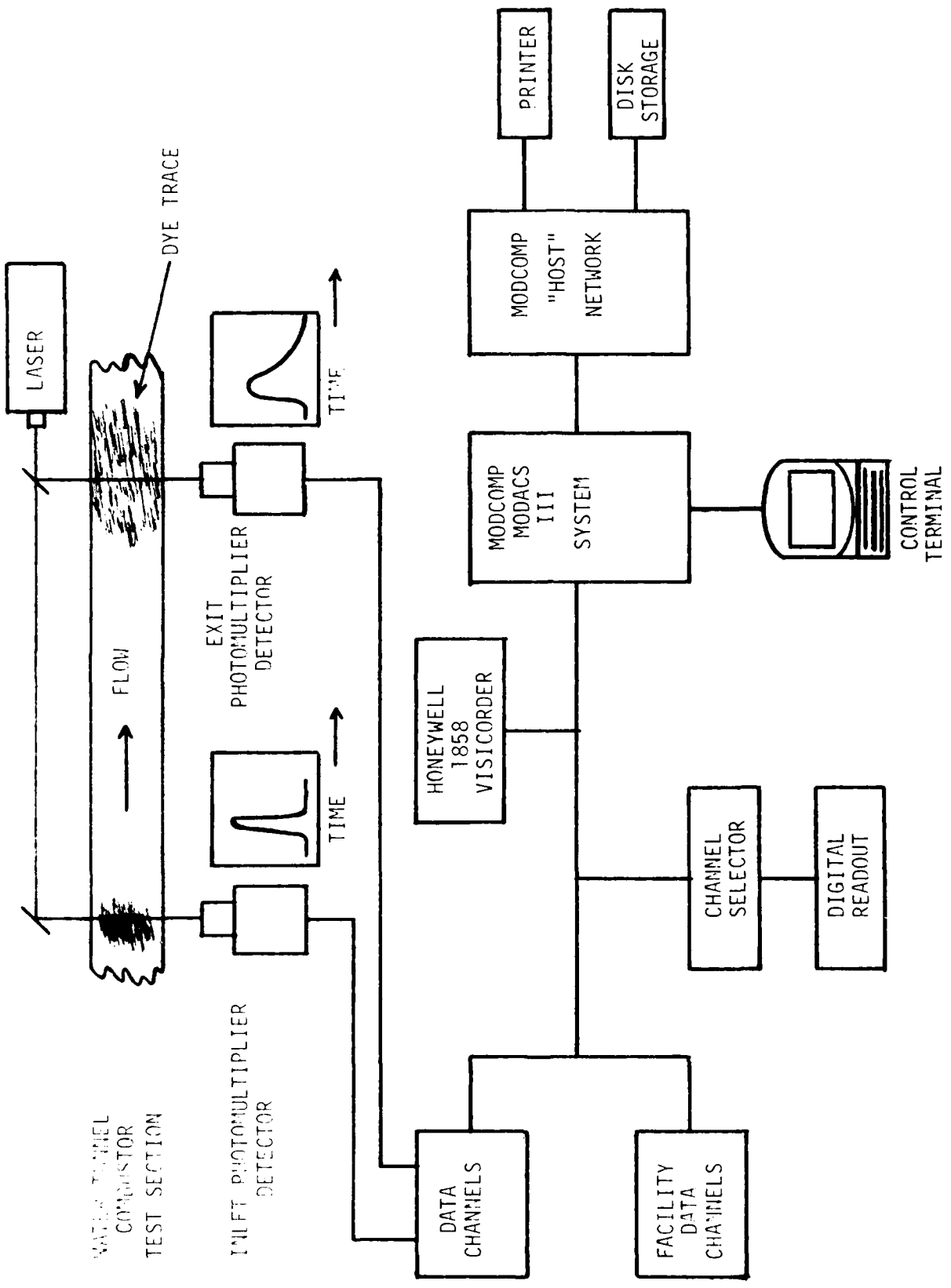


Figure 6. Block Diagram of Water Tunnel Instrumentation System

SECTION VI TEST PROGRAM

The UES test program was designed to achieve two primary objectives. These objectives were: obtaining a qualitative understanding of the internal flow processes of a unique mixing chamber design through the utilization of flow visualization techniques; and the obtaining of quantitative information of the mixing and flow characteristics of fluid passing through the mixing chamber from residence time data. The following paragraphs describe the test program undertaken to accomplish each of these objectives.

6.1 FLOW VISUALIZATION STUDIES

The flow visualization study was undertaken to obtain qualitative data describing the internal fluid flow characteristics of advanced side dump combustor configurations. The configuration under study in this program was the dual inlet side dump combustor, shown in Figure 4. This investigation was accomplished using improved flow visualization capabilities of the AFWAL/PORT Water Tunnel facility that were made as part of the overall research and development effort. Improvements were made in probe designs for the injection of air and dyes; the improvement and refinement of flow visualization techniques; and through the acquisition and modification of facility hardware.

The flow visualization study reported on herein presents the results of simulated high velocity fluid flow using water as the fluid medium at Reynold's Numbers that nearly match that of high velocity gas flows. The information obtained and presented provides an insight into the mixing characteristics of the side dump mixing chamber and details flow formations and flow patterns. In addition, visual data is provided that can aid in the evaluation of new 3-D computer simulations of similiar fluid flows. Actual fluid flow patterns can be analyzed to determine the accuracy of computer simulations.

In the test program conducted, visual information was obtained for variations in design parameters of the basic dual inlet side dump combustor configuration and for a few specialized configurations to study unique flows visualization methods or techniques. Visual information was

obtained from freehand sketches of flow observations, photographs, and movies. The technique used for flow visualization was the "light-sheet" method. A high intensity light source focused to a narrow plane beam illuminates injected gas bubbles or particles in a narrow cross-section of the moving fluid. Table 1 is a matrix of flow pattern sketches made for the various configurations of the dual inlet side dump combustor design using this method.

5.2 INJECTION PROBE

In order to properly conduct the residence time studies of the multi-ducted inlet combustor configurations, it was first necessary to conduct a study of dye injection probes and injection procedures. It was desirable to have the capability to inject a minute quantity of colored dye tracer into the fluid stream that would disperse completely, quickly, and uniformly in a small volume of the fluid. This injected dye tracer would then be the stimulus to the system which could be detected and analyzed to determine residence times. Figure 7 shows the progression of injection probe designs that were studied to achieve the desired results. The 3-prong probe with bleed gave the best results. Its unique design dispersed the injected dye quickly and evenly with minimum trail off. Photographs presented in Figure 8 show an injected dye pulse using the 3-prong probe with bleed at a total flow rate of 300 GPM. Notice that the dye has dispersed almost completely in the inlet fluid in a distance of 16 inches in 0.126 seconds. The dyed fluid is approximately 3 inches long and represents an inlet pulse at the detector of less than 0.1 seconds. Figure 9 is a typical plot of the dye concentration-time function as a result of dye injection at a flow rate of 300 GPM.

Configuration	Flow Rate (GPM)	Combustor Length (in.)	Gas Generator Flow		Combustor Dome Height (in.)		Notes											
			Percent of Total Flow	(GPM)	20	125	0	1	5	10	20	0	1	2	3	4	5	6
30 Degree Dual Inlet $A_N/A_C = 0.29$	300	X	X					X	X	X	X							
	300	X						X										Port at Bottom
	300	X						X										Port at Top
	300	X	X															Divider Installed
	300	X																
	300	X	X					X	X	X	X	X	X	X	X	X	X	
45 Degree Dual Inlet $A_N/A_C = 0.29$	300	X	X					X	X	X	X	X	X	X	X	X	X	
	300	X						X										
	300	X	X					X										
	300	X																
	300	X	X															
	300	X																
60 Degree Dual Inlet $A_N/A_C = 0.29$	300	X	X					X										
	300	X						X										
	300	X	X					X										
	300	X																
	300	X	X															
	300	X																

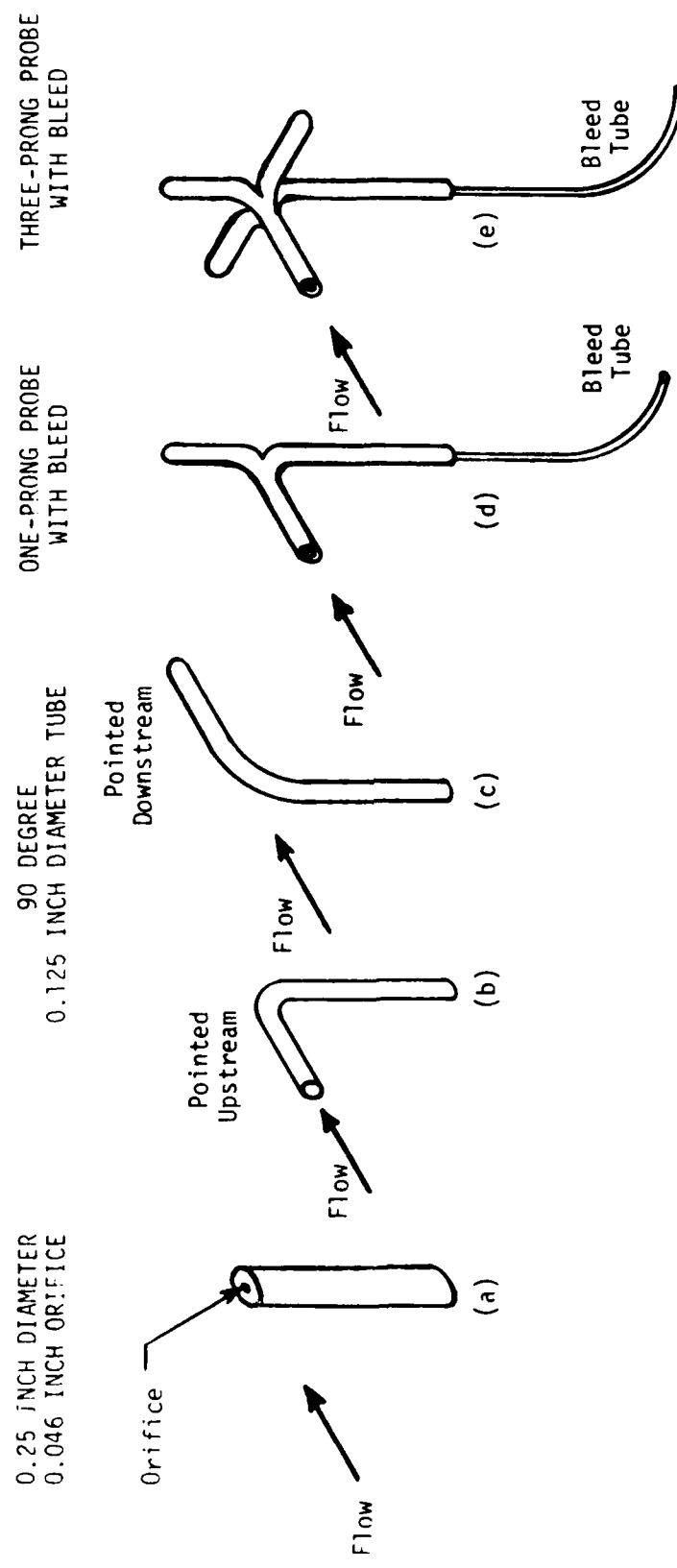
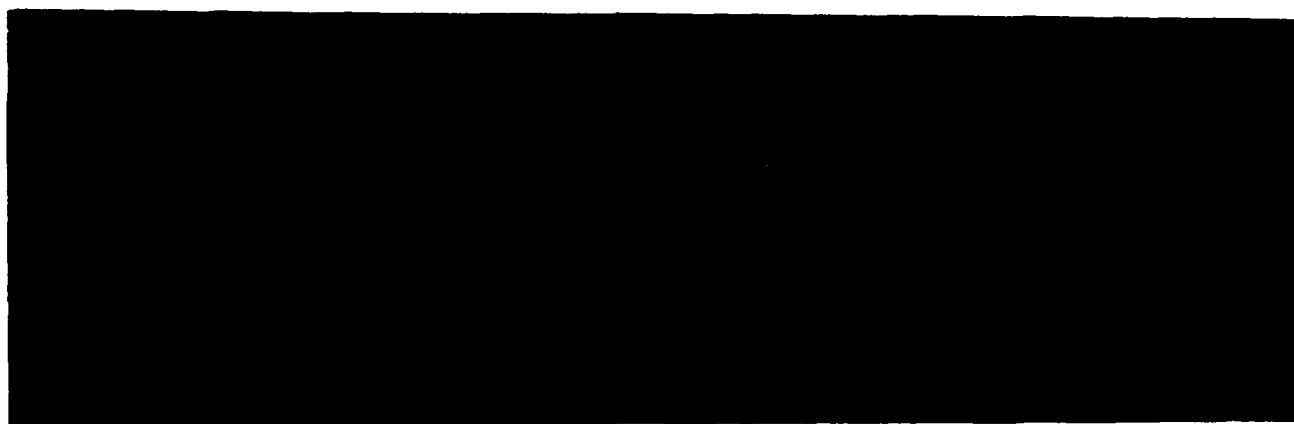
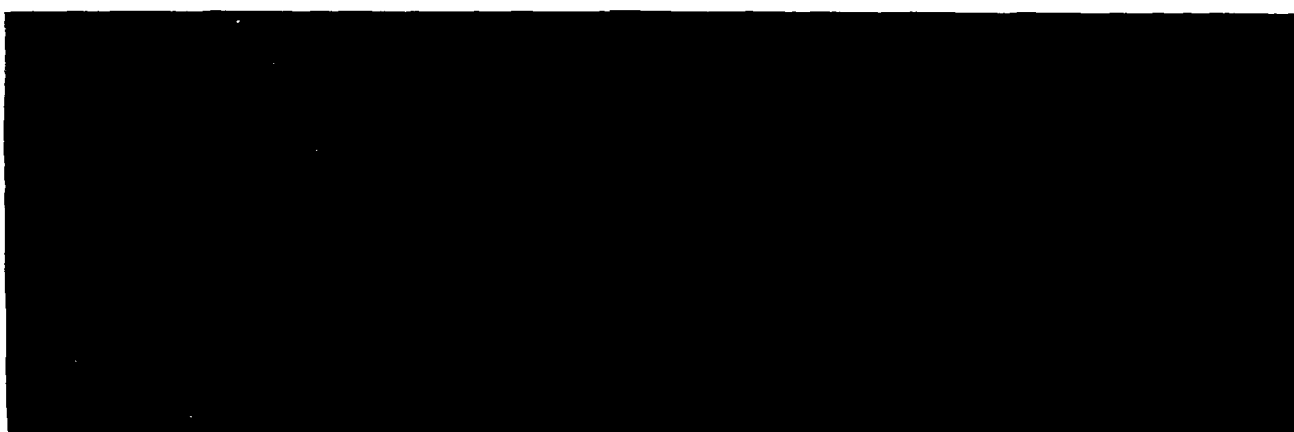


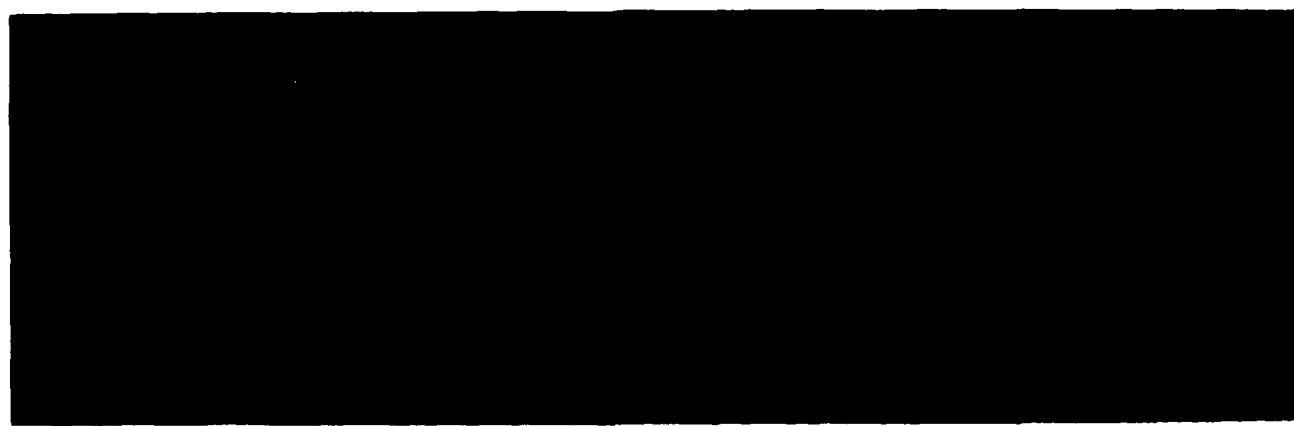
Figure 7. Dye Tracer Injection Probe Designs



← 16 in. →
TIME = 0.0 sec.



← 16 in. →
TIME = 0.063 sec.



← 16 in. →
TIME = 0.126 sec.

Figure 8. Photographs of Dye Injection In Inlet Duct

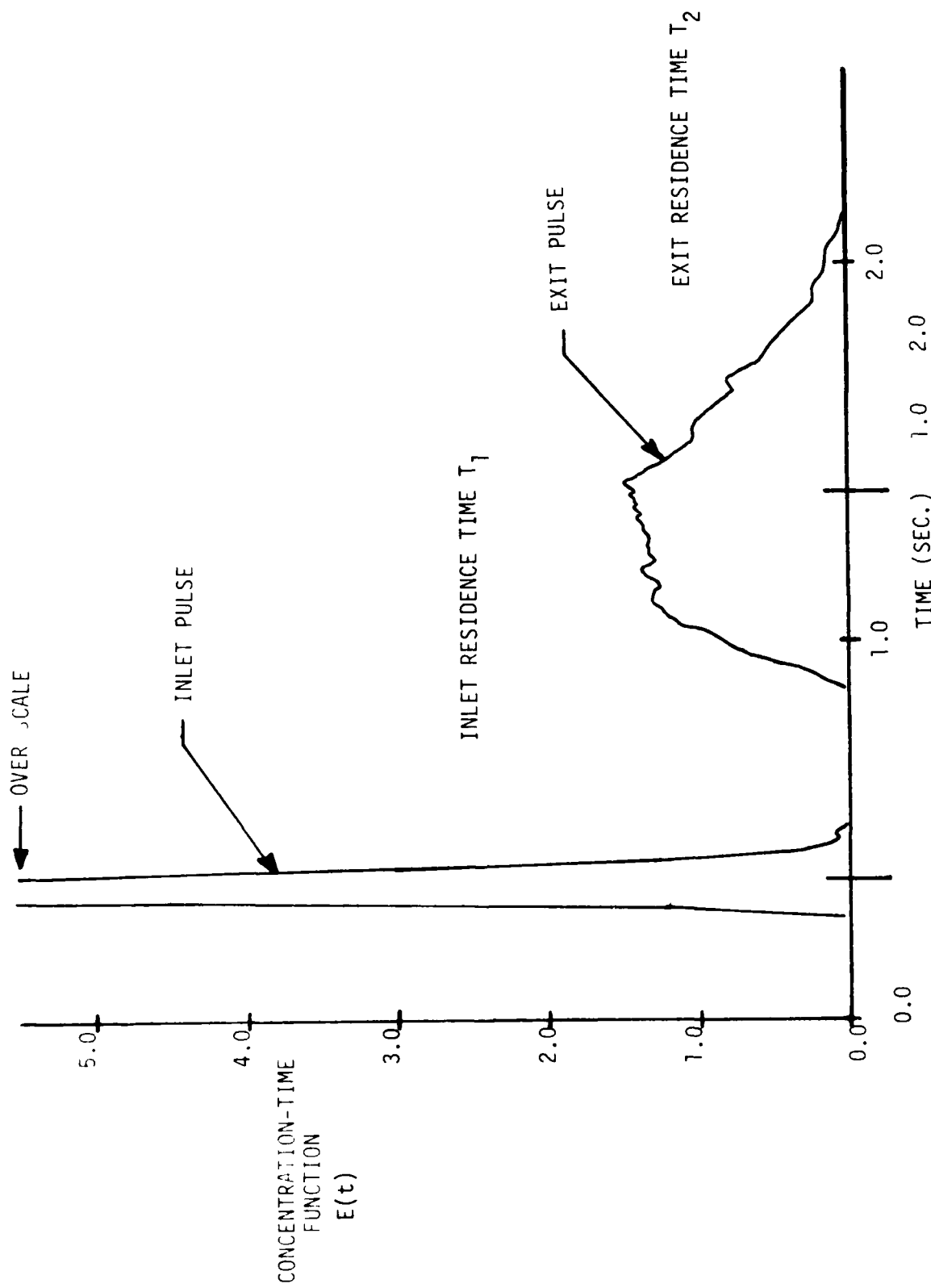


Figure 9. Concentration-Time Function Curve for Dye Injection

6.3 RESIDENCE TIME STUDIES

Combustor residence times were determined for the 30, 45, and 60 degree dual inlet side dump combustor configurations. Tests were conducted using the AFWAL/PORT Water Tunnel at total flow rates of 200, 300, and 400 gallons per minute. Combustor dome plate positions from 0.0 to -6.0 inches from the longitudinal zero reference point (Refer to Figure 4) were studied. The combustor dome plate was moved in increments of 0.5 inches for the 300 gallon per minute flow rate and in increments of 1.0 inch for the 200 and 400 gallon per minute flow rates. The inlet duct Reynolds numbers for the water flow test conditions are given in Table 2. The inlet duct Reynolds numbers are based on the hydraulic diameter determined from the inlet duct cross-sectional area. All residence time tests were conducted at water temperatures between 80 and 90 degrees Fahrenheit.

6.4 SPECIALIZED STUDIES

In conjunction with residence time studies, additional specialized studies were performed to aid in developing an understanding of the side dump combustor flow processes. A gas generator flow study was conducted to determine the effects of injected flows upon combustor flow patterns and residence times. An investigation was also made to determine the effects on combustor flow patterns of inlet turning vanes.

TABLE 2
INLET DUCT REYNOLDS NUMBERS

TUNNEL TOTAL FLOW RATE (GPM)	INLET DUCT REYNOLDS NUMBER (Re_I) @ 78°F
200	125,640
300	188,480
400	251,300

$Re_I = \frac{(D_{H_I}) (GPM) (0.0292)}{\nu}$
 D_H = Hydraulic Diameter = 0.22 ft.
 ν = Kinematic Viscosity = $1.083 \times 10^{-5} \text{ ft}^2/\text{sec.}$ @ 78°F

SECTION VII

DATA PRESENTATION AND DISCUSSION

This section presents the results obtained during the research and development effort to obtain qualitative and quantitative data to describe the internal fluid flow characteristics of advanced dual inlet side dump combustor configurations using hydrodynamic simulation. Studies were conducted to obtain internal fluid flow characteristics using visual observation techniques and information regarding the residence time of combustor flows using the stimulus-response method. The following paragraphs detail flow visualization and residence time results obtained for various configurations of the dual inlet side dump combustor.

7.1 FLOW VISUALIZATION DATA

Flow visualization data was obtained from freehand sketches, photographs, and high speed movies. Data were obtained from the observation of injected air bubbles highlighted with a high intensity light sheet. The light sheet was approximately 1/4 inch wide and could be positioned perpendicularly, axially, or radially to the axis of the combustor. First efforts were directed at developing techniques to achieve good quality flow visualization data. Tests were undertaken to determine the optimum fluid flow rate through the combustor, the type of bubble injection, the quantity of air bubbles, and the proper photographic exposures to achieve good bubble traces with good contrast and resolution. A total flow rate of 300 gallons per minute (GPM) was judged to provide the optimum conditions for visual and photographic observations. This flow rate maintained a reasonable bubble size and yet allowed for photographic exposures that gave good quality and long bubble traces. At a too slow flow rate (200 GPM) the buoyancy effects of the air bubbles became a factor. Bubbles would rise to the top of the chamber and collect, and the bubble size was considered too large (approximately 3/16 inch in diameter) to represent true flow patterns. At a high flow rate (400 GPM) the bubbles became very small as a result of increased system pressure, making traces hard to distinguish. Also, because exposure times had to be shortened to obtain good bubble traces,

the lighting requirements were insufficient. A flow rate of 300 GPM also gave very good visual observations from which freehand sketches could be made that represented averaged characteristics of flow patterns.

Since the only light source during visual and photographic observations was the light sheet, a fairly long exposure time was required. The best results were obtained for photographic exposures of 1/4 second. The film used for still shots was Kodak Kodacolor film with an ASA of 400. For studies of flow characteristics, injection patterns, and circulation regions requiring high speed movies, a frame speed of 400 frames per second was necessary for stop action; for general observation 50 frames per second gave the best results. Kodak Ektachrome Color High Speed Movie Film #7250 was used for all movies.

7.1.1 Baseline Configuration Flow Patterns

Presented in Figures 10, 11, and 12 are freehand sketches of observed fluid flow patterns for the three inlet angle configurations of the dual inlet side dump combustor configuration. The flow patterns are for dome plate positions of 0.0, -2.0, and -4.0 inches and at a balanced total inlet flow of 300 GPM and a nozzle area ratio of 0.29. There are a number of important observations to be made from each set of flow pattern sketches.

First, the flow patterns for each configuration are almost identical at and just downstream of the inlet ducts (4.0 inch axial station). The two helical vortices are strong and symmetrical, but as the inlet angle increases, the vortices are less strong further downstream (6 to 8 inch axial station). The most significant effect of inlet angle occurs in the dome region of the combustor. Here, a vortex is formed that joins the two side vortices with its axis perpendicular to the combustor axis. This vortex was formed for the 30 and 45 degree inlet configurations at the dome position of 0.0 inches but not for the 60 degree inlet until the dome plate had been moved back at least 1.0 inch. At the 0.0 inch dome plate position, the two vortices directly attached themselves to the dome plate for the 60 degree inlet configuration.

As the dome plate was moved to a greater depth, the dome vortex grew in the dome region with a corresponding reduction in vortex

Inlet Configuration: Dual 30 Degrees
Total Combustor Flow: 300 GPM Balanced
Combustor Length: 39.0 Inches
 A_t/A_c : 0.29

Gas Generator Flow: None

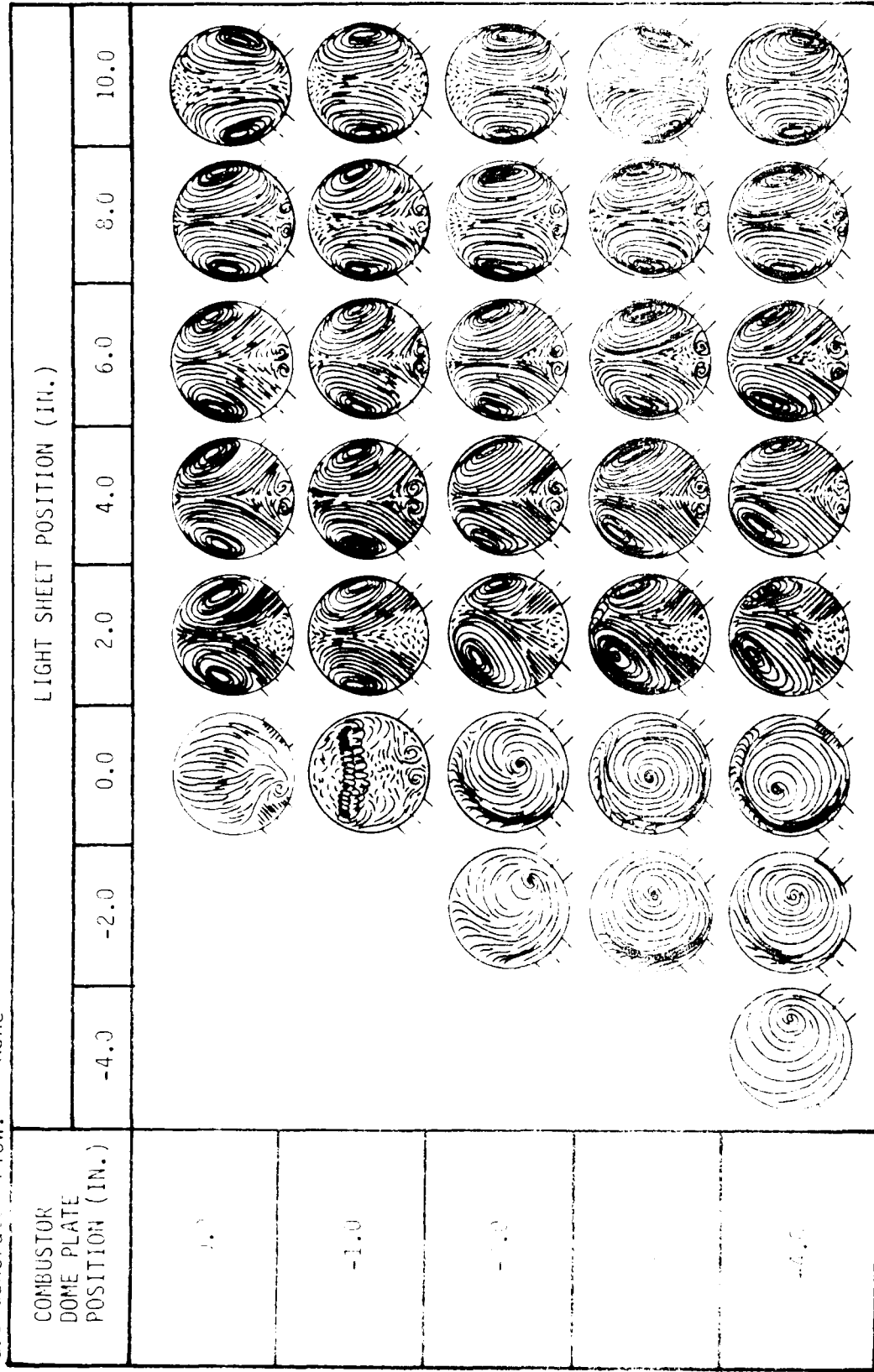


Figure 10. Flow Visualization Sketches - 30 Degree Inlets

Inlet Configuration: Dual 45 Degrees
 Total Combustor Flow: 300 GPM Balanced
 Combustor Length: 39.9 Inches
 A_N/A_C : 0.29
 Gas Generator Flow: None

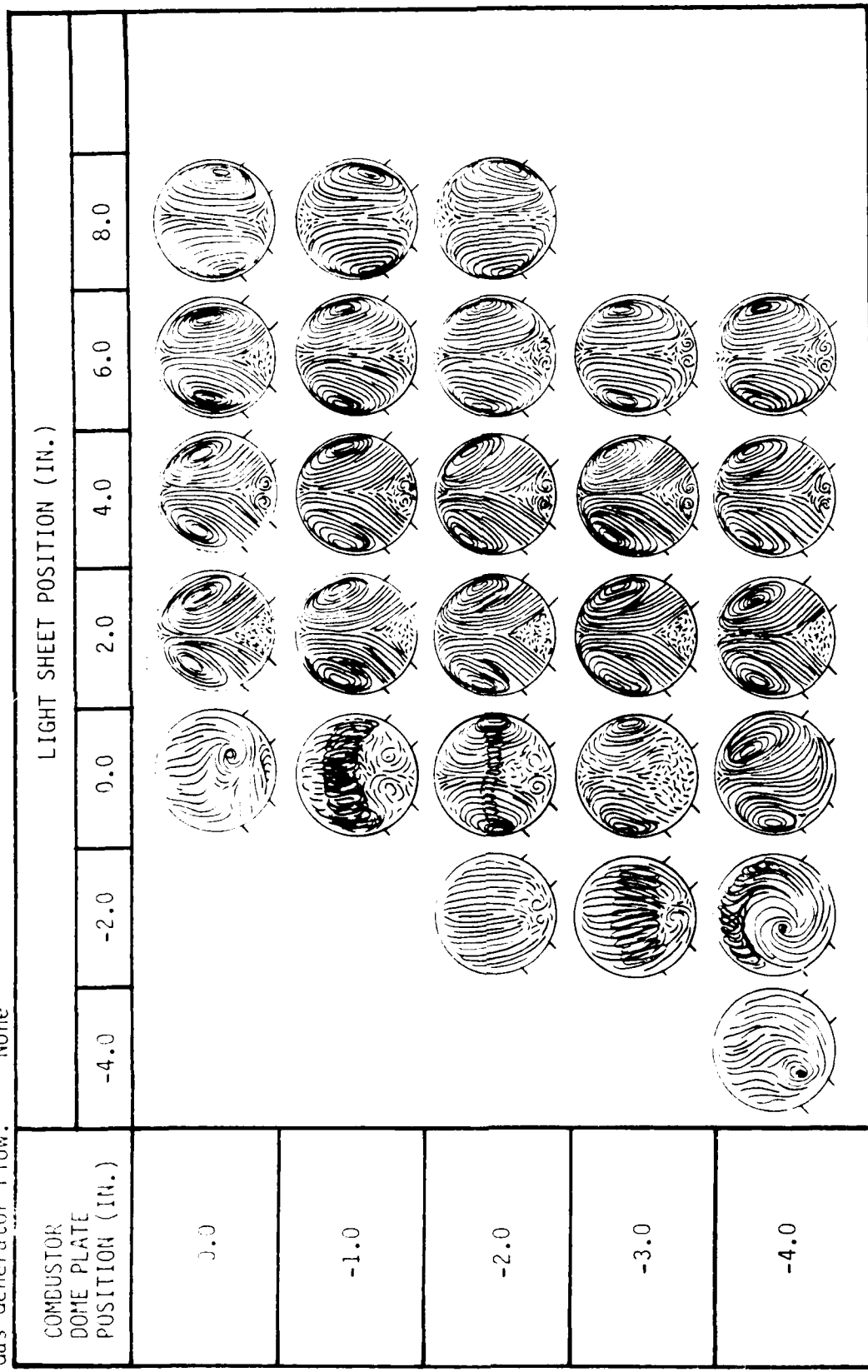


Figure 11. Flow Visualization Sketches - 45 Degree Inlets

Inlet Configuration: Dual 60 Degrees
 Total Combustor Flow: 300 GPM Balanced
 Combustor Length: 39.0 Inches
 A_N/A_C : 0.29
 Gas Generator Flow: None

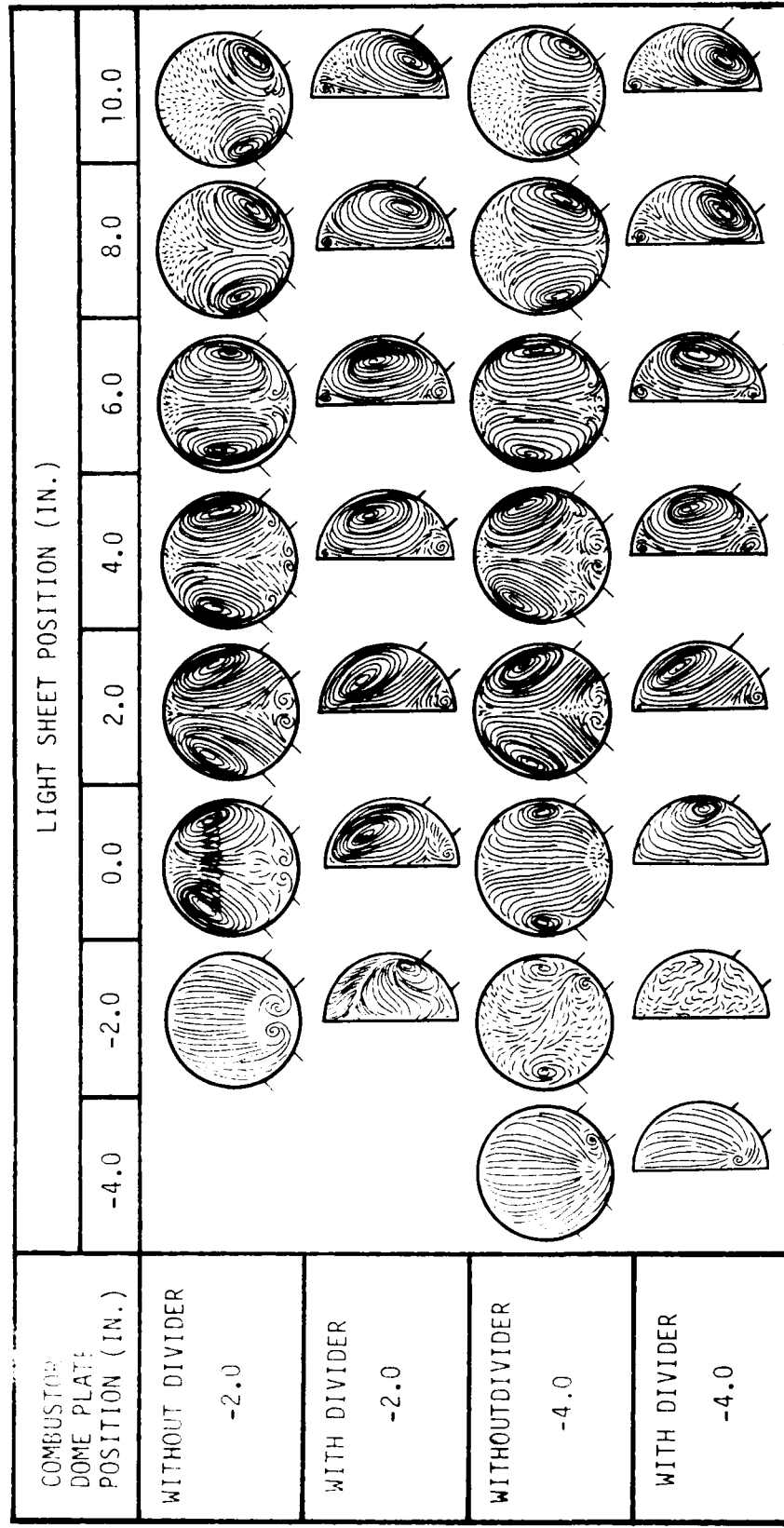


Figure 22. Effect of Combustor Centerline Divider on Flow Patterns for 60 Degree Configuration

Inlet Configuration: Dual 45 Degrees
Total Combustor flow: 300 GPM Balanced
Combustor Length: 39.0 Inches
 A_N/A_C : 0.29

Gas Generator Flow: None

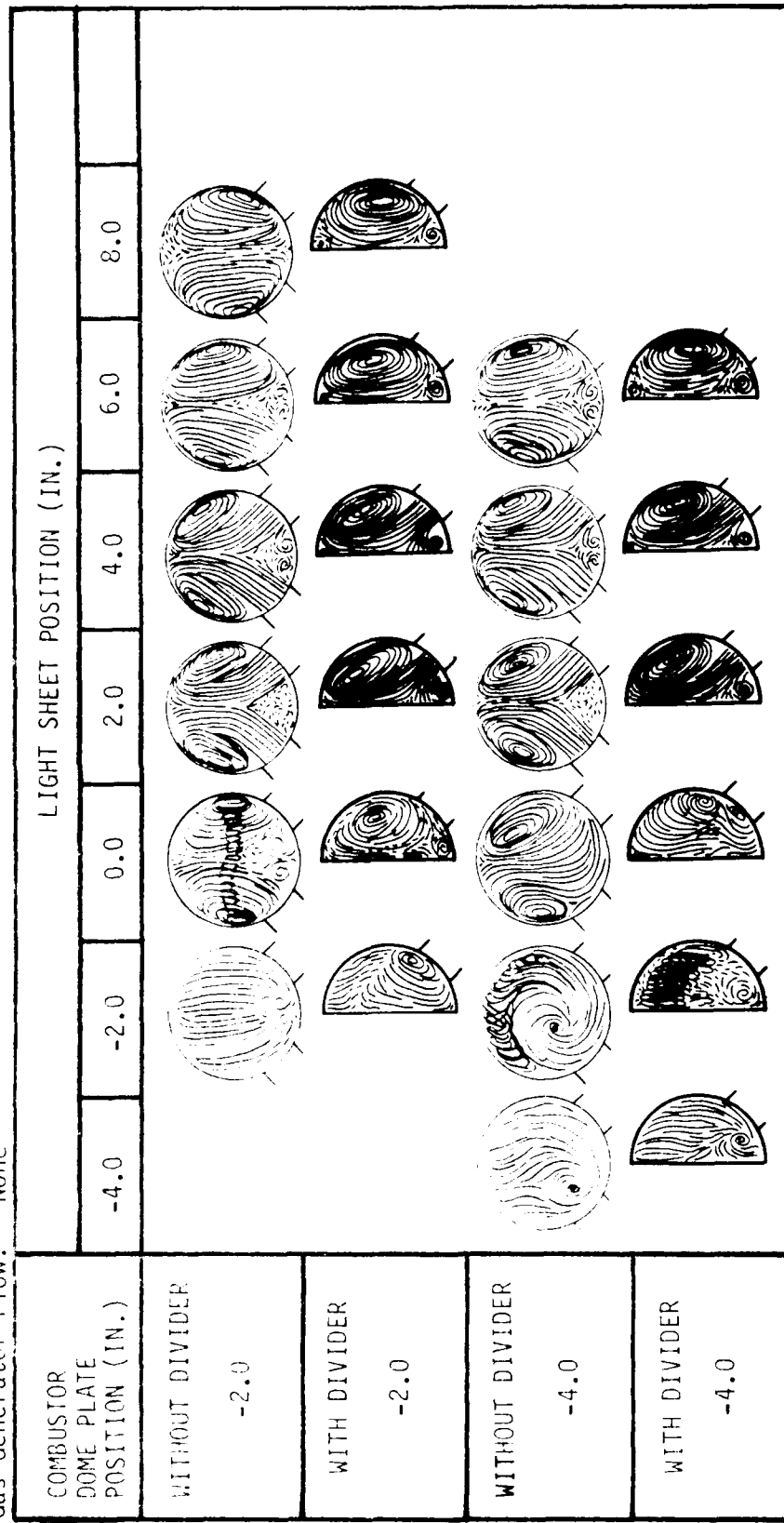


Figure 21. Effect of Combustor Centerline Divider on Flow Patterns for 45 Degree Configuration

Inlet Configuration: Dual 30 Degrees
 Total Combustor Flow: 300 GPM Balanced
 Combustor Length: 39.0 Inches
 A_N/A_C : 0.29

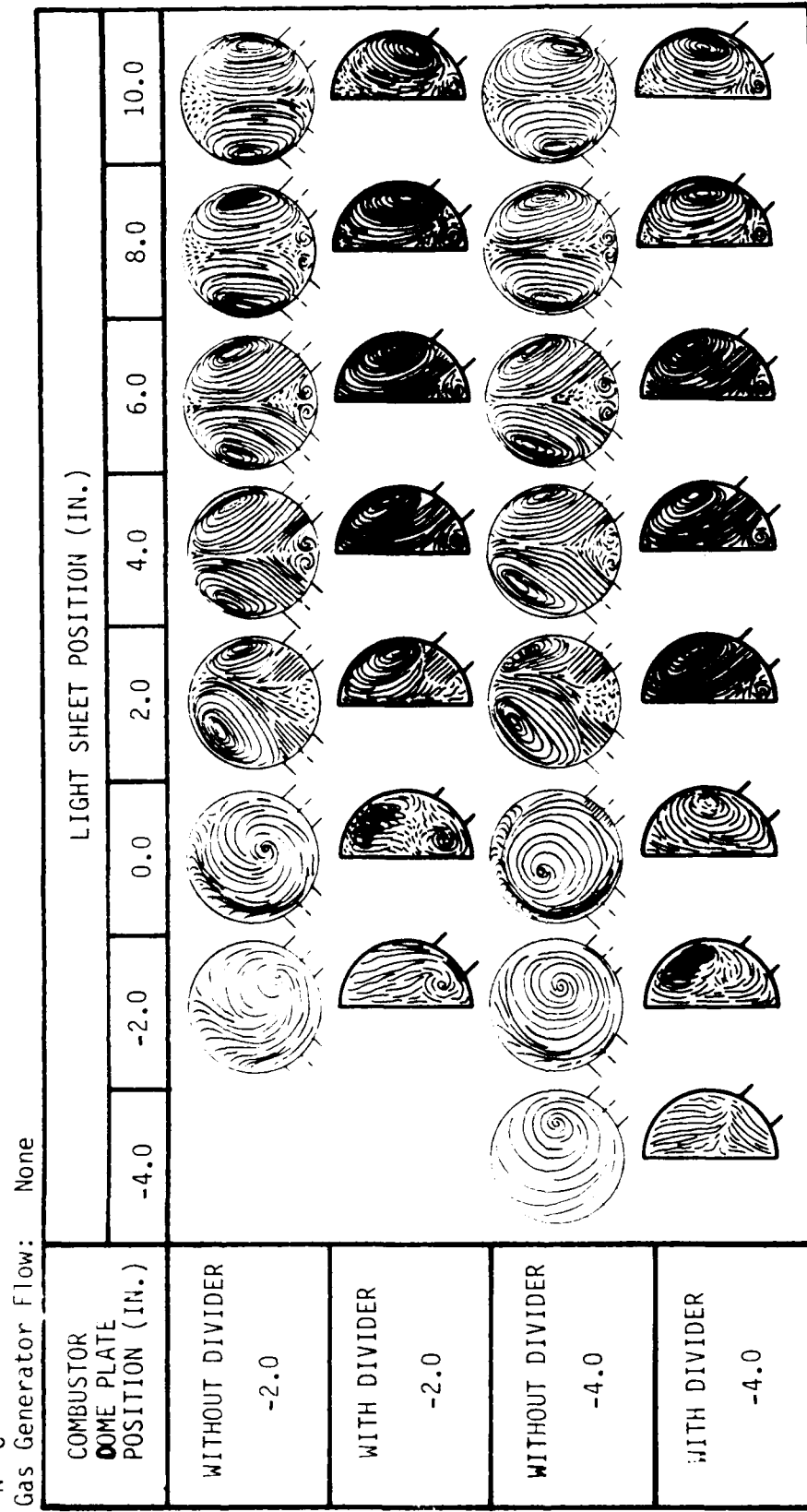


Figure 20. Effect of Combustor Centerline Divider on Flow Patterns for 30 Degree Configuration

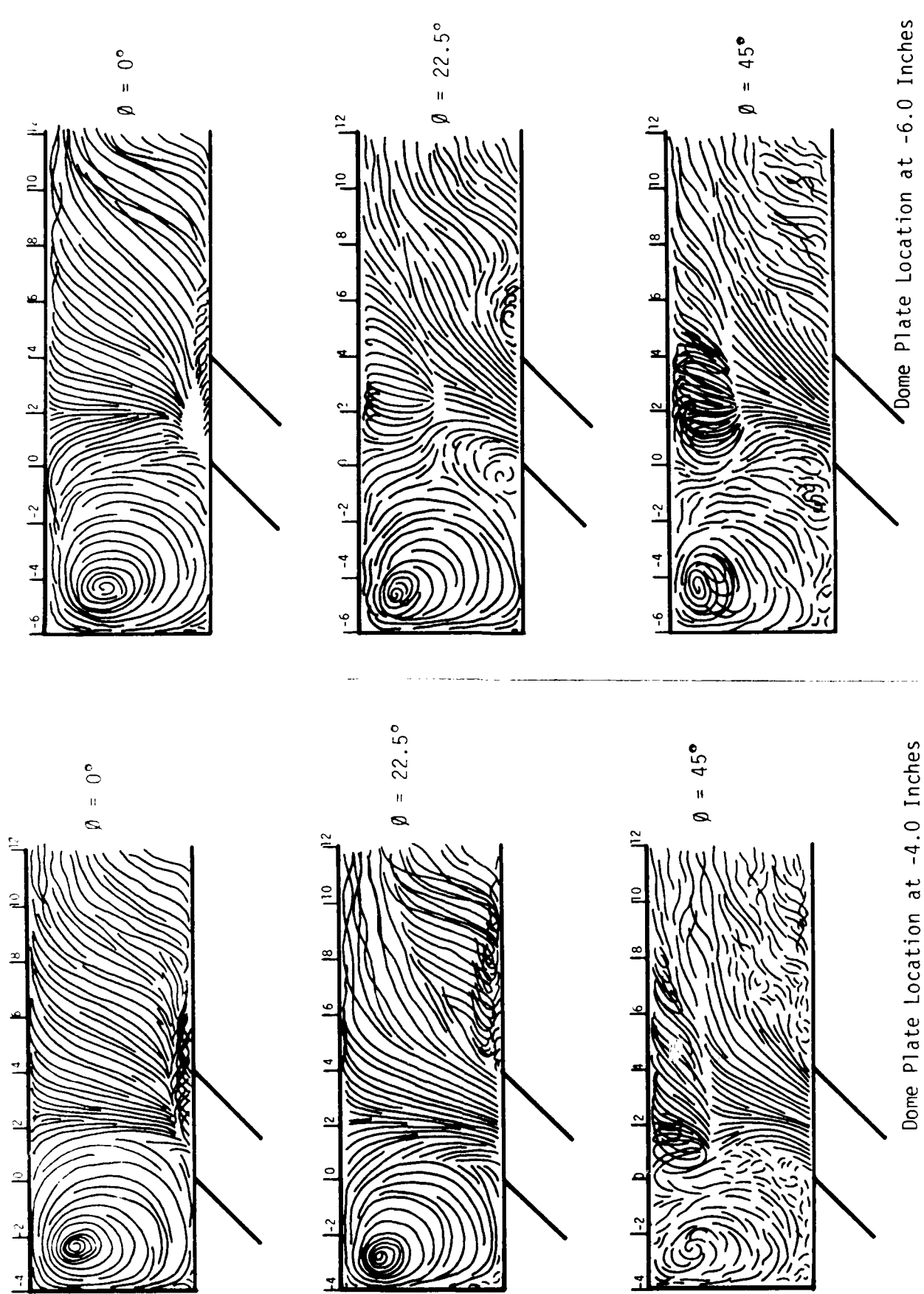


Figure 19. Radial Flow Pattern Sketches of the 60 Degree Inlet Configuration (Concluded)

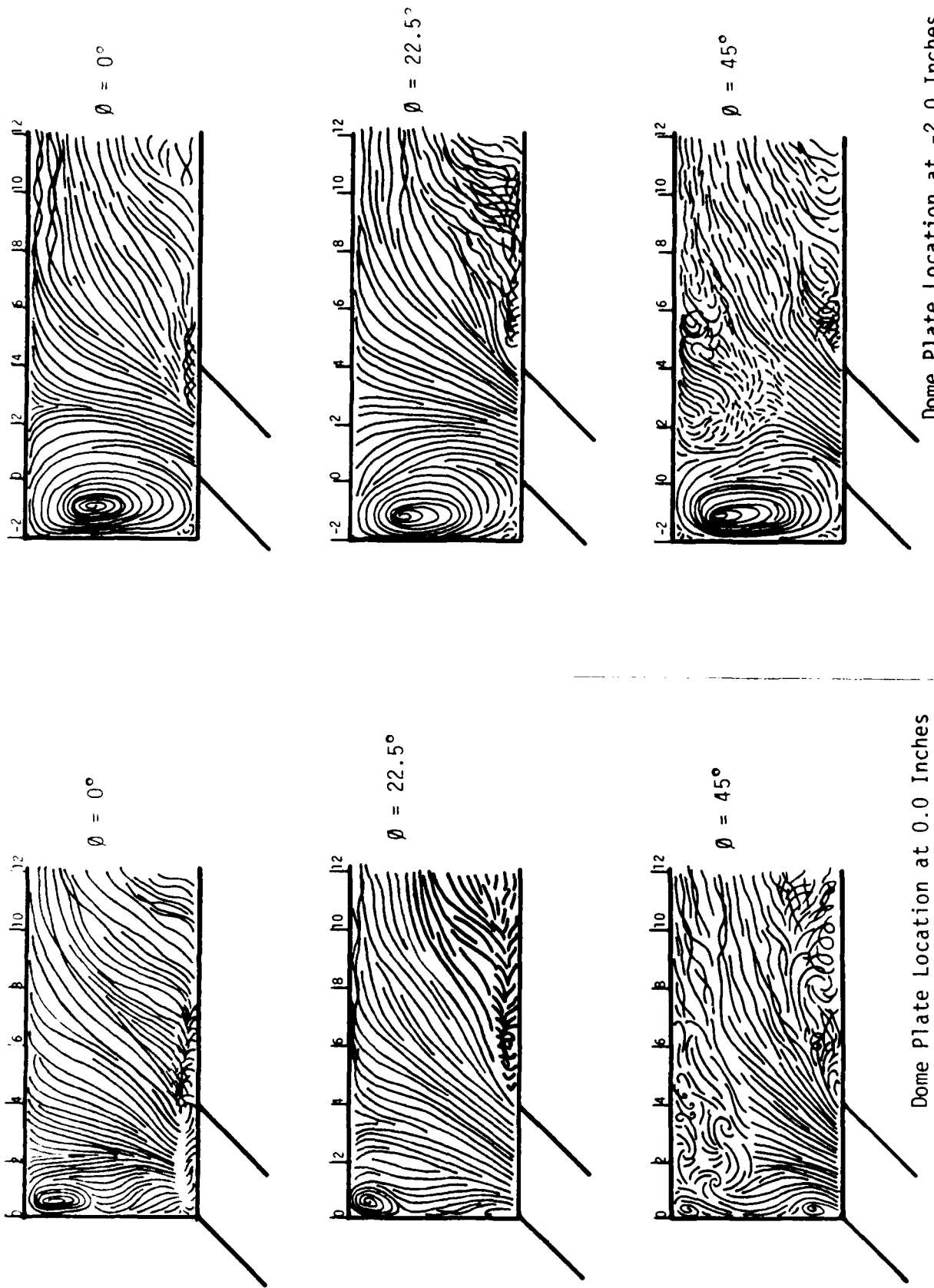


Figure 19. Radial Flow Pattern Sketches of the 60 Degree Inlet Configuration

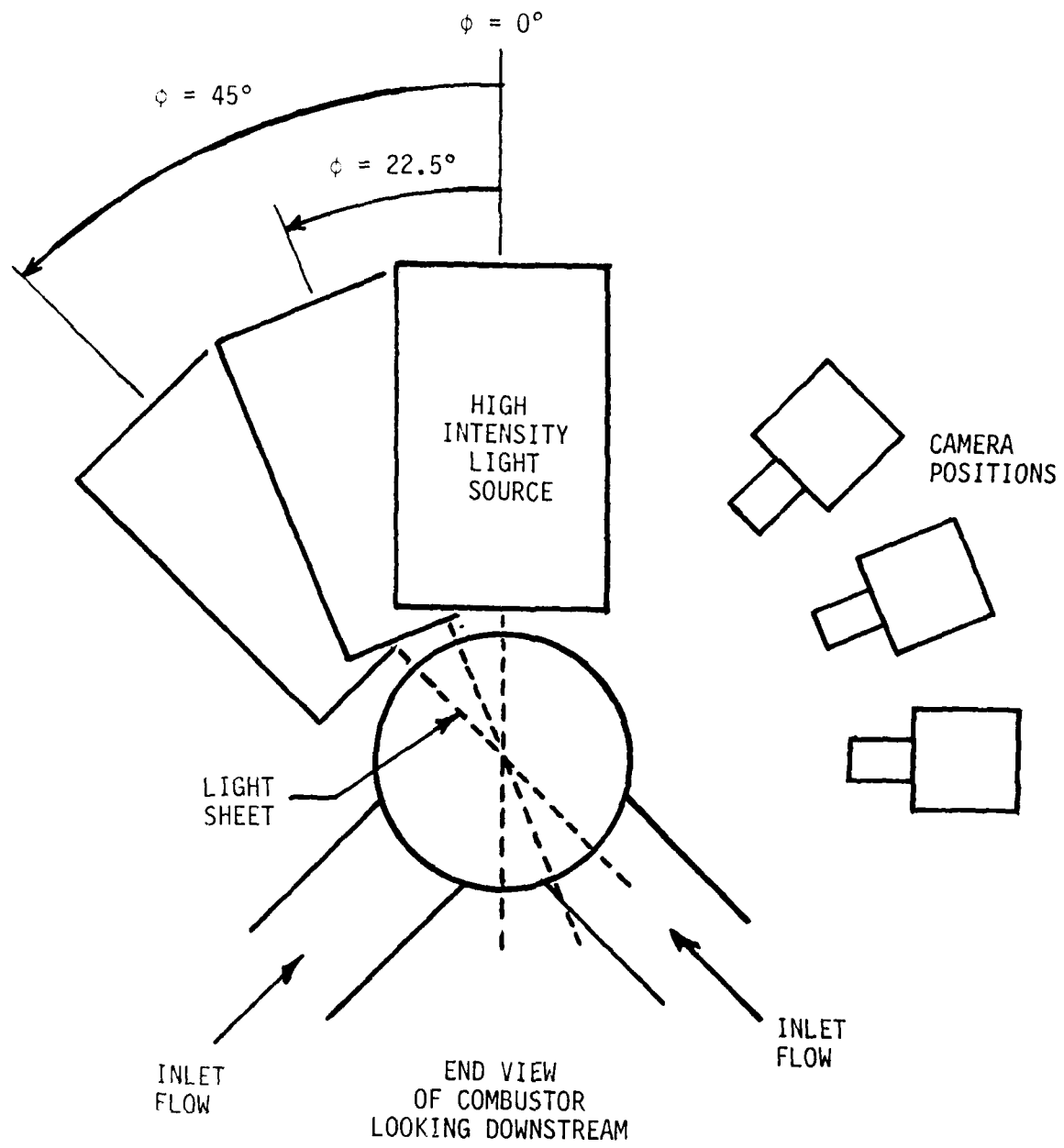


Figure 18. Test Setup for Viewing Radial Flow Patterns

stations. A fixture was designed, fabricated and installed that allowed observation of flow patterns at different radial positions about the axis of the combustor. Figure 18 is a diagram of the test setup for obtaining radial flow pattern sketches. Figure 19 shows freehand sketches made using this setup for various dome plate positions of the 60 degree dual inlet side dump combustor configuration.

The sketches detail quite clearly the formation of the dome vortex and the inlet flow. The dome vortex expands to fill the volume just upstream of the inlet ducts. As the dome volume increases, the dome circulation expands while decreasing in strength. Also visible is the stagnation point of the inlet flow against the top of the combustor. The stagnation point appears near the 2.0 inch longitudinal station and does not noticeably change as the dome volume increases. Another flow formation that agrees with the cross sectional views is the small vortices that are found at the bottom of the combustor between the inlet ducts. These vortices initiate at about the 2.0 inch station and are dissipated before the 6.0 inch station.

7.1.4 Combustor Symmetry Study

In the development of 3-D computer codes to simulate combustor flows, it has been necessary to use configuration symmetry to reduce computational time. Such a configuration utilizes a combustor configuration that has one inlet and a solid boundary at the line of symmetry on the combustor axis. It was of interest to determine how well this configuration duplicates the actual dual inlet configuration flow patterns. A combustor divider was designed and fabricated that attached to the dome plate at the line of symmetry and extended into the combustor for a distance of 13.5 inches. This distance was well past the inlet area and provided a good simulation of symmetry flow in the area of most interest.

Presented in Figures 20, 21, and 22 are freehand sketches of combustor flow patterns for the 30, 45, and 60 degree inlet configurations, respectively, for different dome plate positions. Sketches are for the combustors with and without the combustor divider to show the difference in flow patterns. From the flow patterns, it can be seen that there is almost no difference in the patterns beyond the

Inlet Configuration: Dual 45 Degrees
 Total Combustor Flow: 300 GPM Balanced
 Dome Plate Position: -4.0 Inches
 A_N/A_C : 0.29
 Gas Generator Flow: None

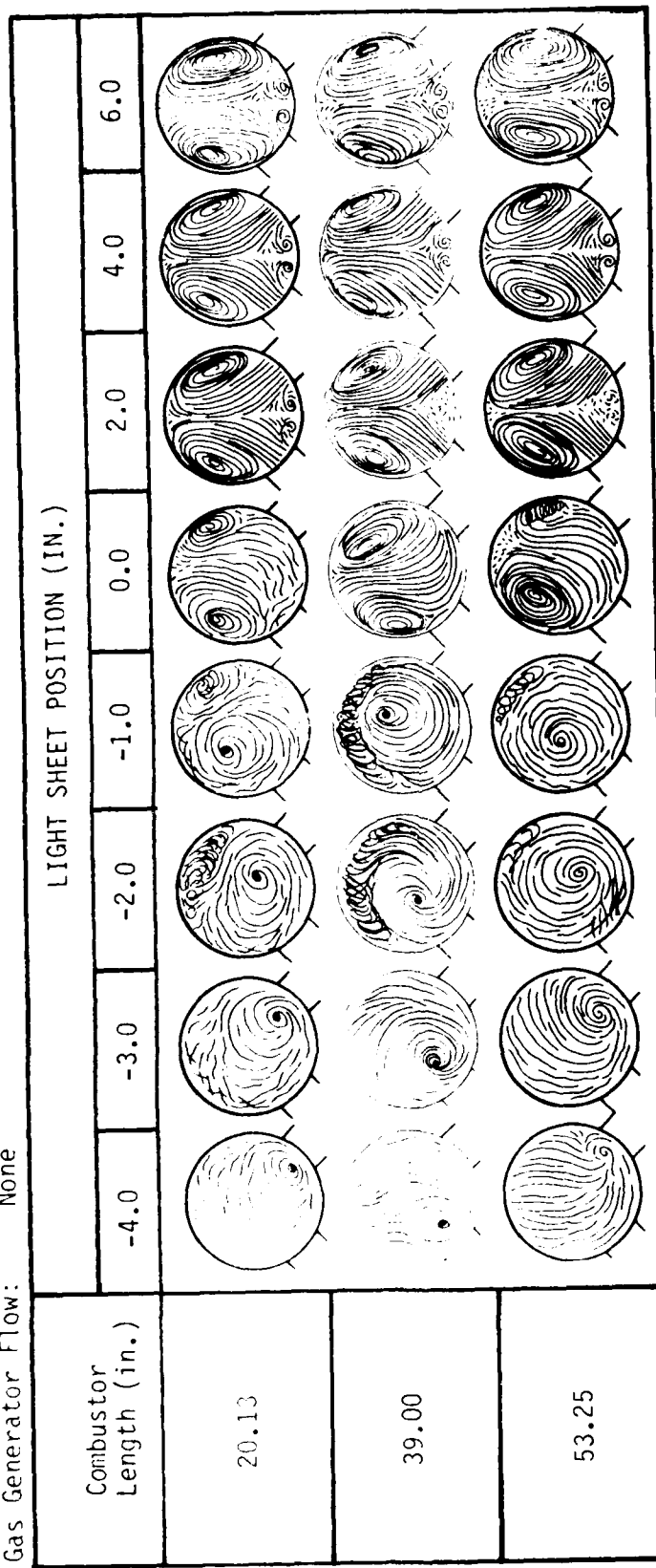


Figure 17. Flow Visualization Sketches for Various Combustor Lengths for 45 Degree Inlet Configuration

Inlet Configuration: Dual 45 Degree
 Total Combustor Flow: 300 GPM Balanced
 Dome Plate Position: -2.0 Inches
 A_t/A_c : 0.29
 Gas Generator Flow: None

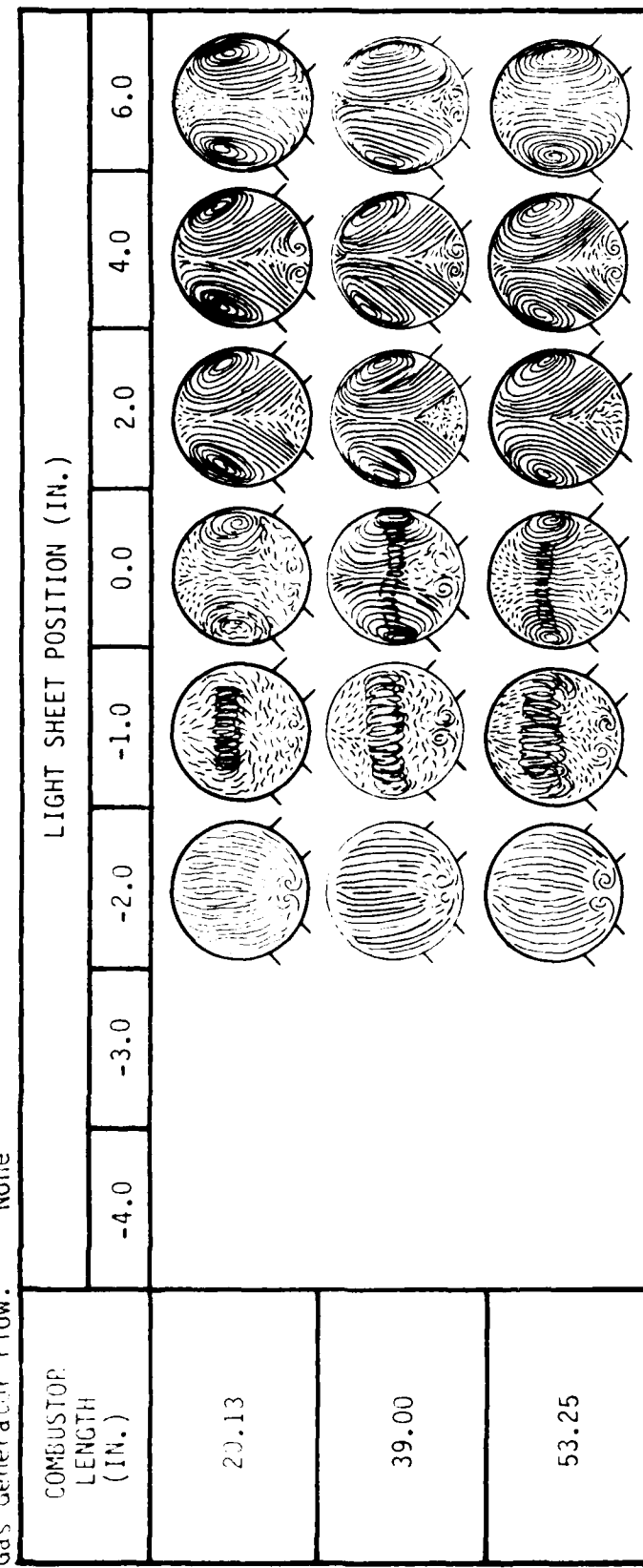


Figure 16. Flow Visualization Sketches for Various Combustor Lengths for 45 Degree Configuration

Inlet Configuration: Dual 45 Degrees
 Total Combustor Flow: 300 GPM Balanced
 Dorne Plate Position: 0.0 Inches
 A_N/A_C : 0.29
 Gas Generator Flow: None

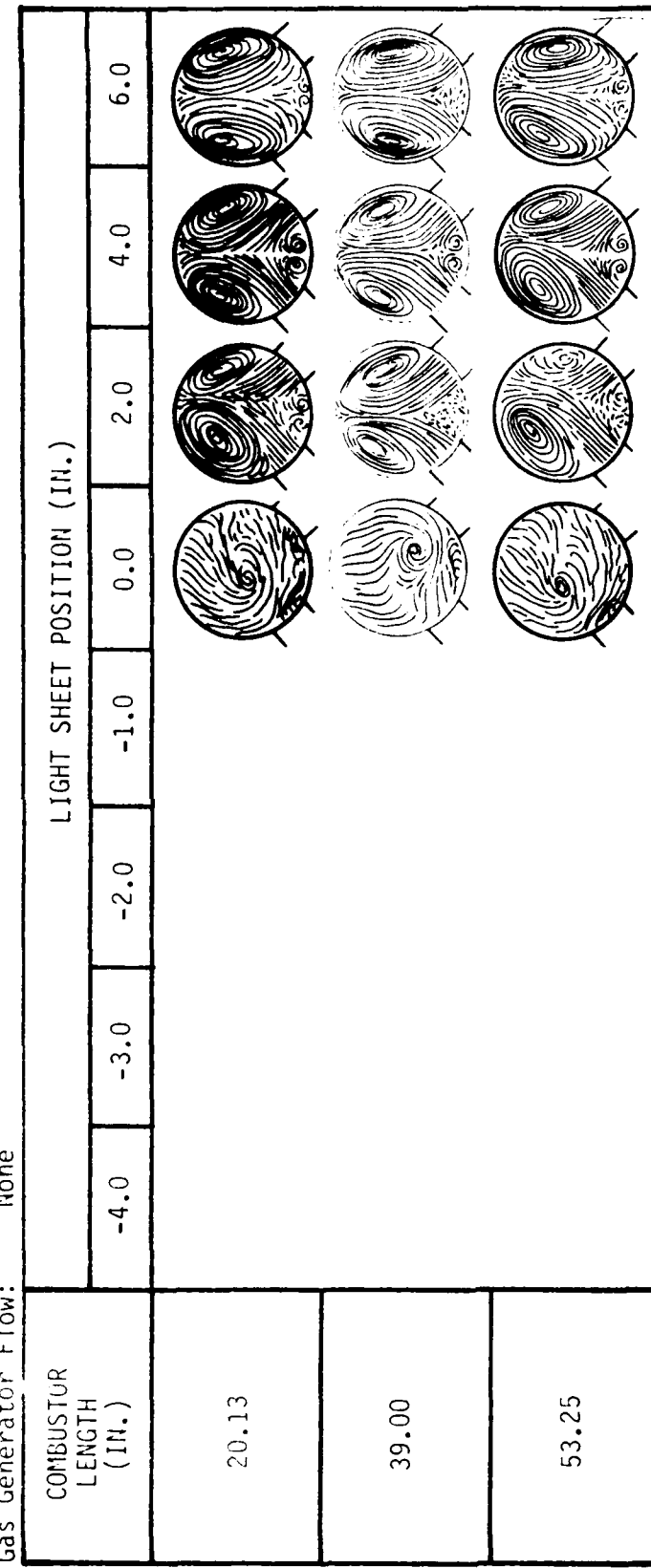
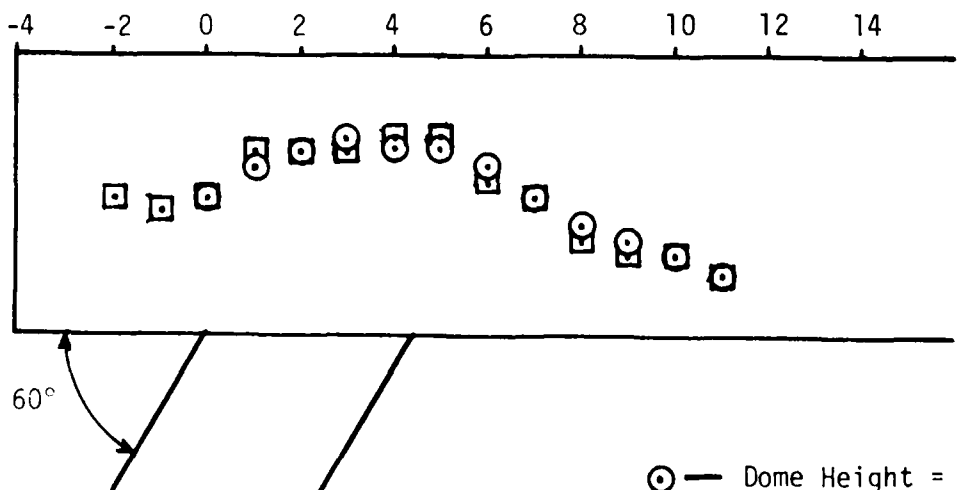
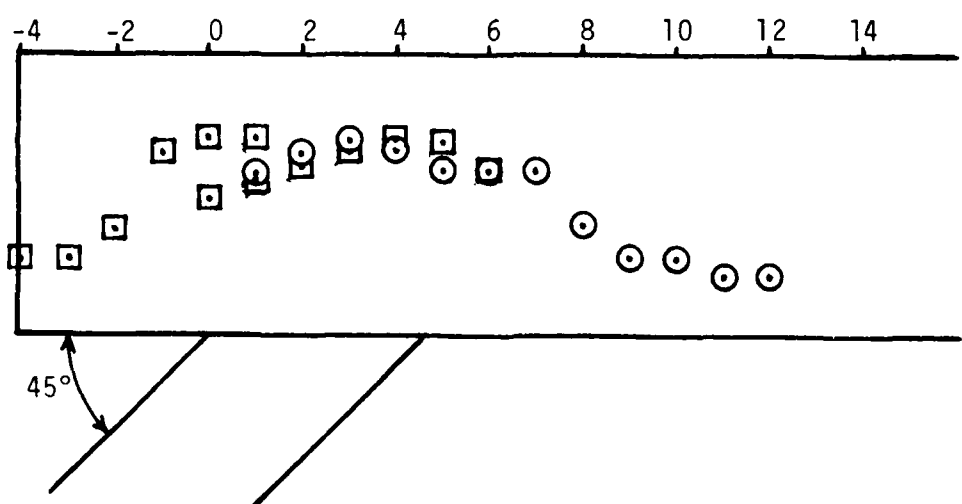
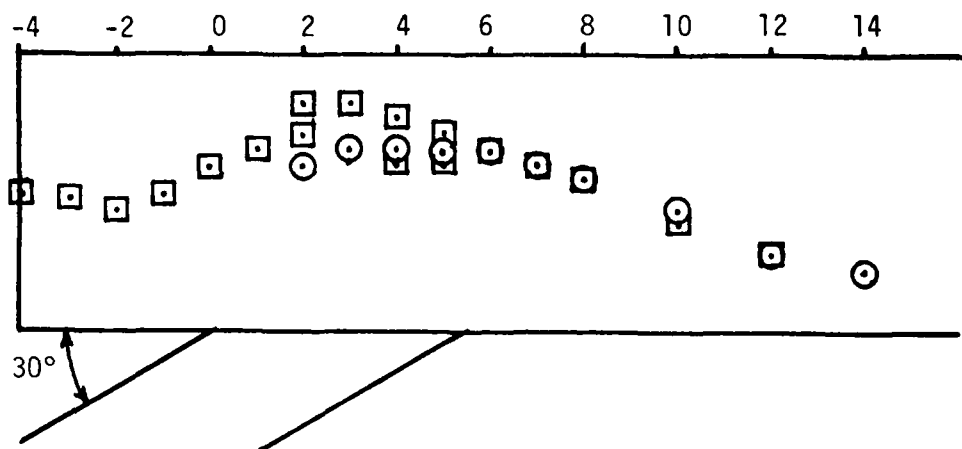


Figure 15. Flow Visualization Sketches for Various Combustor Lengths for 45 Degree Configuration



Data From Flow
Visualization
Sketches

○ — Dome Height = 0.0 in.
□ — Dome Height = -4.0 in.

Figure 14. Relative Vortex Center Versus Longitudinal Station

TEST CONDITIONS

45 DEGREE INLETS
330 GPM TOTAL COMBUSTOR FLOW

DOME PLATE 
POSITION = 0.0 IN.

DOME PLATE
POSITION = -2.0 IN.


DOME PLATE
POSITION = -4.0 IN.




4.0
2.0
0.0
-2.0
-4.0
LIGHT POSITIONS (IN.)

Figure 13. Photographs of Combustor Flow Patterns at Various Longitudinal Stations

strength. When the dome vortex strength weaken sufficiently, it would separate and one side vortex would attach itself to the dome plate. This would occur from either side or the situation would oscillate between the two sides. It should be noted that this breaking and separation of the dome region vortex occurred for different dome plate positions depending on the inlet angle. For the 30 degree case, the separation occurred at the -2.0 inch dome position; for the 45 degree case at the -4.0 inch dome position; and for the 60 degree case at the -6.0 inch position. Shown in Figure 13 are typical photographs of combustor flow patterns for the 45 degree configuration to show the comparison between freehand sketches and photographs.

Additional data obtained from the flow patterns was the relative position of the vortex center at different longitudinal stations for each of the inlet angles studied. Figure 14 presents plots for each inlet angle configuration of the relative vortex center along the combustor centerline for 0.0 and -4.0 inch dome plate positions. The plots show how the vortex centers are forced to higher positions at the inlet openings. Notice how the vortex center drops slowly for the 30 degree case and quickly for the 60 degree case. Data was taken from flow pattern sketches.

7.1.2 Effect of Combustor Length on Combustor Flow Patterns

To determine if there were any effects on the internal flow patterns for variations in combustor lengths, the AFWAL/PORT Water Tunnel combustor was modified to allow for variation of combustor length. Hardware was designed and fabricated that would reduce the combustor length to 20.13 inches or extend the combustor to a length of 53.25 inches. The baseline combustor length was 39.0 inches. Figures 15, 16, and 17 show the combustor flow patterns for the three combustor lengths at dome plate position of 0.0, -2.0 and -4.0 inches, respectively. The sketches show almost no effect of combustor length on the internal fluid flow patterns either in the dome region or downstream of the inlets.

7.1.3 Radial Flow Patterns Data

Efforts were undertaken to modify and improve the flow visualization capabilities of the Water Tunnel facility to allow observation of fluid flow patterns at other than cross sectional

Inlet Configuration: Dual 60 Degrees
 Total Combustor Flow: 300 GPM Balanced
 Combustor Length: 39.0 Inches
 $\Delta N/A_c$: 0.29

Gas Generator Flow: None

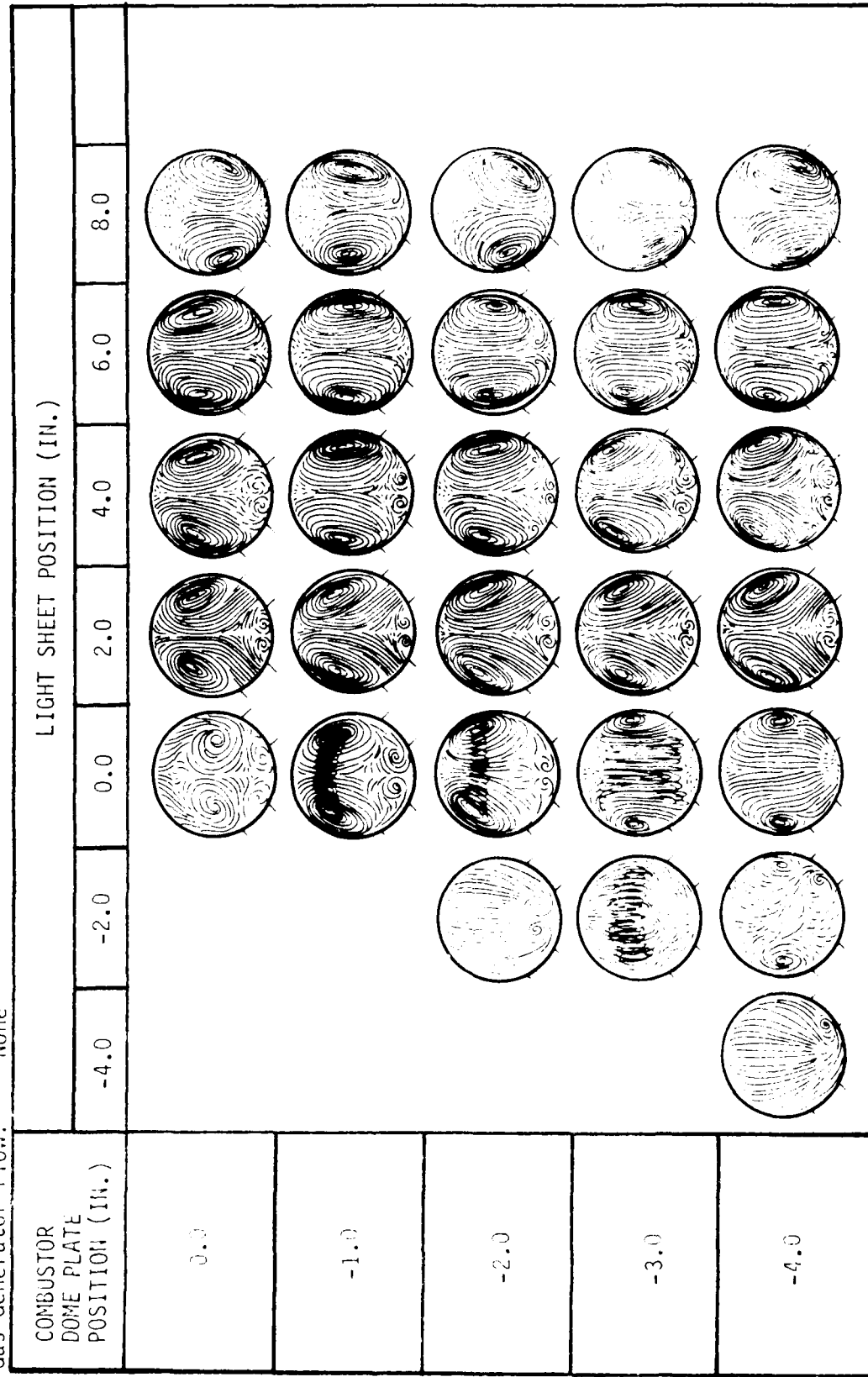


Figure 12. Flow Visualization Sketches - 60 Degree Inlets

4.0 inch longitudinal station. The only difference beyond the 4.0 inch station is the formation of a small vortex at the very top of the combustor for the 45 degree configuration.

The flow pattern differences upstream of the 4.0 inch combustor axial station were considerably greater when compared to flow patterns without the combustor divider. There is very little symmetry in the dome region flow pattern due mainly to vortex circulation perpendicular to the combustor axis. The dome region flow formation was not duplicated by the divider flow. The dome region flow with the divider installed was a more stable flow than without the divider. This was most likely due to the fact there was only one vortex in the dome region with the divider installed which is not the case without the divider.

These results demonstrate that using symmetry may not correctly simulate actual combustor flow patterns that are occurring in actual configurations. Figure 23 shows photographs of combustor flow patterns for the 45 degree configuration with the combustor divider installed. These photographs give a comparison between flow pattern sketches and photographic data.

7.1.5 Inlet Turning Vane Study

A study was conducted to determine the effects of inlet turning vanes upon the flow patterns in the dome region of the combustor configurations. Aluminum inlet vanes were installed in inlet ducts at the intersection of the inlet duct and combustor tube. Figure 24 details the inlet vane and installation in the test configuration. Inlet vanes were only tested with the 45 degree inlet configuration. Comparisons of combustor flow patterns with and without the inlet turning vanes are shown in Figure 25 for dome plate positions 0.0, -1.0, -2.0, and -4.0 inches.

The flow patterns show that the only noticeable effect of the inlet turning vanes is on the patterns in the dome region. The effect is only seen for dome plate positions of 0.0, -1.0, and -2.0 inches. At a dome plate position of -4.0 inches, there appears to be no effect. Where there are flow pattern differences, the inlet turning vanes cause the dome vortex to separate, and both side vortices

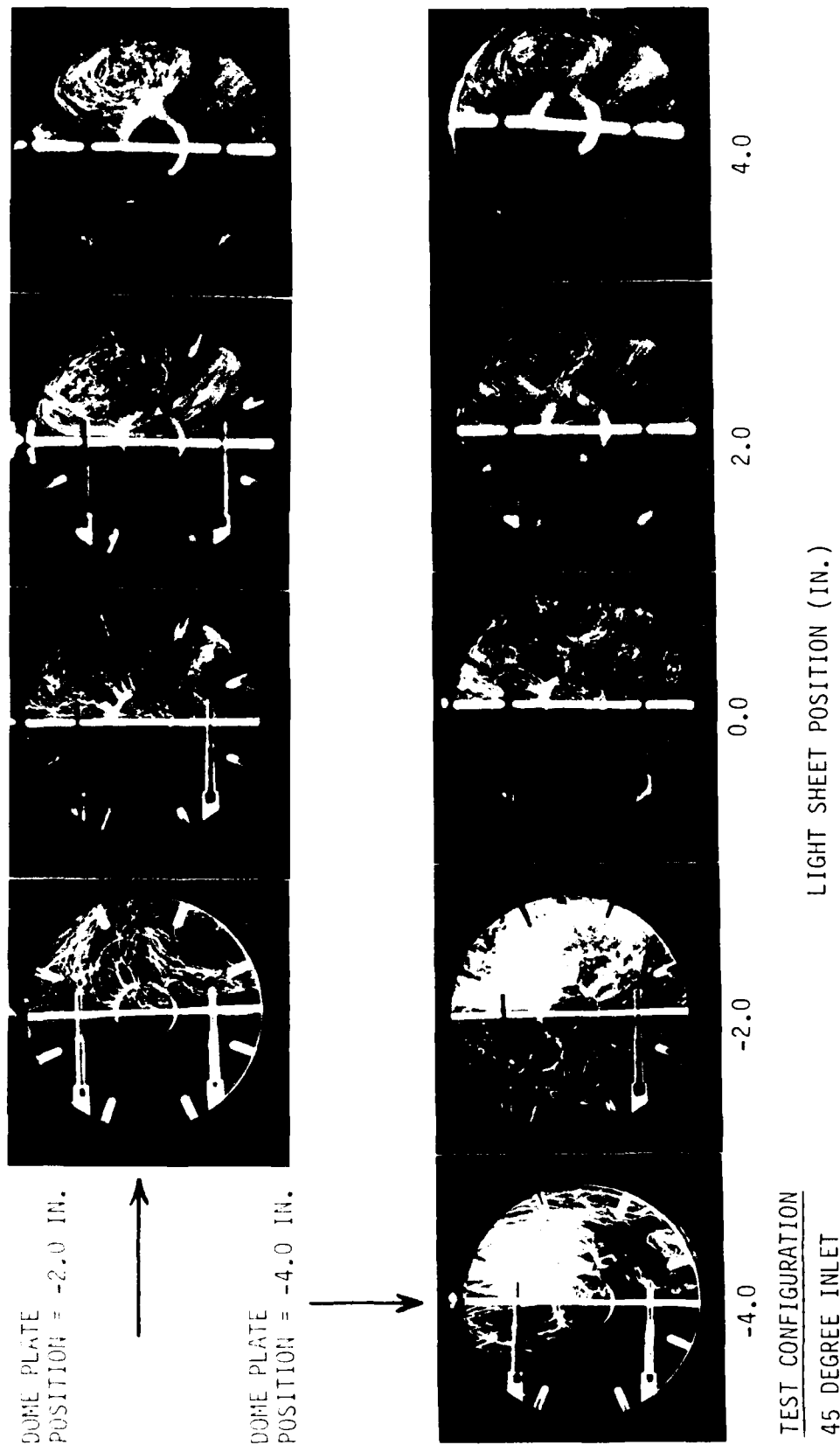


Figure 23. Photographs of Combustor Flow Patterns with Divider Installed

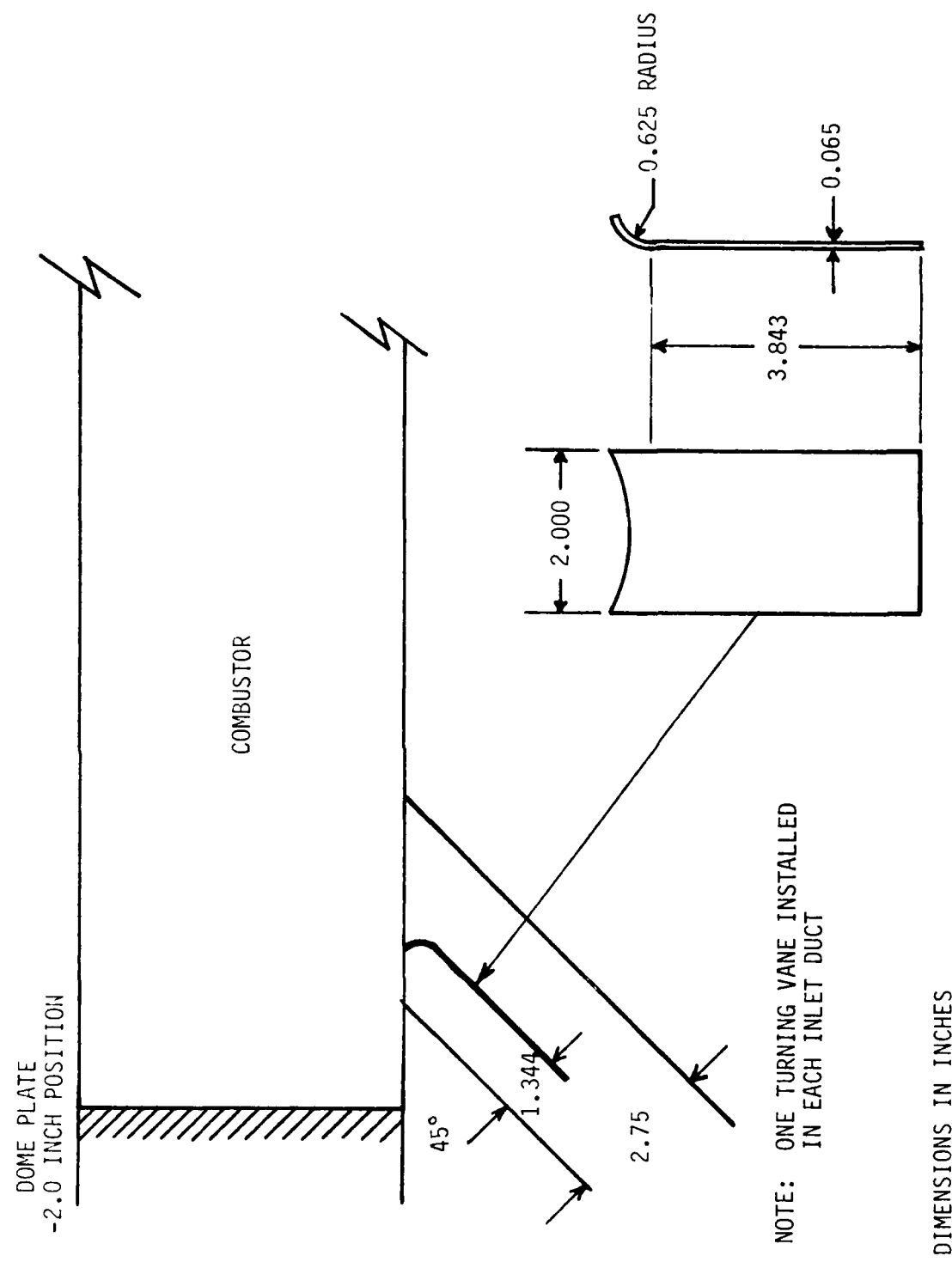


Figure 24. Inlet Turning Vane Configuration

Inlet Configuration: Dual 45 Degrees
 Total Combustor Flow: 300 GPM Balanced
 Combustor Length: 39.0 Inches
 A_N/A_C : 0.29
 Gas Generator Flow: None

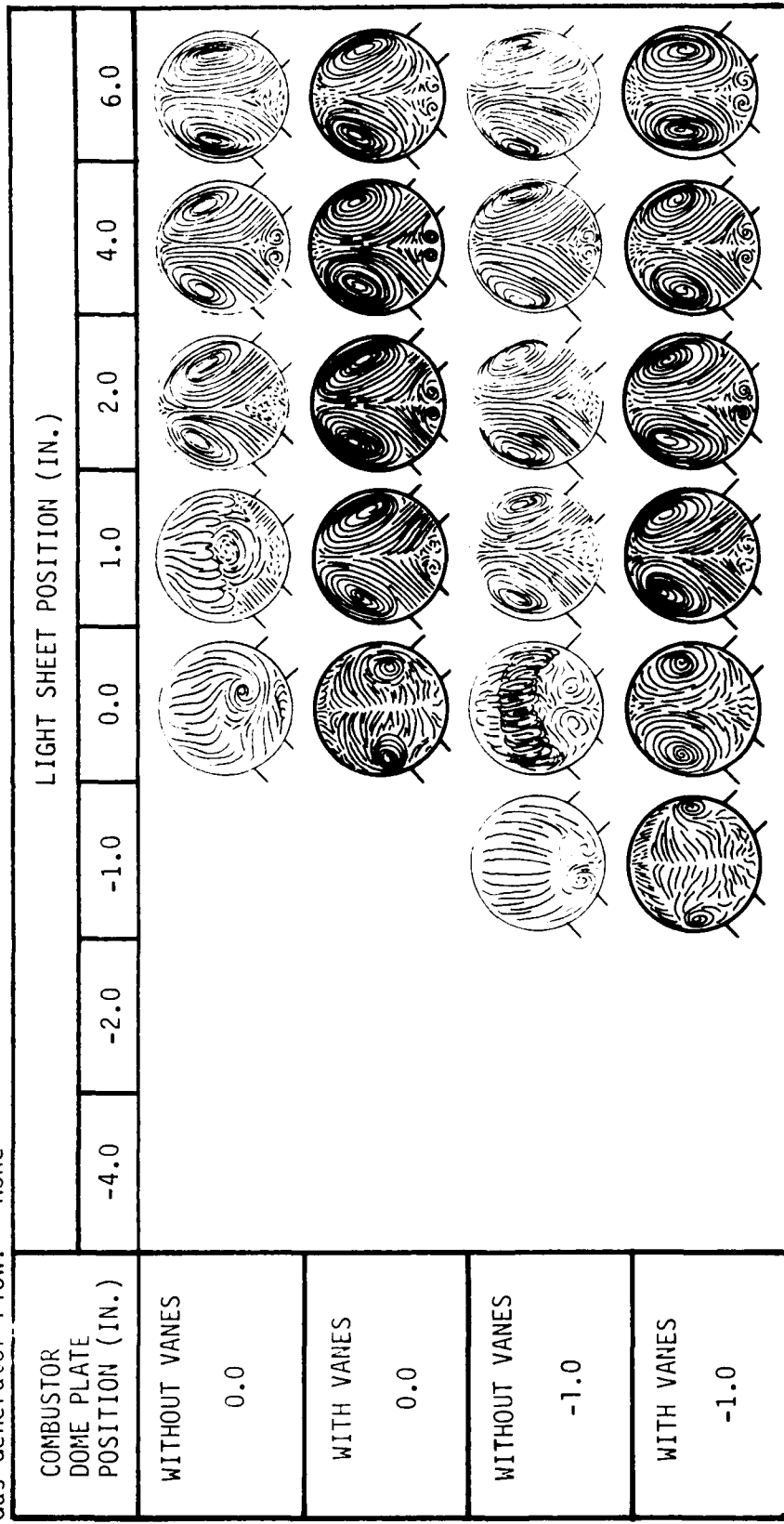


Figure 25. Effect of Inlet Turning Vanes on Combustor Flow Patterns for 45 Degree Configuration

Inlet Configuration: Dual 45 Degrees
 Total Combustor Flow: 300 GPM Balanced
 Combustor Length: 39.0 Inches
 A_N/A_C : 0.29
 Gas Generator Flow: None

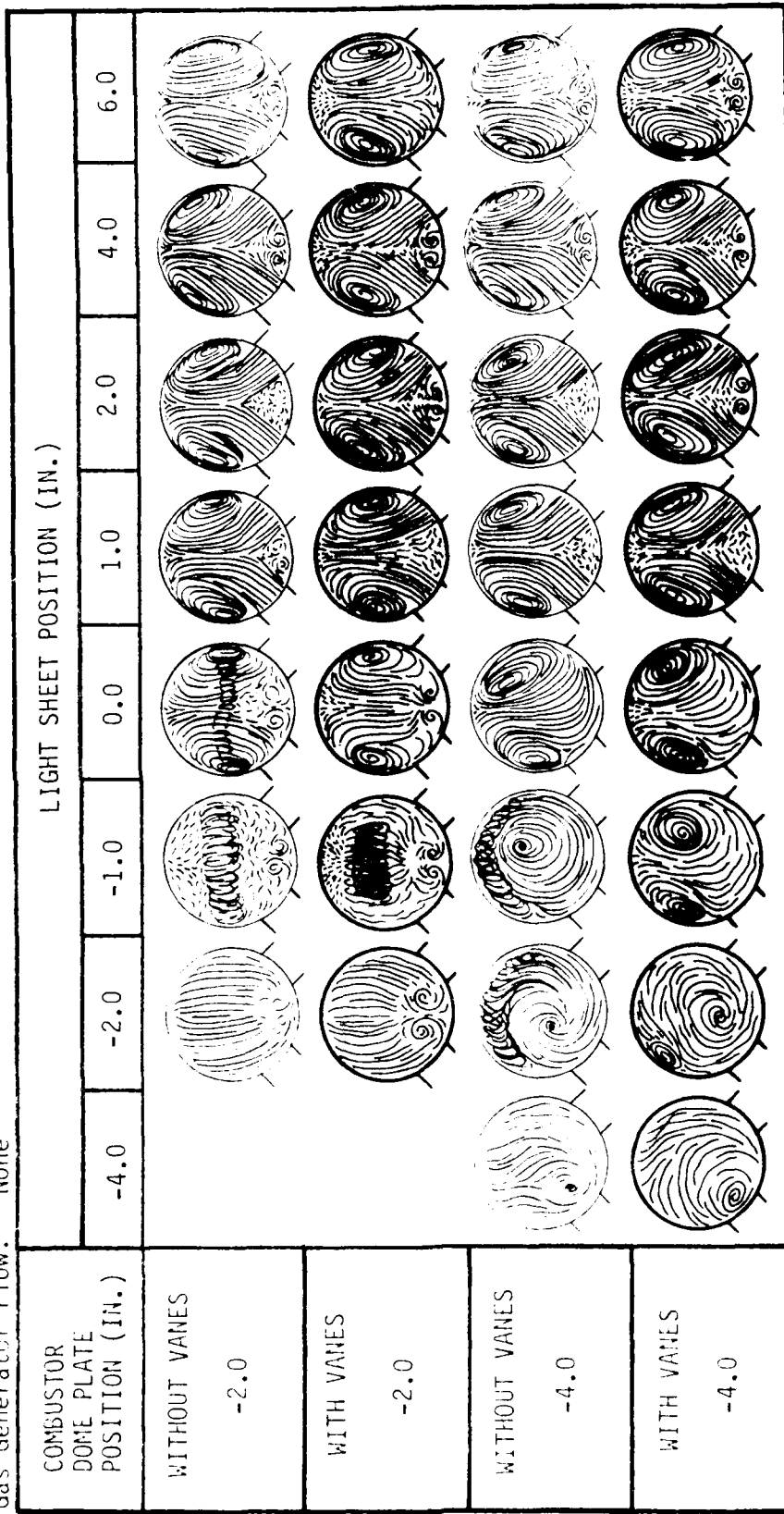


Figure 25. Effect of Inlet Vanes on Combustor Flow Patterns
for 45 Degree Configuration (CONCLUDED)

attach themselves to the dome plate as for dome position 0.0 and -1.0 inches. For a dome plate position of -2.0 inches the dome vortex is still joined, but the dome region flow patterns are somewhat modified. There appears to be no effect downstream of the inlet ducts.

7.1.6 Gas Generator Flow Visualization Study

An extensive investigation was conducted to evaluate the effects of dome plate fluid injection upon the flow characteristics of the dual inlet side dump combustor. The dome plate injection simulates possible gas generator flows in actual combustors. The diameter of the gas generator port for this study was 1.187 inches. Gas generator flows were measured in percent of the total combustor flow which was 300 GPM. Gas generator flows tested were 5, 10, and 20 percent of the total combustor flow. Various dome plate port configurations were also investigated. Figures 26 and 27 show freehand sketches of gas generator flows with the injection port at different positions for the 30 and 45 degree inlet configurations, respectively. Sketches of the combustor flow patterns without gas generator flows are also included for comparison. The gas generator flow for these flow patterns was 20 percent of the total combustor flow. Figure 28 is a series of photographs showing the effect of gas generator flows for different gas generator port configurations for comparisons with the freehand sketches.

Shown in Figure 29 are freehand sketches of gas generator flow patterns for flows through the center port configuration only for the 45 degree configuration. For these flows, the mass flow through the gas generator port was varied to determine the effect on the dome region flow patterns. Sketches are presented for 0, 5, 10, and 20 percent mass flows through the gas generator port. Shown in Figure 30 are unique side view photographs showing the dome region circulation for 0, 10, and 20 percent gas generator flows. The dome plate was located at the -2.0 inch position. Also shown is the test setup that was used to obtain these photographs. Figure 31 shows photographs of combustor flow patterns for different gas generator mass flow rates.

From sketches and photographs, it can be seen that there is a very significant effect upon the dome region flow due to gas generator port location and the amount of mass flow injected into the combustor.

Inlet Configuration: Dual 30 Degrees
Total Combustor Flow: 300 GPM Balanced
Combustor Length: 39.0 Inches
 A_N/A_C : 0.29

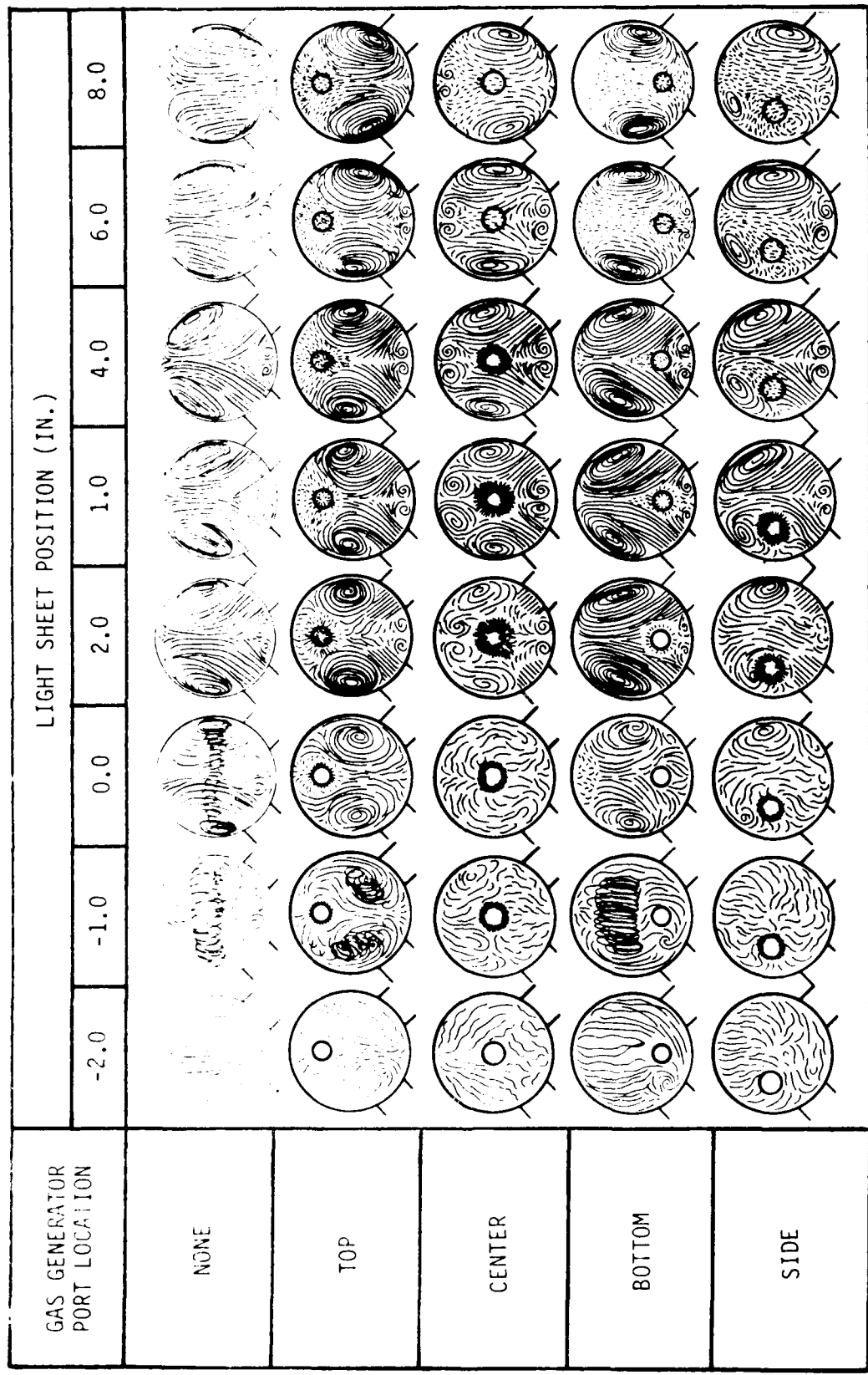
Gas Generator Flow: 20 Percent of Total



Dome Plate Position: -2.0 Inches

Figure 26. Effect of Gas Generator Port Location on Combustor Flow Patterns for 30 Degree Configuration

Inlet Configuration: Dual 45 Degrees
 Total Combustor Flow: 300 GPM Balanced
 Combustor Length: 39.0 Inches
 A_N/A_C : 0.29
 Gas Generator Flow: 20 Percent of Total



Dome Plate Position: -2.0 Inches

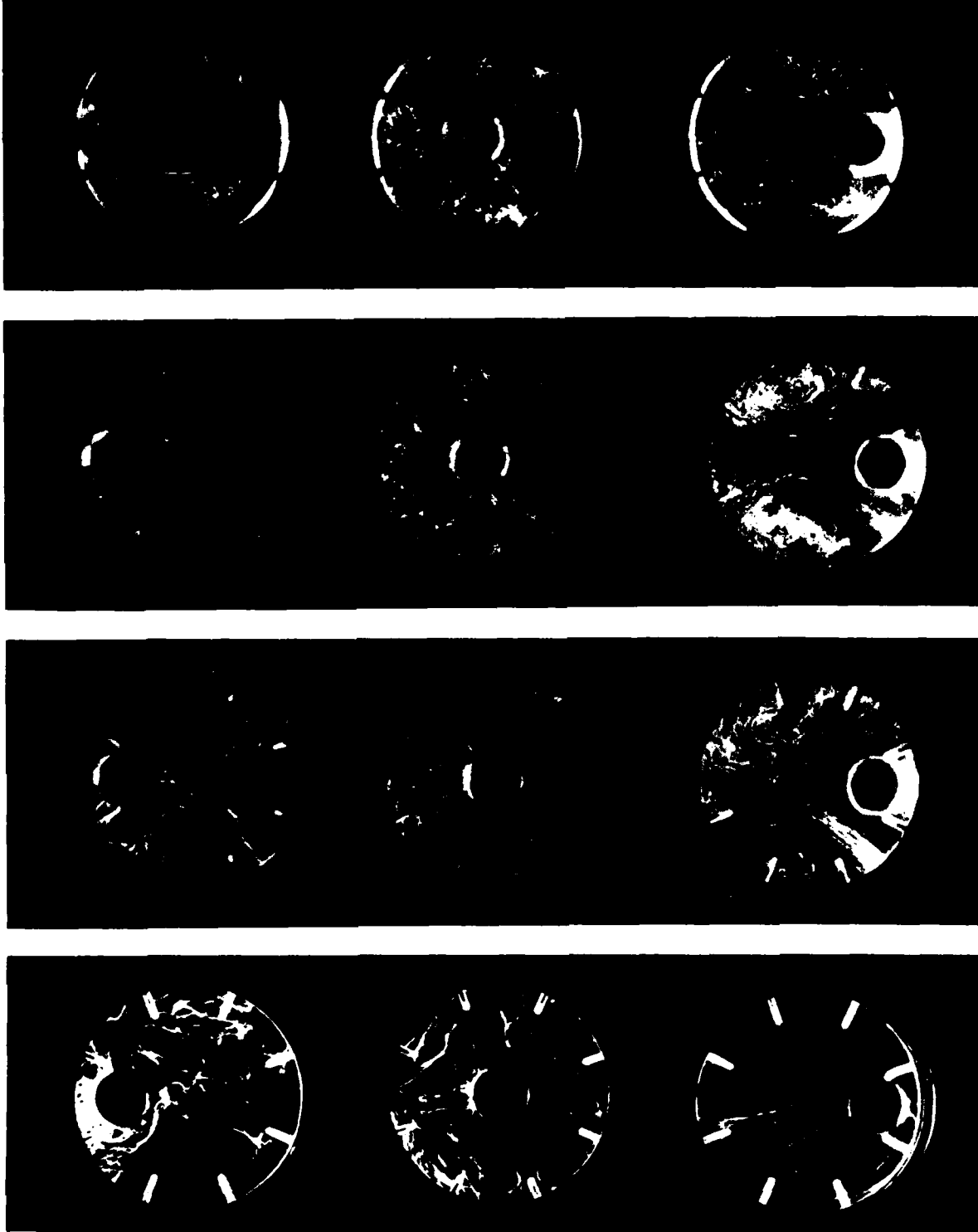
Figure 27. Effect of Gas Generator Port Location on Combustor Flow Patterns for 45 Degree Configuration

GAS GENERATOR
PORT POSITION

TOP

CENTER

BOTTOM



Done Plate Position: -2.0 Inches LIGHT SHEET POSITION (IN.)
-2.0 2.0 4.0 8.0

Figure 28. Photographs of Gas Generator Flow for Various Port Locations
for 45 Degree Configuration - 300 GPM

Inlet Configuration: Dual 45 Degrees
Total Combustor Flow: 300 GPM Balanced
Combustor Length: 39.0 Inches
 A_N/A_C : 0.29

Dome Plate Position: -2.0 Inches

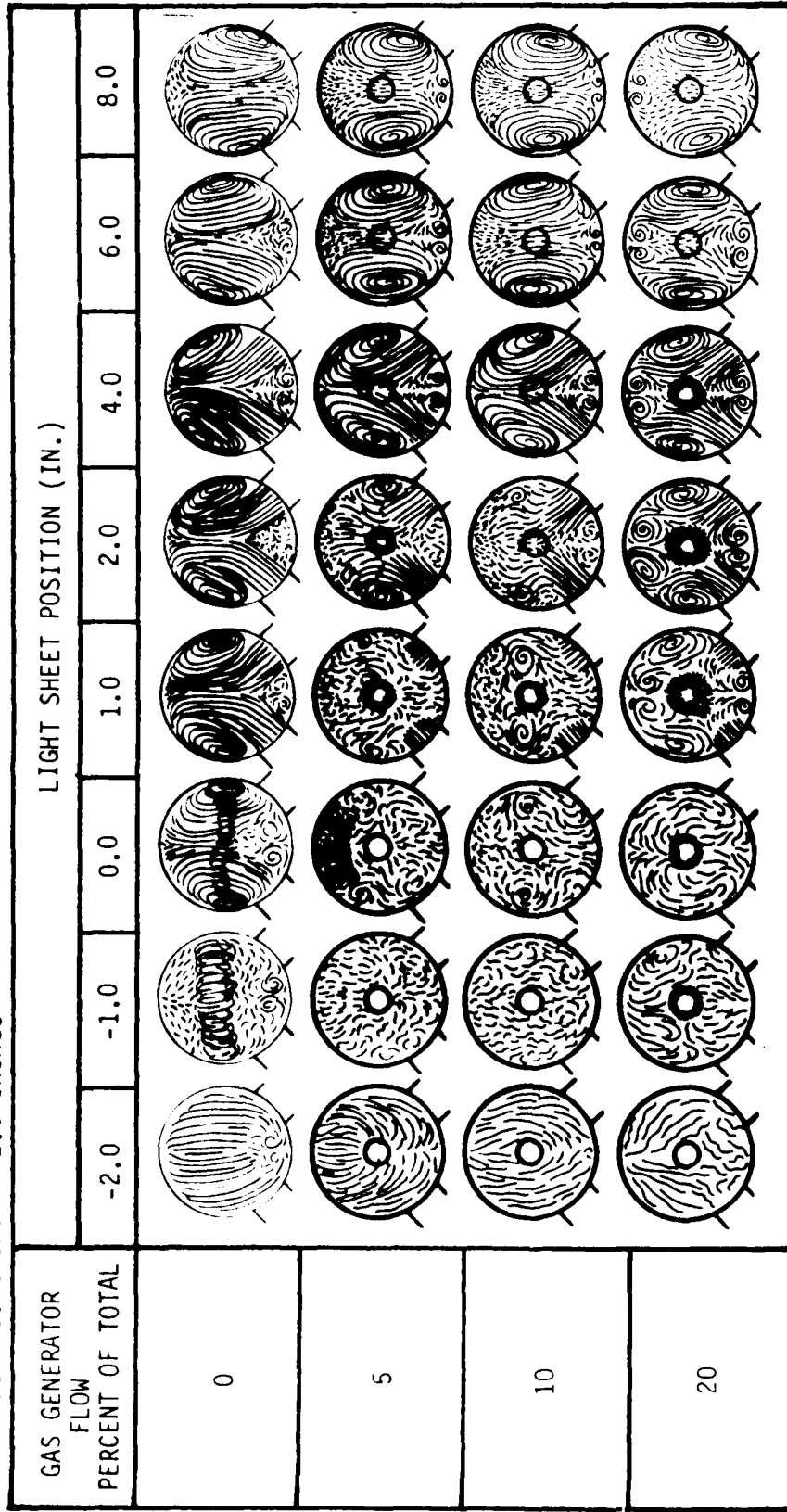
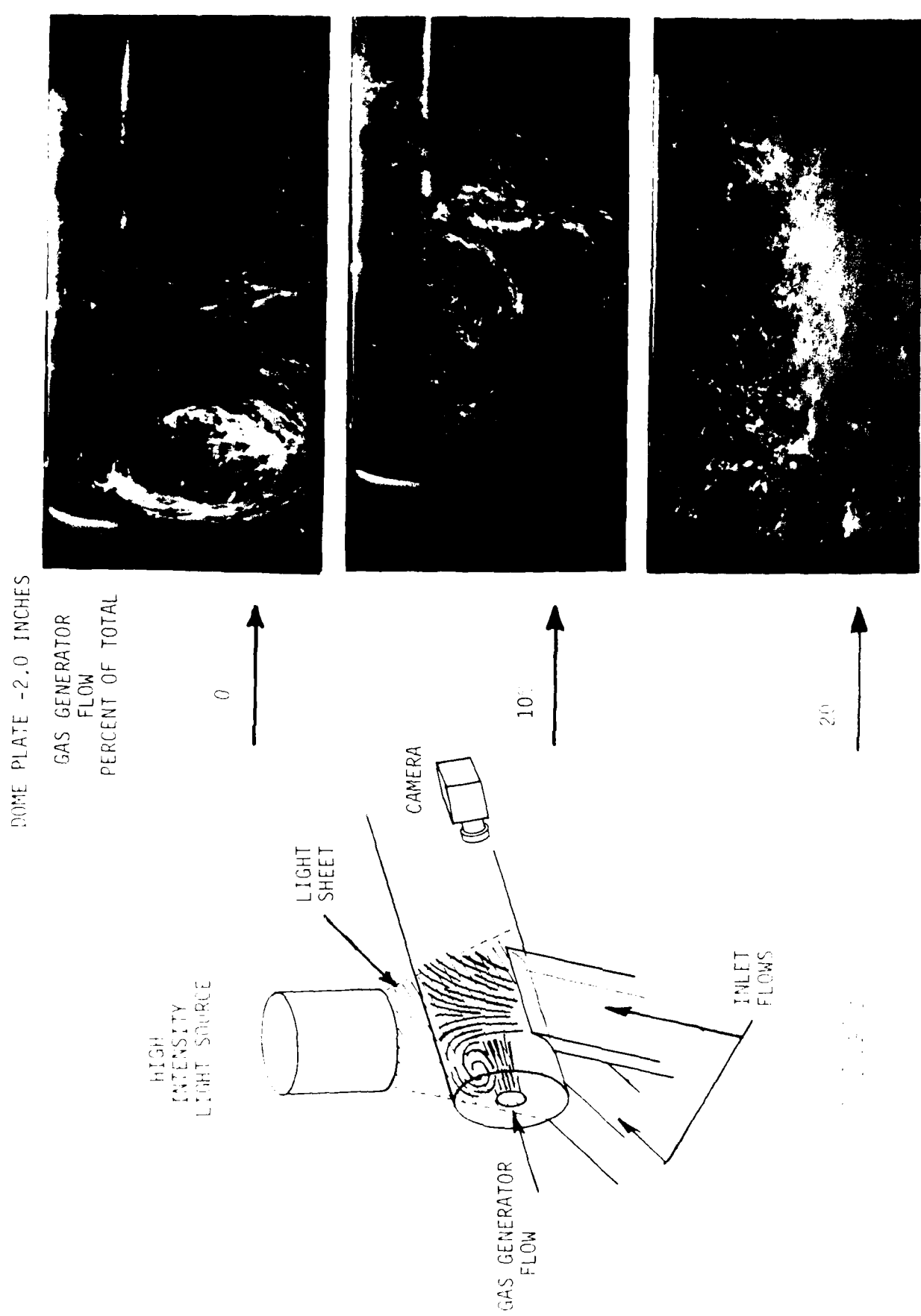


Figure 29. Effect of Gas Generator Flow on Combustor Flow Patterns for 45 Degree Configuration





GAS GENERATOR FLOW
PERCENT OF TOTAL

0%
10%
20%

TOTAL COMBUSTOR FLOW = 300 GPM
DOME PLATE POSITION = -2.0 IN.
LIGHT SHEET POSITION = 4.0 IN.

Figure 31. Photographs of 45 Degree Inlet Configuration Flow Patterns
Showing Effects of Gas Generator Flows

When the gas generator port is located at the top of the dome plate, the injected flow completely destroys the dome region circulation. The resulting dome region flow doesn't appear to have any consistent flow pattern. In the inlet region of the combustor, the top injected flow separates the side vortices and forces them down and causes them to dissipate sooner than without the gas generator flow. When the injection port is at the bottom of the dome plate, the dome region vortex is not disturbed and appears to be more stable. This flow also caused the side vortices to dissipate at a much faster rate beyond the inlet area. The greatest effect of dome plate gas generator flows appears to occur when the injection port is at the center of the dome plate. The flow patterns for this configuration show that the dome region vortex is destroyed and the side vortices are broken down into smaller vortices. The combustor side vortex flows are almost completely dissipated at the 8.0 inch combustor station. Even more disruption occurs when the gas generator port is offset to the side of the center position. These effects appear to occur even for gas generator flow as small as 5 percent of the total combustor flow.

7.2 RESIDENCE TIME MEASUREMENT TECHNIQUE AND RESULTS

Prior to conducting the investigation into residence times of combustor flows, it was necessary to develop a reliable and accurate method for determining residence times. The method employed was the stimulus-response method as described in (3). This method requires that a tracer be injected into a fluid stream and its characteristics observed before and after it passes through the reactor under consideration. Ideally, it would be desirable to have an infinite step pulse of zero duration to stimulate the system, but this is not possible in real circumstances. Therefore, efforts were undertaken to achieve the best tracer pulse from which information could be derived from the system. These efforts involved the design of unique dye injection and dispersion probes and the development of injection techniques.

A design was required that injected a very minute quantity of dye without leaving a stream of dye after being shut off and it also needed to disperse the dye into the total fluid volume as fast as possible. The 3-prong probe design with bleed achieved these goals, Figure 7. Trail

off of dye after injection was greatly reduced with the use of an internal bleed tube. A bleed tube was mounted inside the injection probe tube and was just inside the injection tube opening. The bleed tube came out of the injection tube and was allowed to bleed water from the system. When an injection occurred, a portion of the injected dye would be removed through the bleed tube. The amount of bleed could be regulated using a small vernier valve on the bleed tube. This technique resulted in very clean and minute dye injections. The dye injection probe design also had fabricated onto it three prongs that aided in the dispersal of the injected dye. A portion of the ejected dye would be drawn along each proturbance causing quick and even dispersion. This was the result of studying high speed movies (400 frames per second) of dye injections using the 90 degree tube probe design. Figure 8 shows a typical dye injection pulse using the three-prong probe with the bleed tube in a straight section of an inlet duct. The total flow rate for this test was 300 GPM and the fluid velocity in the inlet duct was approximately 9 feet per second. Notice that the pulse had very little trail off of dye and was uniformly dispersed in a distance of 16 inches. The inlet detection of this pulse would typically be on the order of 150 milliseconds and very near a step pulse as shown in Figure 9.

With a technique developed for dye injection and a data acquisition system capable of storing and processing dye concentration time histories, effective residence time measurement could be accomplished. Residence time tests were conducted of the three inlet angle configurations and at total combustor flow rates of 200, 300, and 400 GPM. Table 3 is the test matrix of residence time tests conducted in the research program. A complete listing of reduced residence time data is given in Appendix C. Equations that were used in residence time determination and data reduction are presented in Appendix D. Tables 4 and 5 detail the combustor volumes for each combustor inlet configuration and the fluid flow rates for each of the total flow conditions, respectively. Presented in Table 6 are the calculated residence times for the various inlet configurations and total flow rates.

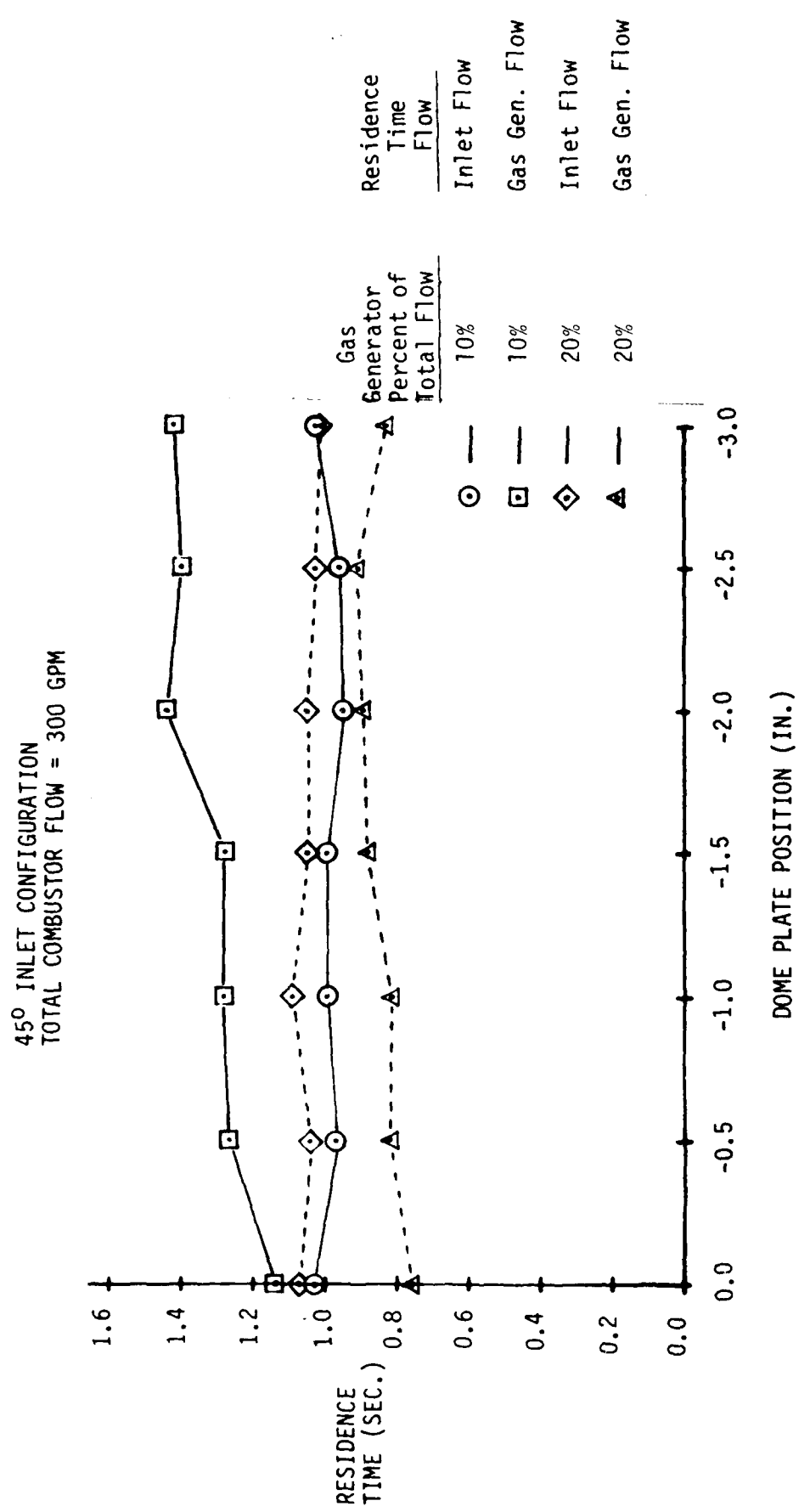


Figure 37. Gas Generator and Inlet Flow Residence Times Versus Dome Plate Position

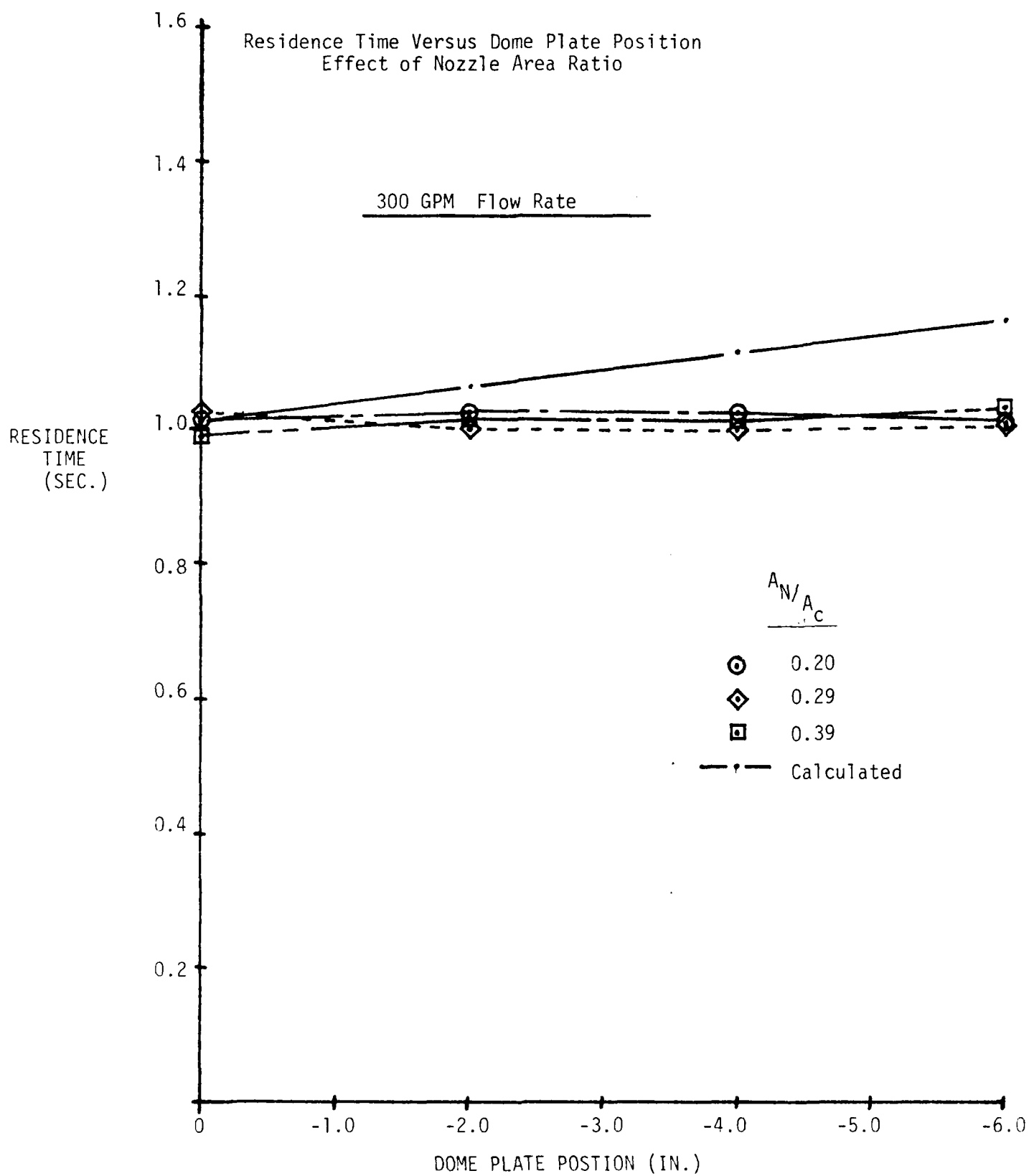


Figure 36. Effect of Nozzle Area to Combustor Area Ratios on Residence Times

through the three combustor configurations. In each case, the measured residence time is constant as the dome plate height was increased. This was also the case for the effect of different nozzle area to combustor area ratios upon residence time. The results of this investigation are presented in Figure 36 and show again almost constant residence times for area ratios of 0.20, 0.29, and 0.39 as the dome plate was moved upstream.

7.2.2 Gas Generator Effects on Residence Times

In order to study the effects of gas generator flow upon residence times, it was necessary to obtain residence times for both the inlet duct flow and for the gas generator flow. For the gas generator flows, this was accomplished by arranging the inlet detection equipment so a dye trace injected through the gas generator could be observed to obtain the residence time of the gas generator flow. Figure 37 presents the results for gas generator flows equal to 10 and 20 percent of the total combustor flow. Data are presented for both the inlet and gas generator flows for different dome plate positions. The data shows that the inlet residence times are almost constant for changes in dome plate position. However, there is a slight decrease in residence time for the 20 percent gas generator flow case which would be expected due to reduced inlet velocity and mass flow. Residence times for the gas generator flows are quite different from inlet residence times. Also there is considerable difference in the residence times between 10 and 20 percent gas generator flows. When the gas generator flow was 10 percent, the residence time at dome plate position 0.0 inches was approximately 10 percent greater than the inlet flow. At the -3.0 inch dome plate position, the gas generator residence time was approximately 40 percent greater than the inlet flow residence time. For a gas generator flow of 20 percent, the residence time of the gas generator flow was only about 75 percent of the inlet residence time for dome plate position 0.0 inches and was approximately 85 percent at a dome position of -3.0 inches.

These results indicate that the residence times of dome plate flows are greatly influenced by dome plate position and gas generator mass flow. This appears to be in agreement with what was observed from flow visualization data which showed considerable effect of gas generator flows upon the flows in the dome region. It appears that for even small

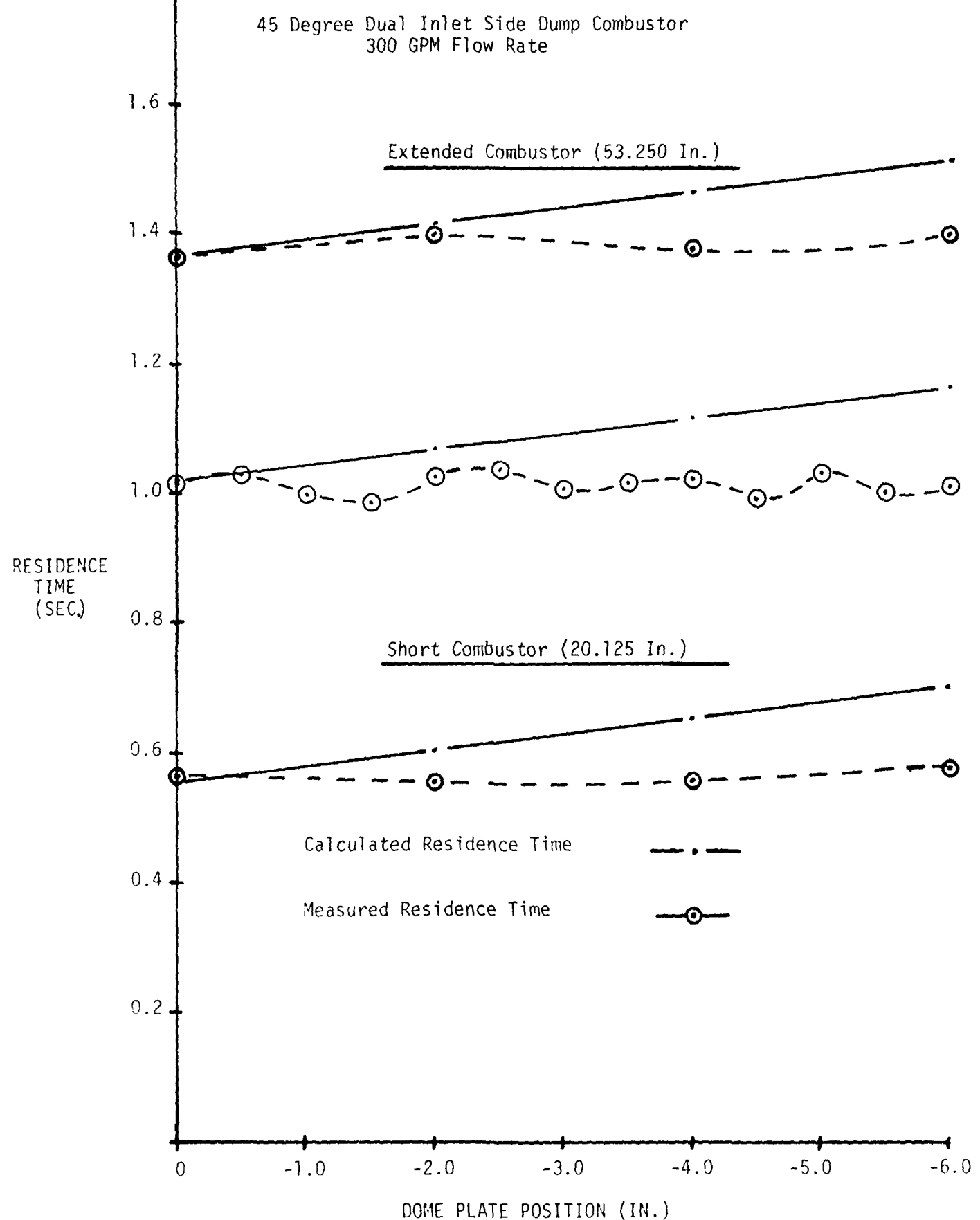


Figure 35. Effects of Combustor Lengths on Residence Times

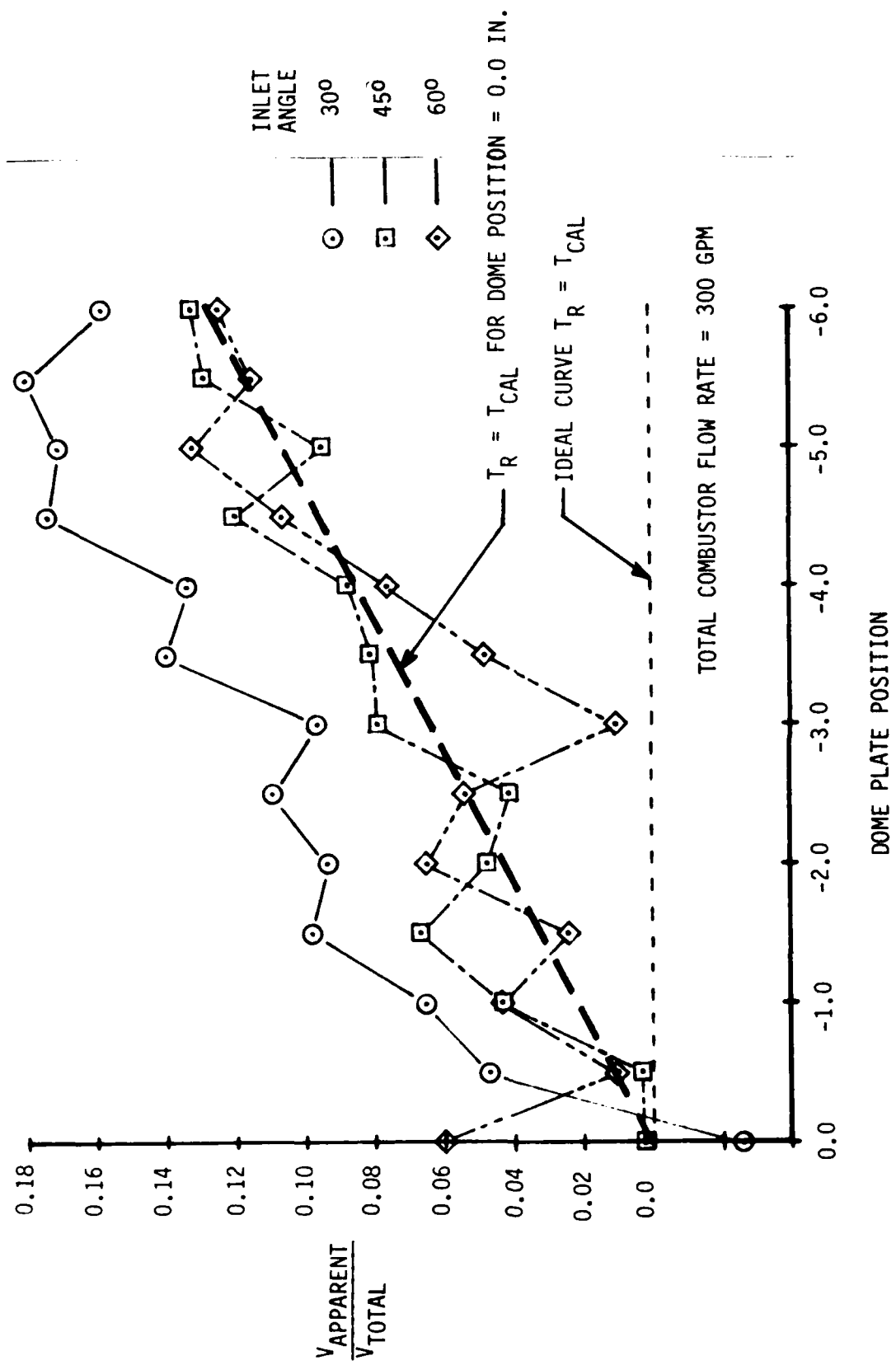


Figure 34. Ratio of Apparent Stagnation Volume to Total Combustor Volume Versus Dome Plate Position

-6.0 inch position. This shows how the dome region volume is not being completely utilized by the inlet flows. In Figure 34 the ineffective use of the dome region volume is shown by a plot of the ratio of apparent combustor stagnation volume to total combustor volume versus dome plate position. Plots are presented for the 30, 45, and 60 degree inlet configurations for a total flow rate of 300 GPM. Also plotted are the curves for two theoretical cases, one when the apparent combustor stagnation volume is equal to zero and the second for the case when the apparent combustor stagnation volume is equal to the volume of the dome region. It is of interest to note that each data curve generally parallels the curve for the case when the apparent combustor stagnation volume equals the dome region volume. The curve for the 30 degree inlet duct configuration is considerably offset vertically from the 45 and 60 degree data. This shift equates to an approximate increase of five (5) percent in addition to the dome region volume that appears as stagnation volume. The 45 degree data are just above or on the dome region curve, whereas the 60 degree data are on or below the dome region curve. Note that the definition of stagnate volume used here does not mean completely stationary fluid. It means that the velocity of the fluid within the region is considerably less than the main body of fluid and does not totally interchange with the incoming fluid. One last point to make regarding this plot is that each data curve appears have a peak and corresponding a dip. It is felt that the peaks are due to the slowing of the dome region vortex velocity as the dome plate is moved further upstream. The dip in the curves may be the result of dome vortex separation. When the dome region vortex separates, it may interact more completely with the dome region flow.

Residence time data were also obtained for changes in combustor length and in the nozzle area to combustor area ratios. These residence times are also for a total flow rate of 300 GPM. Shown in Figure 35 are plots of residence time versus dome plate position for three combustor lengths (20.13, 39.0, and 53.25 inches). The calculated residence times are based on the total combustor volume and the total combustor flow rate. From the data it appears there is no noticeable effect of combustor length upon the residence time of the fluid passing

60 Degree Inlet Configuration

Dome Plate Position - 0.0 In.

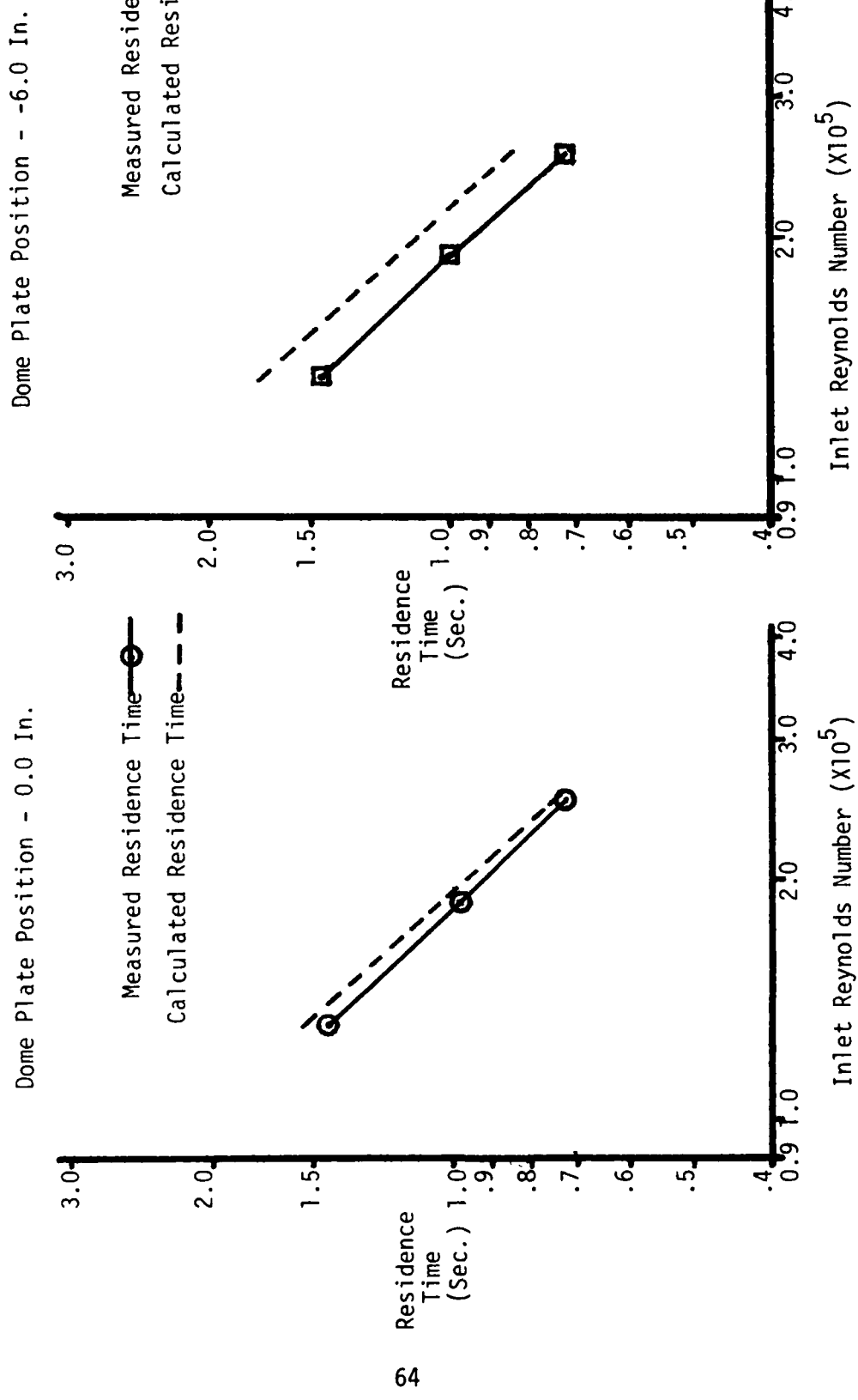


Figure 33. Residence Times Versus Inlet Reynolds Numbers (Concluded)

45 Degree Inlet Configuration

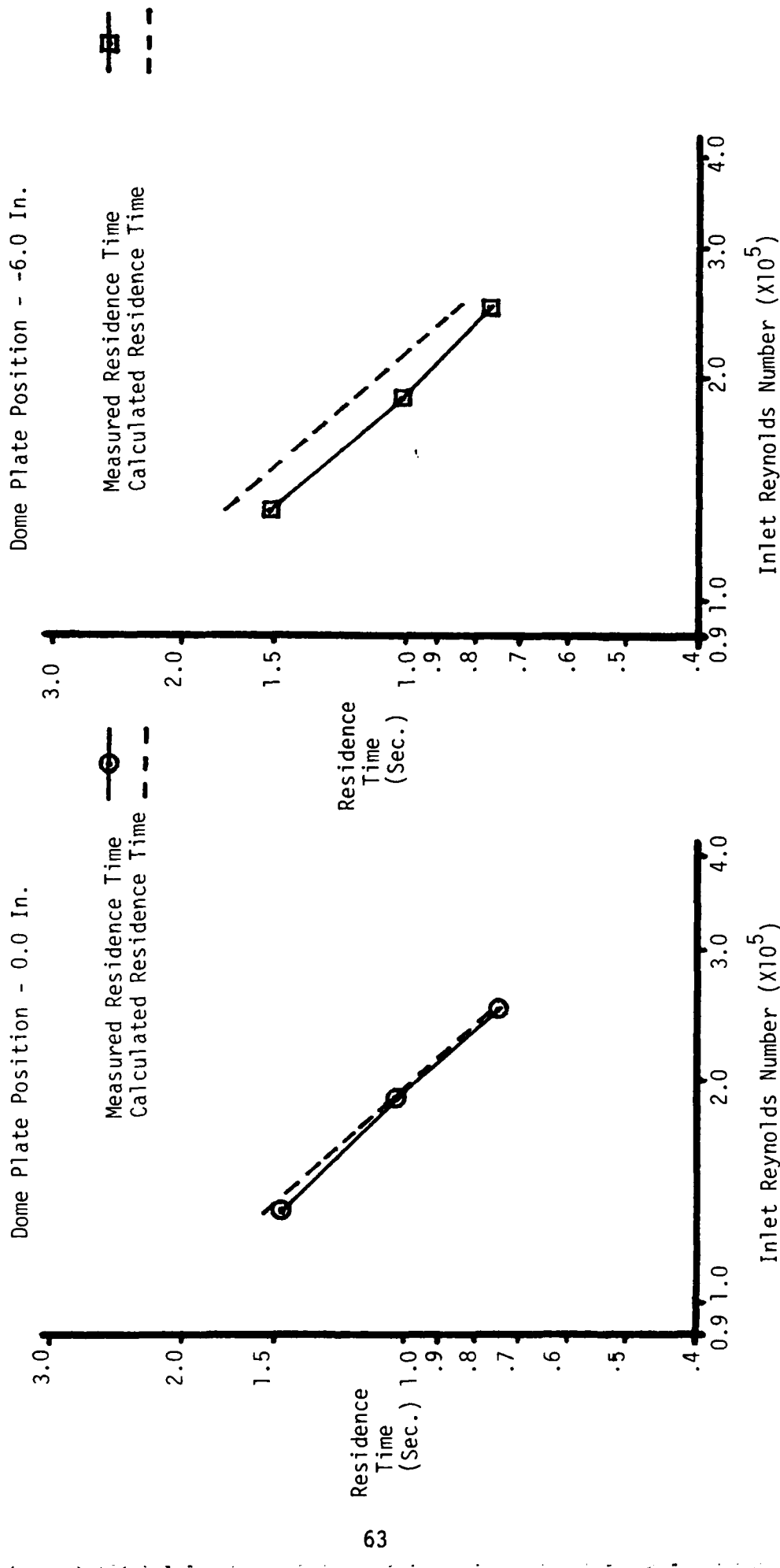


Figure 33. Residence Times Versus Inlet Reynolds Number (Continued)

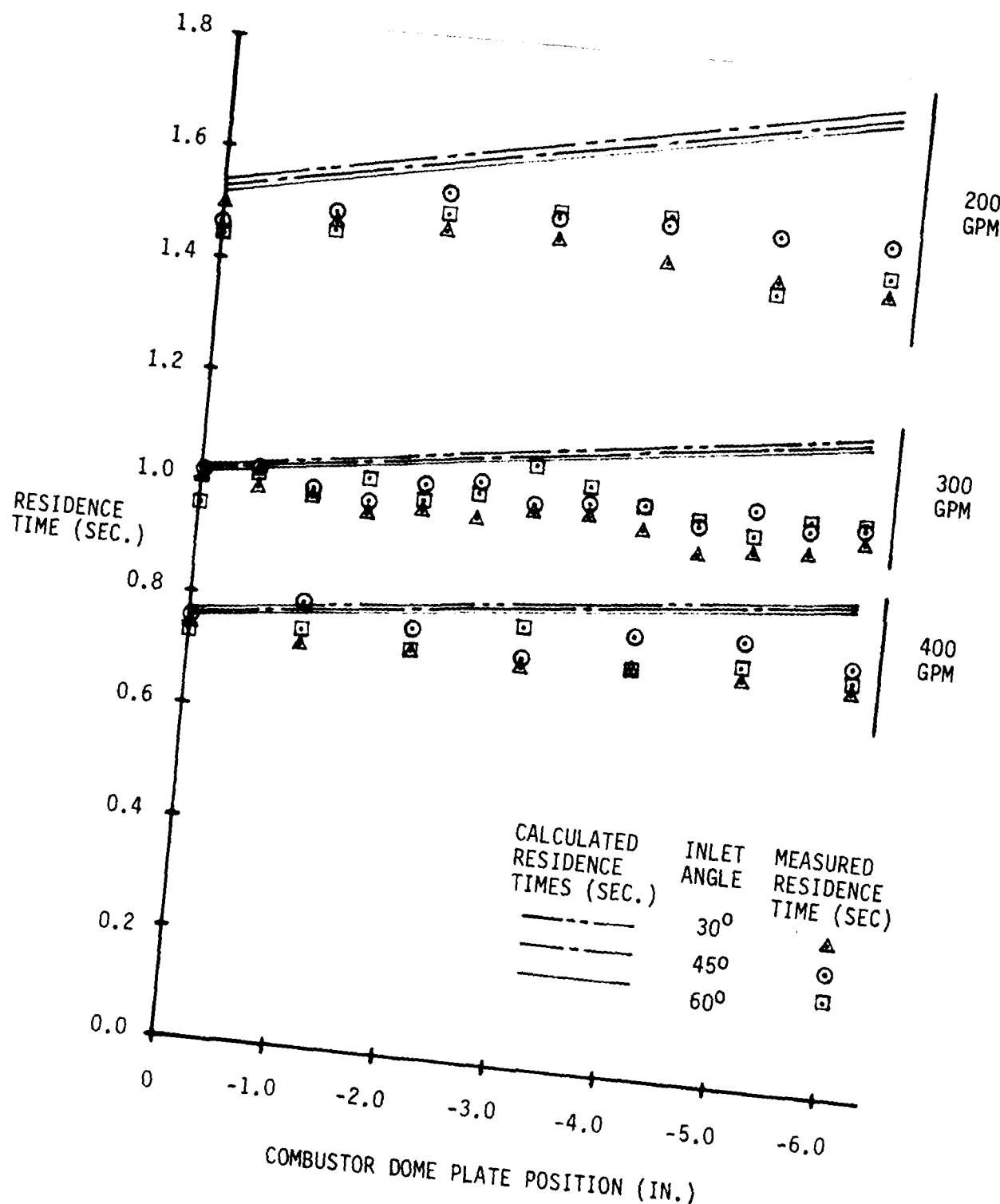


Figure 32. Dual Inlet Side Dump Combustor Residence Times

7.2.1 Residence Time Measurement Results

Presented herein are the results of the investigation to determine fluid flow residence times for variations of the dual inlet side dump combustor configuration. Data are presented showing the effect of dome plate height, combustor length, nozzle area ratio, and Reynolds Number. Figure 32 is a plot of calculated and measured residence times versus dome plate position. The zero position was taken as the upstream edge of the inlet opening, and positions upstream of that position are taken as negative. Plots are presented for the three inlet angles that were studied (30, 45, and 60 degrees) and for three total combustor flow rates.

As can be seen in Figure 32, the calculated residence times are linear functions with positive slopes reflecting the linear volume increase as the dome plate was moved upstream. The measured residence times, however, are not linear and are almost constant for all dome positions. It should be noted that for each flow rate and almost every dome plate position, the 30 degree inlet configuration had the shortest residence time, whereas the 45 and 60 degree inlet configuration residence times tend to overlap and cross over each other. The fluctuations occurring in the residence times were felt to be a result of flow instability in the dome region and the separation of the dome vortex as the dome position was moved further upstream. These processes were shown in the flow pattern sketches previously discussed. The dome region instability and vortex separation effects were possibly more acute because of the fact that dye injections were made from only one of the inlet ducts for residence time determinations.

Figure 33 shows plots of residence time versus the inlet Reynolds Number due to variations in the total combustor flow. Plots are given for dome plate positions of 0.0 and -6.0 inches and for the three inlet duct configurations (30, 45, and 60 degrees). Also plotted are the curves for the calculated residence times. The data curves are generally linear plots and parallel to the calculated values showing no effect for the range of Reynolds Numbers tested. Once again, the effect of dome position is noted. There is a noticeable offset between the calculated and measured residence time curves when the dome plate is moved to the

TABLE 6. CALCULATED RESIDENCE TIMES

Inlet Angle (Deg.)	Total Flow (GPM)	Calculated Residence Times (sec.)	
		DOME PLATE POSITION (IN.)	
		0.0	-6.0
30	200	1.540	1.760
	300	1.026	1.173
	400	0.770	0.880
45	200	1.525	1.746
	300	1.017	1.164
	400	0.763	0.873
60	200	1.518	1.738
	300	1.012	1.159
	400	0.759	0.869

TABLE 4. COMBUSTOR VOLUMES FOR VARIOUS TEST CONFIGURATIONS

Reactor Volume (in. ³)		
Test Configuration Inlet Angles (Deg.)	DOME PLATE POSITION (in.)	
	0.0	-6.0
30	1,185.47	1,355.12
45	1,174.47	1,344.12
60	1,168.98	1,338.63

TABLE 5. FLUID FLOW RATES FOR VARIOUS TOTAL FLOWS

Total Flow (GPM)	Fluid Flow Rate (in. ³ /sec.)
200	770
300	1,155
400	1,540

Combustor Configuration	Flow Rate (GPM)	Combustor Length (in.)	Nozzle Area Ratio An/Ac	Combustor Dome Height (in.)			
				0.20	0.29	0.39	0.50
30 Degree Dual Inlet Side Dump	200	X	X	X	X	X	X
	300	X	X	X	X	X	X
	400	X	X	X	X	X	X
45 Degree Dual Inlet Side Dump	200	X	X	X	X	X	X
	300	X	X	X	X	X	X
	300	X	X	X	X	X	X
	300	X	X	X	X	X	X
	300	X	X	X	X	X	X
	300	X	X	X	X	X	X
	300	X	X	X	X	X	X
	300	X	X	X	X	X	X
	300	X	X	X	X	X	X
	300	X	X	X	X	X	X
	300	X	X	X	X	X	X
	300	X	X	X	X	X	X
	300	X	X	X	X	X	X
	300	X	X	X	X	X	X
	300	X	X	X	X	X	X
	300	X	X	X	X	X	X
	300	X	X	X	X	X	X
	300	X	X	X	X	X	X
	300	X	X	X	X	X	X
	300	X	X	X	X	X	X
	300	X	X	X	X	X	X
	300	X	X	X	X	X	X
	300	X	X	X	X	X	X
	300	X	X	X	X	X	X
	300	X	X	X	X	X	X
	400	X	X	X	X	X	X
60 Degree Dual Inlet Side Dump	200	X	X	X	X	X	X
	300	X	X	X	X	X	X
	400	X	X	X	X	X	X

* - Inlet Detection Below Dome Plate Surface at Gas Generator Port.

** - Inlet Detection Above Dome Plate Surface at Gas Generator Port.

TABLE 3. Residence Time Measurement Test Matrix

gas generator flows (less than 10 percent) the effect is to reduce or eliminate the dome region circulation. For gas generator flows greater than 10 percent, the injected flow is able to cause the large side vortices to dissipate more rapidly in the axial direction resulting in a reduced residence time for the gas generator flows.

7.2.3 Dispersion Characteristics of Combustor Configurations

The dispersion number for a flow through a closed vessel is given by Leverspiel (3) as D/uL . The dispersion number varies from zero for plug flow to infinity for backmix flow and is the reciprocal of the axial Peclet number for the mass transfer. For the "one-shot" tracer input technique that was utilized to conduct residence time measurements, the dispersion number can be determined from the difference in variances of the concentration-time curves for the input tracer. Dispersion numbers calculated from residence time data are presented in Appendix C and are plotted for the three inlet configurations and flow rates in Figure 38. The dispersion numbers are given for dome plate positions of 0.0 to -6.0 inches. The data shows different results for each of the three inlet configurations. In the plot for the 60 degree inlet configuration, the data peaks for dome plate positions -2.0 and -3.0 inches but is reduced at 0.0 and -1.0 inches and for dome positions greater than -4.0 inches. The 45 degree dispersion number data shows a peak for dome plate positions -0.5 and -1.0 inches. At dome plate positions -1.5 to -6.0 inches the dispersion number is almost constant or decreasing. In the case of the 30 degree inlet ducts, the dispersion number is constantly decreasing from its value at dome plate position 0.0 inches. Dispersion number data obtained at total flow rates of 200 and 400 GPM agreed very well with the 300 GPM test results.

The peaks in the dispersion number curves appear to be a consequence of the dome region circulation. In examining flow pattern sketches and the plots of dispersion number, the greater values of dispersion number occur when the dome region circulation appears to be the strongest. This would seem to be the logical result since a stronger dome circulation would mean that a greater portion of the inlet fluid is being diverted into the dome region. Even with the peaks in the dispersion number data, the largest delta change is less than 0.015. The

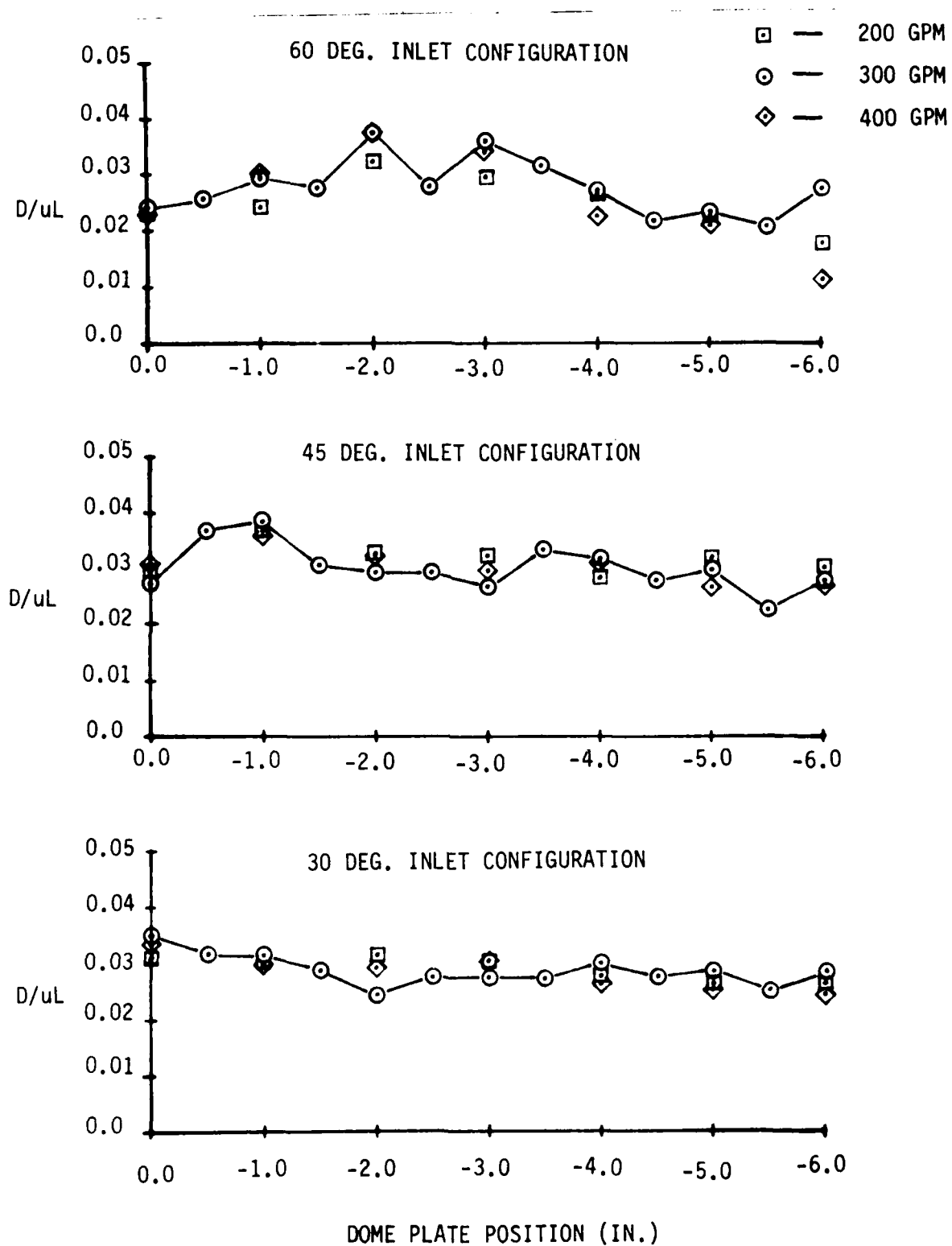


Figure 38. Dispersion Coefficient Versus Dome Plate Position

average value of the dispersion number is approximately 0.025. From Leverspiel (3), a dispersion number of 0.025 represents an intermediate amount of dispersion in the fluid as it flows through the reactor. In Figure 39, residence times are plotted against variance deltas to obtain curves showing the relative amount of dispersion of measured data compared to known dispersion coefficient curves. Data points are plotted from measured residence times and variance deltas for flow rates of 200, 300, and 400 GPM. The data shows increased dispersion as the fluid flow rate is increased. The 300 GPM case is very near the curve for an intermediate amount of dispersion.

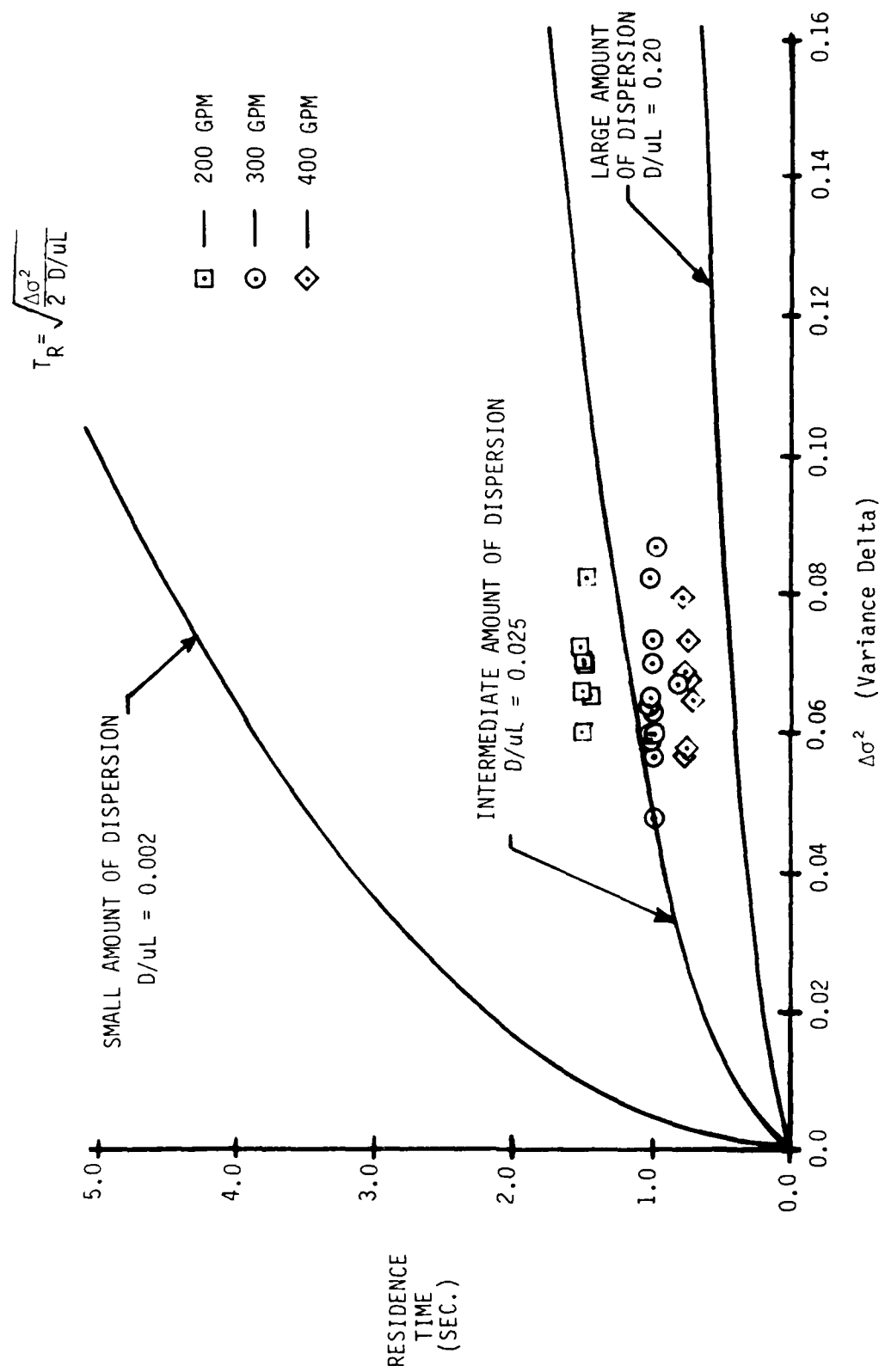


Figure 39. Residence Time Versus Variance Delta

SECTION VIII

CONCLUSIONS AND RECOMMENDATIONS

Flow visualization and residence time studies have been conducted that have provided qualitative and quantitative data of internal fluid flow characteristics of dual inlet side dump combustor configurations. Data have been compiled and organized to detail the mixing characteristics, flow formations, residence times, and dispersion characteristics of the combustor configuration for controlled variations in design parameters and flow conditions. The following paragraphs present the conclusions and make recommendations for possible future work and possible implementation of program results to new combustor designs.

8.1 CONCLUSIONS

The first conclusion that can be made regarding the efforts of this research and development program is that flow visualization can provide a worthwhile method of obtaining qualitative information of the internal fluid structure and mixing characteristics of fluid mixing chambers. Such information can assist greatly in the development of new combustor designs, mathematical modelling, and simulations. Flow visualization techniques should be improved to obtain even higher quality flow visualization data and to obtain quantitative information.

Flow visualization results show that for variations in basic design parameters of the dual inlet side dump combustor configuration, the flow patterns at and downstream of the inlet duct area were almost constant. The only noticeable variation from this conclusion occurred when gas generator flows were introduced. Gas generator flows tended to dissipate more rapidly the two axial helical vortices downstream of the combustor inlets. Forward of the inlet area the flow patterns were significantly altered for variations in both combustor design parameters and for gas generator flows.

The mean residence times of the dual inlet side dump combustor configurations were essentially constant for variations in dome plate height, nozzle area to combustor area ratios, and combustor length. The most significant difference between measured and calculated residence

times occurs for the 30 degree inlet configuration and the least difference occurs for the 60 degree inlet configuration. These differences occurred for variations in the combustor dome plate height. As the dome plate was moved upstream, the volume of the combustor was increased. Since the calculated residence time is the ratio of combustor volume to fluid flow rate, the calculated residence time increased as the dome plate was moved upstream. This was not the result for the measured residence times. Measured residence times remained essentially constant as the dome region volume increased. There were some variations in measured residence times, but this is thought to be due to the instability of the flow in the dome region as the dome plate was moved to a greater depth. These same results were obtained for each inlet angle, combustor length, and nozzle area to combustor area ratio tested. It would appear that the inlet fluid interacts very little with the dome region flow. The greatest activity occurred for dome plate positions from 0.0 to approximately -2.0 inches. For dome plate positions greater than -2.0 inches the dome circulation weakens and eventually separates and attaches to the dome plate.

The mean residence times for fluid injected through the dome plate gas generator port showed considerable differences for variations in dome plate height and for mass flow rates of the injected fluid. The residence time of injected gas generator flows increased as the combustor dome plate was moved upstream to greater depths. At gas generator flows of 20 percent of the total flow, the gas generator flow residence times were considerably less than the residence times of the inlet flows. At 10 percent of total combustor flow, the gas generator flow residence times were almost equal to the inlet residence times at a dome plate position of 0.0 inches and increased in value as the dome plate height was increased. These results tend to agree more closely with the calculated values of residence times for increased dome region volumes.

The results of the study of dispersion characteristics show that fluid passing through the dual inlet side dump combustor configuration will experience an intermediate amount of dispersion as it passes through the combustor. Dispersion coefficients were noticed to increase in value

for some dome plate positions depending on the inlet angles. This may indicate a more complete or a more stable mixing pattern for those configurations.

8.2 RECOMMENDATIONS

As a result of the research and development program just completed, several recommendations can be made regarding the results and possible future efforts in the area of hydrodynamic simulation. The recommended studies would increase utilization of test facilities and help develop more efficient and reliable propulsion systems for future flight vehicles.

1) Efforts should be continued to refine and improve upon the flow visualization techniques utilized at the AFWAL/PORT Water Tunnel test rig. Such programs increase the understanding of combustor and mixing flows and assist in the development of new combustor designs.

2) Efforts should be undertaken to establish the correlation between hydrodynamic simulation and cold and hot fluid flow patterns. Such studies are necessary in the development of computer simulations and methods to increase the utilization of hydrodynamic simulation in combustor studies. As part of such an effort, work needs to be done to demonstrate the effect of heat on fluid flow mixing patterns.

3) Hydrodynamic simulation studies should be conducted to evaluate new combustor designs which have gas generator injections that complement the dome region circulation. Present gas generator injection designs tend to disrupt or destroy the circulation in the dome region. These studies could also examine combustor designs that have no dome region volume causing the inlet vortices to be permanently attached to the dome plate and not joined as for present designs. Also, new designs could include combustors that have internal forms or bodies that would remove unwanted or unnecessary flow formations. An example of such a design would be a fillet shape between the dual inlets of the present design to eliminate the small vortices that form between the inlets.

APPENDIX A
HOLOGRAPHY DIAGNOSTIC TECHNIQUES FOR RAMJET FLOWS
FINAL REPORT
SPECTRON DEVELOPMENT LABORATORIES, INC.

HOLOGRAPHY DIAGNOSTIC TECHNIQUES FOR RAMJET FLOWS

FINAL REPORT

By

James E. Craig

SDL No. 83-2239-01F

31 March 1983

Prepared For:

AERO PROPULSION LABORATORY
Air Force Wright Aeronautical Laboratory
Wright-Patterson AFB, Ohio 45433

Attn: Dr. Roger Craig
Ramjet Technology Division

**SPECTRON
DEVELOPMENT
LABORATORIES
INC.**

3303 Harbor Boulevard, Suite G-3
Costa Mesa, California 92626 (714) 549-8477

TABLE OF CONTENTS

	<u>Page</u>
ABSTRACT.....	1
1.0 INTRODUCTION.....	2
2.0 THE EXPERIMENT.....	4
2.1 Holocamera.....	4
2.2 Ramjet Facility.....	7
2.3 Test Matrix.....	7
3.0 RESULTS.	10
3.1 Fuel Atomization Study.....	10
3.2 Combustor Study.....	19
4.0 SUMMARY.	21
5.0 RECOMMENDATIONS.....	22

LIST OF FIGURES

<u>Figure</u>	<u>Page</u>
1 HOLOCAMERA INSTALLATION IN AFAPL RAMJET FACILITY.....	5
2 ATOMIZATION STUDY.....	6
3 CROSSFLOW FUEL ATOMIZATION.....	12
4 FUEL ATOMIZATION STUDY - ORIFICE INJECTOR.....	14
5 FUEL ATOMIZATION STUDY - PINTLE INJECTOR.....	15
6 DROPLET SIZE ANALYSIS - ORIFICE INJECTOR.....	16
7 DROPLET VELOCITY ANALYSIS - ORIFICE INJECTOR.....	18
8 DROPLET SIZE ANALYSIS - COMBUSTION STUDY.....	20
9 DETERMINING PARTICLE SIZE DISTRIBUTION FROM THE HOLOGRAPHICALLY RECORDED FOURIER TRANSFORM.....	23

ABSTRACT

Holographic diagnostics have been demonstrated as excellent techniques for investigating air/fuel delivery processes in ramjets. The crucial steps of fuel atomization, vaporization, and mixing are revealed with excellent resolution. Fuel jet atomization results in very small ($10 \mu\text{m} - 20 \mu\text{m}$) droplets for typical inlet crossflow velocities ($\approx 150 \text{ m/s}$). The droplet number density is very high and results in optically dense regions.

In the presence of combustion, very small droplets ($10 \mu\text{m} - 20 \mu\text{m}$) are observed for typical flow conditions and somewhat larger droplets ($30 \mu\text{m} - 40 \mu\text{m}$) are observed for lower inlet velocities (100 m/s).

1.0 INTRODUCTION

While the concept of a ramjet propulsion system is exceedingly simple, in fact, the fuel and air flow processes are extremely complex. Fuel injected normally to the inlet air flow is atomized as a result of the large slip velocity. Fuel vaporization increases rapidly as atomization increases the amount of liquid surface area exposed to the hot inlet air flow. Turbulence within the inlet flow rapidly mixes the vapor phase fuel and air into a combustible mixture. At the dump stage, the mixture is ignited by the hot gases in the recirculation zone. In theory, the flame is tied to the inlet lip and somehow spans the inlet flow in the shape of a cone pointing downstream; whereas in practice, the combustion fronts probably oscillate about the combustion chamber. At the flame front, fuel remaining in the liquid phase experiences a large increase in heat transfer due to higher temperatures and slip velocities. For efficient combustion all of the fuel must vaporize, mix with air, and react.

Fuel atomization is a crucial process in the engine operation as rapid vaporization cannot occur if the fuel is poorly atomized (i.e., large droplets say 100 μm). Hence, the objective of this work was to demonstrate holographic droplet imaging within a ramjet combustor. A second objective was added on site at AFAPL to investigate crossflow atomization for orifice type injectors. This additional task was accomplished without funding increase at the expense of a major portion of the data reduction effort. We describe the successful use of holographic imaging of droplets within an operating ramjet combustor.

Image resolution of 5 μm is attained. Droplets within the 15 - 40 μm range are observed for a rather low speed inlet atomization condition; whereas for more typical inlet conditions, smaller droplets are observed. We also display an example of the cross flow atomization data where the field of view includes the fuel injector and the atomization mechanisms are observed. This data is rich in both basic mechanism type information as well as quantitative data on droplet size, velocity, number density and penetration for various fuel and air operating conditions.

RD-A153 753

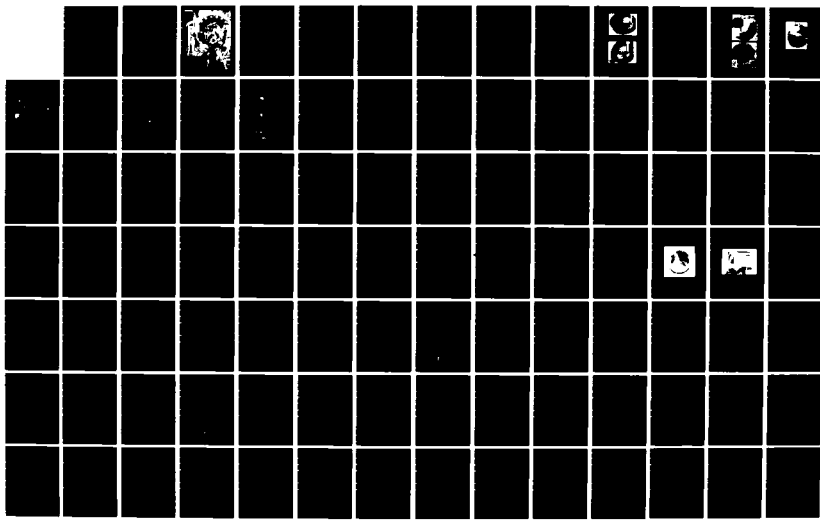
MULTI-DUCTED INLET COMBUSTOR RESEARCH AND DEVELOPMENT
(U) UNIVERSAL ENERGY SYSTEMS INC DAYTON OH G D STREBY
MAR 85 AFWAL-TR-85-2004 F33615-81-C-2074

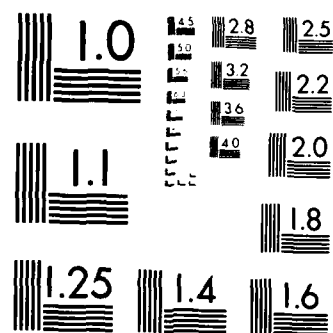
2/3

UNCLASSIFIED

F/G 21/5

NL





MICROCOPY RESOLUTION TEST CHART
NATIONAL BUREAU OF STANDARDS 1963 A

2.0 THE EXPERIMENT

An experiment was planned in which holographic droplet imaging would be demonstrated within a ramjet combustor. Previous to this program AFAPL had procured a stainless steel combustion chamber with 3 optical ports. The pertinent dimensions are 6 inch I.D. and 3 x 5 inch optical ports. Quartz windows were used during these tests and provided excellent optical access to the combustion chamber even in the presence of combustion. A Spectron Holocamera was provided for the experiment. The experiment included a fuel injector characterization phase and a combustion chamber investigation.

2.1 Holocamera

A Spectron Holocamera was installed at the AFAPL ramjet facility. The field of view was modified to conform to the orientation of the combustor windows (Figure 1). The receiving optics were modified to account for the reduced object to hologram distance resulting in a resolution of 30 μm for about 1X magnification and a resolution of 5 μm for 5X magnification.

For 1X magnification, the field of view (Figure 2a) was about 4 inches (100 mm) in diameter and was centered in the upstream and downstream portion of the window. For 5X magnification, the field of view was 0.8 inch (20 mm) in diameter and was centered at three positions during the atomization tests. For the combustion runs, the holocamera could not be positioned upstream of the center of the window because of the ignitor plumbing.

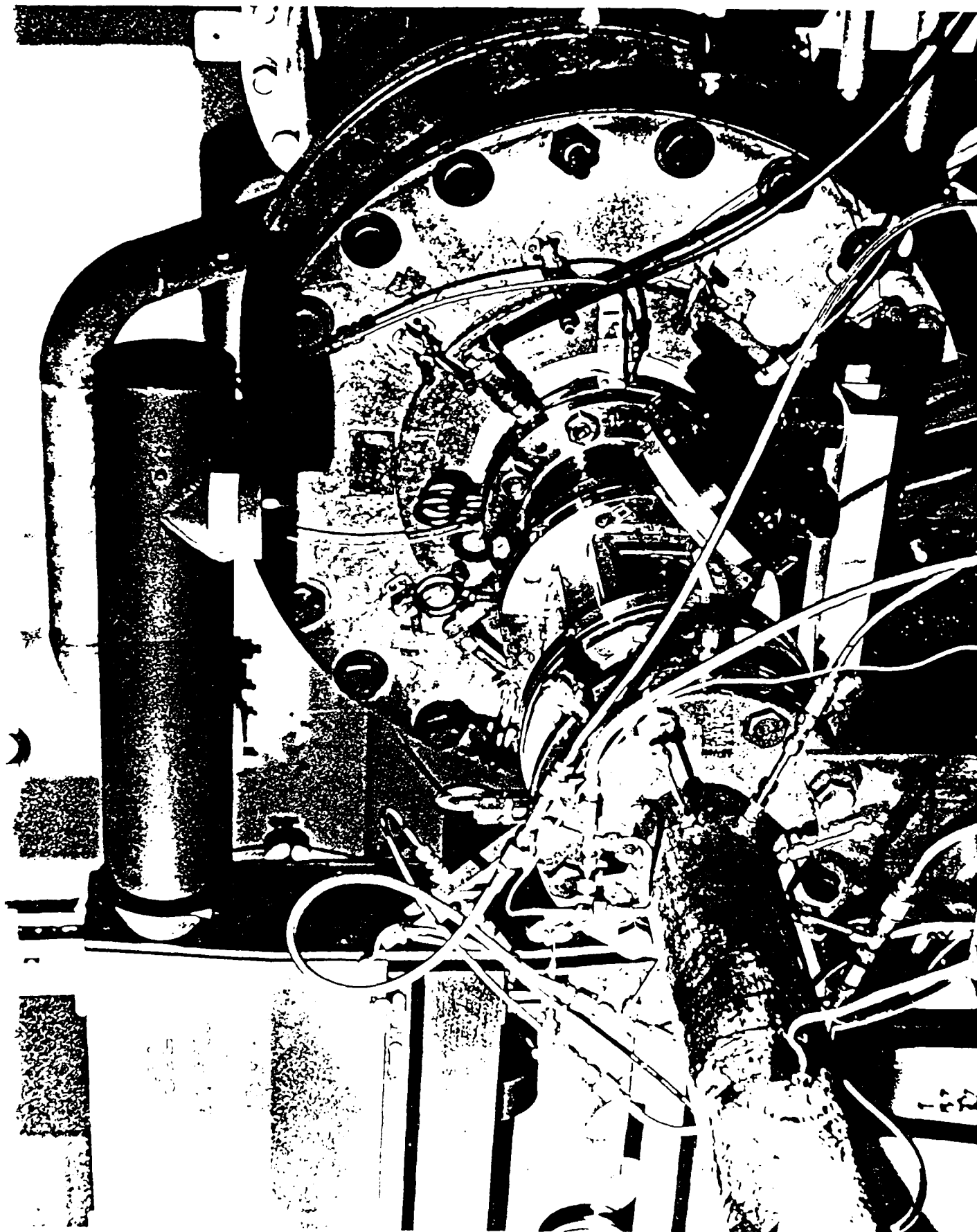


FIGURE 1. HOLOCAMERA INSTALLATION IN AFAPL RAMJET FACILITY

ATOMIZATION STUDY

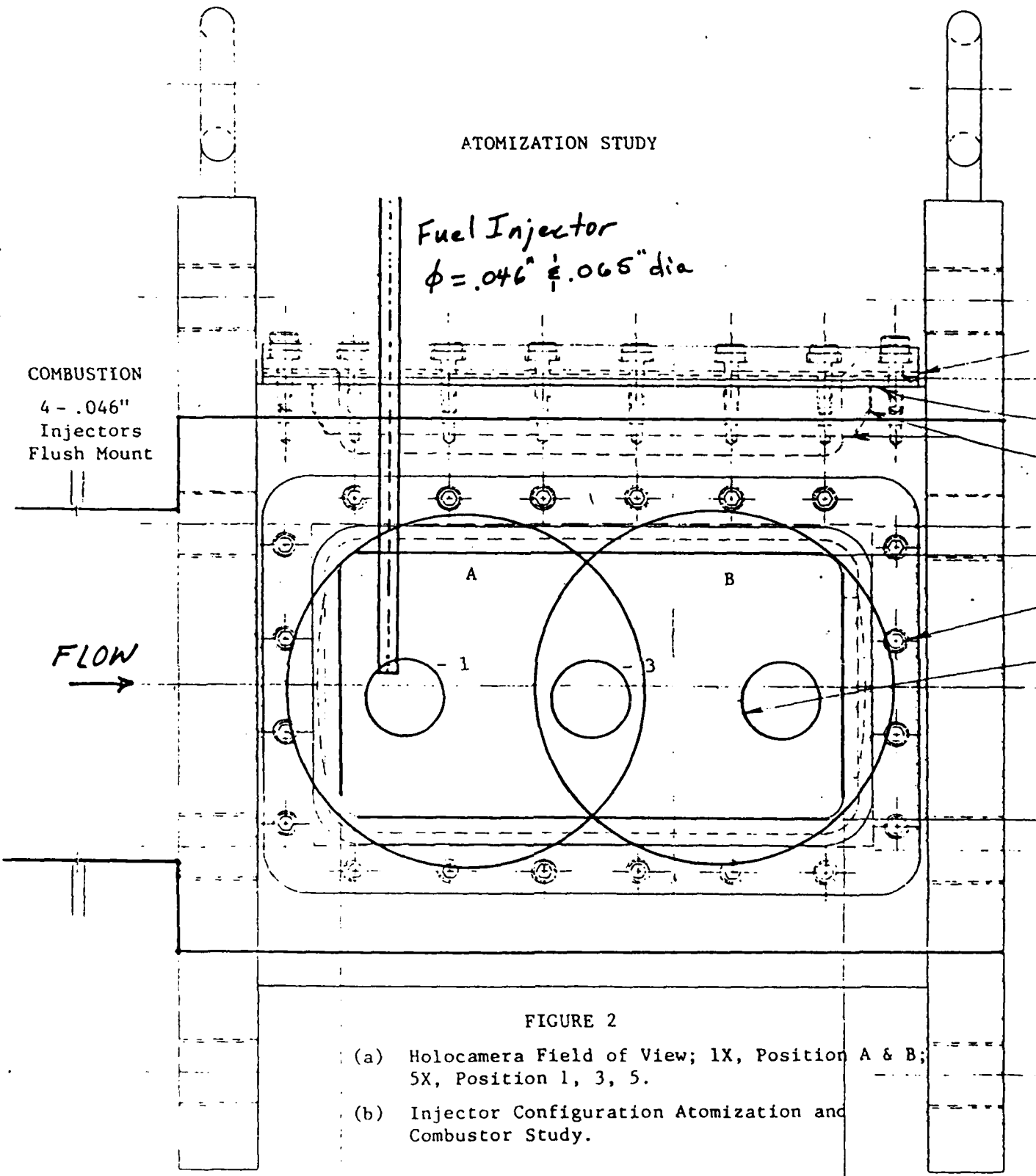


FIGURE 2

- (a) Holocamera Field of View; 1X, Position A & B;
5X, Position 1, 3, 5.
- (b) Injector Configuration Atomization and
Combustor Study.

5.62(A)(F.)

9.5.2 (A.2.1)

2.2 Ramjet Facility

The facility was configured for fuel atomization and combustion studies (Figure 2). For the fuel atomization study, a single injector was installed in a window blank in the 12 o'clock position allowing observation in the vertical plane through the other two windows. The fuel injector tip was adjusted to the duct centerline at a position about 2.3 inches (58. mm) downstream of the dump station. The centerline velocity at this position is approximately equal to the centerline velocity in the inlet. For the combustion study, four fuel injectors were installed in the inlet duct about 9 inches (229. mm) upstream of the dump station.

The atomization study was conducted for two orifice type injector sizes and a Pintle injector. The orifice type fuel injectors are designed to produce fuel jet momentums of the same magnitude as the air crossflow. For such a condition, air and fuel deflections or reactions to the interaction are approximately equal; thus providing sufficient penetration to fill the inlet with fuel and yet a sufficient air drag is encountered to atomize the fuel jet. Pintle type centerbody injectors are designed to atomize in still air and their performance in strong cross flows is not well understood. Inlet air velocities of 50 m/s and 150 m/s and temperatures of 300°k and 550°k were used.

2.3 Test Matrix

The test matrix was divided into three basic categories: fuel injector, air flow, and holocamera. The fuel injector specification included type, size, flow rate, and location. The air flow

specification includes velocity, temperature, and mass flow. The holocamera specification includes position, field of view, magnification, and exposure (single or double pulse). The specification for the test matrix is documented in Table 1.

TABLE I

FUEL INJECTOR		AIR FLOW		HOLOCAMERA	
ORIFICE DIAMETER (mm)	MASS FLOW (g/sec)	IGNITOR	ELDCTRY (mA/sec)	TEMPERATURE (m/s)	POSITION IN WINDOW
1.65	11.0	No	200	555°K	SP
	11.0			A & B	0.8X
	6.8				
	6.8				
	11.0				
	11.0				
	6.8				
	6.8				
	11.0				
	11.0				
	6.8				
	6.8				
	11.0				
	11.0				
	6.8				
	6.8				
	11.0				
	11.0				
	6.8				
	6.8				
	11.0				
	11.0				
	6.8				
	6.8				
	11.0				
	11.0				
	6.8				
	6.8				
	11.0				
	11.0				
	6.8				
	6.8				
	11.0				
	11.0				
	6.8				
	6.8				
	11.0				
	11.0				
	6.8				
	6.8				
	11.0				
	11.0				
	6.8				
	6.8				
	11.0				
	11.0				
	6.8				
	6.8				
	11.0				
	11.0				
	6.8				
	6.8				
	11.0				
	11.0				
	6.8				
	6.8				
	11.0				
	11.0				
	6.8				
	6.8				
	11.0				
	11.0				
	6.8				
	6.8				
	11.0				
	11.0				
	6.8				
	6.8				
	11.0				
	11.0				
	6.8				
	6.8				
	11.0				
	11.0				
	6.8				
	6.8				
	11.0				
	11.0				
	6.8				
	6.8				
	11.0				
	11.0				
	6.8				
	6.8				
	11.0				
	11.0				
	6.8				
	6.8				
	11.0				
	11.0				
	6.8				
	6.8				
	11.0				
	11.0				
	6.8				
	6.8				
	11.0				
	11.0				
	6.8				
	6.8				
	11.0				
	11.0				
	6.8				
	6.8				
	11.0				
	11.0				
	6.8				
	6.8				
	11.0				
	11.0				
	6.8				
	6.8				
	11.0				
	11.0				
	6.8				
	6.8				
	11.0				
	11.0				
	6.8				
	6.8				
	11.0				
	11.0				
	6.8				
	6.8				
	11.0				
	11.0				
	6.8				
	6.8				
	11.0				
	11.0				
	6.8				
	6.8				
	11.0				
	11.0				
	6.8				
	6.8				
	11.0				
	11.0				
	6.8				
	6.8				
	11.0				
	11.0				
	6.8				
	6.8				
	11.0				
	11.0				
	6.8				
	6.8				
	11.0				
	11.0				
	6.8				
	6.8				
	11.0				
	11.0				
	6.8				
	6.8				
	11.0				
	11.0				
	6.8				
	6.8				
	11.0				
	11.0				
	6.8				
	6.8				
	11.0				
	11.0				
	6.8				
	6.8				
	11.0				
	11.0				
	6.8				
	6.8				
	11.0				
	11.0				
	6.8				
	6.8				
	11.0				
	11.0				
	6.8				
	6.8				
	11.0				
	11.0				
	6.8				
	6.8				
	11.0				
	11.0				
	6.8				
	6.8				
	11.0				
	11.0				
	6.8				
	6.8				
	11.0				
	11.0				
	6.8				
	6.8				
	11.0				
	11.0				
	6.8				
	6.8				
	11.0				
	11.0				
	6.8				
	6.8				
	11.0				
	11.0				
	6.8				
	6.8				
	11.0				
	11.0				
	6.8				
	6.8				
	11.0				
	11.0				
	6.8				
	6.8				
	11.0				
	11.0				
	6.8				
	6.8				
	11.0				
	11.0				
	6.8				
	6.8				
	11.0				
	11.0				
	6.8				
	6.8				
	11.0				
	11.0				
	6.8				
	6.8				
	11.0				
	11.0				
	6.8				
	6.8				
	11.0				
	11.0				
	6.8				
	6.8				
	11.0				
	11.0				
	6.8				
	6.8				
	11.0				
	11.0				
	6.8				
	6.8				
	11.0				
	11.0				
	6.8				
	6.8				
	11.0				
	11.0				
	6.8				
	6.8				
	11.0				
	11.0				
	6.8				
	6.8				
	11.0				
	11.0				
	6.8				
	6.8				
	11.0				
	11.0				
	6.8				
	6.8				
	11.0				
	11.0				
	6.8				
	6.8				
	11.0				
	11.0				
	6.8				
	6.8				
	11.0				
	11.0				
	6.8				
	6.8				
	11.0				
	11.0				
	6.8				
	6.8				
	11.0				
	11.0				
	6.8				
	6.8				
	11.0				
	11.0				
	6.8				
	6.8				
	11.0				
	11.0				
	6.8				
	6.8				
	11.0				
	11.0				
	6.8				
	6.8				
	11.0				
	11.0				
	6.8				
	6.8				
	11.0				
	11.0				
	6.8				
	6.8				
	11.0				
	11.0				
	6.8				
	6.8				
	11.0				
	11.0				
	6.8				
	6.8				
	11.0				
	11.0				
	6.8				
	6.8				
	11.0				
	11.0				
	6.8				
	6.8				
	11.0				
	11.0				
	6.8				
	6.8				
	11.0				
	11.0				
	6.8				
	6.8				
	11.0				
	11.0				
	6.8				
	6.8				
	11.0				
	11.0				
	6.8				
	6.8				
	11.0				
	11.0				
	6.8				
	6.8				
	11.0				
	11.0				
	6.8				
	6.8				
	11.0				
	11.0				
	6.8				
	6.8				
	11.0				
	11.0				
	6.8				
	6.8				
	11.0				
	11.0				
	6.8				
	6.8				
	11.0				
	11.0				
	6.8				
	6.8				
	11.0				
	11.0</				

3.0 RESULTS

The fuel atomization and the combustor studies are summarized in the following sections. In the fuel atomization study we show how orifice type injectors perform for typical air crossflow conditions. The injector performance is described in terms of droplet penetration size and velocity. The mechanisms of the liquid air interaction appears to result in a nonsteady jet breakup very near the injector tip. The unsteady action manifests itself in the injector wake where vortical structures are observed. Vaporization and mixing processes within the injector wake are critical steps within the engine fuel delivery system. In the combustion study, we describe droplets observed in the combustion chamber during two standard firing sequences. Droplets about 5 μm to 10 μm were observed for typical inlet conditions ($V=150 \text{ m/s}$); and, for inlet velocities about 60% of typical, droplets between 20 μm and 40 μm are observed.

3.1 Fuel Atomization Study

The fuel atomization study included many air and fuel flow parameters; however, the fuel jet penetration is most sensitive to the air/fuel momentum flux ratio, and the fuel jet breakup is most sensitive to Weber number. The air/fuel momentum flux ratio is defined as

$$n = \frac{\rho V_{\text{air}}^2}{\rho V_{\text{fuel}}^2}$$

(ρV^2 : as momentum flux)

and the jet Weber number is defined as

$$We = \frac{\rho_{air} V_{air}^2 \phi_J}{\sigma_J}$$

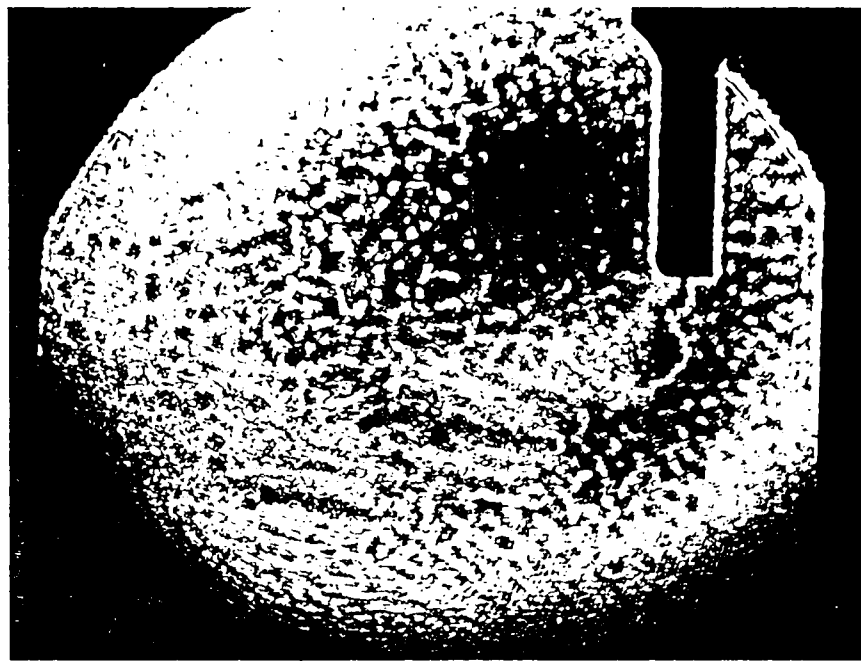
ϕ_J : Jet diameter

σ_J : Fuel Surface Tension

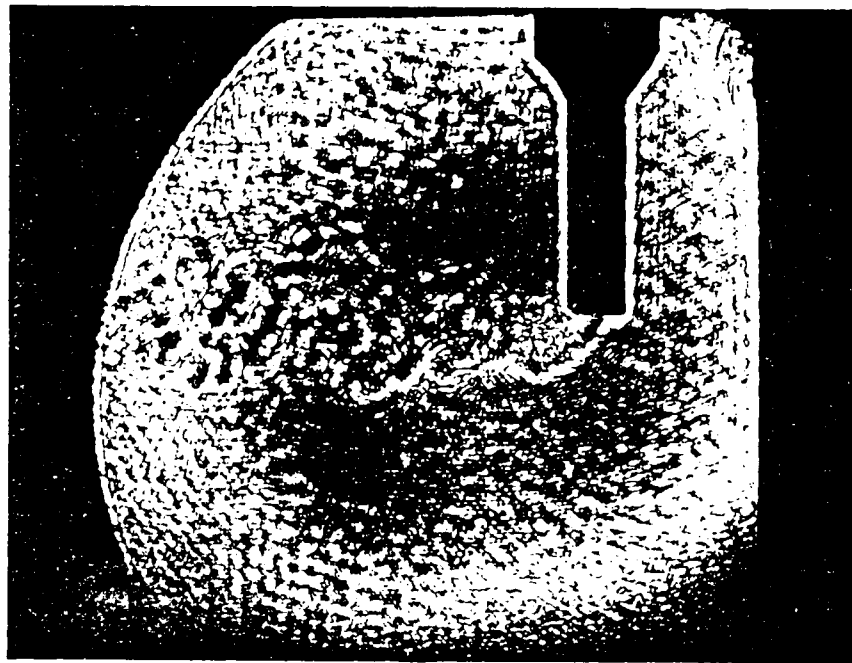
For very small momentum ratios (air/fuel) the jet penetration is large and the breakup mechanism can be the natural hydrodynamic Rayleigh instability. For larger ratios, the penetration is reduced and the jet breakup is very energetic.

The cases of small and equal momentum ratios are shown in Figure 3. For the low air velocity case (a), the fuel jet ($\phi = 1.1$ mm) penetrates about 25 diameters (27 mm), and the breakup mechanism is observed to be stripping from the air/fuel interface typical of Weber numbers above 100. The results of mass and heat transfers from the fuel jet are observed in its wake where turbulent mixing processes are observed between the air fuel mixture. The Reynolds number based on jet diameter is 2000. The eventual failure of the jet appears to be a nonsteady process resulting in fluctuating amounts of mass being released into the air flow.

For the high air flow case, the fuel jet penetrates only 6 diameters. The fuel jet is deformed within one diameter of the exit, and within the next few diameters the breakup is complete. Irregular distortions appear in the leading edge of the jet which and within a few diameters result in a nonsteady fuel delivery. That is the fuel appears



(a) Velocity = 50 m/s
Temperature = 300°K



(b) Air Velocity = 150 m/s
Temperature = 300°K

FIGURE 3. URGSKEEN FUEL ATOMIZATION
(Flow Right to Left, this Figure Only)

to be distributed in a nonuniform manner into the injector wake. The injector Reynolds number is 33,000. These nonuniformities persist into the injector wake where they take the form of vortices.

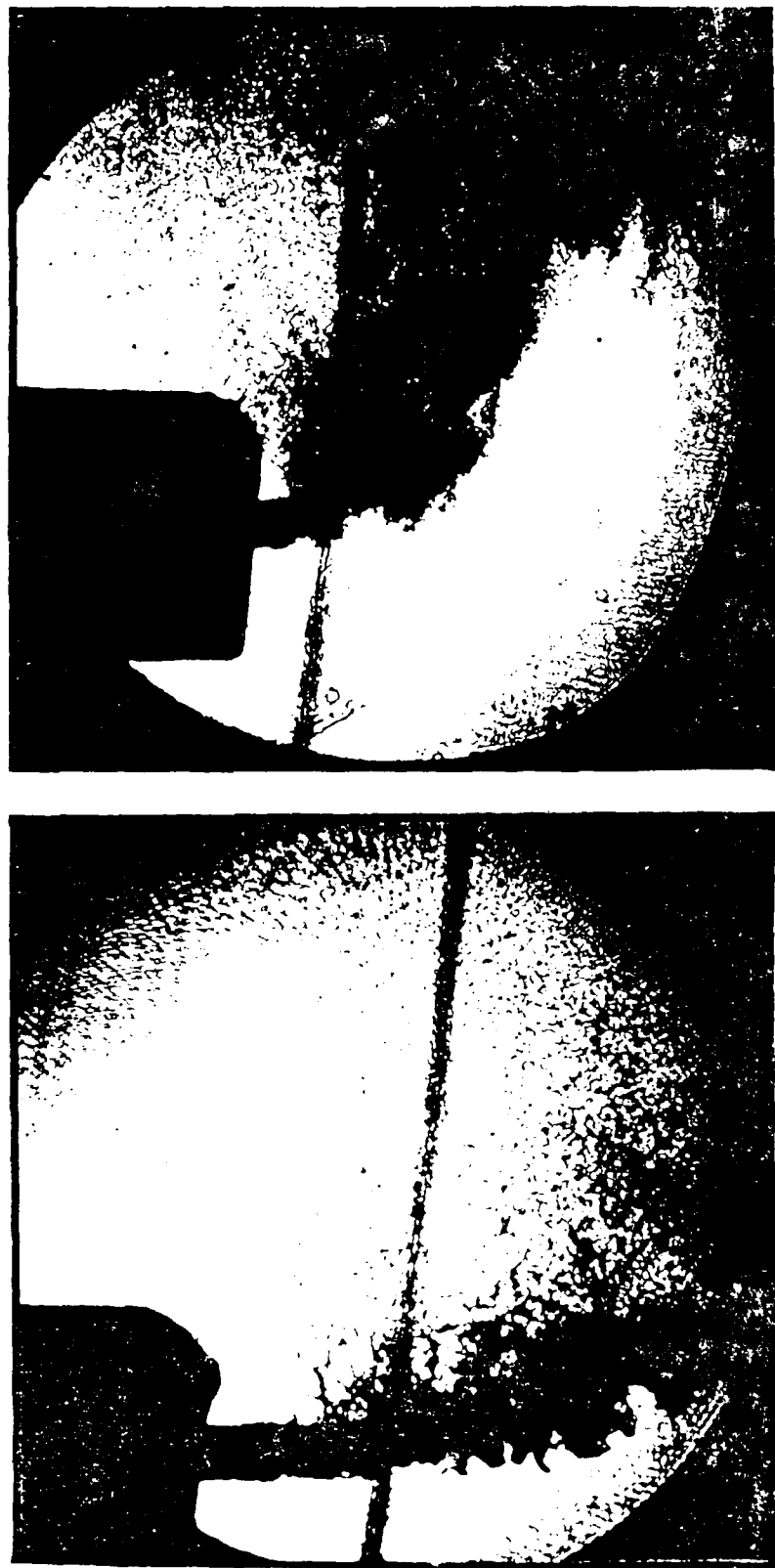
The mechanism of breakup is shown in Figure 4 with higher magnification. The jet deformations and fragments are resolved to about 5 μm . In the low air speed case, the fuel droplets are distributed over a larger region and are larger in size than in the high air flow case; hence the number density appears to be much higher in the high air flow case. In both cases the optical density prohibits imaging in portions of the fuel jet.

The center body type fuel injector is shown in Figure 5. The center body type injector operates by producing a diverging sheet of fuel of decreasing thickness, which exhibits an instability and fragments. In the absence of crossflow, the atomization is very efficient; however, the effect of high velocity crossflow may be detrimental to the atomization efficiency. Preliminary observations of Figure 5 indicate that the crossflow produces a significant effect on the atomization, particularly with the portion of the sheet which is initially injected upstream. This portion of the sheet fails due to aerodynamic loading long before the hydrodynamic instabilities occur. The primary result may be that portions of the fuel may be atomized by a different mechanism (i.e. aerodynamic) and therefore result in different size droplets in the presence of a strong crossflow.

A very cursory droplet size analysis was conducted for the high and low crossflow conditions. A portion of the droplet image at Position 5 (about 2 x 2 mm) is shown in Figure 6. For the low crossflow

FUEL ATOMIZATION STUDY

50 m/s Air Velocity 150 m/s
11. gm/s Fuel Rate 11. gm/s
300 Weber Number 2700
1.18 mm Injector Diameter 1.18 mm



Scale — 1 mm

FIGURE 4. FUEL ATOMIZATION STUDY - SWIRL INJECTOR



FIGURE 5. FUEL ATOMIZATION STUDY - PINTLE INJECTOR

LIST OF FIGURES (CONTINUED)

<u>FIGURES</u>	<u>PAGE</u>
10. FLOWFIELD IN (r-z) PLANE FOR $\alpha = 45^\circ$, H = 0 INCHES	
FIRST PLOT	43
FLOWFIELD IN (r-z) PLANE FOR $\alpha = 45^\circ$, H = 0 INCHES	
SECOND PLOT	44
FLOWFIELD IN (r-z) PLANE FOR $\alpha = 45^\circ$, H = 0 INCHES	
THIRD PLOT	45
FLOWFIELD IN (r-z) PLANE FOR $\alpha = 45^\circ$, H = 0 INCHES	
FOURTH PLOT	46
11. FLOWFIELD IN (r- θ) PLANE FOR $\alpha = 60^\circ$, H = 2 INCHES	
FIRST PLOT	47
FLOWFIELD IN (r- θ) PLANE FOR $\alpha = 60^\circ$, H = 2 INCHES	
SECOND PLOT	48
FLOWFIELD IN (r- θ) PLANE FOR $\alpha = 60^\circ$, H = 2 INCHES	
THIRD PLOT	49
FLOWFIELD IN (r- θ) PLANE FOR $\alpha = 60^\circ$, H = 2 INCHES	
FOURTH PLOT	50
12. FLOWFIELD IN (r-z) PLANE FOR $\alpha = 60^\circ$, H = 2 INCHES	
FIRST PLOT	51
FLOWFIELD IN (r-z) PLANE FOR $\alpha = 60^\circ$, H = 2 INCHES	
SECOND PLOT	52
FLOWFIELD IN (r-z) PLANE FOR $\alpha = 60^\circ$, H = 2 INCHES	
THIRD PLOT	53
FLOWFIELD IN (r-z) PLANE FOR $\alpha = 60^\circ$, H = 2 INCHES	
FOURTH PLOT	54
13. FLOWFIELD IN (r- θ) PLANE FOR $\alpha = 60^\circ$, H = 0 INCHES	
FIRST PLOT	55
FLOWFIELD IN (r- θ) PLANE FOR $\alpha = 60^\circ$, H = 0 INCHES	
SECOND PLOT	56
FLOWFIELD IN (r- θ) PLANE FOR $\alpha = 60^\circ$, H = 0 INCHES	
THIRD PLOT	57
FLOWFIELD IN (r- θ) PLANE FOR $\alpha = 60^\circ$, H = 0 INCHES	
FOURTH PLOT	58

LIST OF FIGURES

<u>FIGURES</u>	<u>PAGE</u>
1. WATER TUNNEL COMBUSTOR CONFIGURATION.	23
2. GENERAL FLOW PATTERN IN CROSS-SECTIONAL PLANE	24
3. FLOW PATTERN IN THE VERTICAL (r - z) PLANE (LIGHT SOURCE PLACED PARALLEL TO DUCT AXIS)	25
4. LOCATION OF INJECTION PORTS AND A TYPICAL FINITE- DIFFERENCE GRID	26
5. FINITE-DIFFERENCE GRID FOR -2 INCH DOME POSITION.	27
6. FLOWFIELD IN (r - θ) PLANE FOR $\alpha = 45^\circ$, $H = 2$ INCHES FIRST PLOT.	29
FLOWFIELD IN (r - θ) PLANE FOR $\alpha = 45^\circ$, $H = 2$ INCHES SECOND PLOT	30
FLOWFIELD IN (r - θ) PLANE FOR $\alpha = 45^\circ$, $H = 2$ INCHES THIRD PLOT.	31
FLOWFIELD IN (r - θ) PLANE FOR $\alpha = 45^\circ$, $H = 2$ INCHES FOURTH PLOT	32
7. FLOWFIELD IN (r - z) PLANE FOR $\alpha = 45^\circ$, $H = 2$ INCHES FIRST PLOT.	33
FLOWFIELD IN (r - z) PLANE FOR $\alpha = 45^\circ$, $H = 2$ INCHES SECOND PLOT	34
FLOWFIELD IN (r - z) PLANE FOR $\alpha = 45^\circ$, $H = 2$ INCHES THIRD PLOT.	35
FLOWFIELD IN (r - z) PLANE FOR $\alpha = 45^\circ$, $H = 2$ INCHES FOURTH PLOT	36
8. FINITE DIFFERENCE GRID FOR THE 0 INCH DOME POSITION . . .	37
9. FLOWFIELD IN (r - θ) PLANE FOR $\alpha = 45^\circ$, $H = 0$ INCHES FIRST PLOT.	39
FLOWFIELD IN (r - θ) PLANE FOR $\alpha = 45^\circ$, $H = 0$ INCHES SECOND PLOT	40
FLOWFIELD IN (r - θ) PLANE FOR $\alpha = 45^\circ$, $H = 0$ INCHES THIRD PLOT.	41
FLOWFIELD IN (r - θ) PLANE FOR $\alpha = 45^\circ$, $H = 0$ INCHES FOURTH PLOT	42

TABLE OF CONTENTS

<u>SECTION</u>		<u>PAGE</u>
1.0	INTRODUCTION.	1
2.0	DESCRIPTION OF THE FLOW GEOMETRY.	2
3.0	EQUATIONS GOVERNING THE FLOW.	4
4.0	MODIFICATION TO THE FLOW3D PROGRAM.	8
	4.1 Brief Details of FLOW3D.	8
	4.2 Simulation of Geometry	8
	4.3 Simulation of the Boundary Conditions.	9
	4.4 Prescription of the Initial Guess.	10
	4.5 Modifications to MODS.	10
	4.6 Modification to Improve Convergence.	10
	4.7 New Input Data	11
5.0	COMPUTATIONAL DETAILS	12
	5.1 Finite - difference Grid	12
	5.2 Accuracy of the Computations	12
6.0	RESULTS AND DISCUSSION.	14
	6.1 General Flow Pattern	14
	6.2 Comparison with Flow Visualizations.	16
	6.3 Effect of Dome Positions	16
	6.4 Effect of Injection Angle.	17
	6.5 Other Calculations	18
	6.6 Summary.	19
7.0	SUMMARY	20
8.0	ACKNOWLEDGEMENTS.	21

ANALYTICAL CHARACTERIZATION
OF FLOWFIELDS IN
DUCTED-ROCKET COMBUSTOR GEOMETRIES

S.P. VANKA[†]

UNIVERSAL ENERGY SYSTEMS
4401 Dayton-Xenia Road
Dayton, Ohio 45432

[†]Summer Consultant. Permanent affiliation
Argonne National Laboratory, Argonne, Illinois 60439

ANALYTICAL CHARACTERIZATION
OF FLOWFIELD IN
DUCTED-ROCKET COMBUSTOR GEOMETRIES

S.P. Vanka*

UNIVERSAL ENERGY SYSTEMS, INC.
4401 Dayton-Xenia Road
Dayton, Ohio 45432

*Summer Consultant. Permanent Affiliation
Argonne National Laboratory, Argonne, Illinois 60439

APPENDIX B
ANALYTICAL CHARACTERIZATION OF FLOWFIELD IN
DUCTED-ROCKET COMBUSTOR GEOMETRIES

DR. S. P. VANKA

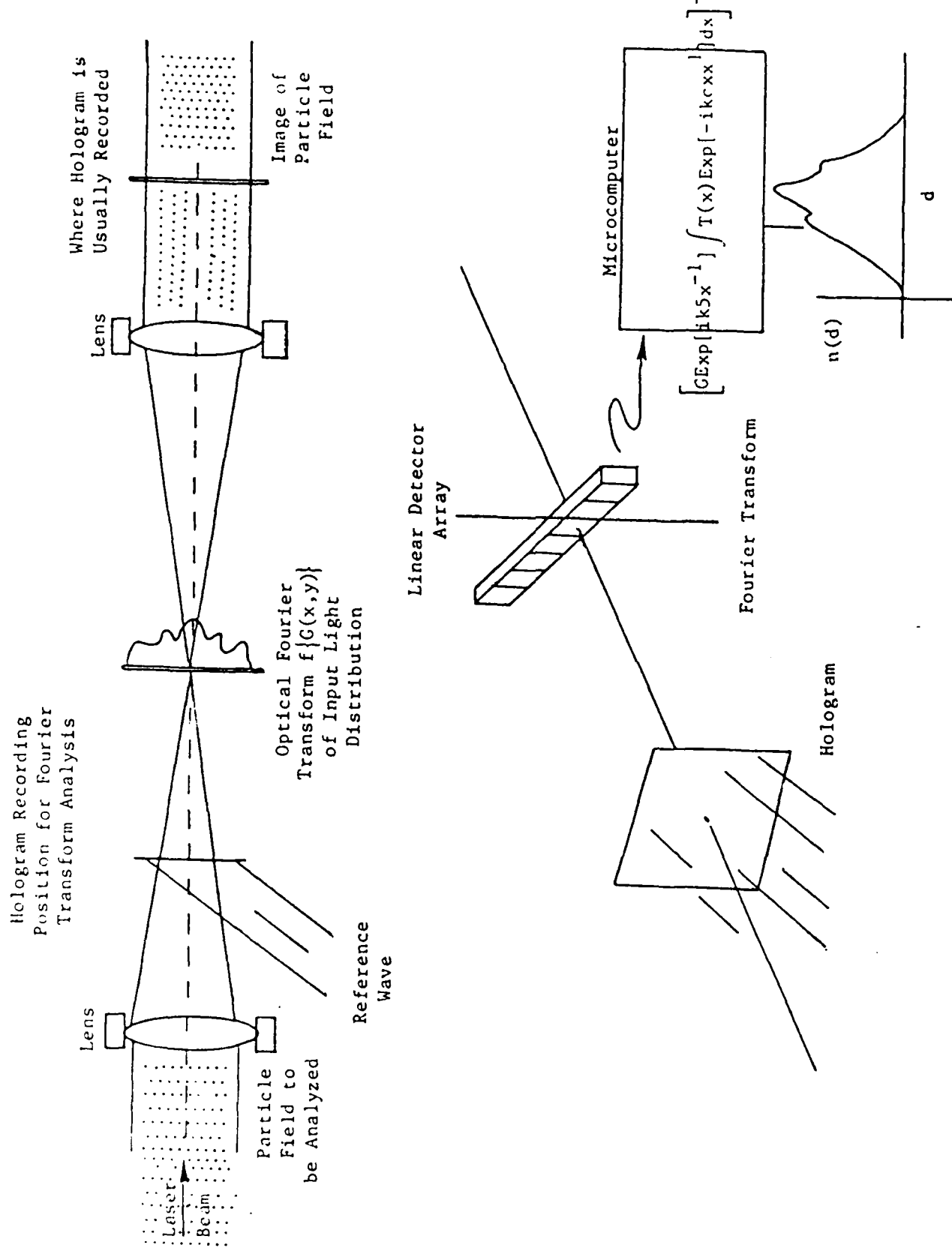


FIGURE 9. DETERMINING PARTICLE SIZE DISTRIBUTION FROM THE HOLOGRAPHICALLY RECORDED FOURIER TRANSFORM

5.0 RECOMMENDATIONS

Holographic diagnostics are shown to provide excellent droplet images within the high speed flows in ramjet combustion chambers. The holographic technique apparently provides high resolution even in the presence of turbulent reacting flow; whereas point scattering probes (LDV) can suffer broadening effects or dramatically reduced resolutions in the presence of such flows. However, tedious data reduction currently limits the ability to utilize the scope and resolution of the data.

We recommend that Fourier transform holographic data reduction techniques be investigated and developed to provide droplet size and velocity data (Figure 9). Such a capability could be combined with other recent advances in holographic technology to provide near real-time image and Fourier transform analysis. This ability would dramatically improve current understanding of ramjet fuel delivery processes.

We recommend that holographic interferometry be used to visualize the heat and mass transfer processes within the injector wake. Interferometry is a very sensitive technique for detecting temperature and concentration variations present in the injector wake.

4.0 SUMMARY

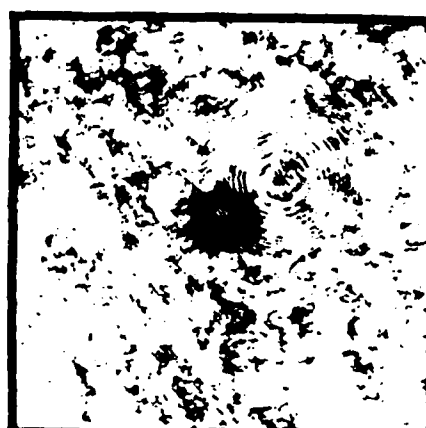
This very cursory review of about 100 holographic images has been presented to demonstrate the utility of holographic diagnostics in a combustion environment. For an intermediate inlet crossflow velocity, excellent droplet images in the 20 μm to 40 μm range were recorded in the presence of combustion. For the more typical inlet crossflow condition, smaller droplets (5 μm - 15 μm) at higher number density produced images with slightly degraded signal/noise ratio.

Holographic observation of crossflow fuel atomization reveals a process rich in complex fluid interactions. The physics of this process is certainly not limited to liquid atomization, but also includes mass and heat transfer processes and fuel/air mixing processes. For typical crossflow velocities, the mechanism of the fuel/air interaction appears to result in nonsteady jet breakup and, hence, nonsteady fuel delivery. The unsteadiness appears to persist into the injector wake where vortex-like structures are observed. The flow visualization of the injector wake also reveals mixing processes between fuel vapor and air. Higher magnification holography of specific pieces of the crossflow injection reveals droplet size and velocity with resolutions of 5 μm and 1 m/s , respectively. Images of the injector tip reveal the structure of the liquid-gas interface and the instability mechanisms of breakup. Droplets are observed within the injector wake whose size depends on the crossflow velocity.

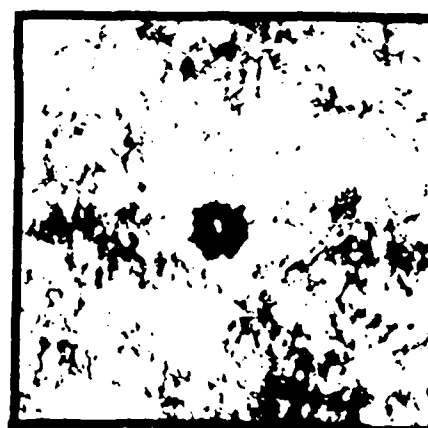
DROPLET ANALYSIS - COMBUSTION STUDY



Large $\phi = 38 \times 48 \mu\text{m}$



Typical $\phi = 33 \mu\text{m}$



Small $\phi = 24 \mu\text{m}$

FIGURE 8. DROPLET SIZE ANALYSIS - COMBUSTION STUDY

3.2 Combustor Study

For the combustor study, four injectors were flush mounted 9 inches (229. mm) upstream of the dump station at 90° intervals about the inlet duct. The combustor was operated at two conditions:

Condition	\dot{M}_{air}	\dot{M}_{fuel}	$\phi_{injector}$
1	1.14 kg/sec	11.4 gm/s	1.1 mm
2	0.68 kg/sec	6.8 gm/s	1.1 mm

Condition 1 corresponds to the high crossflow atomization case described in Section 3.1, in which the breakup resulted in droplet sizes ranging from 10 - 20 μm . The crossflow velocity for condition 2 is about 100 m/s which is about midway between the conditions discussed in Section 3.1; hence one would expect atomization for condition 2 to result in droplet sizes about midway between 15 μm and 60 μm or about 30 μm - 40 μm . Images were recorded for conditions 1 and 2 before and after ignition in the combustion chamber. Ignition is accomplished by a gas phase flame injected into the combustion chamber at the dump station. The inlet velocity is reduced when the combustor is ignited.

The reconstructed images for both conditions 1 and 2 in the absence of combustion revealed fairly noisy images with very small droplets. For condition 1 with combustion, the crossflow droplet images were fairly noisy, but small droplets in the 5 - 15 μm range were observed. For condition 2 with combustion, the droplet images have better contrast and a few representative images are shown in Figure 8. Droplet sizes in the 20 μm to 40 μm range were typical, a result which is consistent with the lower crossflow velocity condition.

DROPLET VELOCITY ANALYSIS - ORIFICE INJECTOR

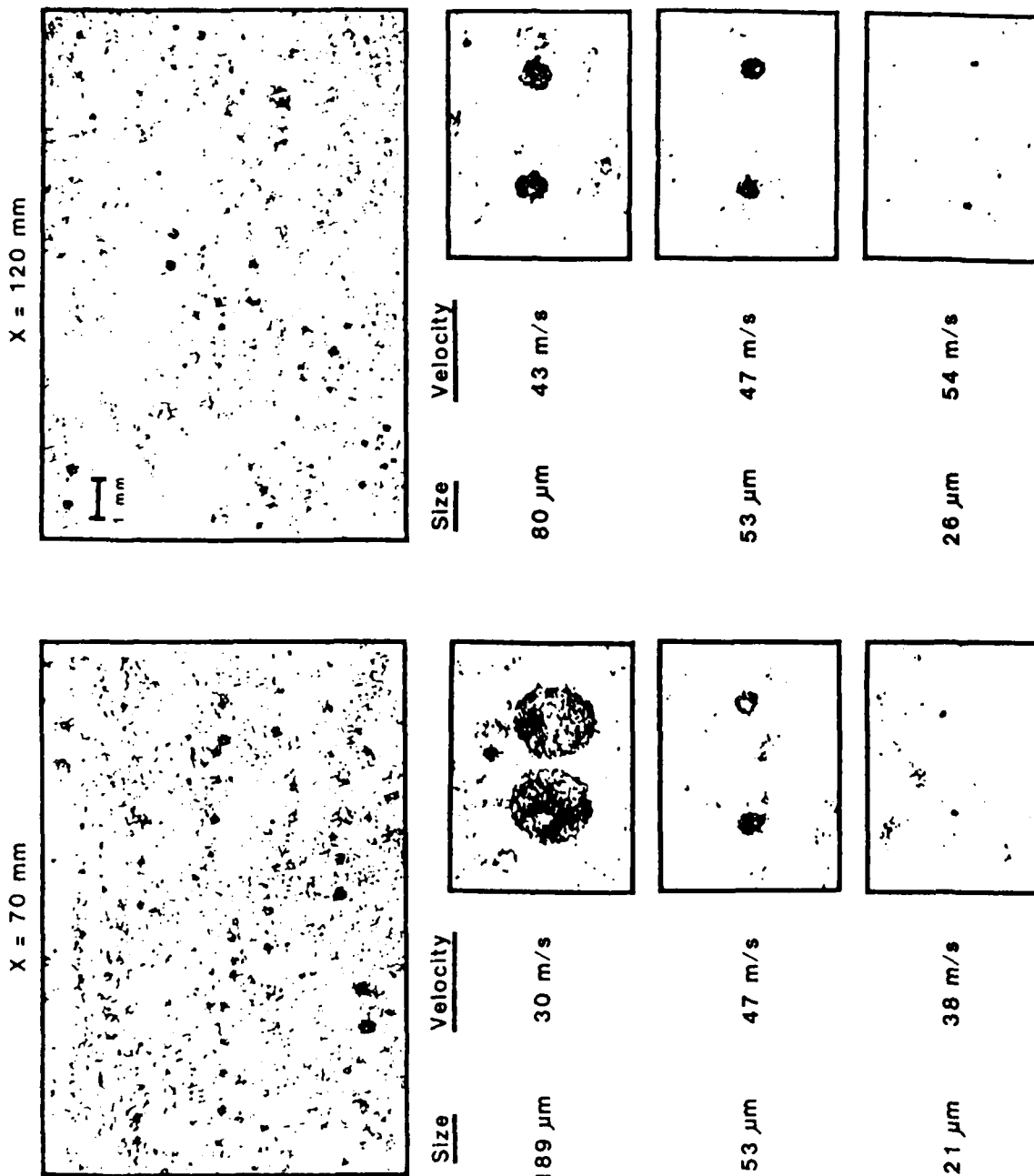


FIGURE 7. DROPLET VELOCITY ANALYSIS - ORIFICE INJECTOR

condition, droplet images exhibit excellent signal to noise, and highly magnified images of droplets from 20 μm to 200 μm are produced with a resolution of 5 μm . A typical droplet size (by no means the average) is about 60 μm . For the high crossflow condition the atomization is to much smaller droplets and correspondingly higher number density. The signal to noise ratio of the image is degraded by the small droplet size and the increased number density. However, this type of image may be well suited for statistical sampling. High magnification images of individual droplets from 8 μm to 22 μm are produced with varying degrees of resolution.

A droplet velocity analysis was conducted for images at Positions 3 and 5 for the low crossflow condition (see Figure 7). The time interval between the images was 6 μsec . At Position 3, the droplet velocities range from 30 m/s to 47 m/s, and at Position 5, the droplet velocities are essentially equal to the gas velocity (taken to be 50 m/s). This velocity data is in general agreement with droplet relaxation scaling laws which predict a velocity equilibrium in about 1 ms or 50 μm , as follows:

$$t = \frac{\rho_L \phi}{\rho \Delta u}$$
$$x = \Delta U t$$

For the high crossflow condition double droplet images could not be found in the higher number density images.

50 m/s
11. gm/s
1.18 mm
300

Air Velocity
Fuel Rate
Injector Diameter
Weber Number

150 m/s
11. gm/s
1.18 mm
2700

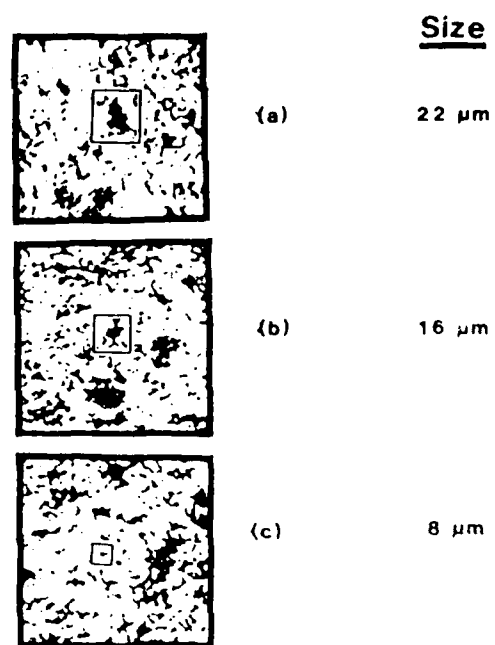
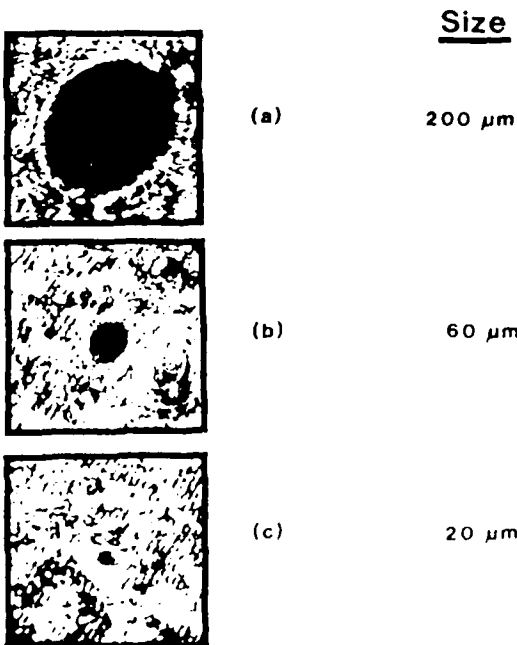
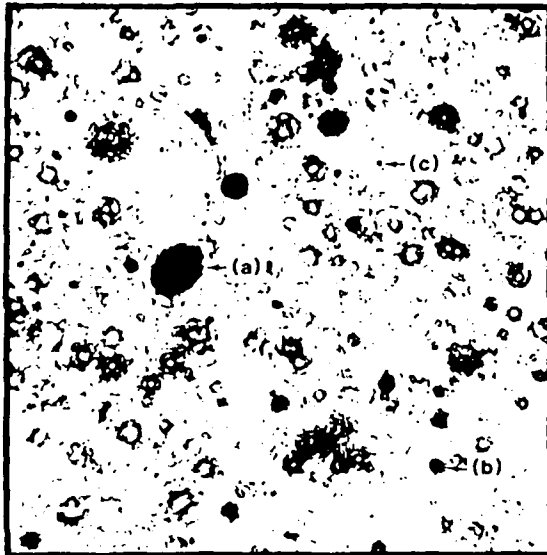


FIGURE 6. DROPLET SIZE ANALYSIS - ORIFICE INJECTOR

LIST OF FIGURES (CONTINUED)

<u>FIGURES</u>	<u>PAGE</u>
14. FLOWFIELD IN (r-z) PLANE FOR $\alpha = 60^\circ$, H = 0 INCHES FIRST PLOT	59
FLOWFIELD IN (r-z) PLANE FOR $\alpha = 60^\circ$, H = 0 INCHES SECOND PLOT	60
FLOWFIELD IN (r-z) PLANE FOR $\alpha = 60^\circ$, H = 0 INCHES THIRD PLOT	61
FLOWFIELD IN (r-z) PLANE FOR $\alpha = 60^\circ$, H = 0 INCHES FOURTH PLOT	62

LIST OF TABLES

	<u>PAGE</u>
TABLE 1. FINITE-DIFFERENCE GRID USED IN COMPUTATIONS. . . . (H = 2 INCHES)	28
Table 2. FINITE-DIFFERENCE GRID USED IN COMPUTATIONS. . . . (H = 0 INCHES)	38

1.0 INTRODUCTION

The author spent a period of eight weeks with the Ramjet Technology Division, Wright-Patterson AFB, Ohio as a summer consultant through Universal Energy Systems, Dayton, Ohio. During this period, calculations were performed of the development of three-dimensional flow fields in ducted-rocket combustor geometries. The calculations were made with a modified version of a three-dimensional fluid flow computer program, FLOW3D, developed by the author. The present computations were performed for cold flow conditions for parametric ranges corresponding to flow visualization tests currently under progress at the WPAFB facilities. Flow patterns for two different dome positions and for two-different injection angles were investigated. The computed flow fields were plotted as velocity vector plots in selected cross-sectional planes. The computations were performed on the CYBER computer systems at the WPAFB.

The present report documents the work performed during this assignment. In the following sections, brief details are presented of the flow geometry considered, the equations solved, the computer program used and the details of the computations. The results are presented in Section 6.

2.0 Description of the Flow Geometry

Figure 1 shows a sketch of the ducted rocket combustor geometry. The air flow enters the combustor through two side arm inlet ports located symmetrically about a diameter of the circular duct. The position of the dome plate D can be varied, along with the mass flow through the side arms, and the angle of the injection, α .

Experimental investigations are currently in progress at WPAFB's water tunnel to investigate the flow field development in the geometry of Figure 1. The flow visualization is achieved by injecting small air bubbles into the stream and making photographs with a narrow slit of a high intensity light source. Two illustrative flow patterns observed for nominal flow rate and geometric configurations are shown in Figures 2 and 3.* Figure 2 shows a typical flow pattern in cross-sectional planes between the inlet ports and the nozzle. In the dome region (between dome plate and the injection port), the flow is very complex and for certain conditions, bistable. It appears that the flow also becomes asymmetrical although the side inlets are symmetrically placed and have equal flow rates. The flow pattern shown in Figure 2 is seen nearly for the entire duct (excluding some sections of the dome region), with a decreasing strength of the vortex as the flow proceeds to the nozzle.

Figure 3 shows the observed flow with the light slit placed parallel to the duct axis. Only the flow near the inlet port is shown. The flow entering the combustor is split between the dome region, and the downstream combustor region. The flow going into the dome region creates an eddy and flows back to the nozzle. The resulting patterns are highly three-dimensional and contain complex, embedded recirculation zones.

*Complete results of the flow visualization studies are documented in separate reports by UES.

Downstream of the inlet ports, the flow tends to straighten out, and the two pairs of counter rotating vortices in the cross-section decay in their strength. The result of these complex flow patterns is a complete mixing of the fuel injected either through the dome plate, or through the inlet-air ports. Knowledge of the flow patterns and the ability to predict the transport processes is of much importance for efficient design.

3.0 Equations Governing the Flow

In the present work, the partial differential equations governing the mean (time averaged) three-dimensional flow field have been solved with the appropriate boundary conditions. The equations have been solved numerically by a finite-difference calculation procedure. The set of differential equations solved is described below along with the boundary conditions. The modifications to a computer code FLOW3D are described in Section 4.

General form of the Equation

The equations governing the three-dimensional flow can be expressed by the following general form

$$\operatorname{div} (\vec{G} \phi) = \operatorname{div} (\Gamma_\phi \operatorname{grad} \phi) + S_\phi \quad (3.1)$$

where ϕ represents a general transported quantity. ϕ may stand for a general scalar (enthalpy, turbulent kinetic energy, etc.), and for the three velocities (u, v, w). For mass continuity, ϕ can be made to unity. \vec{G} represents the mass flow vector, and Γ_ϕ is an effective diffusion coefficient. S_ϕ represents the 'source' terms in the equation and contains terms such as the pressure gradients (in the momentum equations), the production and dissipation of kinetic energy of turbulence, etc. The expressions for divergence and gradient in the (r, θ, z) system (currently used) are given below.

$$\operatorname{div} \phi = \frac{1}{r} \frac{\partial(r\phi)}{\partial r} + \frac{\partial\phi}{r\partial\theta} + \frac{\partial\phi}{\partial z} \quad (3.2)$$

$$\operatorname{grad} \phi = \frac{\partial\phi}{\partial r} \vec{i} + \frac{\partial\phi}{r\partial\theta} \vec{j} + \frac{\partial\phi}{\partial z} \vec{k} \quad (3.3)$$

where $\vec{i}, \vec{j}, \vec{k}$ are the unit normal vectors in the three coordinate directions.

The term S_ϕ appearing in the individual equations is given below.

Mass continuity NONE

θ -momentum (u-velocity)

$$S_u = \frac{-\partial p}{r\partial\theta} - \frac{\rho uv}{r} + \frac{\partial}{r\partial\theta} \left(\frac{\mu \partial u}{r\partial\theta} + \frac{2\mu v}{r} \right) + \frac{\partial}{\partial r} \left(\mu r \left(\frac{\partial v}{r\partial\theta} - \frac{u}{r} \right) \right) + \frac{\partial}{\partial z} \left(\frac{\mu}{r} \frac{\partial w}{\partial\theta} \right) + \frac{\mu}{r} \left(\frac{\partial u}{\partial r} + \frac{\partial v}{r\partial\theta} - \frac{u}{r} \right) \quad (3.4)$$

r -momentum

$$S_v = \frac{-\partial p}{\partial r} + \frac{\rho u^2}{r} + \frac{\partial}{r\partial\theta} \left(\mu \frac{\partial u}{\partial r} \right) + \frac{1}{r} \frac{\partial}{\partial r} \left(\mu r \frac{\partial v}{\partial r} \right) - \frac{\partial}{r\partial\theta} \left(\frac{\mu u}{r} \right) - \frac{2\mu}{r} \left(\frac{1}{r} \frac{\partial u}{\partial\theta} + \frac{v}{r} \right) \quad (3.5)$$

z -momentum

$$S_w = \frac{-\partial p}{\partial z} + \frac{\partial}{\partial z} \left(\mu \frac{\partial w}{\partial z} \right) + \frac{1}{r} \frac{\partial}{\partial r} \left(\mu r \frac{\partial v}{\partial z} \right) + \frac{\partial}{r\partial\theta} \left(\mu \frac{\partial u}{\partial z} \right) \quad (3.6)$$

Kinetic Energy of Turbulence

$$S_k = P - \rho \epsilon \quad (3.7)$$

$$P = \mu_t \left[2.0 \left\{ \left(\frac{\partial u}{r\partial\theta} + \frac{v}{r} \right)^2 + \left(\frac{\partial v}{\partial r} \right)^2 + \left(\frac{\partial w}{\partial z} \right)^2 \right\} + \left(\frac{\partial u}{\partial z} + \frac{\partial w}{r\partial\theta} \right)^2 + \left(\frac{\partial w}{\partial r} + \frac{\partial v}{\partial z} \right)^2 + \left(\frac{\partial u}{\partial r} + \frac{\partial v}{r\partial\theta} - \frac{u}{r} \right)^2 \right] \quad (3.8)$$

Dissipation rate of k (ϵ)

$$S_\epsilon = C_1 \frac{\epsilon}{k} P - C_2 \frac{\rho \epsilon^2}{k} \quad (3.9)$$

Further,

$$\mu_t = C_\mu \rho \frac{k^2}{\epsilon} \quad (3.10)$$

and the effective diffusion coefficient Γ_ϕ is given by

$$\Gamma_\phi = \frac{\mu_\ell}{\sigma_{\ell,\phi}} + \frac{\mu_t}{\sigma_{t,\phi}} \quad (3.11)$$

where μ_ℓ , μ_t , are the laminar and turbulent viscosities, and $\sigma_{\ell,\phi}$, $\sigma_{t,\phi}$ are the appropriate laminar and turbulent Prandtl numbers for the transported quantity.

The constants in the turbulence model are given the following values

$$C_1 = 1.47, C_2 = 1.92, C_\mu = 0.09 \quad \text{and}$$

$$\sigma_{t,k} = 1.0, \sigma_{t,\epsilon} = 1.3.$$

The laminar and turbulent Prandtl numbers for the velocities, and the laminar Prandtl numbers for k and ϵ are assigned a value of unity. Because the flow is isothermal, the laminar viscosity and the density are prescribed constant values.

Boundary Conditions

Because the inlet ducts are symmetrically located about a diametrical plane, only one half of the duct (180° , containing one inlet port) is solved for. The boundaries of the domain are the left and right semi circular planes, the duct wall, and the central diametrical plane. The central diameter plane is considered in three sections: two radial planes, (separated by 180°) and a point (line) representing the origin.

The boundary conditions for the present calculations were as follows.

Outer Wall:

$$\begin{aligned} u, v, w &= 0 \\ v = v_{inj}; w = w_{inj} &\text{ at the} \\ &\text{injection (inlet) ports} \end{aligned} \tag{3.12}$$

Inner Radial Lines:

$$u = 0; \frac{\partial v}{\partial \theta} = \frac{\partial w}{\partial \theta} = \frac{\partial k}{\partial \theta} = \frac{\partial \epsilon}{\partial \theta} = 0 \tag{3.13}$$

Dome Plate (z^- boundary)

$$\begin{aligned} u = v = w &= 0 \\ k = 0, \epsilon &= 0 \end{aligned} \tag{3.14}$$

Exit (z^+) boundary

$$\frac{\partial \phi}{\partial z} = 0, \text{ where } \phi = u, v, w, k, \epsilon \tag{3.15}$$

Inlet Ports Region

The inlet ports occupy an azimuthal span of $(\theta_L - \theta_F)$, and an axial distance of $(z_L - z_F)$. Between this region, at the outer wall, the angled flow is represented as a resultant of a radial velocity component v_{inj} and an axial velocity w_{inj} .

The above described equations and the boundary conditions fully define the flow. In addition, near the walls, wall functions have been used to model the near wall turbulence phenomena. We need to now represent them in finite-difference form and solve the finite difference equations.

4.0 Modifications to the FLOW3D Program

4.1 Brief Details of FLOW3D

The above described physical geometry and the boundary conditions have been simulated by modifying a three-dimensional fluid flow computer code FLOW3D [1]. The complete details of FLOW3D are documented separately [1] and hence will not be described here. In the present section, the general features and the capabilities of the code will be described. For details of the finite-differencing and solution procedures, the user is referred to reference [1].

FLOW3D solves the elliptic partial differential equations governing fluid flow and heat transfer in three-dimensions. The turbulence phenomena are modelled through a two-equation ($k \sim \epsilon$) model. Two transport equations, in addition to those for the three momenta, mass and enthalpy are solved to calculate the development of the kinetic energy of turbulence and its dissipation rate. The partial-differential equations are finite-differenced by integrating the differential equations over 'control volumes'. An exponential variation of a flow variable with coordinate distance is assumed in deriving the finite-difference equations. The set of finite-difference equations is solved by a combination of plane-by-plane procedure and an alternate-sweep technique.

The computer code is arranged into several modular subroutines according to their function in the calculation sequence. The subroutines are described in detail in [1]. The problem dependent routines INIT, INPUT, MODS and OUTP have been modified to simulate the geometry and the boundary conditions. The modifications and the input data are described below.

4.2 Simulation of Geometry

The simulation of the geometry is straight-forward. We have used the (r, θ, z) system of coordinates (the source terms of Section 2 have

already been programmed) and prescribed the index KPLAX equal to 2. The top wall (KBYP) index is set to 1, and the indices KBXM, KBYM, KBXP, are set to 3 in order to simulate a symmetry plane. The dome plate is considered as a wall, and the outlet is prescribed with an index (KBZP) of 2. A finite-difference grid consisting of r , θ and z coordinate values is prescribed based on the desired fineness of the grid chosen.

4.3 Simulation of the Boundary Conditions

The only boundary condition we need to simulate is the top inlet to the duct. Since, if nothing is done, the entire top wall will be treated as a wall (zero velocities) we shall have to overwrite the top velocities. As mentioned earlier in Section 1, the inlet flow is at an angle to the duct axis. We need to therefore resolve this flow vector into a radial and an axial velocity. Since the axial velocity vector does not point into the domain, the entire mass flow enters as a v -velocity, carrying with it a radial momentum and an axial momentum. These momenta are convected into the flow domain. Note that the w -velocities are prescribed at locations between the grid lines in the z -direction.

Four separate indices KFINJ, KLINJ, IFINJ, ILINJ have been created. These define the bounds of the inlet port in the z and θ directions (see Fig. 4). The radial velocities for $J = JMAX$ and $I = IFINJ$ to $ILINJ$, and $K = KFINJ$ to $KLINJ$ are prescribed a value equal to (volume flow/inlet area). The axial velocity (w) is prescribed a value of $v_{inj}/\tan(\alpha)$ where α is the angle of the inlet duct with the duct axis. The inlet turbulent kinetic energy, and the inlet value of the dissipation rate are prescribed based on an intensity of turbulence, length scale and the inlet radial velocity. All these operations are performed in a new subroutine BOUND, called MAIN.

4.4 Prescription of the Initial Guess

Some modifications are necessary to INIT subroutine in order to prescribe a realistic initial flow field. The values prescribed in the modified version are as follows.

$K \leq KLINJ$

$u = 0, v = 0, w = m_d/A$, where m_d = dome flow.

If $m_d = 0$, $w = 1.0 \times 10^{-3}$

$$k = k_{inj} \times w^2; \epsilon = \epsilon_{inj} \times k^{3/2}, p = 0 \quad (4.1)$$

$K > KLINJ$

$u = 0, v = 0, w = (m_d + m_{inj})/A$

$k = k_{inj} \times w^2; \epsilon = \epsilon_{inj} \times k^{3/2}$

$$p = 0 \quad (4.2)$$

4.5 Modifications to MODS

Whenever a wall is encountered, MODS modifies the source terms in the equations in order to incorporate the wall functions. However, at the inlet ports (which are on the KBYP wall), we should not modify the near boundary source terms, because there is no wall in that region (it is an inlet). Consequently, the wall functions are skipped in the region $ILINJ \geq I \geq IFINJ$ and $KLINJ \geq K \geq KFINJ$. Appropriate jumps are provided in each subsection of MODS.

4.6 Modification to Improve Convergence

During the earlier part of the iterative procedure, it was found that because of the impingement of the injection jet on the central region, and because of the incorrect velocity field, large pressure corrections are calculated in the impingement zone. Sometimes, these pressure corrections are so large (10^7 N/m^2) as to make the calculations diverge. Since these large pressure corrections are unrealistic (Note: the maximum

pressure in the domain can not exceed the inlet momentum), a trap was placed on their magnitude. The maximum pressure correction was limited to 1.0E4, which corresponds roughly to the inlet momentum from the injection. The p's calculated were trapped as follows.

$$p' = \max (-1.0E4, p')$$

$$p' = \min (1.0E4, p') \quad (4.3)$$

This modification improved the rate of convergence.

ADJST Procedure

No block adjustment was performed in the region upstream of the inlet ports. Because that region is highly three-dimensional with zero net mass flow across any constant -z plane, it was felt that no benefit will be derived from the adjustment procedure.

4.7 New Input Data

The new input data read for the injection with their meaning are:

INJ Denotes if side injection exists. .True. for side inlets. .False. for no side inlet. If INJ is .False. no further data of injection are read

KFINJ
KLINJ } Indices denoting region of inlet ports
IFINJ
ILINJ }

AMINJ GPM flow of the inlet port per 180 degrees.

ANGINJ Angle of side inlet with duct axis

TKEINJ Inlet kinetic energy (per unit velocity square)

$$k = k_{inj} * w^2$$

boundary boundary

TDINJ Inlet dissipation rate ϵ_{inj} , per $k^{3/2}$

$$\epsilon = \epsilon_{inj} * k^{3/2}$$

5.0 Computational Details

5.1 Finite - difference Grid

Finite difference grids with 11×10 (θ, r) grid nodes in the cross-section and with 35 (-2 in dome position), 31 (0 in.), grid nodes in the z-direction were employed in the calculations. A total of 3500 to 4000 nodes were therefore placed in the solution domain. One finite-difference grid is shown in Figure 4 , for a -2in. dome position ($11 \times 10 \times 35$).

The calculations were performed with the sequence-2 code, FLOW3D-2[1]. The calculations were started from the initial guess described in Section 4, and the changes in successive iterations were monitored. Typically 600 iterations were sufficient for the changes (related to residuals) in variables to decrease to an acceptable accuracy ($\frac{\delta u}{w}, \frac{\delta v}{w} \approx 3 \times 10^{-5}, \frac{\delta w}{w} \approx 1.0 \times 10^{-4}$). The dump restart capability was used. Typically, for 600 iterations, the CYBER system A required 1 1/4 hr of computing time.

5.2 Accuracy of the Computations

All calculations presented in Section 6 were performed with a 11×10 grid in the cross-sectional plane, and with 31 and 35 grid nodes in the z-direction. These calculations required a storage of about 170K Octal words, which was just the storage amount available for daytime runs. The biggest finite-difference grid that could be accommodated on the WPAFB computer was $20 \times 15 \times 40$ (12000 nodes) grid, which required a storage of 376000 Octal words (the maximum storage allowed on WPAFB's computer). Because of the slow turnaround of large-memory, large-time jobs, it was not possible to perform calculations with the 12,000 node finite-difference grid. Therefore, it is not possible to assess the magnitude of the finite-differencing errors in the present calculations. It is advocated therefore that these results not be used for precise quantitative comparisons and design purposes.

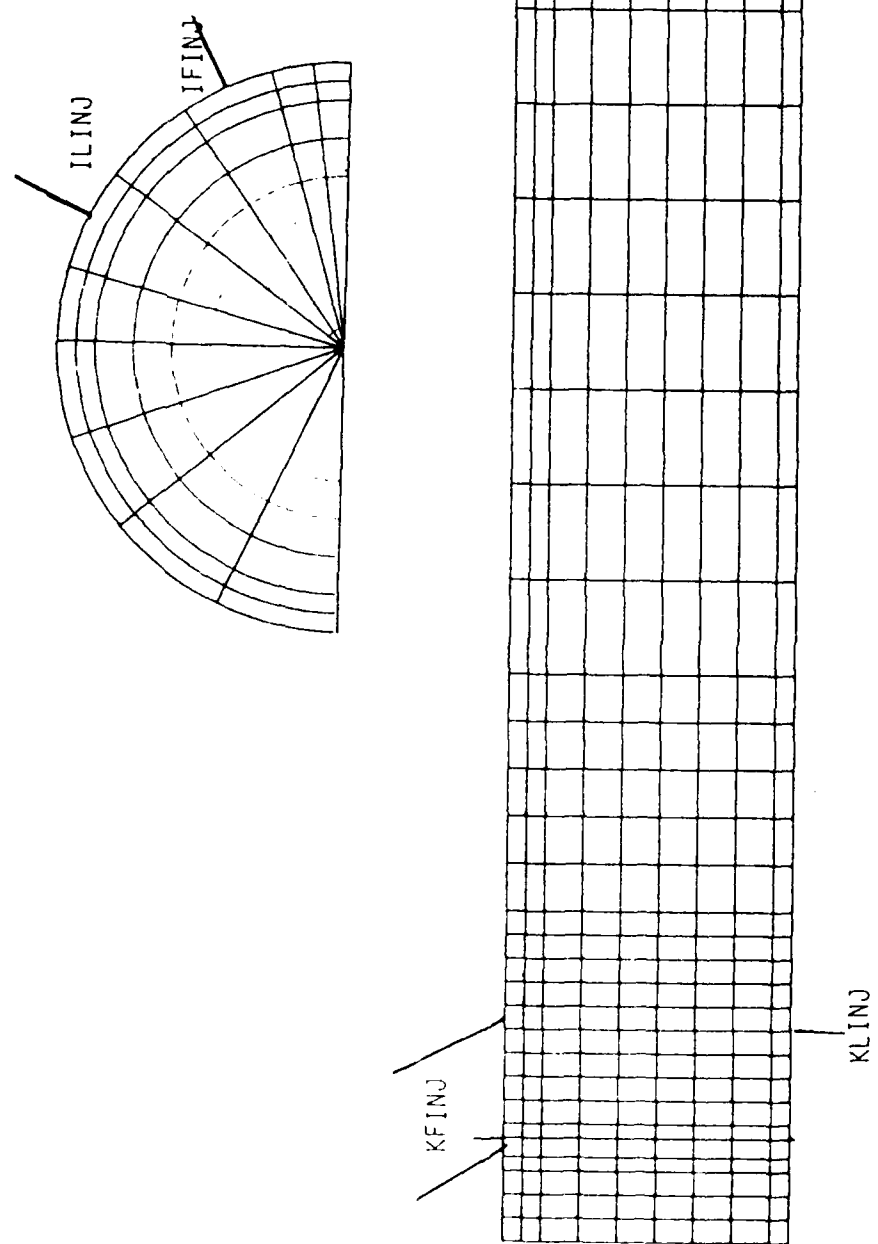


FIGURE 4
LOCATION OF INJECTION PORTS AND A TYPICAL FINITE-DIFFERENCE GRID



FIGURE 3

FLOW PATTERN IN THE VERTICAL (r-z) PLANE
(LIGHT SOURCE PLACED PARALLEL TO DUCT AXIS)



FIGURE 2
GENERAL FLOW PATTERN IN CROSS-SECTIONAL PLANE

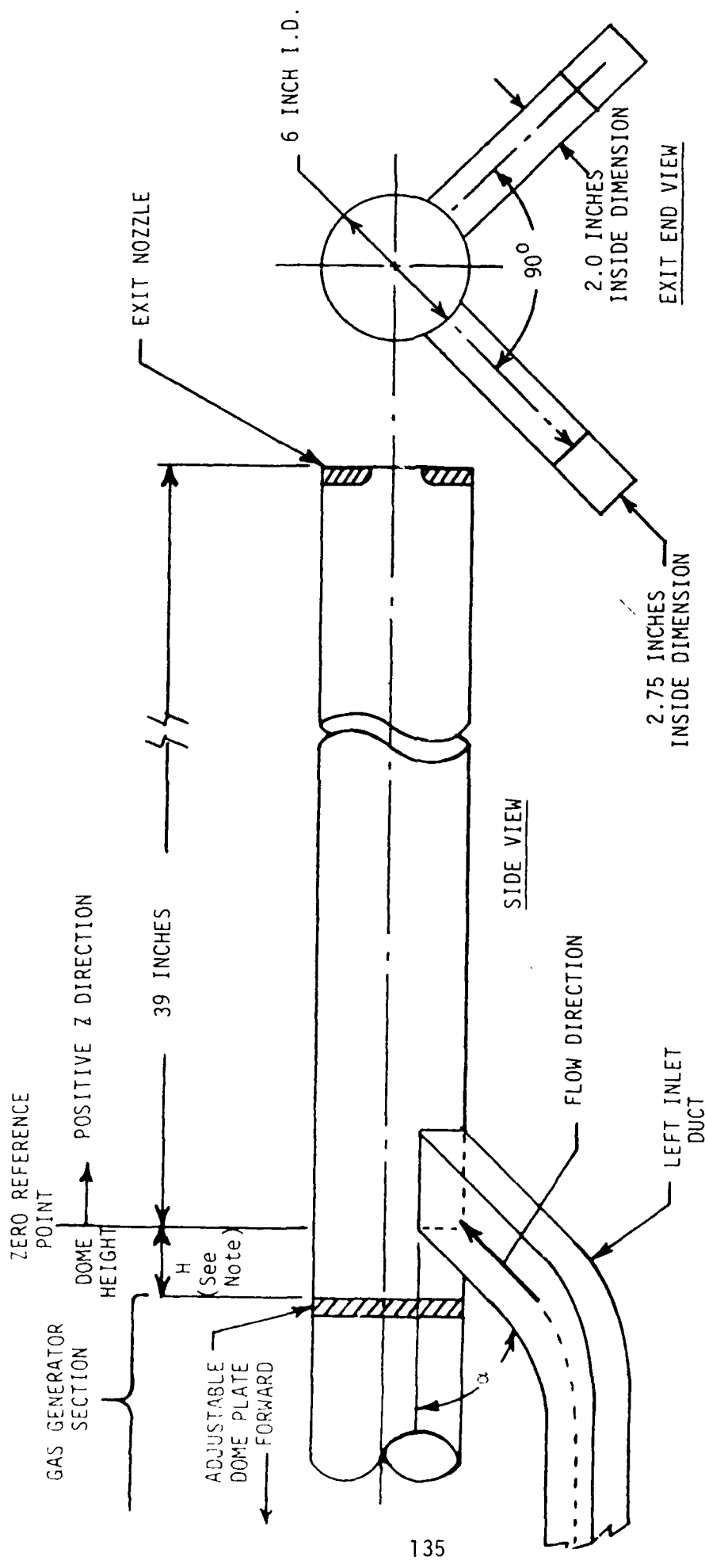


FIGURE 1. WATER TUNNEL COMBUSTOR CONFIGURATION

9.0 References

1. Vanka, S.P. 'FLOW3D: A computer program for modelling three-dimensional recirculating turbulent flows and heat transfer', under preparation as an Argonne National Laboratory report.

8.0 Acknowledgements

The author appreciates the encouragement and opportunity provided by Drs. F.D. Stull and R.R. Craig of Ramjet Technology Division, WPAFB, Ohio to undertake this short assignment. The help provided by Mr. G.D. Streby of UES in discussing the experimental data, and in other administrative matters is very much appreciated. Finally, during this period, I have enjoyed the friendly working atmosphere provided by Dr. R.S. Boray of Ramjet Technology Division, WPAFB, Professor E.F. Brown of VPISU, Virginia and Dr. W.H. Harch of ARL, Melbourne Australia, to whom I offer my special thanks.

7.0 Summary

Computations have been performed of the flow field development in side inlet dump combustor geometries relevant to ducted rockets. The computations have been performed with a modified version of the FLOW3D code. A set of four (4) calculations have been performed with combinations of dome plate positions and injection (inlet) angles, for a volume flow of 150 gpm of water. The calculated results agree qualitatively with the flow visualization data in the WPAFB water tunnel. Some disagreement is observed in the flow region between the dome plate and the inlet ports. This region is characterized by complex interaction of shear driven flow and a spill over inlet flow. The flow velocities are small and in some cases bistable and asymmetrical. Further detailed measurements and improved (mesh refined) calculations are required to improve the predictions.

6.6 Summary

The flow field development in the side inlet dump combustor appears to be very complex. It contains several three-dimensional vortices and recirculation zones. Such complex flow motions can have significant effects on the fuel mixing and combustion characteristics of the combustor. The present calculations reveal some of these features.

The recirculation zones seen in plots at $I=7$ to 9 also have decreased in size. Intuitively, this may appear questionable, but with a deeper look into the flow, this decrease may be due to the following reason. Let us first consider the case of a jet in a cross wind. The more the jet is normal to the flow, we expect a larger recirculation region ahead of the jet. Therefore going from 45° to 60° angle, we expect a larger recirculation angle. However, the present case is somewhat different than that of a jet in a cross wind. First, there is no other cross flow except that produced by the inlet flow itself. Second, if the flow is injected at 90° to the duct axis, we will see a helical flow pattern with an axis at the centre of the cross-stream eddy. In such a case we may not see any flow recirculation behind the inlet jet. Because the flow is coming at an angle to the duct axis the stagnant zone may have been created by the impingement of the inlet jet. The size of this will therefore depend on the injection angle, the smaller the angle, the larger may be the recirculation zone. If the angle is decreased to 30° , the recirculation eddy may be stretched further into the domain.

The above explanation is only a hypothesis and it is tentative. It is necessary to perform more calculations and compare them with flow visualizations in appropriate planes (this may be hard to obtain) to confirm the present findings and explanations.

6.5 Other Calculations

Figures 13-14 show the flow patterns for a case with 60° injection and $0''$ dome position. We now observe the effects of both the injection angle and the dome position. For this case, the dome eddy is compressed further to the extent that it appears as a ring vortex (at $I=6$). The effect of the higher injection angle on the flow ahead of the inlet jet is similar to that discussed in Section 6.4.

dome plate. As a result, the two-vortex pattern begins to form at the dome plate itself, but is not clearly formed because of the interaction with the dome plate. There are no qualitative differences in the cross-sectional plane between the 0" and the 2" cases. The two vortex pattern behaves similar to the 2" base case.

In the (r-z) planes, because now the injection is nearer to the dome plate, the dome region eddy is compressed and is smaller. The shape of the eddy is triangular at planes I=4 and I=5. The recirculation region observed in front of the inlet jet is nearly of the same size and shape. But for some other minor differences, the main effects of the smaller dome height are

- a) to compress the dome recirculation region and
- b) to alter its shape by making the eddy to form near the central region.

6.4 Effect of Injection Angle

Another parameter considered towards investigating for an optimum design is the angle of flow injection (with the duct axis). In the base case this was 45°. To investigate the effects of a change in the injection angle, calculations have been performed for a configuration in which the dome height is 2" but the injection angle is 60°. A larger injection angle implies the same radial (v) velocity but a smaller axial-velocity component.

The results for the 60°, 2" dome position are shown in Figs. 11-12. Again, the qualitative patterns in the cross-sectional plane have not changed, but some quantitative differences exist because of the larger radial component of the flow. In the (r-z) plane however, an interesting feature is observed. From Figure 12, at I=5 and 6, it is seen that the recirculation zone in front of the jet has diminished in size considerably.

top wall and the centre. At $I=3$, which is adjacent to the inlet port, we observe the characteristics of the inlet flow and the eddy in the dome region.

It can be seen that the flow is very much three-dimensional, and contains several vortices which vary in size three-dimensionally. Such a flow will have significant effect on the mixing of fuel with the air and will influence the combustion phenomena significantly. In the ducted rocket case however, there will be a central injection from the gas generator which will further complicate the flow field.

6.2 Comparison with Flow Visualizations

A large number of photographs have been taken by UES of the flow development in the present geometry. Photographs have been taken of the cross-sectional flow and of the flow in a plane corresponding to $I=11$ in the notation of Figure 7. Two of these pictures have been shown earlier in Figure 2 and 3. It is seen that good agreement of the cross-sectional two-vortex pattern is obtained. Although the photographs do not reveal the magnitude of the velocities for comparison, the sizes of the two vortices appear to be in good quantitative agreement with the calculated patterns. In the plane along the duct axis, the flow split and the streamline pattern is well predicted. However, the flow visualizations indicate a vortex in the dome region, which is not seen in the calculations. It is not clear whether this vortex is a steady one nor it is known how strong the vortex is. Further investigations, both analytical and experimental, are required to resolve this discrepancy.

6.3 Effect of Dome Position

Figures 8-10 show the finite-difference grid, the cross-sectional and radial flow patterns for a configuration with 45° injection and $0''$ dome position. In this configuration, the injection is directly at the

cross-sectional planes in the dome region show the two-vortex patterns similar to the rest of the flow, except immediately adjacent to the dome plate. The two-vortex pattern continues to exist throughout the flow, albeit with decreasing magnitudes of the velocities. It is also observed that as the flow develops the centre of the larger vortex rotates clockwise towards the injection ports.

The flow pattern in the $(r-z)$ planes is much more complex than that in $(r-\theta)$ planes. We shall first consider the flow pattern at the two azimuthal planes of injection ($I=4$ and 5). Here we observe that the angled inlet jet sets up a vortex pattern between the dome and the first inlet port. This vortex is driven both by shear of the jet, and by the spill over flow from the inlets. At $I=4$, we observe that the angled streamlines from the top wall impinge on the central plane and eventually straighten out. At $I=5$, however, a recirculation zone forms ahead of the bent stream lines. This zone of negative and stagnant flow increases at higher azimuthal angles. For example, at $I=7$ (90°), a large recirculation region spanning up to 2 duct diameters from the inlet port is observed. The dome region vortex still exists, but has a slightly different shape.

The axial recirculation region of $I=7$ decreases in magnitude as we proceed towards larger azimuthal angles. The vortex moves towards the dome and the streamlines now emerge partly from the centre and partly from the top wall. The recirculation eddy is attached to the top wall. At further azimuthal angles we observe the radial outflow corresponding to the cross-sectional flow pattern earlier discussed. The 'fing' streamline between the forward and backward turning flow (at $I=10, 11$) occurs at $2''$ from the inlet ($4''$ from the dome). The flow patterns at $I=1$ and 2 reflect the features of the smaller vortex (shear driven) of the cross-sectional planes. It can be seen that we have taken a section through the vortex, and consequently we observe a zone of zero radial flow between the

6.0 Results and Discussion

6.1 General Flow Pattern

A total of 4 test calculations have been performed in which the dome position and the injection angle have been varied. The general flow patterns observed in these cases have nearly been the same, but the extent of the recirculation zones, and the vortex regions have been different. We shall first present the results for a base case of 45 degrees injection and 2" dome position and discuss the general flow behavior. In Sections (6.3) and (6.4) we present the results displaying the influences of the injection angle and the dome position.

The amount of information that a three-dimensional calculation produces is enormous and difficult to comprehend in a raw form. Even with detailed flow patterns in various cross-sectional planes, the present flow situation is hardly easy to understand, for it contains several three-dimensional vortex regions which are difficult to visualise through two-dimensional plots. Figure 6 shows the flow patterns in the cross-sectional ($r-\theta$) planes at several axial positions. The distances of each K plane are shown in Figure 5 and Table 1. Figure 7 shows the flow patterns along planes of constant θ .

We first observe that the angled (aximuthal direction) injection into the cross-sectional plane sets up two vortices (a total of four in the complete duct). The first one is driven by the convected flow, whereas the second one is a shear driven vortex which is formed behind the inlet jet. The formation of these vortices is strongest at the inlet ports ($K = 6$ to 11), after which the vortices decrease in strength as they flow towards the nozzle. In the region between the dome plate and the inlet port, the flow is also shear driven but some flow spills over from the inlets. The dome flow is therefore very complex. The present calculations of the flow in

In the future investigations, it is planned to refine the grid progressively even beyond the 12000 node grid, by new computational techniques, and assess the magnitude of error reductions achieved with mesh refinement. The results of Section 6 however display good qualitative agreement with flow visualizations, and illustrate the capabilities of the solution technique to predict the dump combustor flow fields.

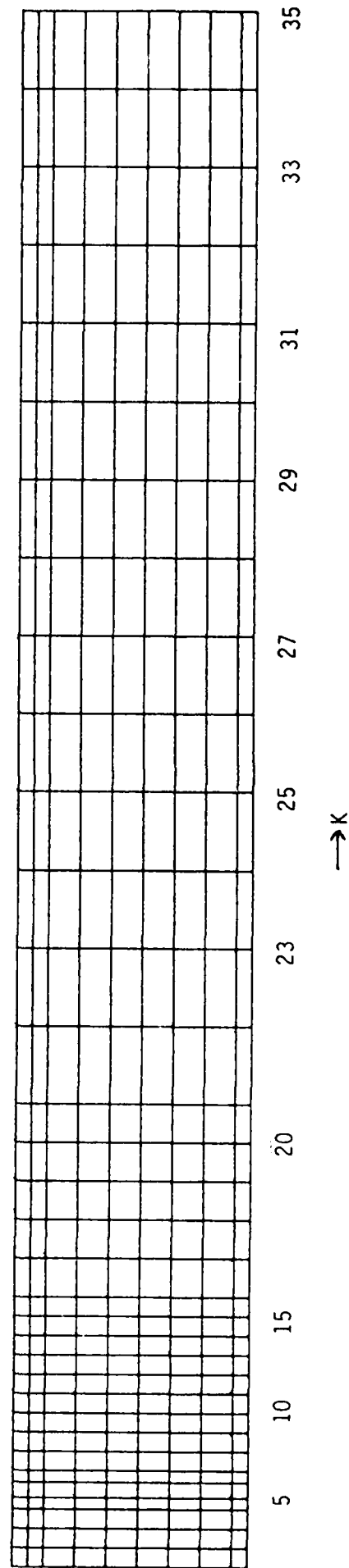
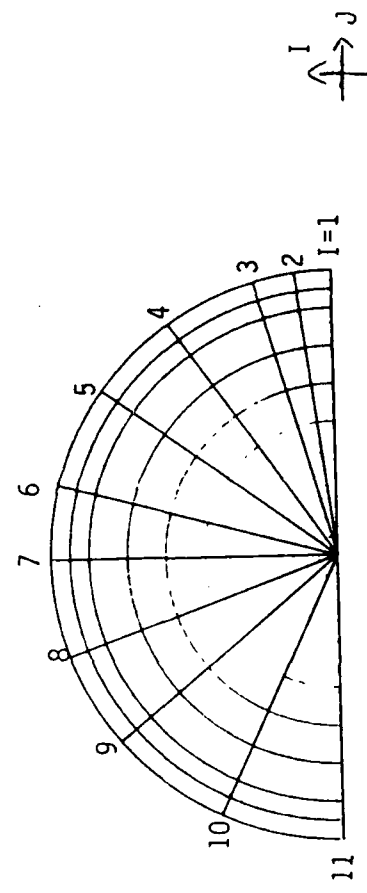


FIGURE 5

FINITE-DIFFERENCE GRID FOR -2 INCH DOME POSITION

Table 1. Finite-Difference Grid Used in Computations
($H = 2$ inches)

X-Grid (degrees)

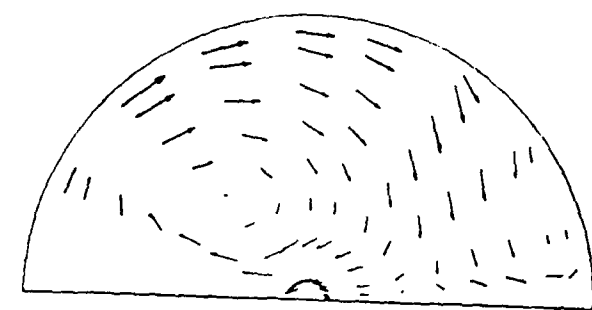
$x(1) = 0.0$	$x(2) = 7.5$	$x(3) = 16.0$
$x(4) = 35.0$	$x(5) = 54.0$	$x(6) = 75.0$
$x(7) = 90.0$	$x(8) = 110.0$	$x(9) = 130.0$
$x(10) = 155.0$	$x(11) = 180.0$	

Y-Grid (inches)

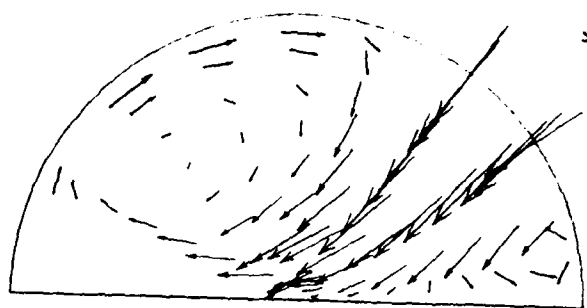
$y(1) = 0.0$	$y(2) = 0.2$	$y(3) = 0.6$
$y(4) = 1.0$	$y(5) = 1.4$	$y(6) = 1.8$
$y(7) = 2.2$	$y(8) = 2.6$	$y(9) = 2.8$
$y(10) = 3.0$		

Z-Grid (inches)

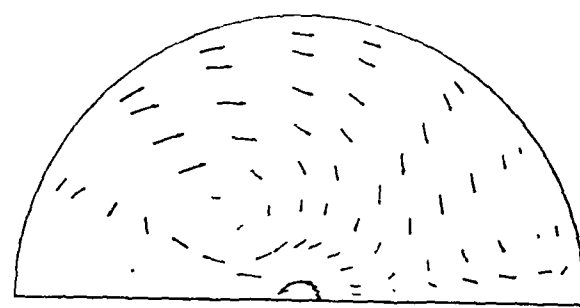
$z(1) = 0.0$	$z(2) = 0.5$	$z(3) = 1.0$
$z(4) = 1.5$	$z(5) = 1.8$	$z(6) = 2.2$
$z(7) = 2.5$	$z(8) = 3.0$	$z(9) = 3.5$
$z(10) = 4.0$	$z(11) = 4.5$	$z(12) = 5.0$
$z(13) = 5.5$	$z(14) = 6.0$	$z(15) = 6.5$
$z(16) = 7.0$	$z(17) = 8.0$	$z(18) = 9.0$
$z(19) = 10.0$	$z(20) = 11.0$	$z(21) = 12.0$
$z(22) = 14.0$	$z(23) = 16.0$	$z(24) = 18.0$
$z(25) = 20.0$	$z(26) = 22.0$	$z(27) = 24.0$
$z(28) = 26.0$	$z(29) = 28.0$	$z(30) = 30.0$
$z(31) = 32.0$	$z(32) = 34.0$	$z(33) = 36.0$
$z(34) = 38.0$	$z(35) = 40.0$	



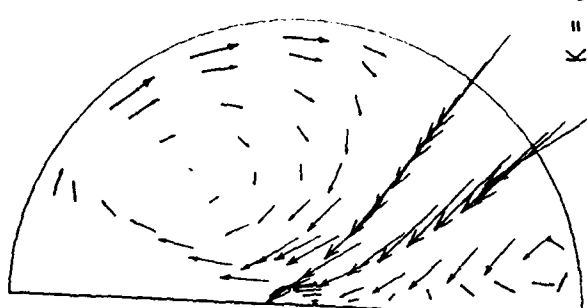
$K = 2$



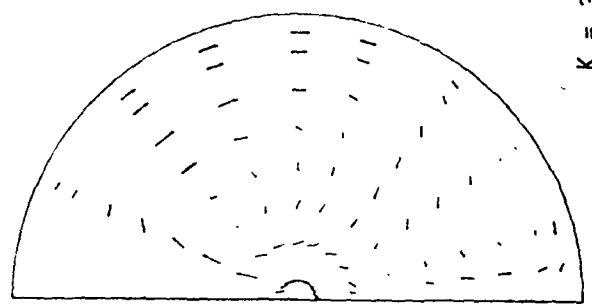
$K = 5$



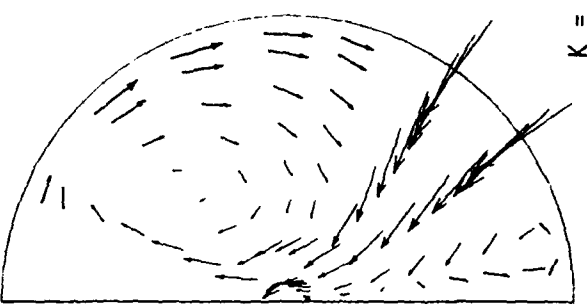
$K = 4$



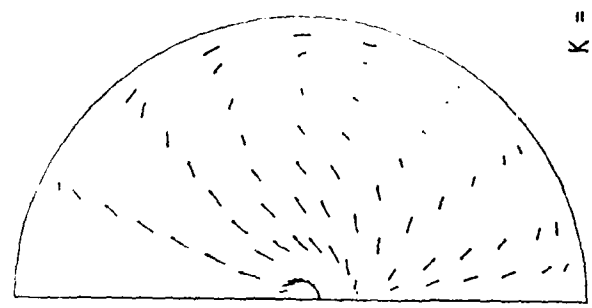
$K = 8$



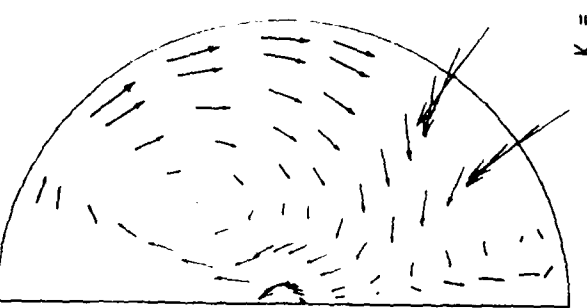
$K = 3$



$K = 7$

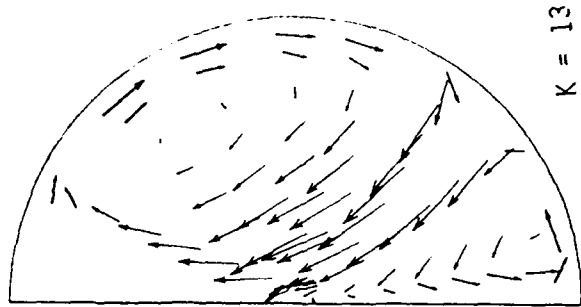


$K = 6$



$K = 9$

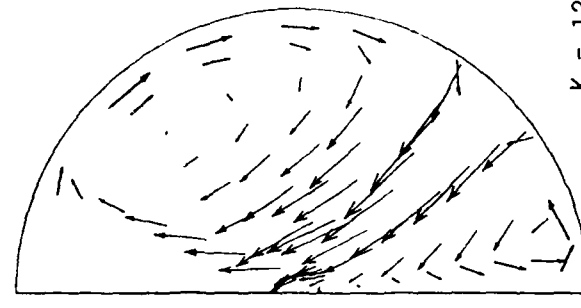
FIGURE 6. FLOWFIELD IN $(r-\theta)$ PLANE FOR $\alpha = 45^\circ$, $H = 2$ INCHES
FIRST PLOT



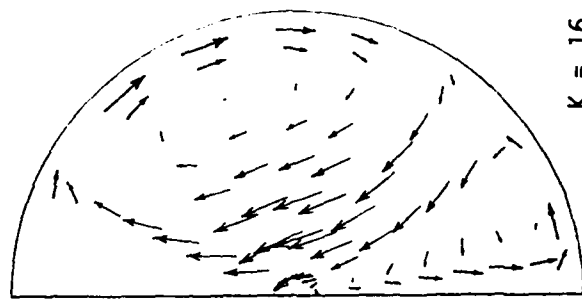
$K = 13$



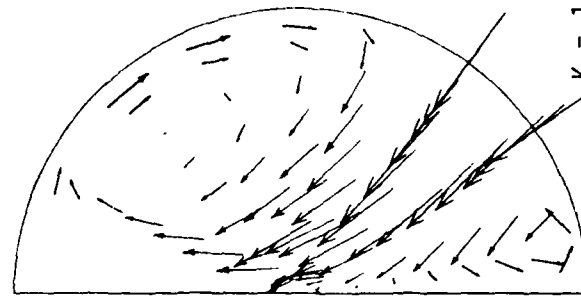
$K = 17$



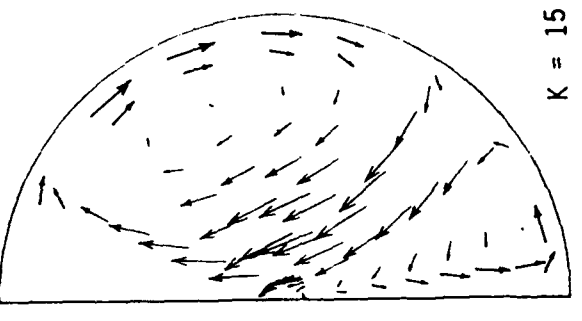
$K = 12$



$K = 16$



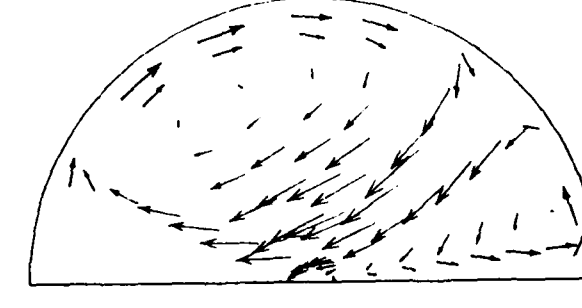
$K = 11$



$K = 15$



$K = 10$



$K = 14$

FIGURE 6 (Contd) FLOWFIELD IN $(r-\theta)$ PLANE FOR $\alpha = 45^\circ$, $H = 2$ INCHES
SECOND PLOT

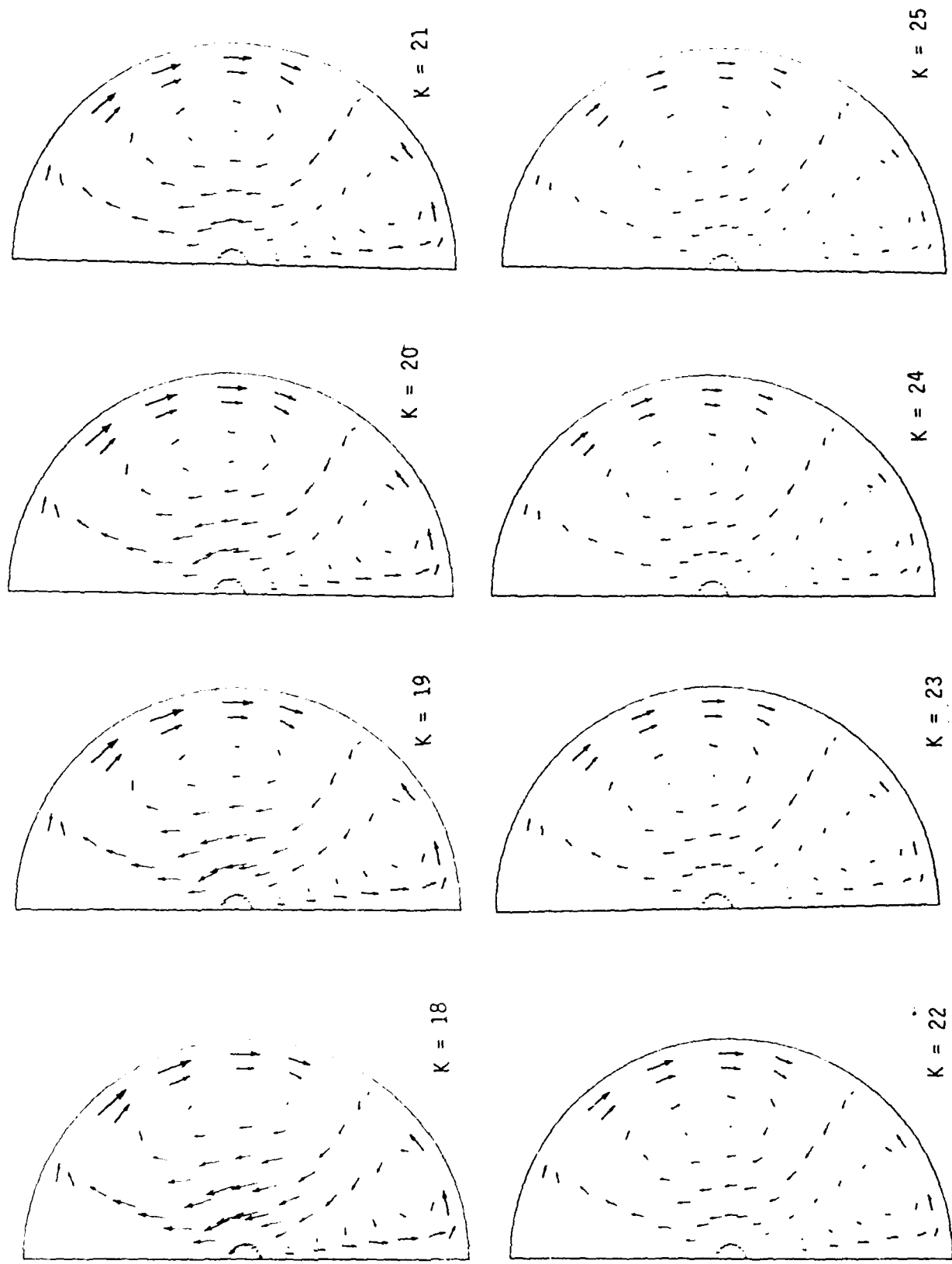


FIGURE 6 (Contd) FLOWFIELD IN $(r-\theta)$ PLANE FOR $\alpha = 45^\circ$, $H = 2$ INCHES
THIN PLATE

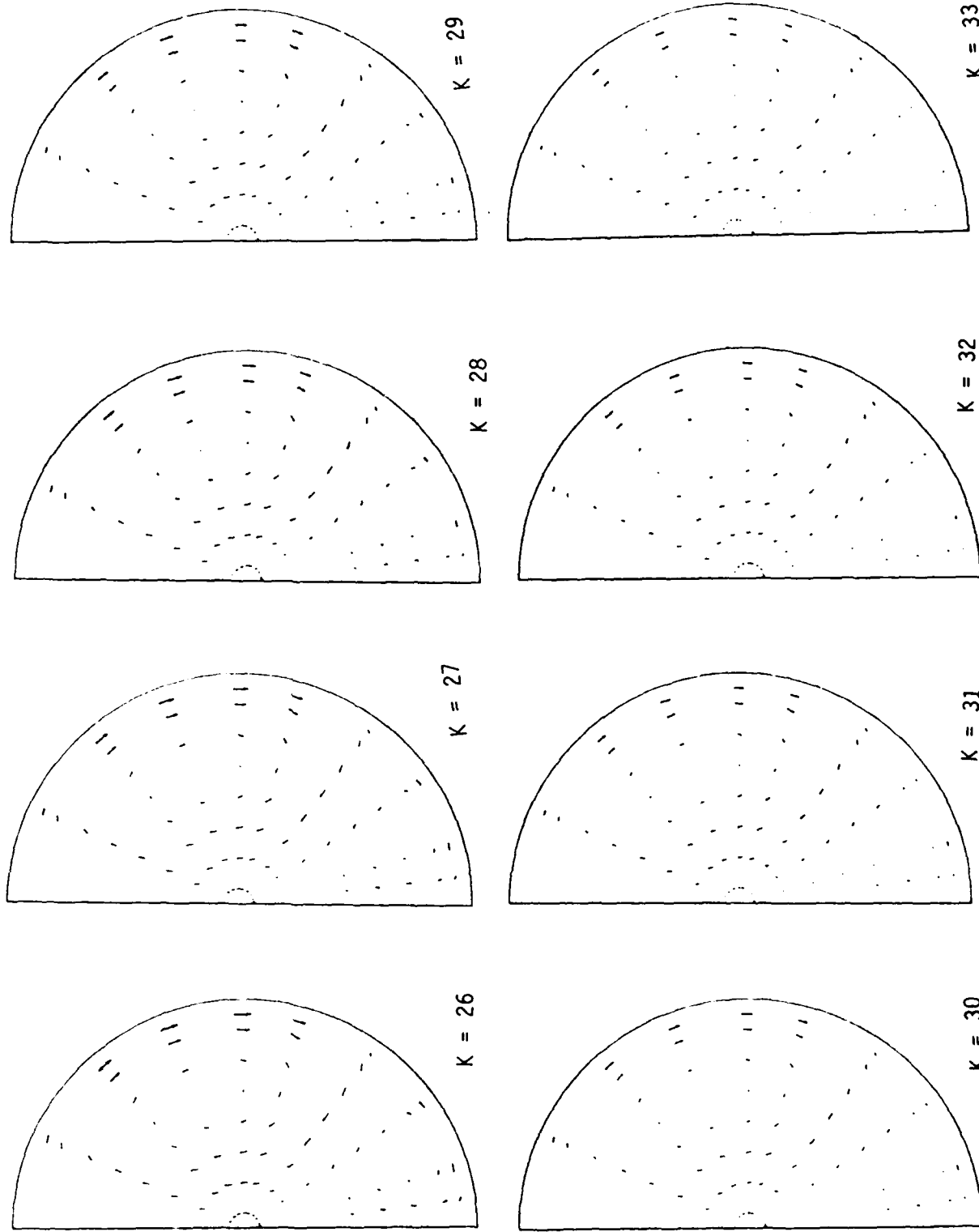
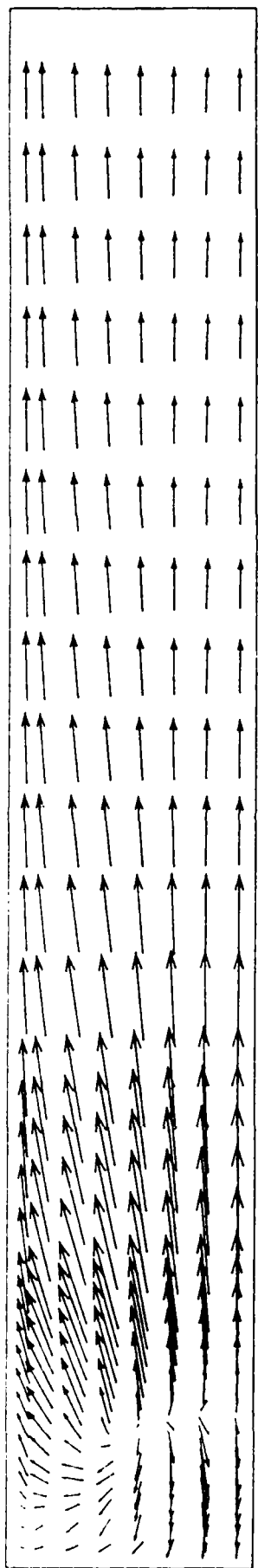
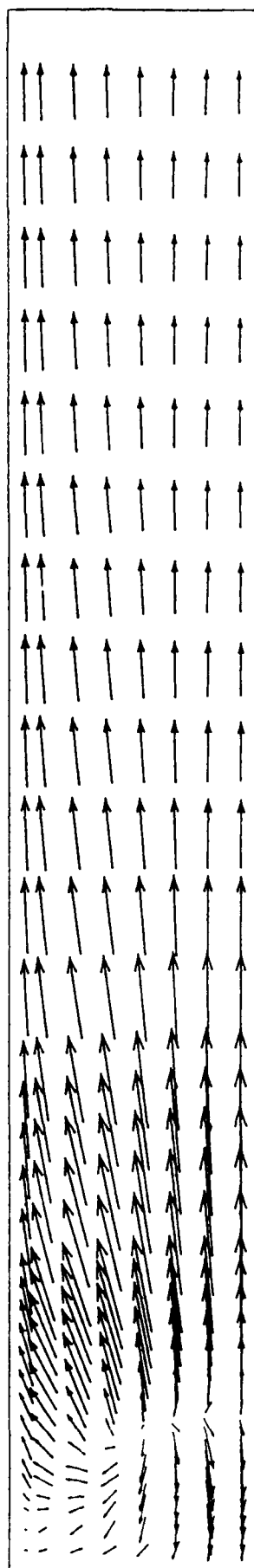


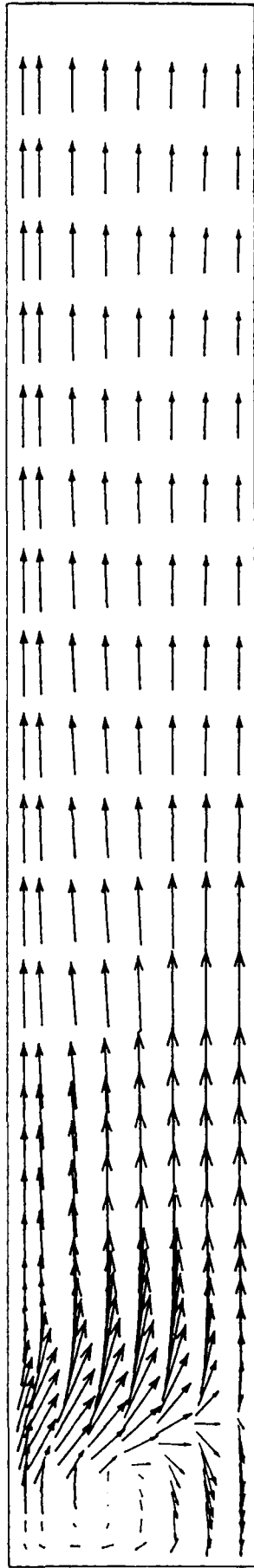
FIGURE 6 (Contd) FLOWFIELD IN $(r-\theta)$ PLANE FOR $\alpha = 45^\circ$, $H = 2$ INCHES
 READING FROM LEFT TO RIGHT



$I = 1$

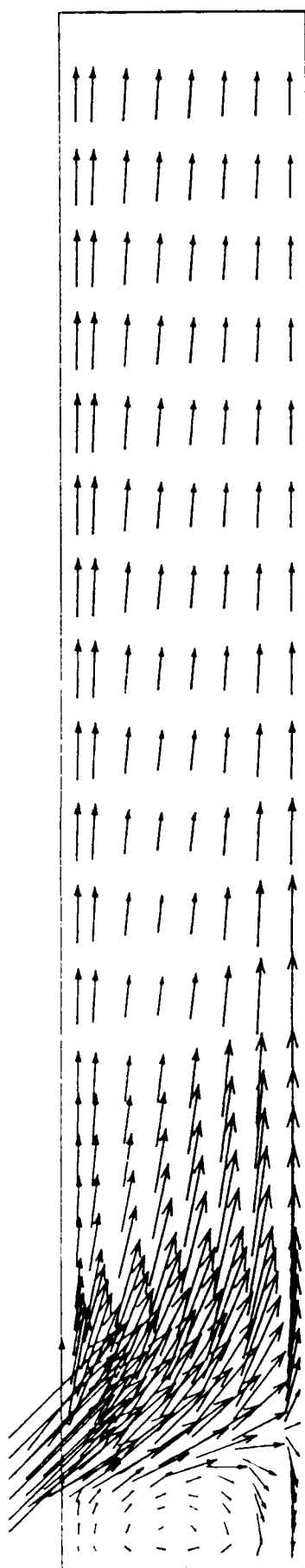


$I = 2$

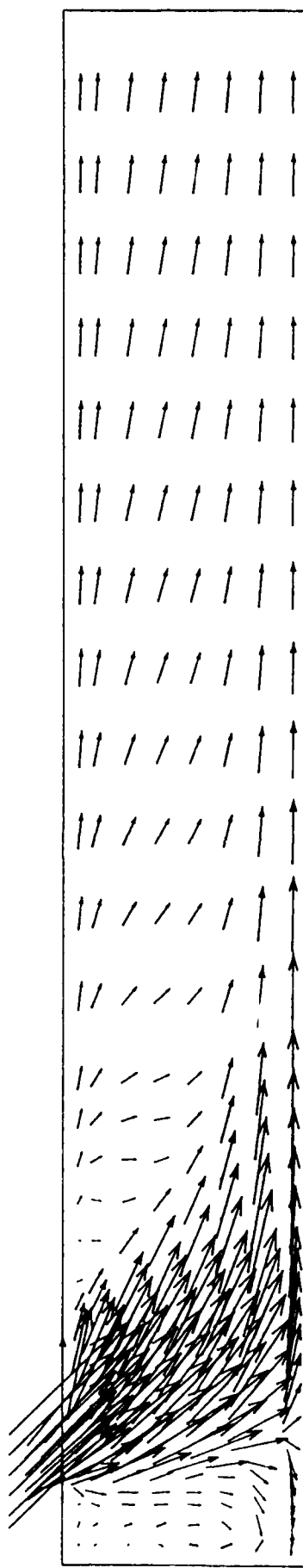


$I = 3$

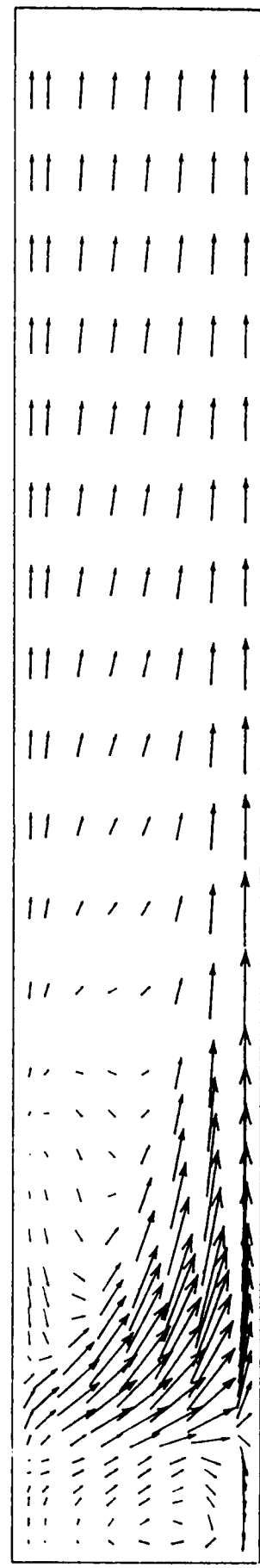
FIGURE 7. FLOWFIELD IN $(r-z)$ PLANE FOR $\alpha = 45^\circ$, $H = 2$ INCHES



$I = 4$



$I = 5$



$I = 6$

FIGURE 7. (Contd) FLOWFIELD IN $(r-z)$ PLANE FOR $\alpha = 45^\circ$, $H = 2$ INCHES

SECOND PLOT

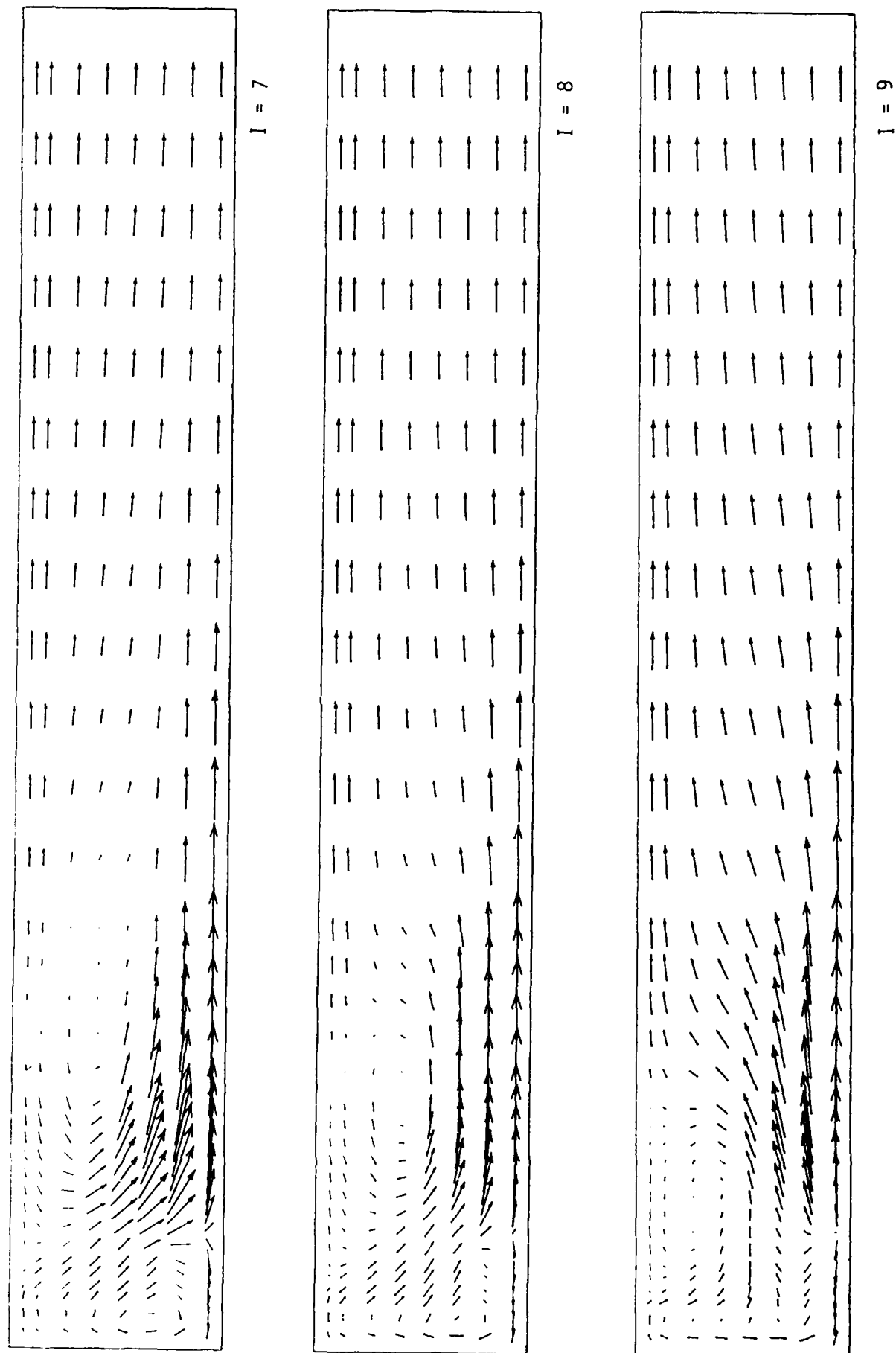
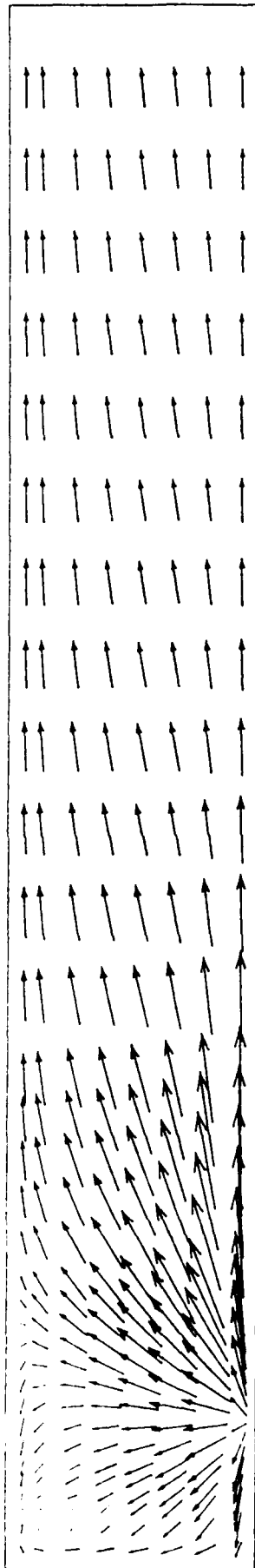
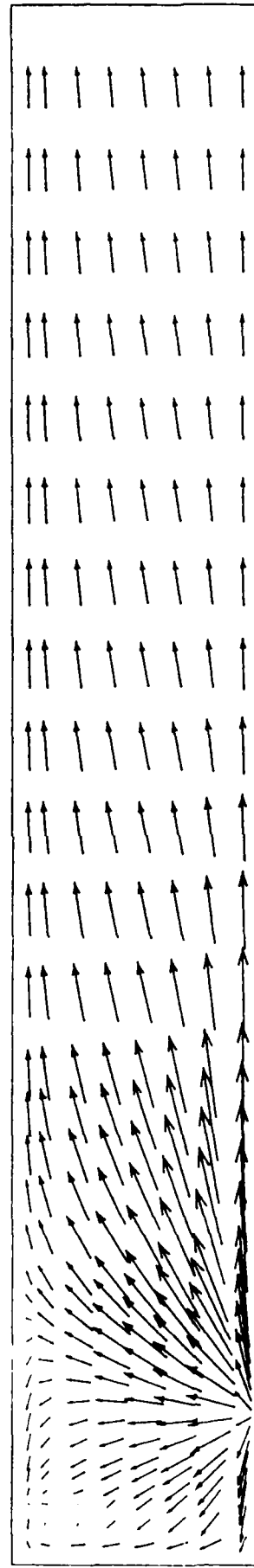


FIGURE 7. (Contd) FLOWFIELD (r - z) PLANE FOR $\alpha = 45^\circ$, $H = 2$ INCHES

THIRD PLOT



$I = 10$



$I = 11$

FIGURE 7. (Contd) FLOWFIELD IN $(r-z)$ PLANE FOR $\alpha = 45^\circ$, $H = 2$ INCHES

FOURTH PLOT

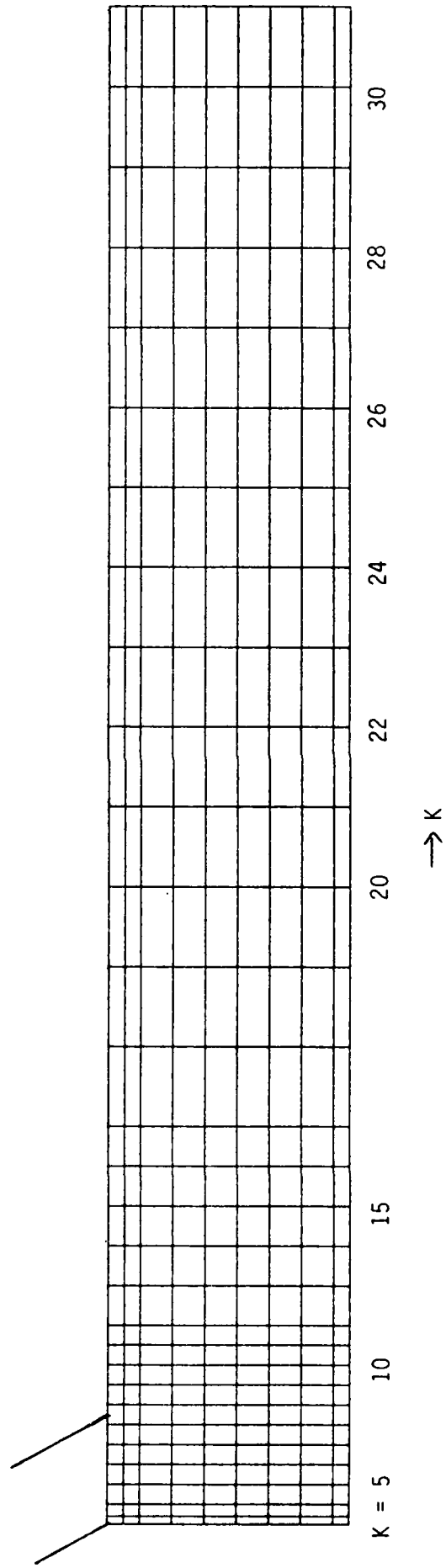
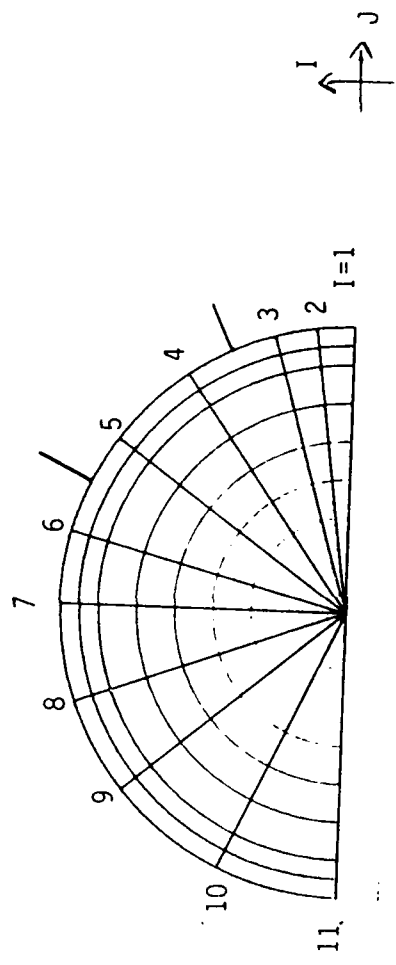


FIGURE 8. FINITE DIFFERENCE GRID FOR THE 0 INCH DOME POSITION

Table 2. Finite-Difference Grid Used in Computations
($H = 0$ inches)

X-Grid (degrees)

$x(1) = 0.0$	$x(2) = 7.5$	$x(3) = 16.0$
$x(4) = 35.0$	$x(5) = 54.0$	$x(6) = 75.0$
$x(7) = 90.0$	$x(8) = 110.0$	$x(9) = 130.0$
$x(10) = 155.0$	$x(11) = 180.0$	

Y-Grid (inches)

$y(1) = 0.0$	$y(2) = 0.2$	$y(3) = 0.6$
$y(4) = 1.0$	$y(5) = 1.4$	$y(6) = 1.8$
$y(7) = 2.2$	$y(8) = 2.6$	$y(9) = 2.8$
$y(10) = 3.0$		

Z-Grid (inches)

$z(1) = 0.0$	$z(2) = 0.2$	$z(3) = 0.5$
$z(4) = 1.0$	$z(5) = 1.5$	$z(6) = 2.0$
$z(7) = 2.5$	$z(8) = 3.0$	$z(9) = 3.5$
$z(10) = 4.0$	$z(11) = 4.5$	$z(12) = 5.0$
$z(13) = 6.0$	$z(14) = 7.0$	$z(15) = 8.0$
$z(16) = 9.0$	$z(17) = 10.0$	$z(18) = 12.0$
$z(19) = 14.0$	$z(20) = 16.0$	$z(21) = 18.0$
$z(22) = 20.0$	$z(23) = 22.0$	$z(24) = 24.0$
$z(25) = 26.0$	$z(26) = 28.0$	$z(27) = 30.0$
$z(28) = 32.0$	$z(29) = 34.0$	$z(30) = 36.0$
$z(31) = 38.0$		

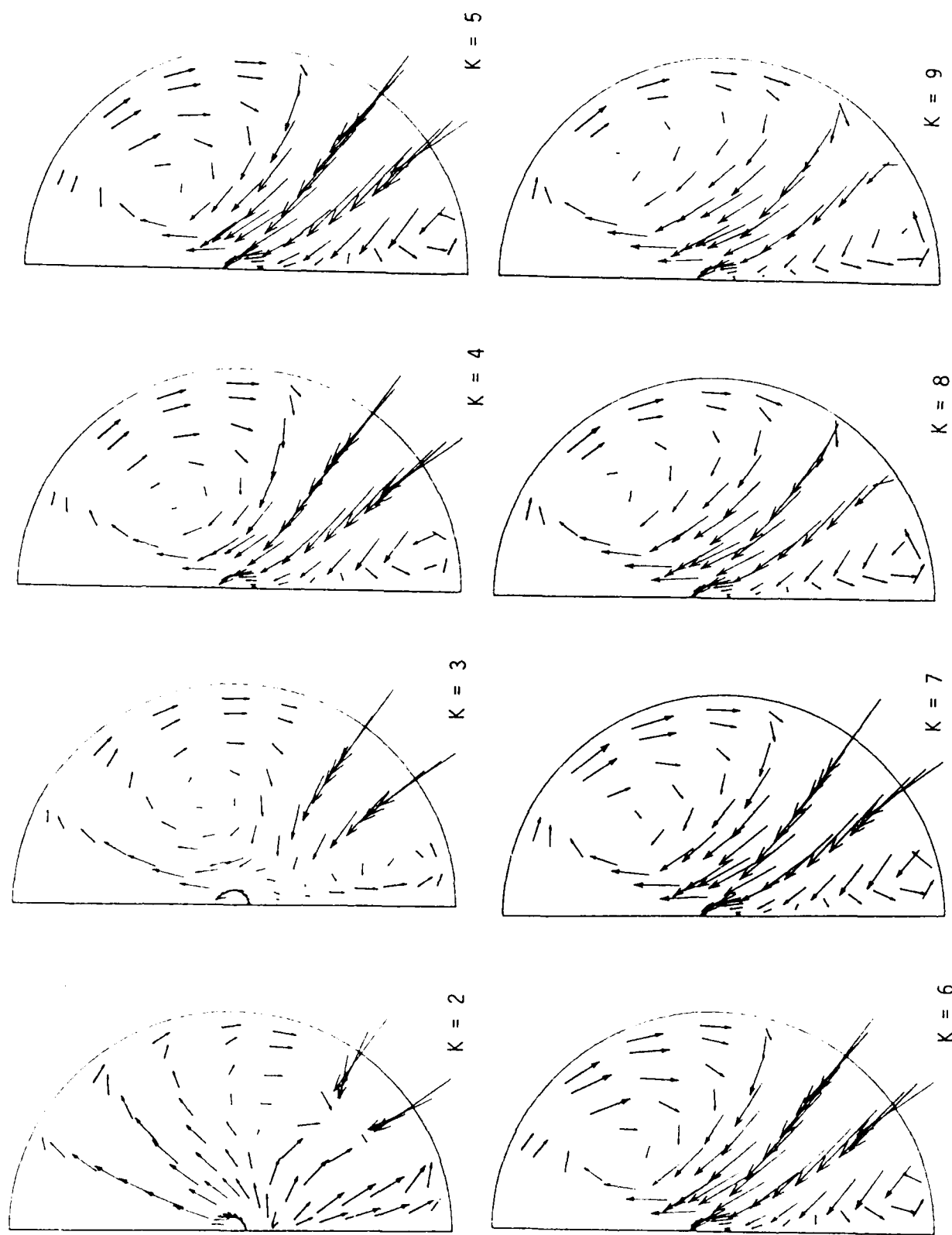
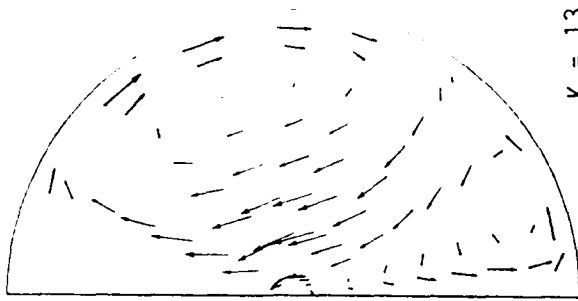
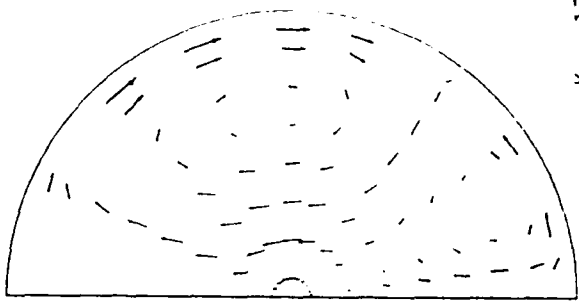


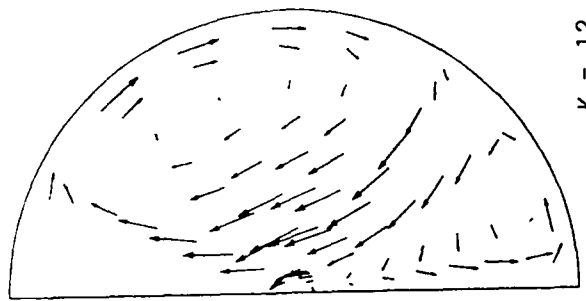
FIGURE 9. FLOWFIELD IN $(r-\theta)$ PLANE FOR $\alpha = 45^\circ$, $H = 0$ INCHES
FIRST PLOT



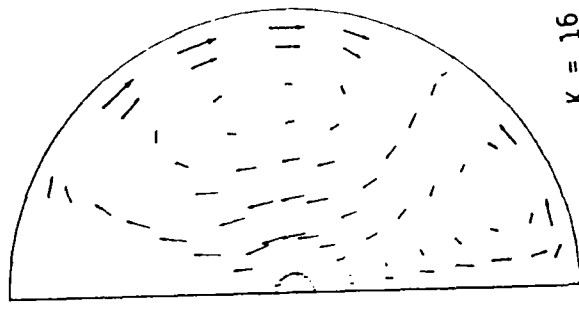
$K = 13$



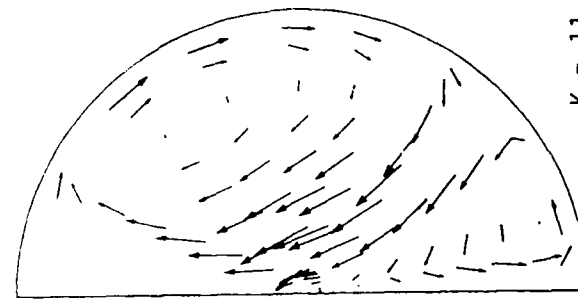
$K = 17$



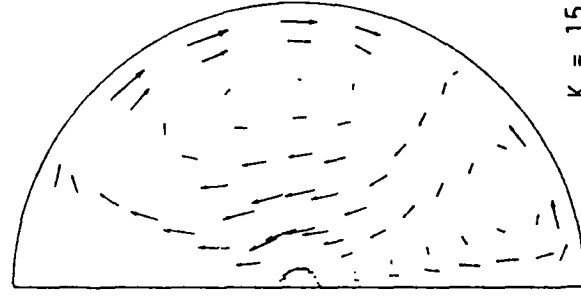
$K = 12$



$K = 16$



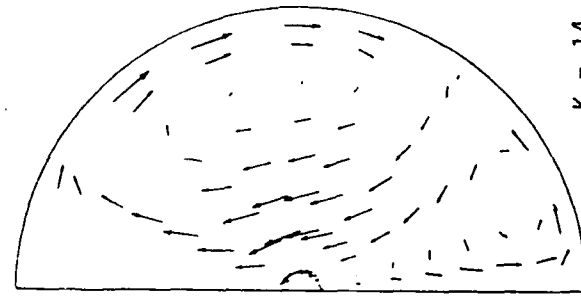
$K = 11$



$K = 15$



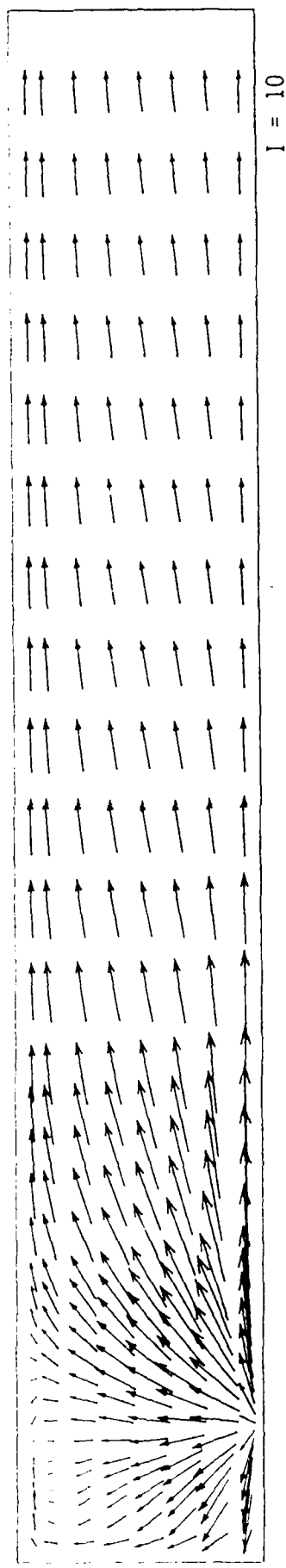
$K = 10$



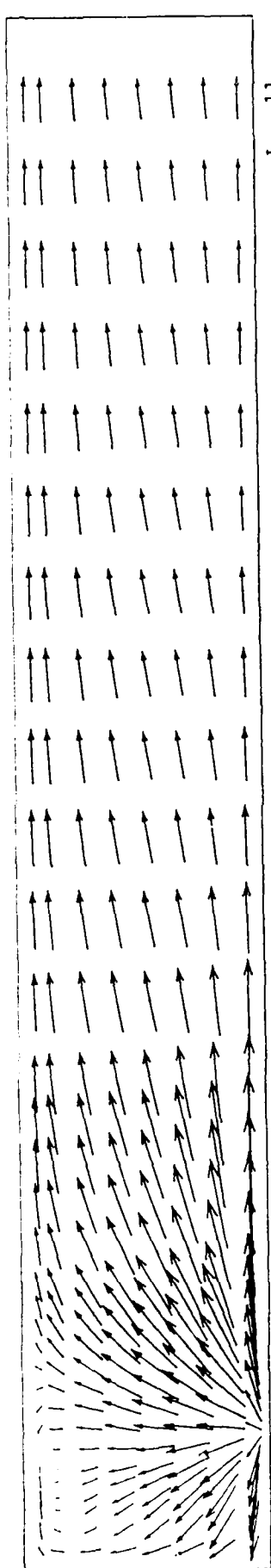
$K = 14$

FIGURE 9. (Contd) FLOWFIELD IN $(r-\theta)$ PLANE FOR $\alpha = 45^\circ$, $H = 0$ INCHES

SECTION D-D



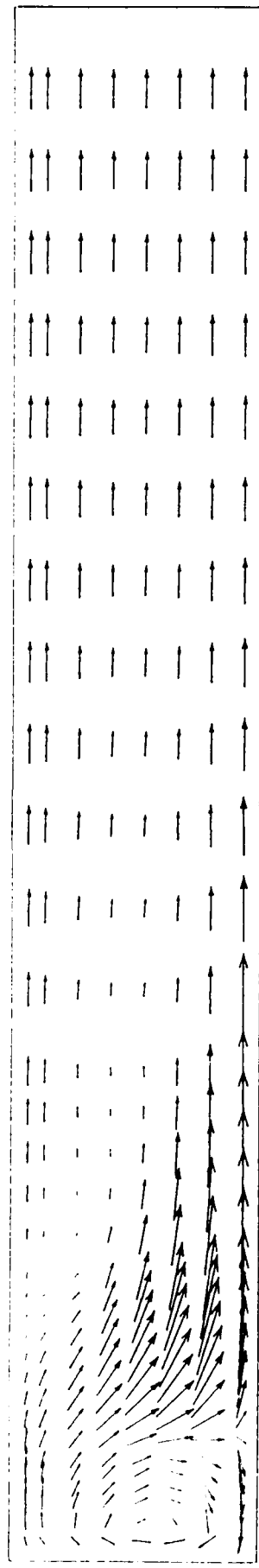
$I = 10$



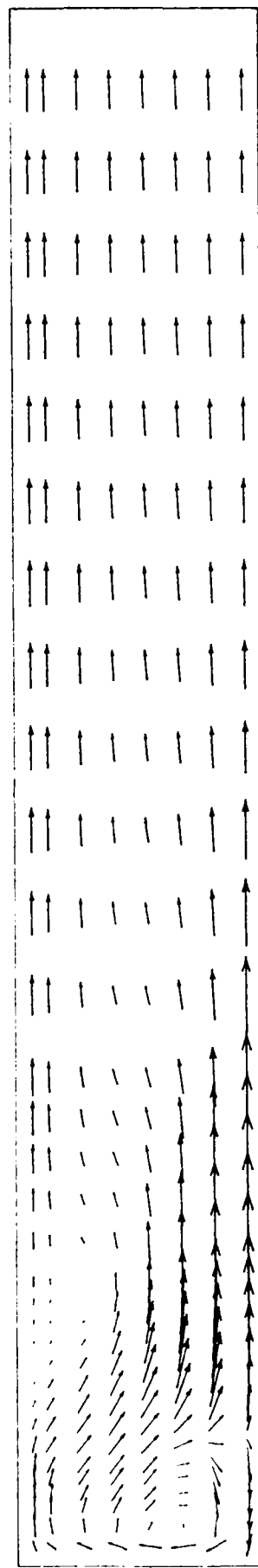
$I = 11$

FIGURE 12. (Contd) FLOWFIELD IN $(r-z)$ PLANE FOR $\theta = 60^\circ$, $H = 2$ INCHES

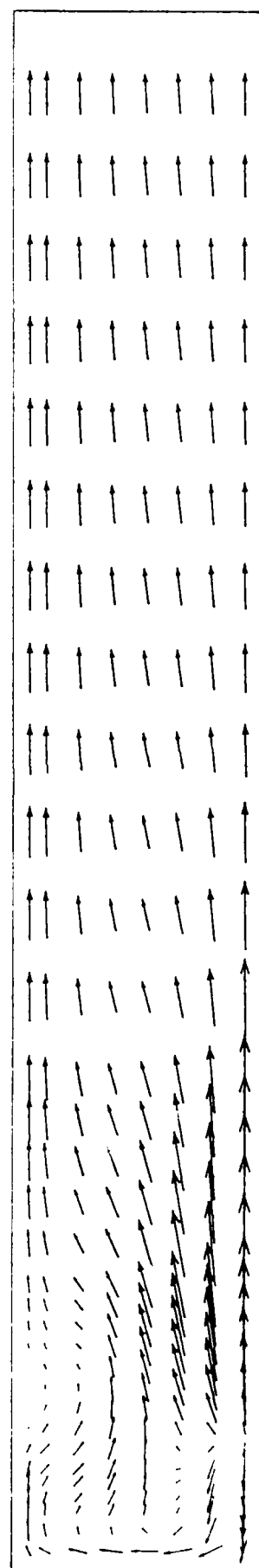
FOURTH PLOT



$I = 7$



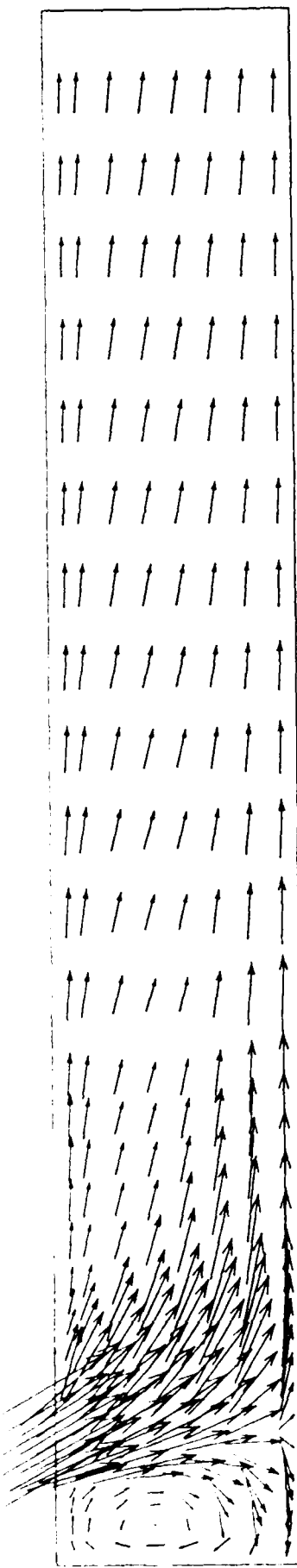
$I = 8$



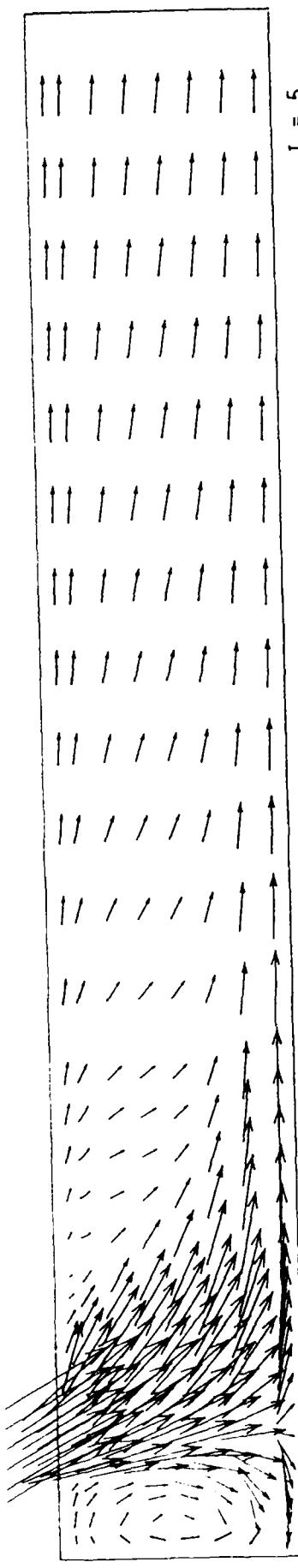
$I = 9$

FIGURE 12. (Contd) FLOWFIELD IN $(r-z)$ PLANE FOR $\alpha = 60^\circ$, $H = 2$ INCHES

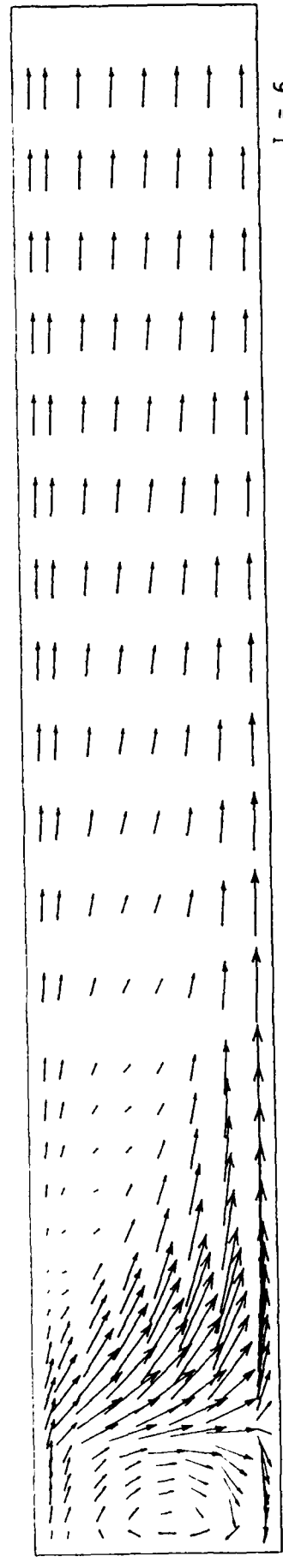
THIRD PLOT



$I = 4$

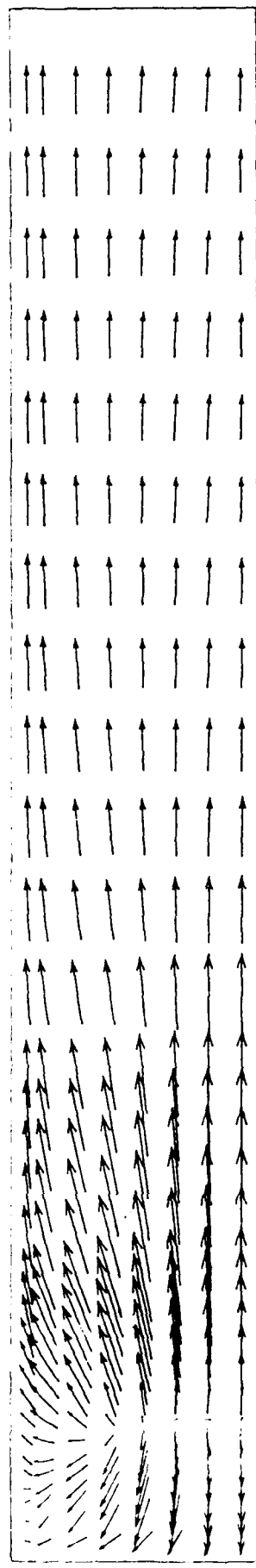


$I = 5$

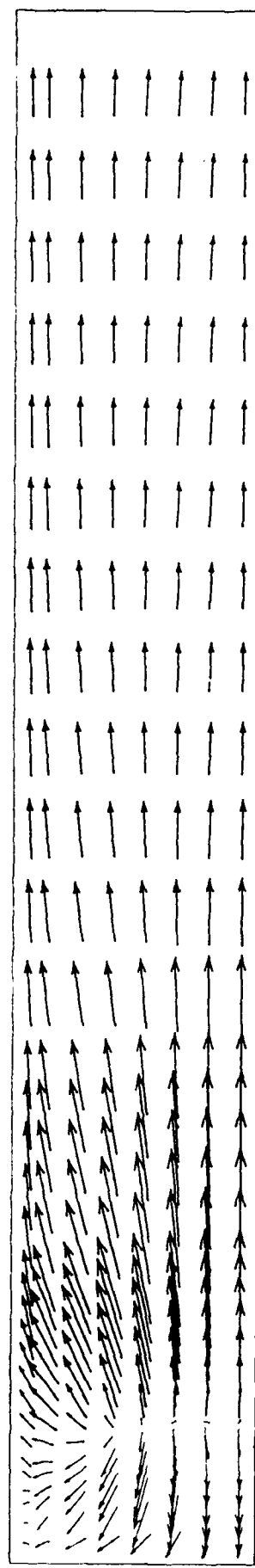


$I = 6$

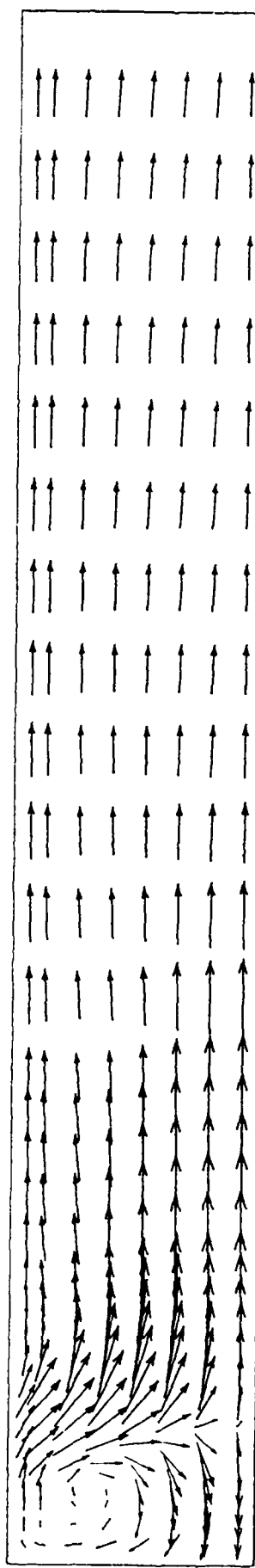
FIGURE 12. (Contd) FLOWFIELD IN $(r-z)$ PLANE FOR $\alpha = 60^\circ$, $H = 2$ INCHES
SECOND PLOT



$I = 1$



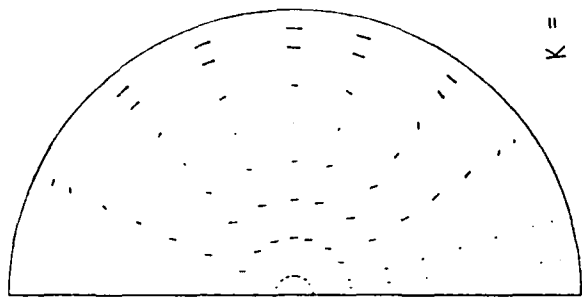
$I = 2$



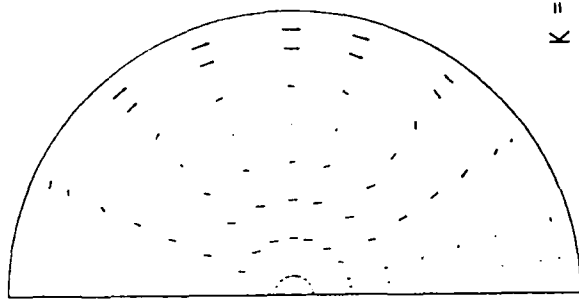
$I = 3$

FIGURE 12. FLOWFIELD IN $(r-z)$ PLANE FOR $\alpha = 60^\circ$, $H = 2$ INCHES

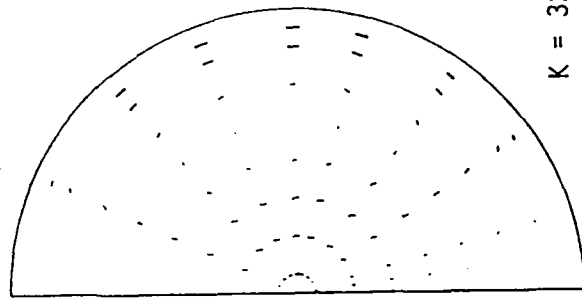
FIRST PLOT



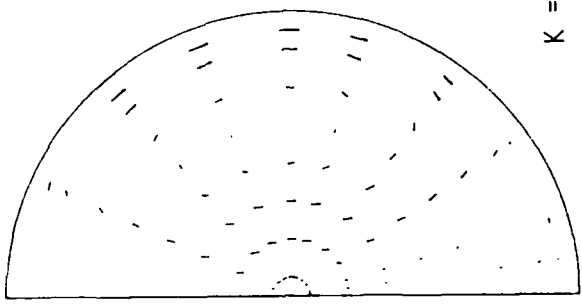
$K = 29$



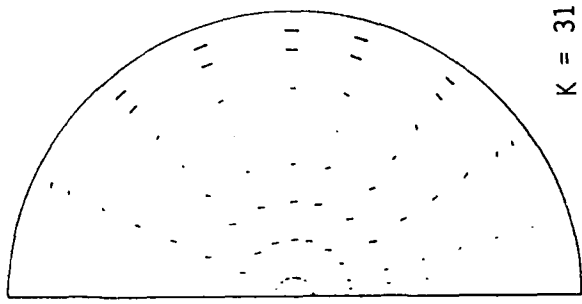
$K = 28$



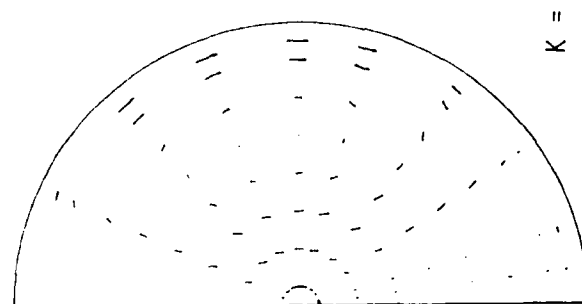
$K = 32$



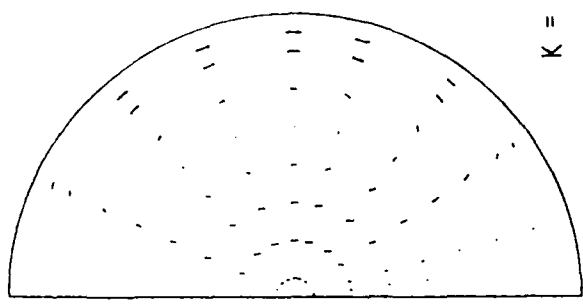
$K = 27$



$K = 31$



$K = 30$



$K = 30$

FIGURE 11. (Contd) FLOWFIELD IN $(r-\theta)$ PLANE FOR $\alpha = 60^\circ$, $H = 2$ INCHES
FOURTH PLOT

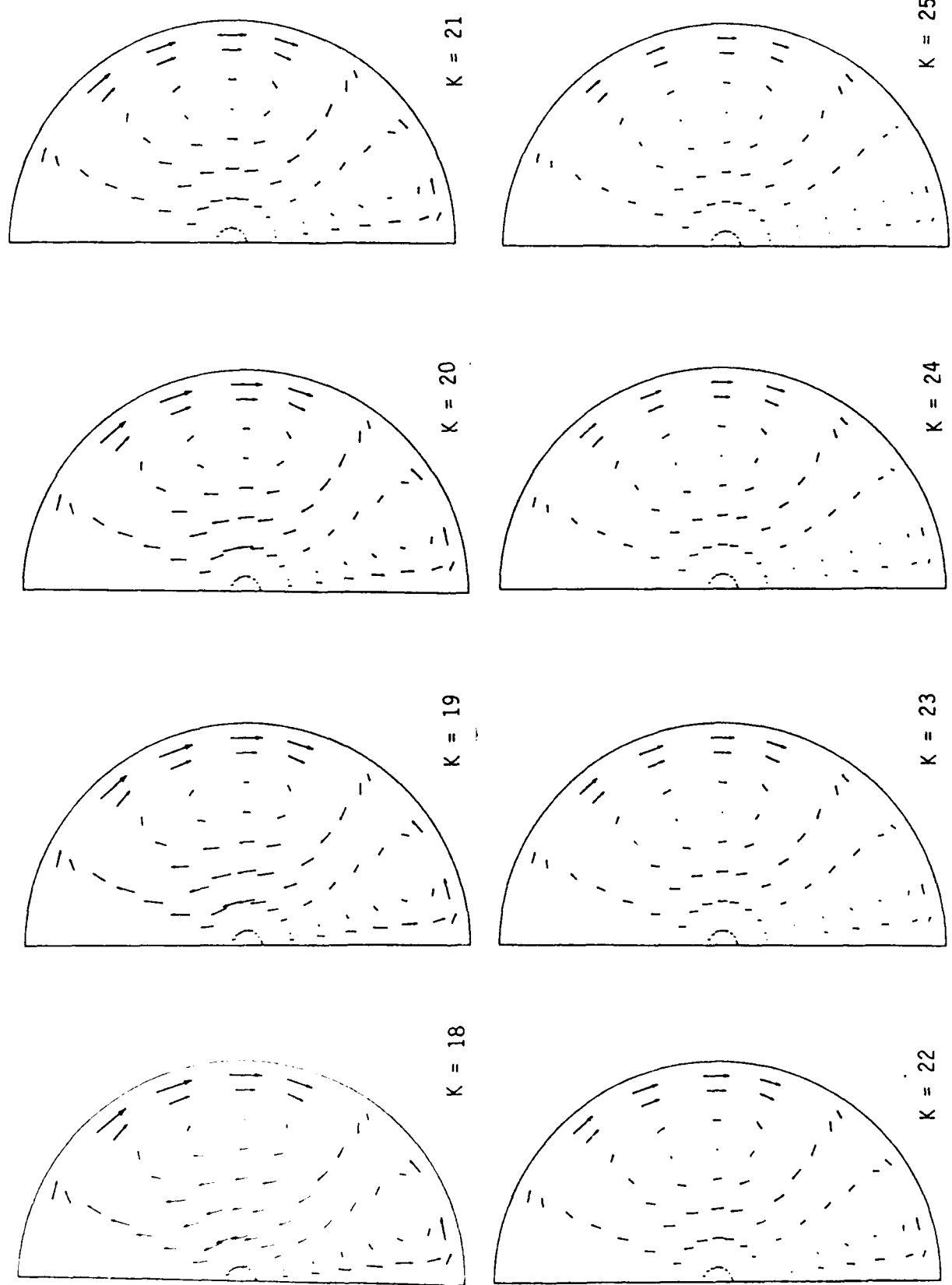
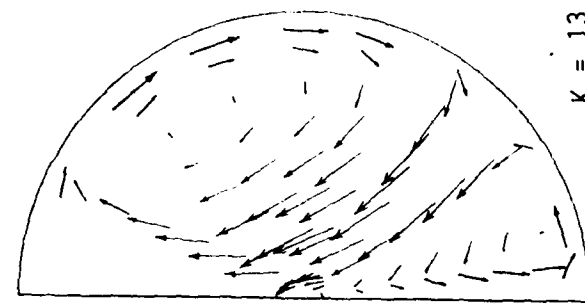
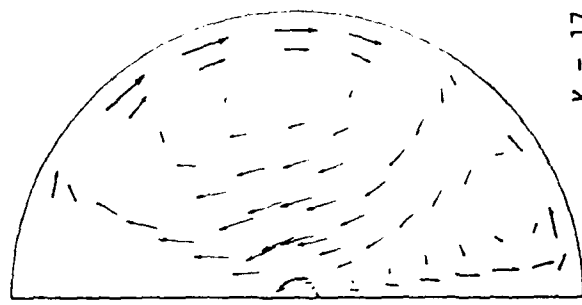


FIGURE 11. (Contd) FLOWFIELD IN $(r-\theta)$ PLANE FOR $\alpha = 60^\circ$, $H = 2$ INCHES

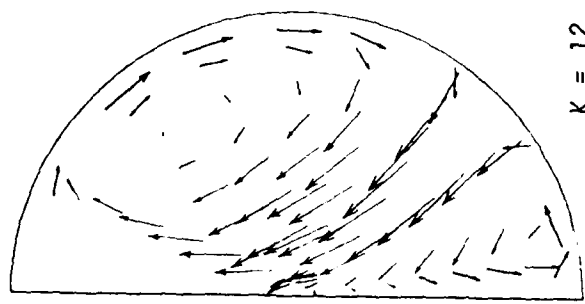
THIRD PLOT



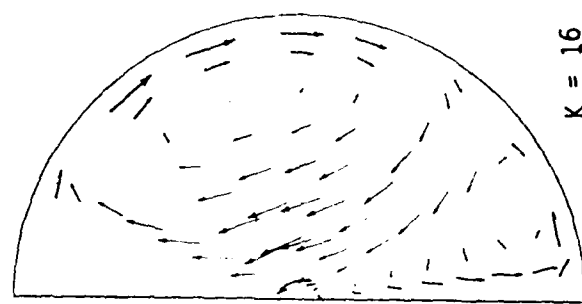
$K = 13$



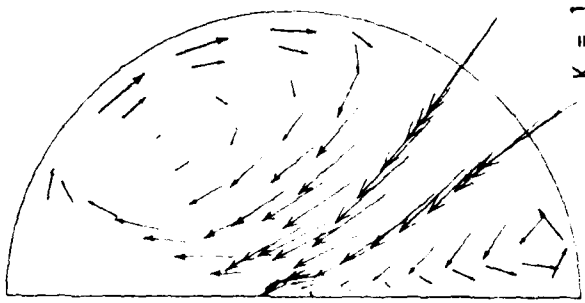
$K = 17$



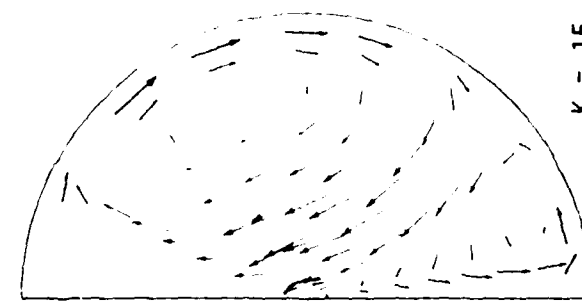
$K = 12$



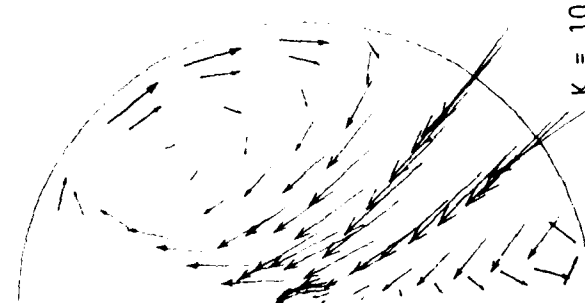
$K = 16$



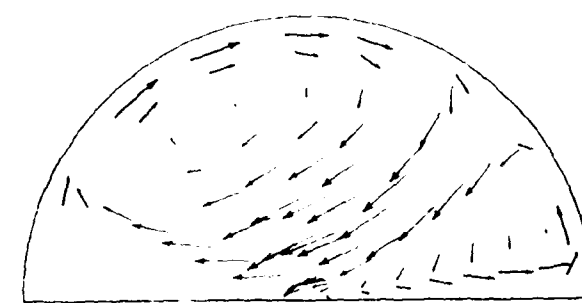
$K = 11$



$K = 15$



$K = 10$



$K = 14$

FIGURE 11. (Contd) FLOWFIELD IN $(r-\theta)$ PLANE FOR $\alpha = 60^\circ$, $H = 2$ INCHES
SECOND DIAM

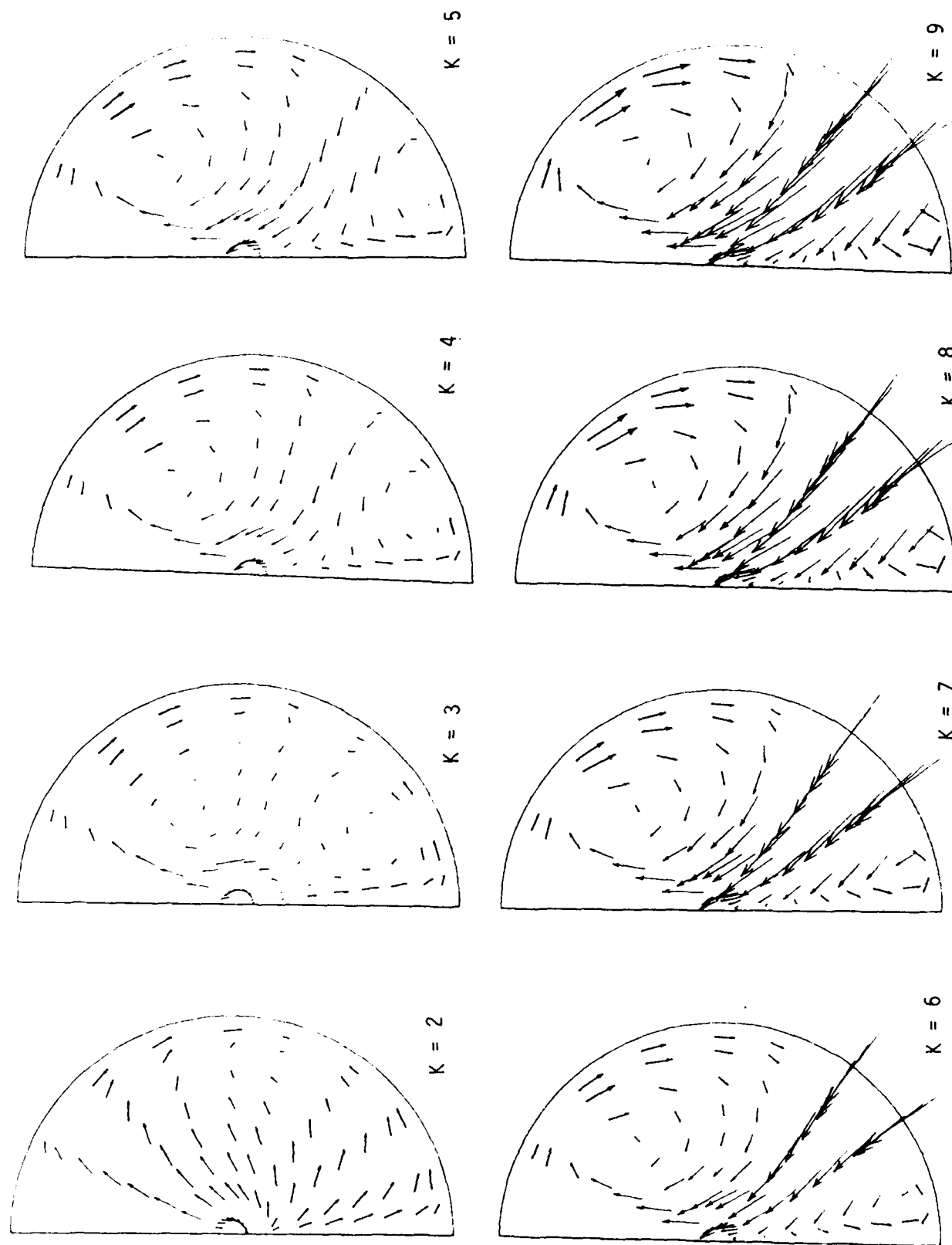


FIGURE 11. FLOWFIELD IN $(r-\theta)$ PLANE FOR $\alpha = 60^\circ$, $H = 2$ INCHES

FIRST PLOT

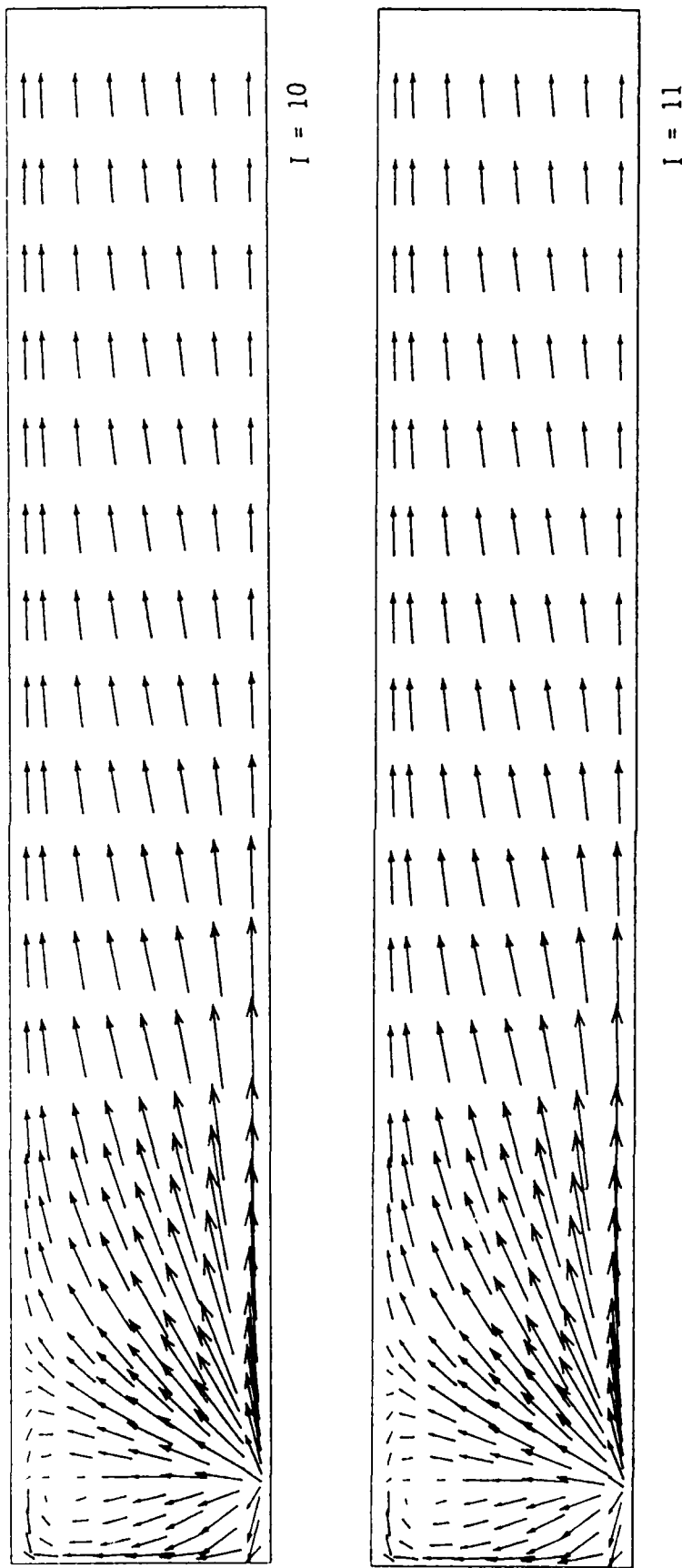
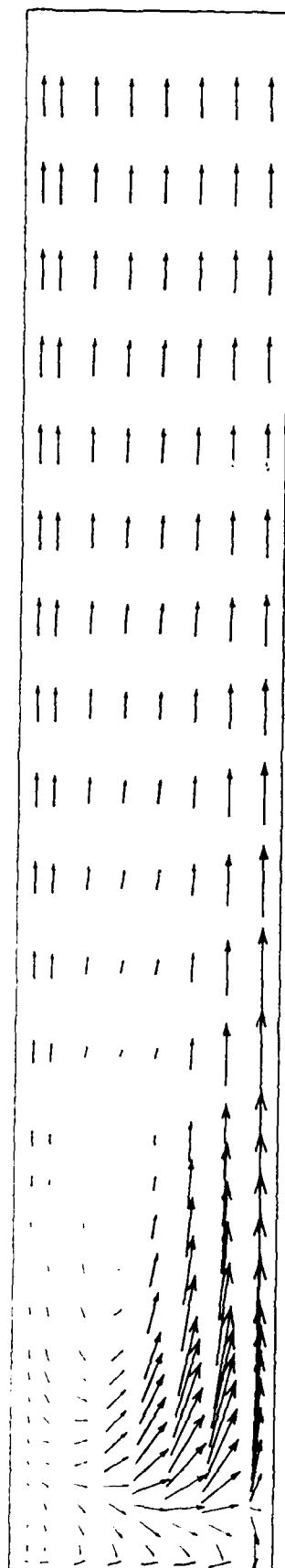
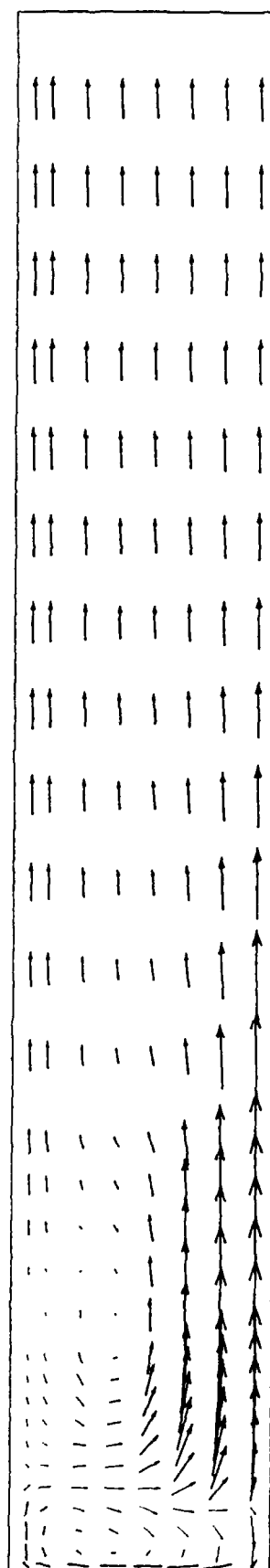


FIGURE 10. (Contd) FLOWFIELD IN $(r-z)$ PLANE FOR $\alpha = 45^\circ$, $H = 0$ INCHES

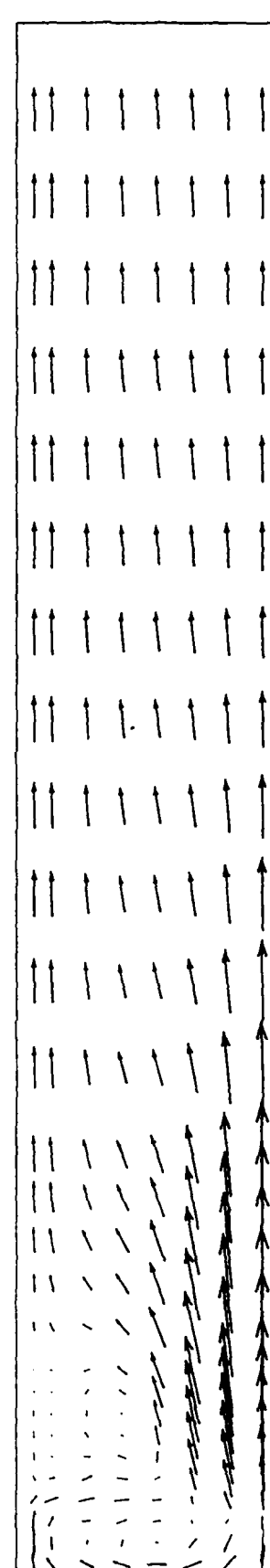
FOURTH PLOT



$I = 7$



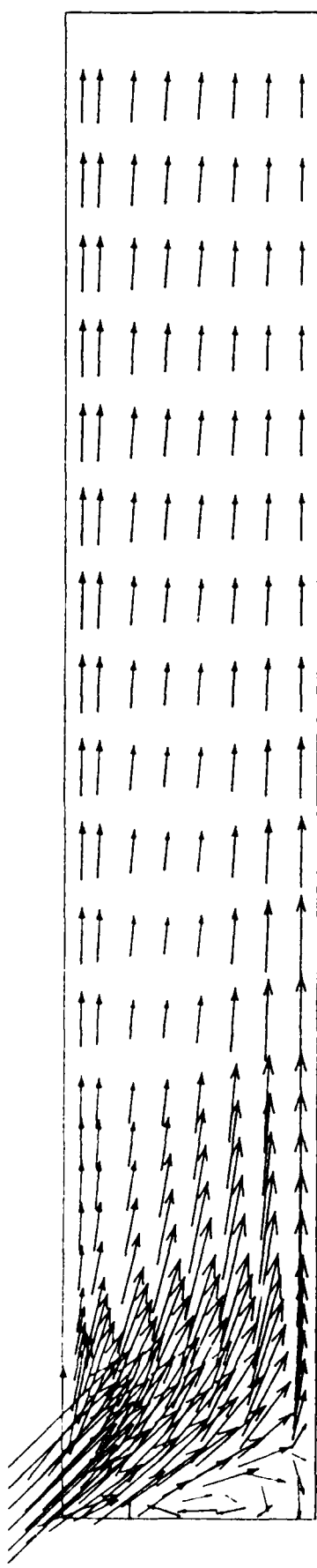
$I = 8$



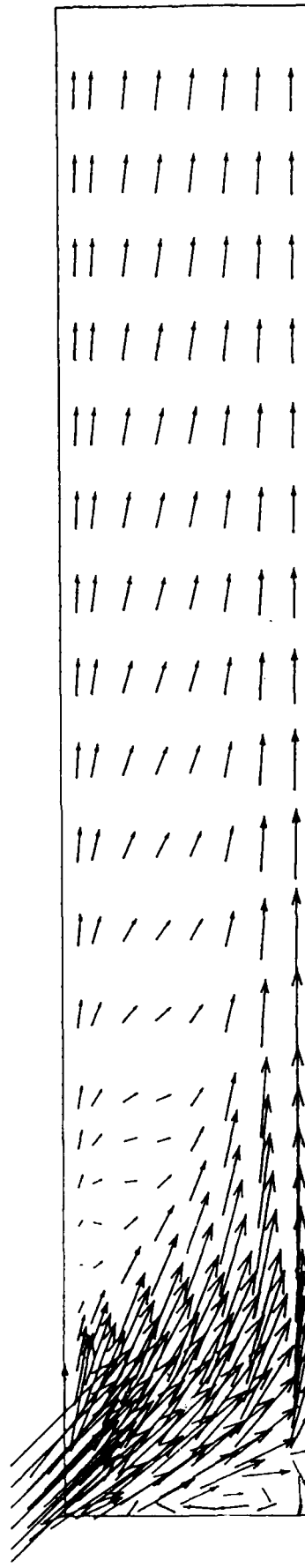
$I = 9$

FIGURE 10. (Contd) FLOWFIELD IN $(r-z)$ PLANE FOR $\alpha = 45^\circ$, $H = 0$ INCHES

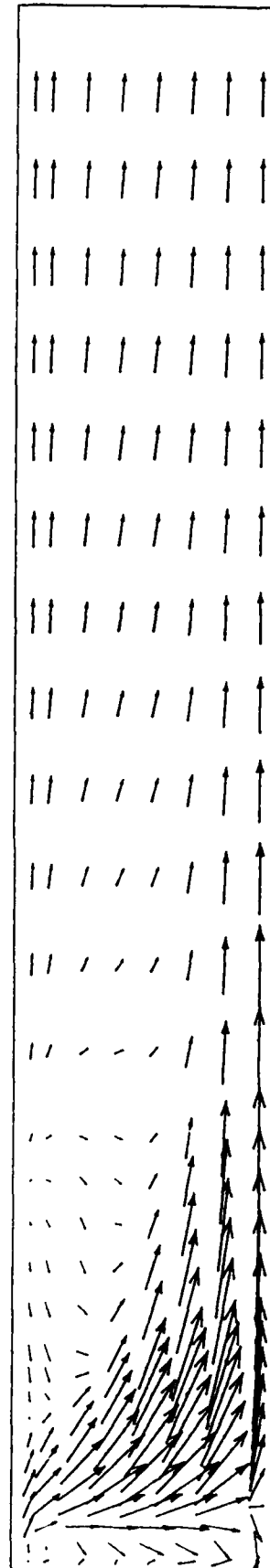
THIRD PLOT



$I = 4$



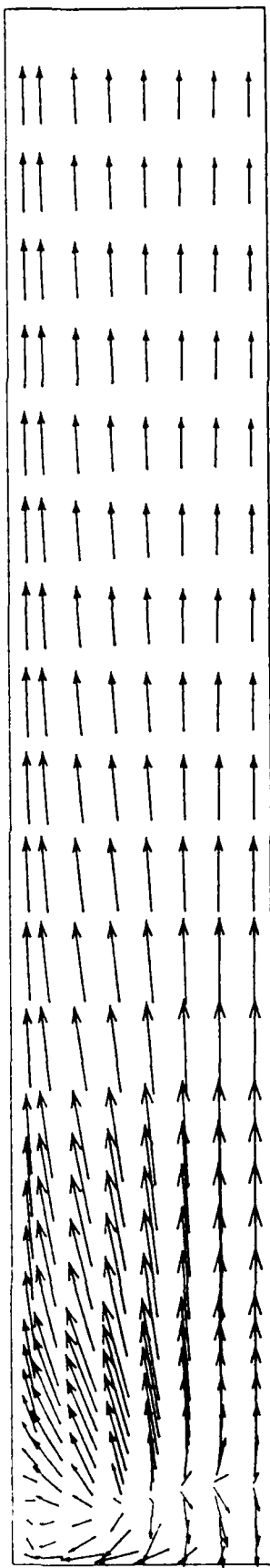
$I = 5$



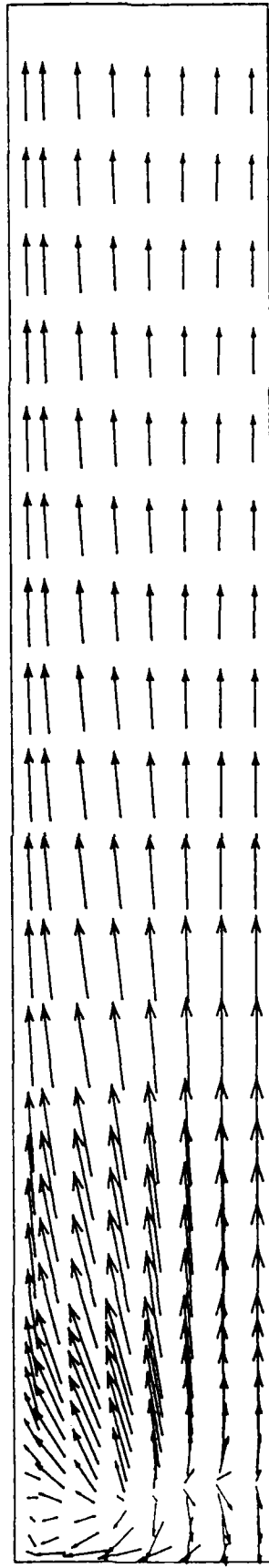
$I = 6$

FIGURE 10. (Contd) FLOWFIELD IN $(r-z)$ PLANE FOR $\alpha = 45^\circ$, $H = 0$ INCHES

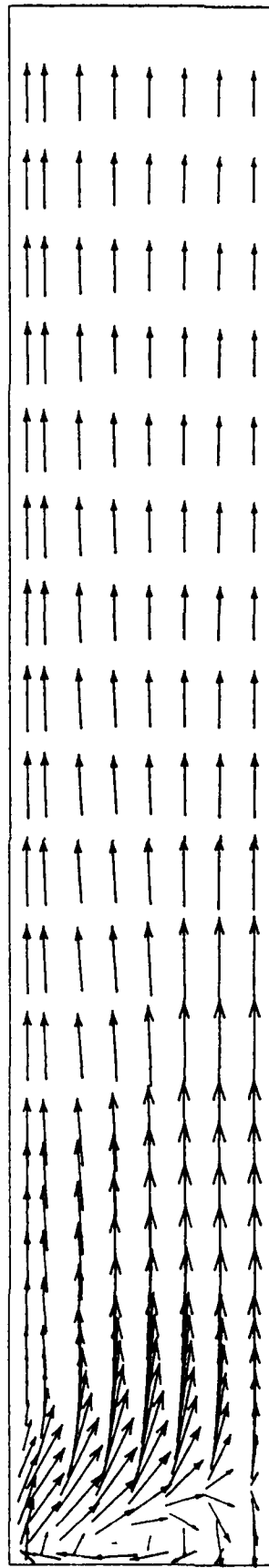
SECOND PLOT



$I = 1$



$I = 2$



$I = 3$

FIGURE 10. FLOWFIELD IN $(r-z)$ PLANE FOR $\alpha = 45^\circ$, $H = 0$ INCHES.

FIRST PLOT

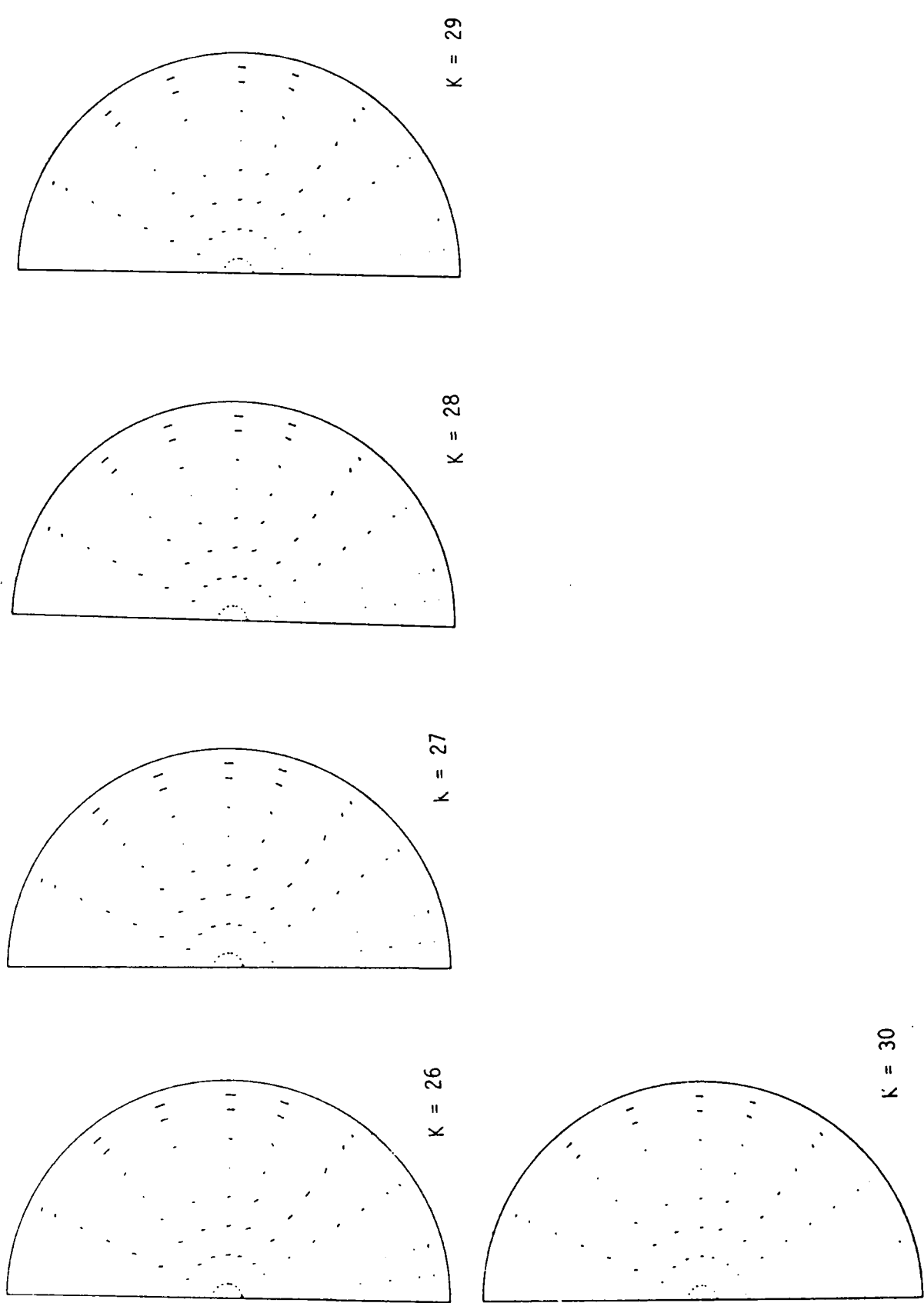


FIGURE 9. (Contd) FLOWFIELD IN $(r-\theta)$ PLANE FOR $\alpha = 45^\circ$, $H = 0$ INCHES

FOURTH PLOT

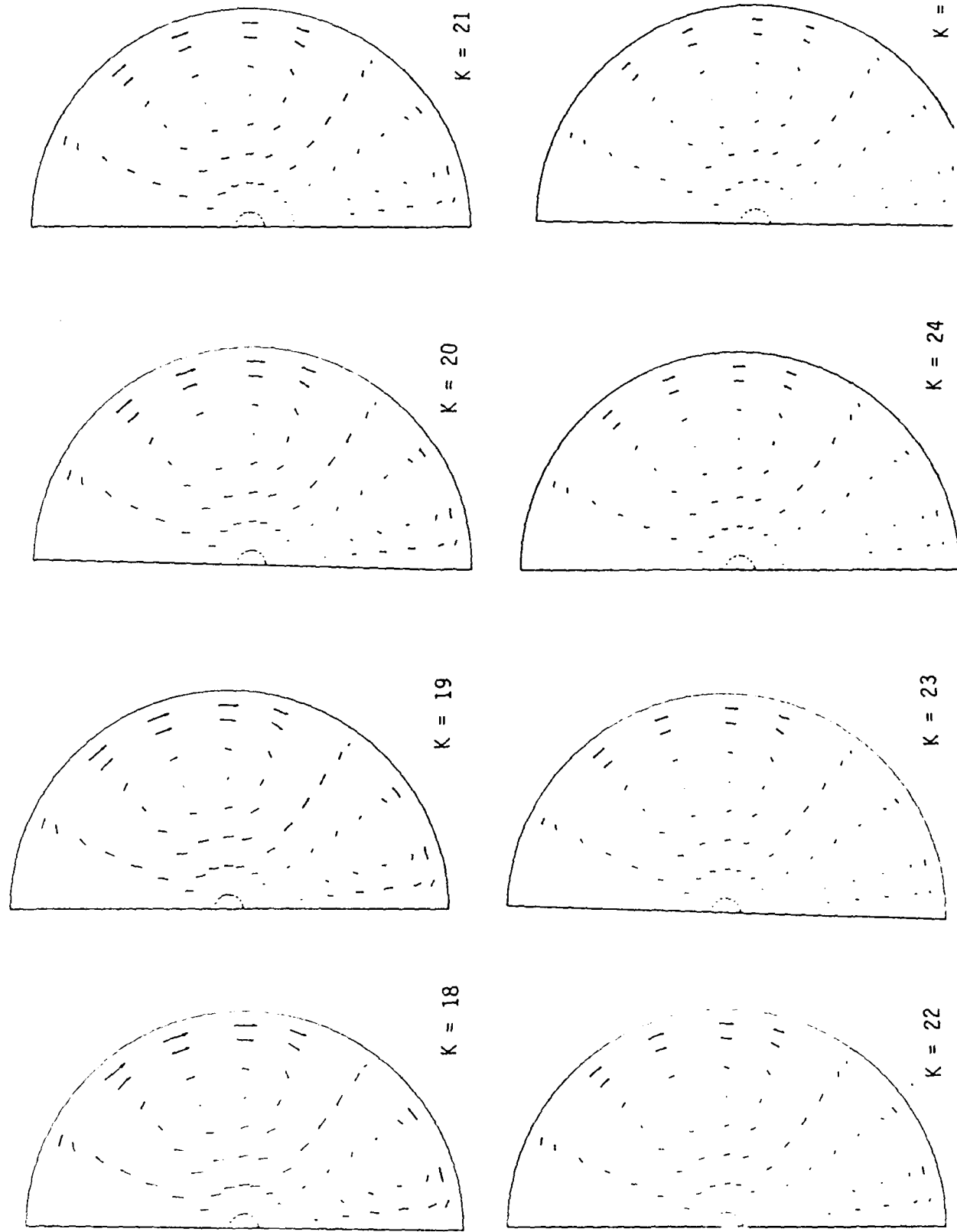


FIGURE 9. (Contd) FLOWFIELD IN $(r-\theta)$ PLANE FOR $\alpha = 45^\circ$, $H = 0$ INCHES

THIRD PLOT

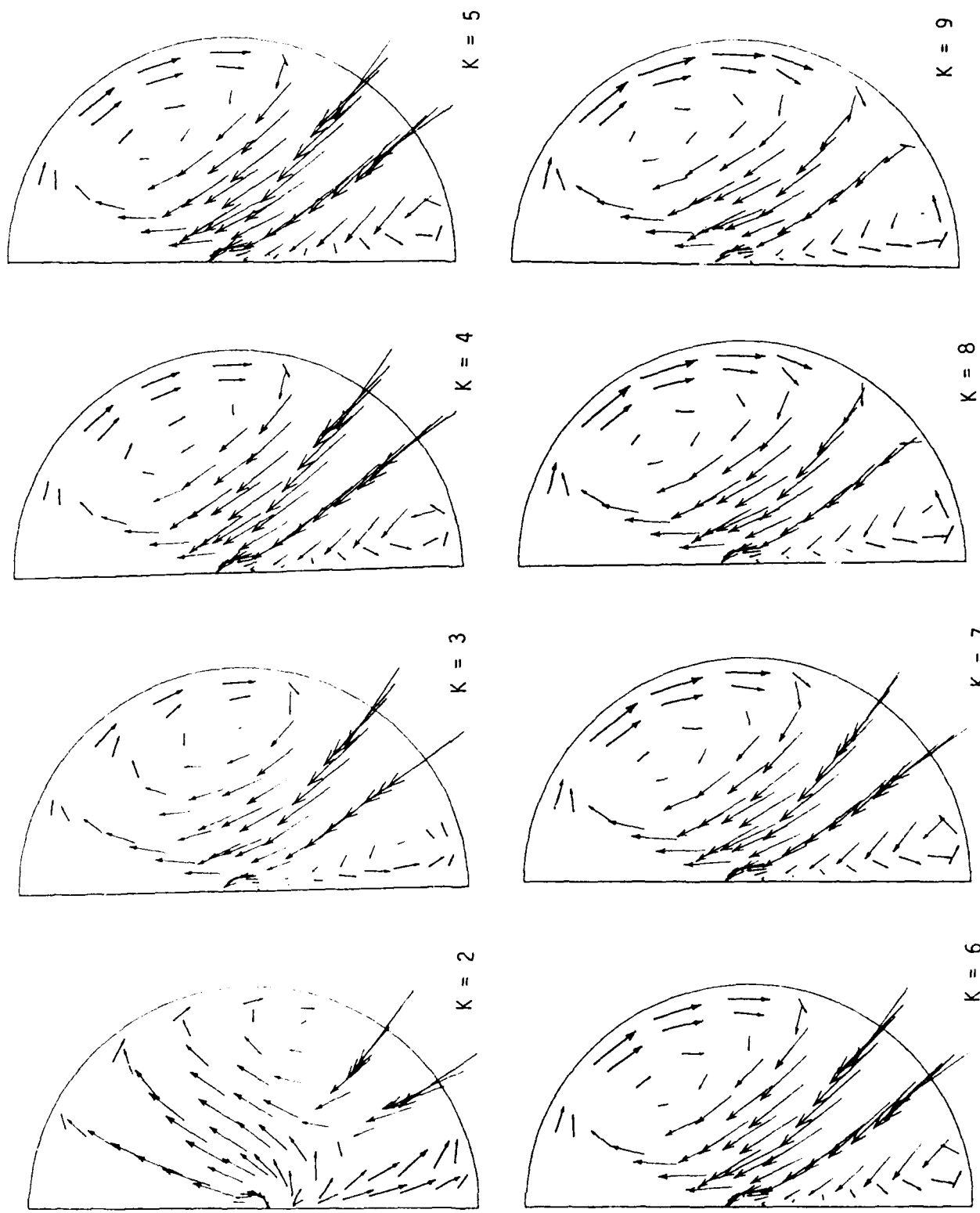
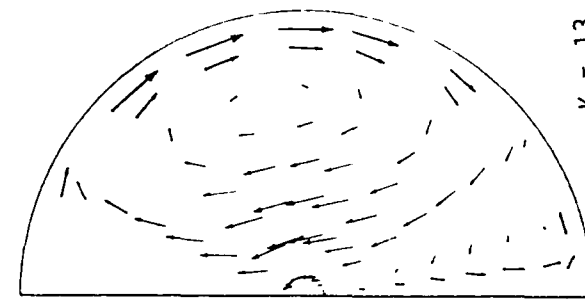
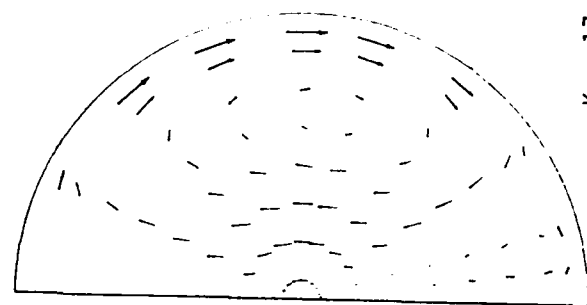


FIGURE 13. FLOWFIELD IN $(r-\theta)$ PLANE FOR $\alpha = 60^\circ$, $H = 0$ INCHES

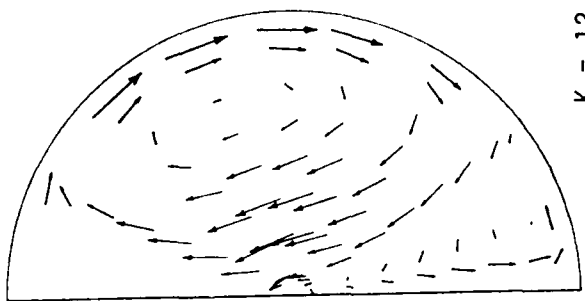
FIRST PLOT



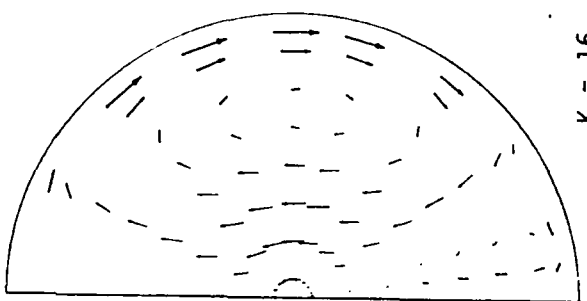
$K = 13$



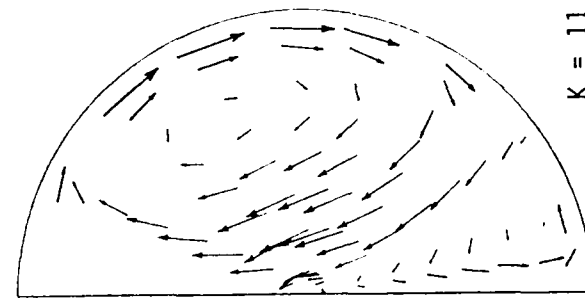
$K = 17$



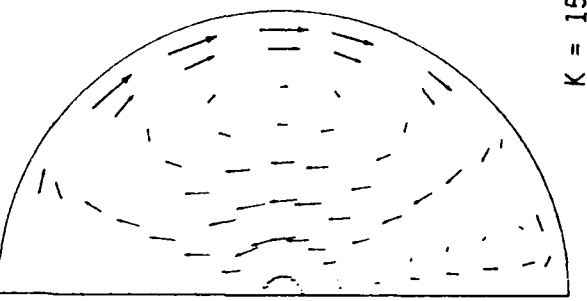
$K = 12$



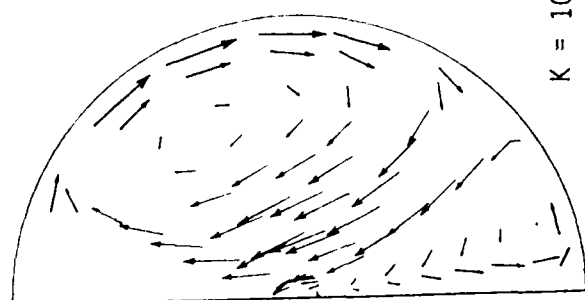
$K = 16$



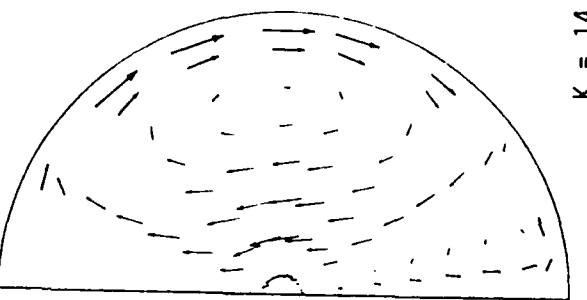
$K = 11$



$K = 15$



$K = 10$



$K = 14$

SECOND PLOT

FIGURE 13. (Contd) FLOWFIELD IN $(r-\theta)$ PLANE FOR $\alpha = 60^\circ$, $H = 0$ INCHES

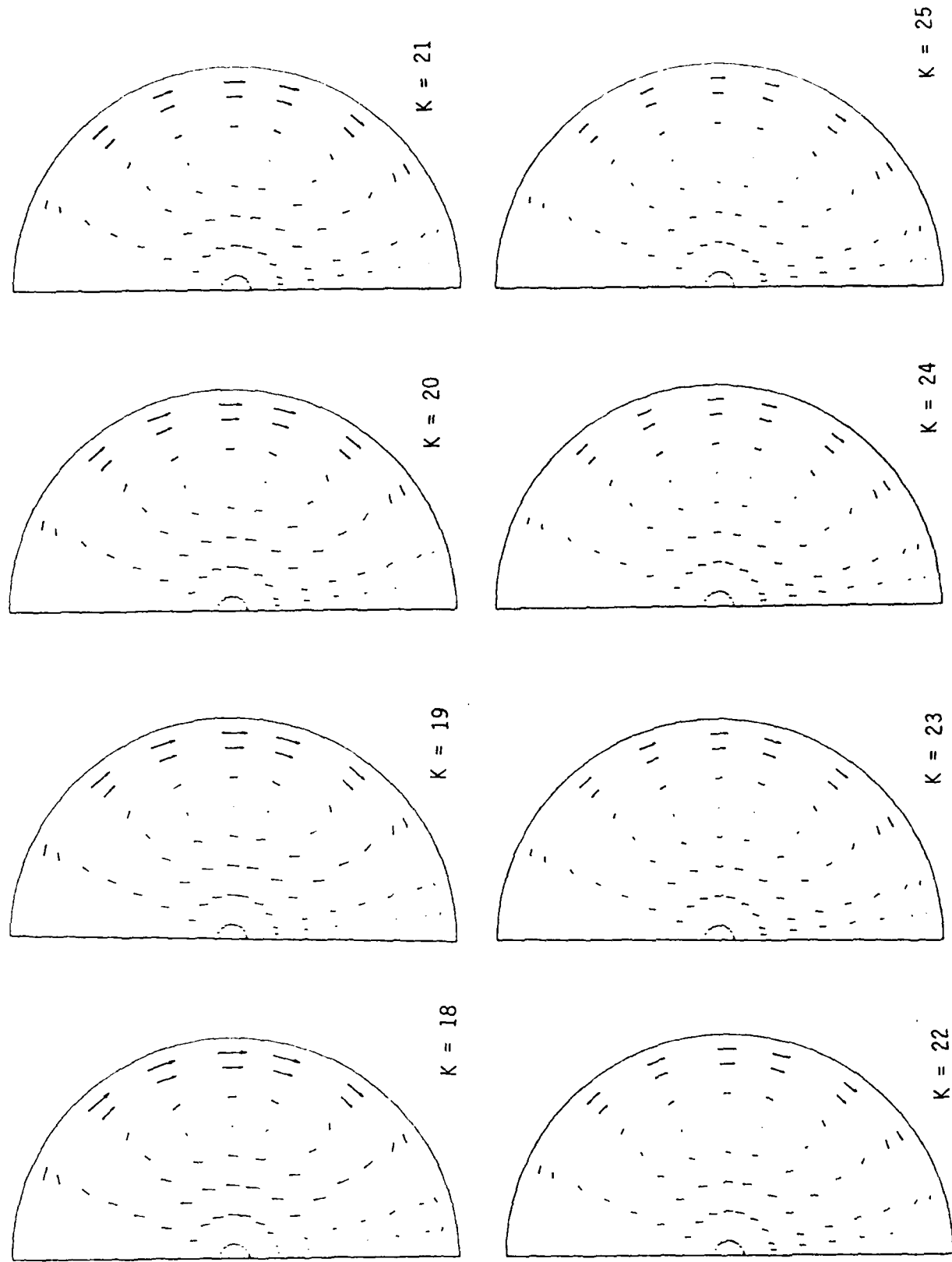
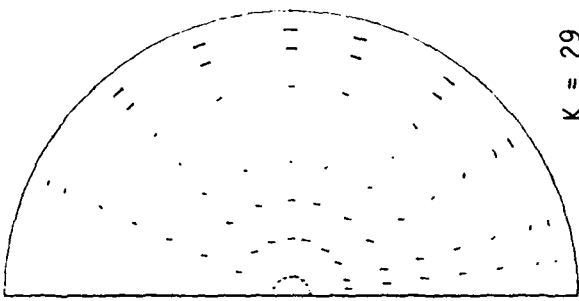
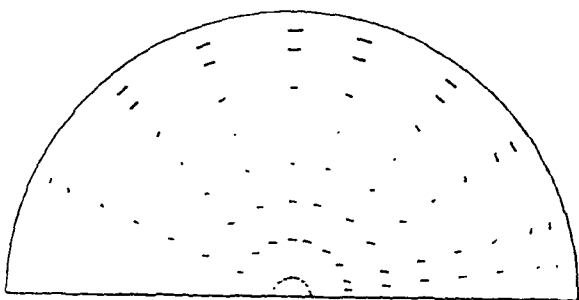


FIGURE 13. (Contd) FLOWFIELD IN $(r-\theta)$ PLANE FOR $\alpha = 60^\circ$, $H = 0$ INCHES

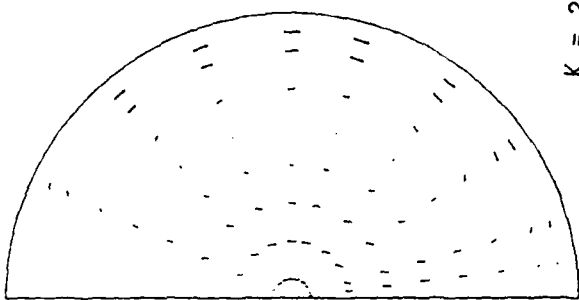
THIRD PLOT



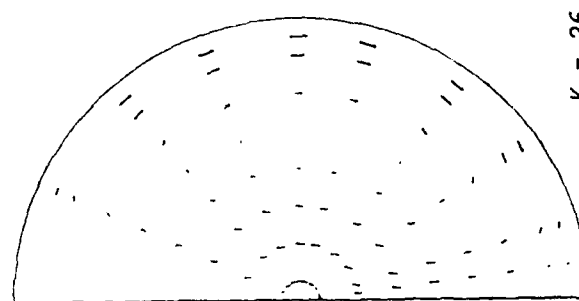
$K = 29$



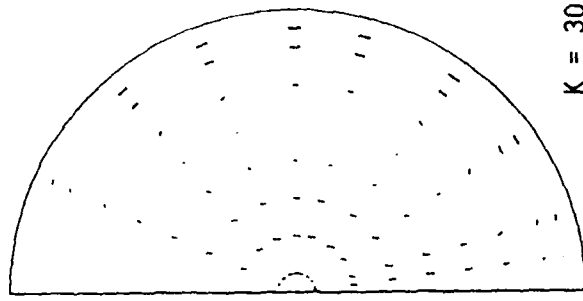
$K = 28$



$K = 27$

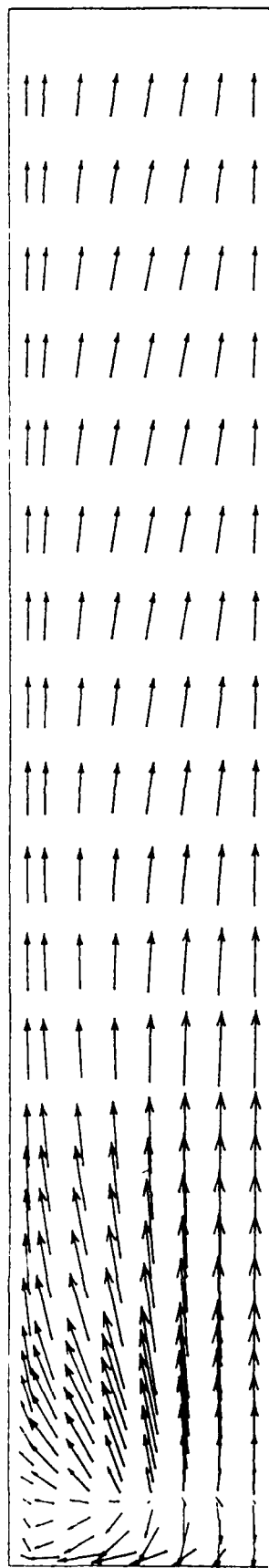


$K = 26$

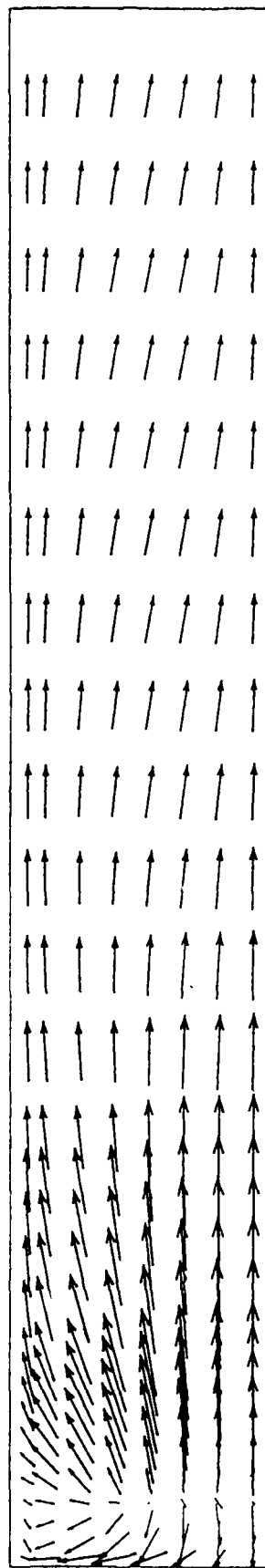


$K = 30$

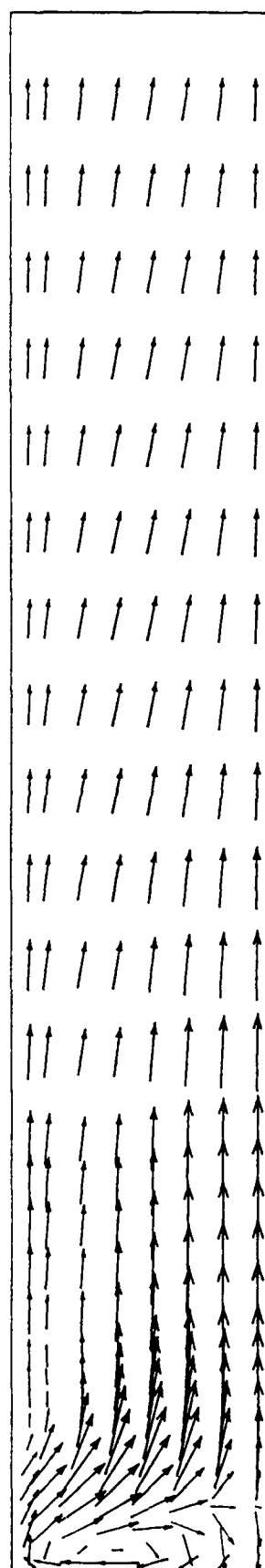
FIGURE 13. (Contd) FLOWFIELD IN $(r-\theta)$ PLANE FOR $\alpha = 60^\circ$, $H = 0$ INCHES
FOURTH PLOT



$I = 1$



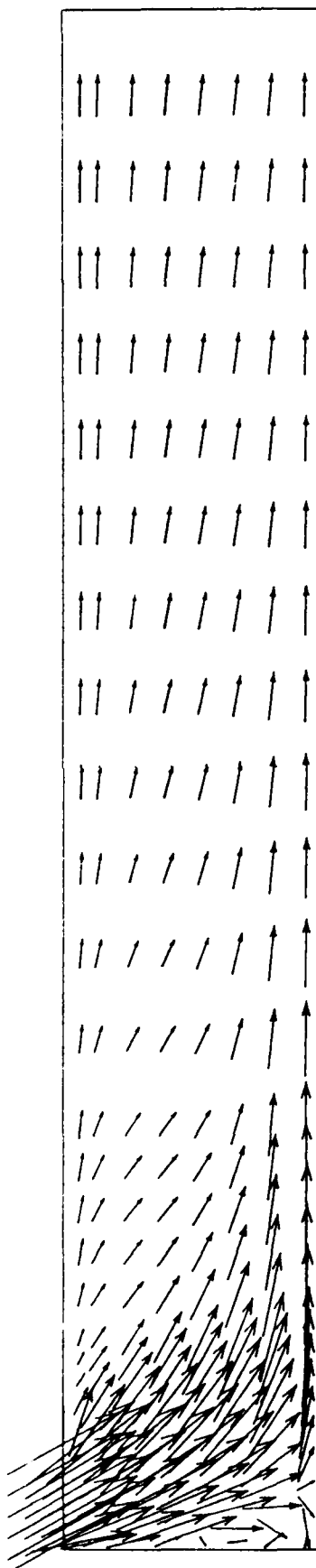
$I = 2$



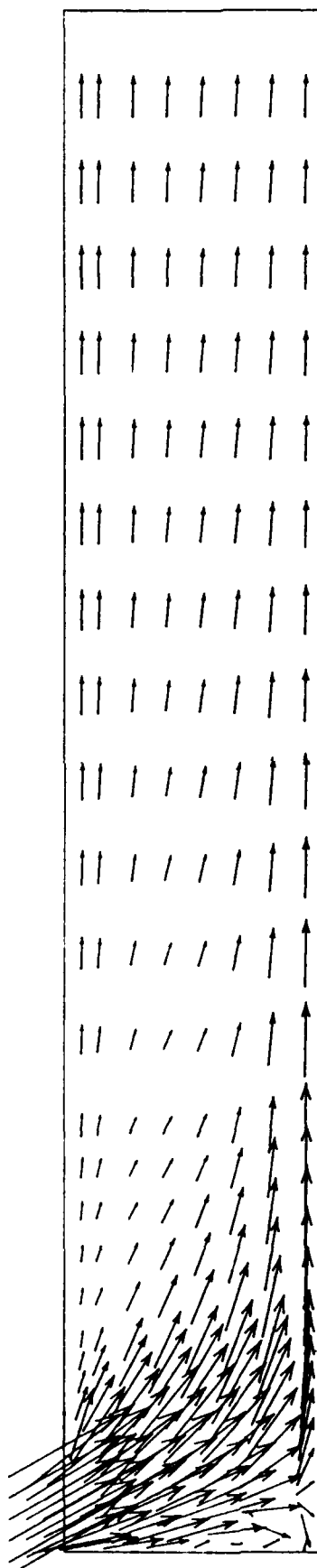
$I = 3$

FIGURE 14. FLOWFIELD IN $(r-z)$ PLANE FOR $\alpha = 60^\circ$, $H = 0$ INCHES

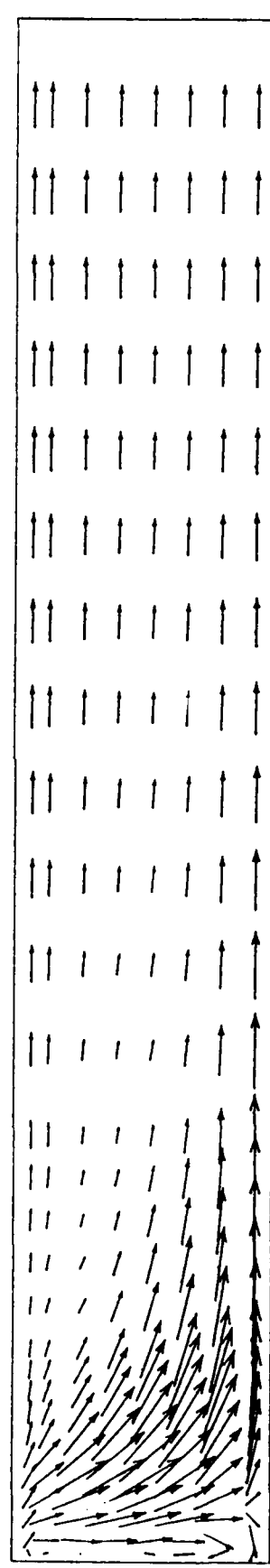
FIRST PLOT



$I = 4$



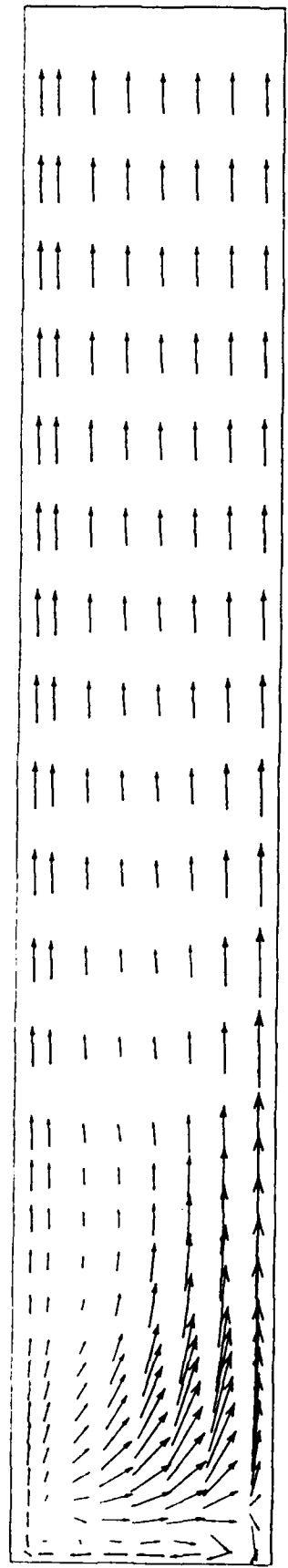
$I = 5$



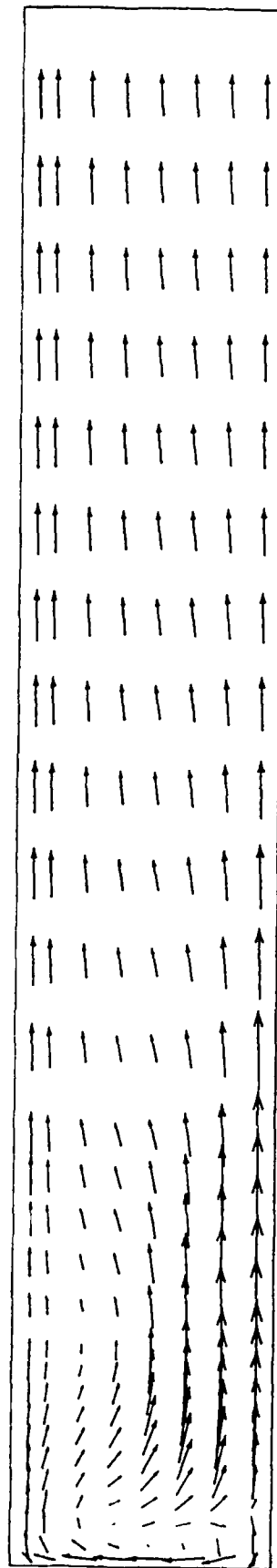
$I = 6$

FIGURE 14. (Contd) FLOWFIELD IN $(r-z)$ PLANE FOR $\alpha = 60^\circ$, $H = 0$ INCHES

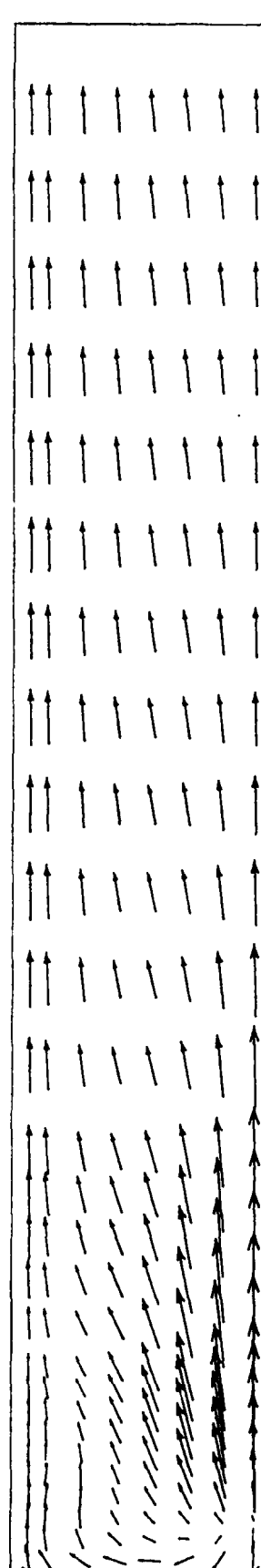
SECOND PLOT



$I = 7$



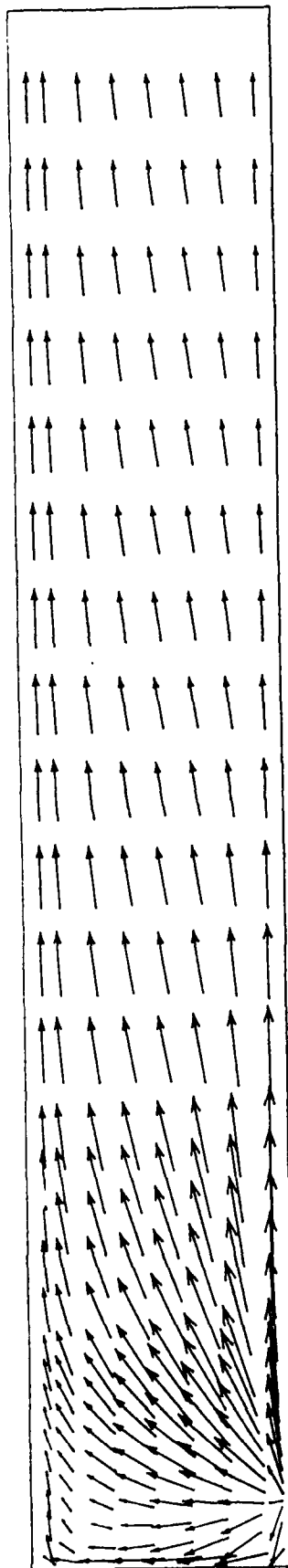
$I = 8$



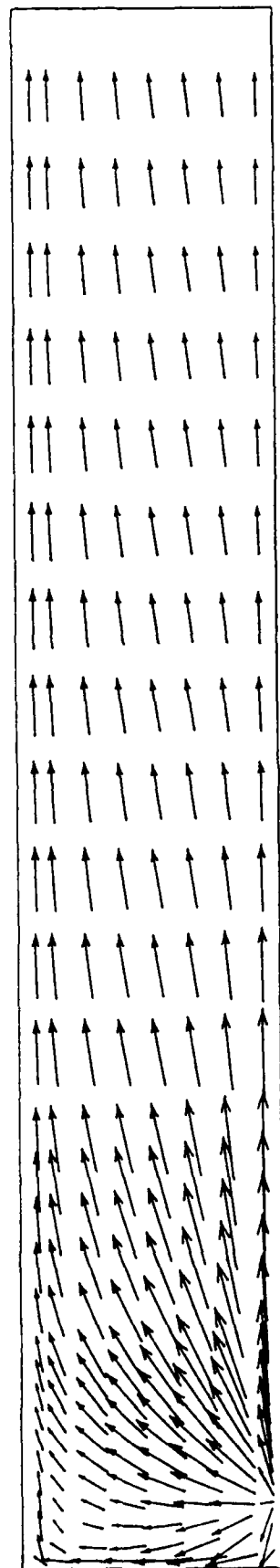
$I = 9$

FIGURE 14. (Contd) FLOWFIELD IN $(r-z)$ PLANE FOR $\alpha = 60^\circ$, $H = 0$ INCHES

THIRD PLOT



$I = 10$



$I = 11$

FIGURE 14. (Contd) FLOWFIELD IN $(r-z)$ PLANE FOR $\alpha = 60^\circ$, $H = 0$ INCHES

FOURTH PLOT

APPENDIX C
AFWAL/PORT WATER TUNNEL
RESIDENCE TIME TEST DATA

AFWAL/PORT WATER TUNNEL TEST RIG

MEASURED RESIDENCE TIME TEST DATA

DOME HEIGHT IN.	RESIDENCE TIMES		STANDARD DEVIATION		VARIANCE		DISPERSION		COEFF.	RESIDENCE		TEST PARAMETERS
	INLET	EXIT	INLET	EXIT	INLET	EXIT	2	2		D/UL	TIME	
	T1	T2	S1	S2			(T2-T1)	(S2-S1)		1ST ITERATION	FINAL VALUE	(T2-T1)
0	.348	1.348	.034	.28	.001156	.0784	1	.077244	.038622	.034893	1	ANG=30 DEG
-.5	.342	1.333	.037	.263	.001369	.069169	.982081	.069037	.034519	.031540	.991	GPM=300
-1	.345	1.327	.057	.263	.003249	.069169	.964324	.068359	.034179	.031259	.982	AN/AC=0.29
-1.5	.342	1.302	.069	.249	.004761	.061504	.9216	.061570	.030785	.028416	.96	LC=39IN.
-2	.344	1.34	.126	.255	.015876	.065025	.992016	.049545	.024772	.023238	.996	GG=0%
-2.5	.343	1.314	.072	.248	.005184	.061504	.942841	.059734	.029867	.027637	.971	
-3	.357	1.351	.051	.247	.002601	.061009	.988036	.059115	.029558	.027373	.994	
-3.5	.339	1.295	.047	.236	.002209	.055696	.913936	.058524	.029262	.027121	.956	
-4	.339	1.314	.036	.251	.001296	.063001	.950625	.064910	.032455	.029822	.975	
-4.5	.354	1.295	.05	.233	.0025	.054289	.885481	.058487	.029243	.027105	.941	
-5	.363	1.318	.049	.242	.002401	.058564	.912025	.061581	.030790	.028420	.955	
-5.5	.356	1.316	.048	.226	.002304	.051076	.9216	.052921	.026461	.024710	.96	
-6	.357	1.345	.04	.247	.0016	.061009	.976144	.060861	.030430	.028115	.988	
0	.358	1.388	.162	.295	.026244	.087025	1.0609	.057292	.028646	.026594	1.03	ANG=45 DEG
-.5	.358	1.385	.081	.305	.006561	.093025	1.054729	.081977	.040989	.036789	1.027	GPM=300
-1	.353	1.352	.029	.295	.000841	.087025	.998001	.086357	.043178	.038517	.999	AN/AC=0.29
-1.5	.366	1.35	.044	.258	.001936	.066564	.968256	.066747	.033373	.030589	.984	LC=39IN.
-2	.362	1.387	.029	.259	.000841	.067081	1.050625	.063048	.031524	.029040	1.025	GG=0%
-2.5	.361	1.397	.029	.262	.000841	.068644	1.073296	.063173	.031586	.029092	1.036	
-3	.359	1.363	.032	.241	.001024	.058081	1.008016	.056603	.028302	.026299	1.004	
-3.5	.367	1.382	.031	.276	.000961	.076176	1.030225	.073008	.036504	.033173	1.015	
-4	.366	1.387	.029	.271	.000841	.073441	1.042441	.069644	.034822	.031791	1.021	
-4.5	.357	1.352	.031	.245	.000961	.060025	.990025	.059659	.029830	.027605	.995	
-5	.38	1.413	.047	.267	.002209	.071289	1.067089	.064737	.032368	.029749	1.033	
-5.5	.363	1.367	.029	.221	.000841	.048841	1.008016	.047618	.023809	.022392	1.004	
-6	.371	1.383	.07	.257	.0049	.066049	1.024144	.059707	.029854	.027326	1.012	
0	.387	1.34	.069	.227	.004761	.051529	.908209	.051495	.025747	.024090	.953	ANG=60 DEG
-.5	.384	1.402	.042	.244	.001764	.059536	1.036324	.055747	.027874	.025931	1.018	GPM=300
-1	.372	1.365	.031	.253	.000961	.064009	.986049	.063740	.031970	.029415	.993	AN/AC=0.29
-1.5	.384	1.409	.045	.255	.002025	.065025	1.050625	.059964	.029982	.027735	1.025	LC=39IN.
-2	.395	1.386	.041	.29	.001681	.0841	.982081	.083923	.041961	.037560	.991	GG=0%
-2.5	.387	1.402	.035	.251	.001225	.063001	1.030225	.059964	.029982	.027735	1.015	
-3	.365	1.44	.031	.307	.000961	.094249	1.153476	.080876	.040438	.036350	1.074	
-3.5	.391	1.436	.037	.278	.001369	.077284	1.092025	.069518	.034759	.031738	1.045	
-4	.385	1.411	.034	.251	.001156	.063001	1.052676	.058750	.029375	.027218	1.026	
-4.5	.392	1.393	.04	.22	.0016	.0484	1.002001	.046707	.023353	.021990	1.001	
-5	.405	1.388	.041	.224	.001681	.050176	.966289	.050187	.025093	.023519	.983	
-5.5	.416	1.43	.063	.224	.004624	.050176	1.028196	.044303	.022151	.020925	1.014	
-6	.396	1.412	.056	.254	.003136	.064516	1.032256	.059462	.029731	.027521	1.016	

AFWAL/PORT WATER TUNNEL TEST RIG

MEASURED RESIDENCE TIME TEST DATA

DOME HEIGHT IN.	RESIDENCE TIMES		STANDARD DEVIATION		VARIANCE		2 (T2-T1)	2 (S2-S1)	D/UL	COEFF.	RESIDENCE TIME TEST	
	INLET	EXIT	INLET	EXIT	INLET	EXIT					TIME (SEC.)	TEST PARAMETERS
	T1 SEC.	T2 SEC.	S1	S2							(T2-T1)	
0	.466	1.958	.057	.391	.003249	.152881	2.226064	.067219	.033609	.030785	1.492	ANG=30 DEG
-1	.472	1.949	.037	.38	.001369	.1444	2.178576	.065653	.032827	.030133	1.476	GPM=200
-2	.462	1.939	.034	.387	.001156	.149769	2.181529	.068123	.034062	.031161	1.477	AN/AC=0.29
-3	.46	1.959	.036	.381	.001296	.145161	2.187441	.065769	.032884	.030181	1.479	LC=39IN.
-4	.478	1.932	.032	.354	.001024	.125316	2.114116	.058791	.029396	.027235	1.454	GG=0%
-5	.486	1.925	.049	.343	.002401	.117649	2.070721	.055656	.027828	.025892	1.439	
-6	.473	1.891	.069	.346	.004761	.119716	2.010724	.057171	.028585	.026543	1.418	
0	.272	1.012	.062	.209	.003844	.043681	.5476	.072748	.036374	.033066	.74	ANG=30 DEG
-1	.264	.983	.031	.186	.000961	.034596	.516961	.065063	.032531	.029866	.719	GPM=400
-2	.271	.994	.04	.186	.0016	.034596	.522729	.063123	.031561	.029071	.723	AN/AC=0.29
-3	.283	.997	.033	.186	.001089	.034596	.509796	.065726	.032863	.030163	.714	LC=39IN.
-4	.289	1.015	.038	.176	.001444	.030976	.527076	.056030	.028015	.026053	.726	GG=0%
-5	.292	1.016	.051	.176	.002601	.030976	.524176	.054133	.027066	.025235	.724	
-6	.288	1.007	.057	.173	.003249	.029929	.516961	.051609	.025805	.024140	.719	
0	.504	1.96	.041	.374	.001681	.139876	2.119936	.065188	.032594	.029938	1.456	ANG=45 DEG
-1	.509	2.002	.042	.428	.001764	.183184	2.229049	.081389	.040694	.036554	1.493	GPM=200
-2	.514	2.057	.04	.416	.0016	.173056	2.380849	.072015	.036007	.032766	1.543	AN/AC=0.29
-3	.501	2.019	.041	.405	.001681	.164025	2.304324	.070452	.035226	.032124	1.518	LC=39IN.
-4	.522	2.043	.042	.376	.001764	.141376	2.313441	.060348	.030174	.027898	1.521	GG=0%
-5	.516	2.034	.042	.404	.001764	.163216	2.304324	.070065	.035032	.031964	1.518	
-6	.508	2.024	.053	.392	.002809	.153664	2.298256	.065639	.032819	.030127	1.516	
0	.275	1.027	.025	.197	.000625	.038809	.565504	.067522	.033761	.030912	.752	ANG=45 DEG
-1	.27	1.062	.022	.224	.000484	.050176	.627264	.079220	.039610	.035688	.792	GPM=400
-2	.292	1.046	.032	.209	.001024	.043681	.583696	.073081	.036540	.033202	.764	AN/AC=0.29
-3	.274	1.001	.023	.186	.000529	.034596	.528529	.064456	.032228	.029631	.727	LC=39IN.
-4	.277	1.061	.023	.206	.000529	.042436	.614656	.068180	.034090	.031185	.784	GG=0%
-5	.28	1.074	.025	.191	.000625	.036481	.630436	.056875	.028437	.026416	.794	
-6	.292	1.056	.092	.205	.008464	.042025	.583696	.057497	.028749	.026682	.764	
0	.36	1.381	.028	.299	.000784	.089401	1.042441	.085009	.042505	.037988	1.021	ANG=45 DEG
-2	.364	1.374	.029	.29	.000841	.0841	1.0201	.081618	.040809	.036646	1.01	GPM=300
-4	.36	1.372	.028	.302	.000784	.091204	1.024144	.088288	.044144	.039272	1.012	AN/AC=0.39
-6	.34	1.346	.029	.29	.000784	.0841	1.012036	.082325	.041163	.036927	1.006	LC=39IN.
												GG=0%
0	.348	1.353	.029	.266	.000841	.070756	1.010025	.069221	.034611	.031616	1.005	ANG=45 DEG
-2	.347	1.384	.061	.378	.003721	.142884	1.075369	.129410	.064705	.054238	1.037	GPM=300
-4	.359	1.402	.031	.295	.000961	.087025	1.087849	.079114	.039557	.035645	1.043	AN/AC=0.20
-6	.356	1.341	.048	.274	.002304	.075076	.970225	.075005	.037503	.033987	.985	LC=39IN.
												GG=0%

AFVAL/PORT WATER TUNNEL TEST RIG

MEASURED RESIDENCE TIME TEST DATA

ME GHT N.	RESIDENCE TIMES		STANDARD DEVIATION		VARIANCE		DISPERSION		COEFF.	RESIDENCE TIME (SEC.)	TEST PARAMETERS	
	INLET T1 SEC.	EXIT T2 SEC.	INLET S1	EXIT S2	INLET S1	EXIT S2	2 (T2-T1)	2 (S2-S1)				
							D/UL 1ST ITERATION	FINAL VALUE				
0	.35	.926	.058	.258	.003364	.066564	.331776	.190490	.095245	.072566	.576	ANG=45 DEG
-2	.349	.921	.026	.23	.000676	.0529	.327184	.159617	.079808	.063885	.572	GPM=300
-4	.355	.91	.062	.205	.003844	.042025	.308025	.123954	.061977	.052374	.555	AN/AC=0.29
-6	.355	.945	.029	.259	.000841	.067081	.3481	.190290	.095145	.072514	.59	LC=20.125 GG=0%
0	.358	1.722	.071	.294	.005041	.086436	1.860496	.043749	.021875	.020678	1.364	ANG=45 DEG
-2	.369	1.78	.033	.318	.001089	.101124	1.990921	.050246	.025123	.023545	1.411	GPM=300
-4	.36	1.731	.031	.296	.000961	.087616	1.879641	.046102	.023051	.021723	1.371	AN/AC=0.29
-6	.362	1.706	.066	.259	.004356	.067081	1.806336	.034725	.017362	.016609	1.344	LC=53.25 GG=0%
0	.445	1.476	.039	.258	.001521	.066564	1.054729	.061668	.030834	.028457	1.027	ANG=45 DEG
-5	.443	1.414	.038	.204	.001444	.041616	.942841	.042607	.021304	.020169	.971	GPM=300
-1	.436	1.433	.067	.224	.004489	.050176	.994009	.045962	.022981	.021661	.997	AN/AC=0.29
1.5	.431	1.427	.075	.22	.005625	.0484	.992016	.043119	.021560	.020398	.996	LC=39IN.
-2	.438	1.356	.053	.187	.002809	.034969	.898704	.035785	.017892	.017092	.948	GG=10%
2.5	.422	1.386	.069	.19	.004761	.0361	.929296	.033723	.016862	.016151	.964	*INLET*
-3	.448	1.478	.04	.258	.0016	.066564	1.0609	.061235	.030617	.028274	1.03	*DETECT*
0	.467	1.533	.034	.292	.001156	.085264	1.136356	.074016	.037008	.033584	1.066	ANG=45 DEG
-5	.468	1.511	.042	.32	.001764	.1024	1.087849	.092509	.046255	.040906	1.043	GPM=300
-1	.462	1.554	.036	.37	.001296	.1369	1.192464	.113717	.056859	.048776	1.092	AN/AC=0.29
1.5	.455	1.501	.051	.297	.002601	.088209	1.092025	.078394	.039197	.035356	1.045	LC=39IN.
-2	.467	1.518	.059	.295	.003481	.087025	1.104601	.075633	.037816	.034241	1.051	GG=20%
2.5	.429	1.463	.18	.272	.0324	.073984	1.069156	.038894	.019447	.018502	1.034	*INLET*
-3	.5	1.519	.113	.232	.012769	.053824	1.038361	.039538	.019769	.018792	1.019	*DETECT*
0	.343	1.482	.229	.413	.089401	.170569	1.297321	.062566	.031283	.028836	1.139	ANG=45 DEG
-5	.458	1.722	.41	.497	.1681	.247009	1.597636	.049389	.024695	.023170	1.264	GPM=300
-1	.476	1.761	.427	.502	.182329	.252004	1.651225	.042196	.021098	.019985	1.285	AN/AC=0.29
1.5	.563	1.342	.47	.514	.2209	.264196	1.635841	.026467	.013234	.012796	1.279	LC=39IN.
-2	.539	1.982	.503	.676	.253009	.456976	2.082249	.097955	.048978	.042981	1.443	GG=10%
2.5	.531	2.033	.596	.71	.355216	.5041	1.965604	.075745	.037872	.034287	1.402	*BELOW*
-3	.502	1.924	.493	.719	.243049	.516961	2.027773	.135080	.067540	.056136	1.424	*SURFACE*
0	.437	1.186	.399	.385	.159201	.149225	.561001	-.01957	-.00978	-.01002	.749	ANG=45 DEG
-5	.42	1.234	.4	.457	.16	.208849	.662596	.073724	.036862	.033465	.814	GPM=300
-1	.434	1.28	.429	.425	.184041	.181476	.665856	-.00385	-.00193	-.00194	.816	AN/AC=0.29
1.5	.503	1.384	.431	.496	.185761	.246016	.776161	.077632	.038816	.035049	.881	LC=39IN.
-2	.493	1.381	.428	.485	.183184	.235225	.797449	.065259	.032630	.029968	.893	GG=20%
2.5	.58	1.492	.574	.632	.329476	.399424	.831744	.084098	.042049	.037629	.912	*BELOW*
-3	.546	1.381	.603	.544	.363609	.295936	.697225	-.09706	-.04853	-.05442	.835	*SURFACE*

AFVAL/PORT WATER TUNNEL TEST RIG

MEASURED RESIDENCE TIME TEST DATA

DOME HEIGHT IN.	RESIDENCE TIMES		STANDARD DEVIATION		VARIANCE		2 (T2-T1)	2 (S2-S1)	DISPERSION D/UL 1ST ITERATION	COEFF. FINAL VALUE	RESIDENCE TIME (SEC.) (T2-T1)	TEST PARAMETERS
	INLET	EXIT	INLET	EXIT	INLET	EXIT						
	T1 SEC.	T2 SEC.	S1	S2								
0	.672	1.552	.502	.43	.252004	.1849	.7744	-.0865	-.04333	-.04802	.88	ANG=45 DEG
-.5	.757	1.655	.544	.502	.295936	.252004	.806404	-.05448	-.02724	-.02909	.898	GPM=300
-1	.903	1.587	.635	.556	.403225	.309136	.467856	-.20111	-.10055	-.12583	.684	AN/AC=0.29
-1.5	.945	1.631	.635	.518	.403225	.268324	.784996	-.17185	-.08592	-.10438	.886	LC=39IN.
-2	1.004	1.901	.687	.606	.471969	.367236	.804609	-.13017	-.06508	-.07567	.897	GG=10%
-2.5	1.104	2.051	.794	.71	.630436	.5041	.896809	-.14087	-.07044	-.08284	.947	*ABOVE*
-3	1.143	2.069	.813	.716	.660969	.512656	.857476	-.17296	-.08648	-.10518	.926	*SURFACE*
0	.697	1.186	.617	.438	.380689	.191844	.239121	-.78975	-.39487	-.78469	.489	ANG=45 DEG
-.5	.759	1.25	.633	.403	.400689	.162409	.241081	-.98838	-.49419	-.1048	.491	GPM=300
-1	.796	1.281	.659	.452	.434281	.204304	.235225	-.97769	-.48884	-.10863	.485	AN/AC=0.29
-1.5	.942	1.373	.711	.506	.505521	.256036	.185761	-.13430	-.67152	-.17989	.431	LC=39IN.
-2	1.02	1.415	.789	.546	.622521	.298116	.156025	-2.0792	-1.0393	-3.7415	.395	GG=20%
-2.5	1.122	1.468	.869	.541	.755161	.292681	.119716	-3.8631	-1.9316	-11.259	.346	*ABOVE*
-3	1.14	1.496	.878	.639	.770884	.408321	.126736	-2.8608	-1.4304	-6.5454	.356	*SURFACE*
0	.533	1.973	.056	.327	.003136	.106929	2.0736	.050054	.025027	.023461	1.44	ANG=60 DEG
-1	.523	1.983	.056	.336	.003136	.112896	2.1316	.051492	.025746	.024089	1.46	GPM=200
-2	.553	2.061	.053	.405	.002809	.164025	2.274064	.070893	.035447	.032306	1.508	AN/AC=0.29
-3	.545	2.066	.078	.393	.006084	.154449	2.313441	.064132	.032066	.029495	1.521	LC=39IN.
-4	.551	2.088	.046	.373	.002116	.139129	2.362369	.057998	.028999	.026897	1.537	GG=0%
-5	.548	1.961	.046	.312	.002116	.097344	1.996569	.047696	.023848	.022426	1.413	
-6	.555	2.016	.044	.286	.001936	.081796	2.134521	.037414	.018707	.017832	1.461	
0	.29	1.016	.063	.173	.003969	.029929	.527076	.049253	.024626	.023110	.726	ANG=60 DEG
-1	.299	1.041	.028	.193	.000784	.037249	.550564	.066232	.033116	.030374	.742	GPM=400
-2	.305	1.083	.049	.232	.002401	.053824	.605284	.084957	.042478	.037967	.778	AN/AC=0.29
-3	.315	1.098	.031	.217	.000961	.047089	.613089	.075239	.037619	.034081	.783	LC=39IN.
-4	.306	1.03	.042	.164	.001764	.026896	.524176	.047946	.023973	.022536	.724	GG=0%
-5	.317	1.067	.034	.163	.001156	.026569	.5625	.045179	.022589	.021314	.75	
-6	.331	1.065	.109	.157	.011881	.024649	.538756	.023699	.011850	.011498	.734	

APPENDIX D

DATA REDUCTION AND ANALYSIS EQUATIONS

AD-A153 753

MULTI-DUCTED INLET COMBUSTOR RESEARCH AND DEVELOPMENT
(U) UNIVERSAL ENERGY SYSTEMS INC DAYTON OH G D STREBY

3/3

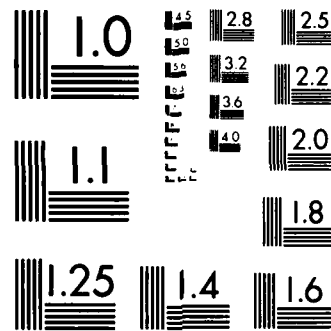
MAR 85 AFWAL-TR-85-2004 F33615-81-C-2074

F/G 21/5

NL

UNCLASSIFIED





MICROCOPY RESOLUTION TEST CHART
NATIONAL BUREAU OF STANDARDS 1964 A

Determination of Dye Calibration Coefficients

Dye calibration coefficients were determined by conducting measurements of different dye concentrations in the AFWAL/PORT closed loop Water Tunnel. With clean clear water in the system flowing at test temperatures (80 - 100°F), initial photomultiplier outputs were recorded. Then measured quantities of dye (Pontamine Fast Orange W Liquid) were injected into the system (normally 3 to 9 milliliters). The dye was allowed to circulate and disperse for several minutes before photomultiplier detector outputs were recorded. After outputs were recorded another quantity of dye would be injected and allowed to disperse. This procedure was continued until approximately 40 milliliters of dye were injected into the system. A total system volume of 3.5×10^6 milliliters was used for system dye calibrations.

The result of the dye calibration test were then plotted on semi-log paper with photomultiplier output versus dye concentration. The resulting plots should be linear on semi-log paper. Figure 1 shows a dye calibration curve plot. Dye calibration coefficients are determined from the slopes of the dye concentration curves.

$$\text{Slope} = \frac{\log V_2 - \log V_1}{C_2 - C_1}$$

$$\text{Calibration Coefficient: } B = \frac{\text{Slope}}{\log e}$$

Photomultiplier
Outlet
V (-Volts)

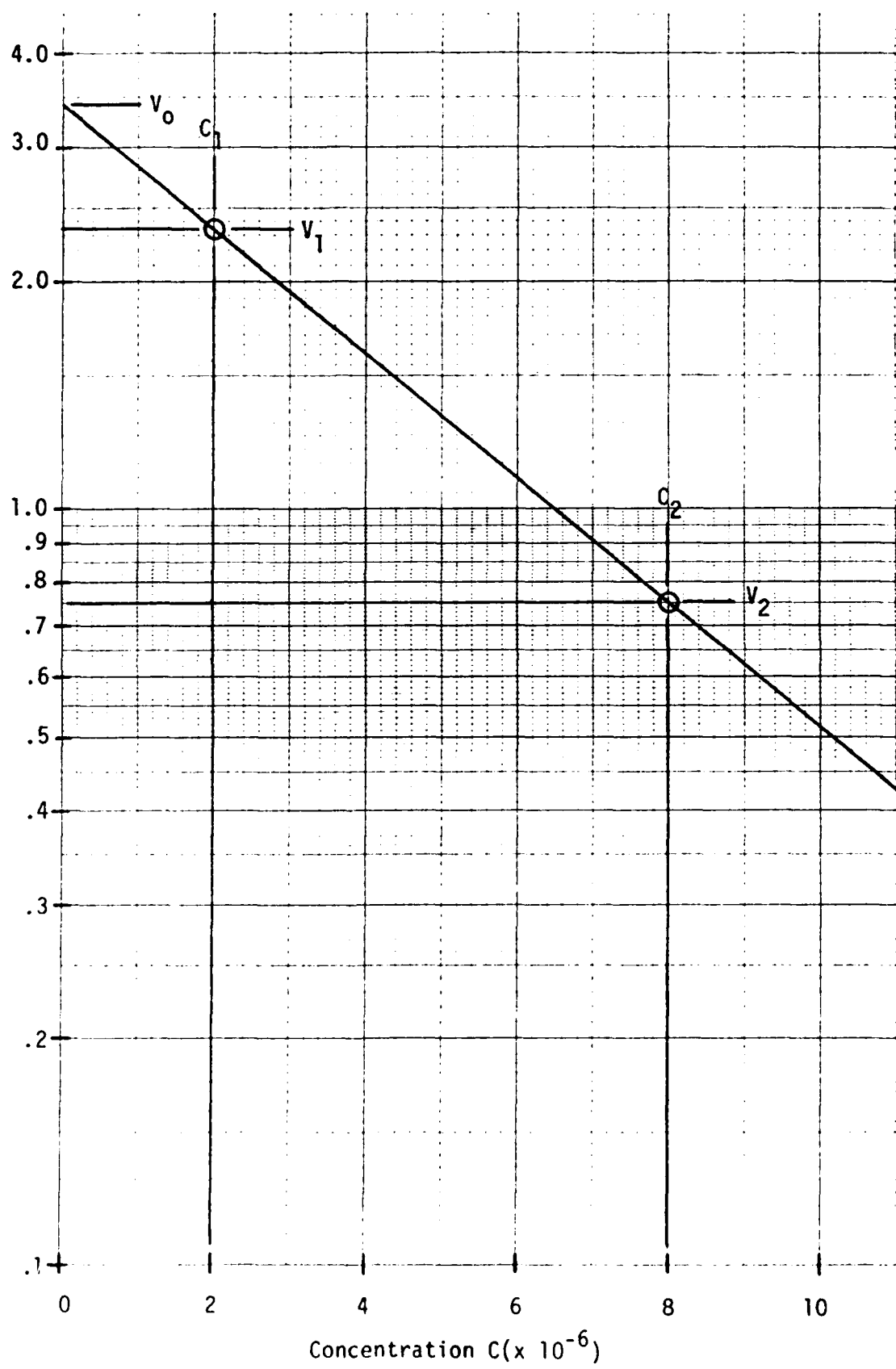


Figure 1 Dye Calibration Curve

Dye calibration coefficients were determined for both inlet and exit photomultiplier detectors.

With the proper dye calibrations obtained, the quantity and concentration could be obtained in either a stationary or moving fluid volume. Dye concentration and dye quantities are determined using the following equations.

$$\text{Concentration: } C = \frac{\ln (V/V_0)}{B}$$

V - Detector Output Voltage

V_0 - Initial Detector Output Voltage

B - Dye Calibration Coefficient

Dye Quantity equals concentration times volume of fluid.

$$\text{Quantity: } Q = (C) \times (\text{Volume})$$

$$\text{or for moving fluid: } Q = (C) \times (\text{Area}) \times (\text{velocity}) \times (\text{time})$$

The dye concentration was determined at inlet and exit points of combustor configurations at short time intervals to obtain concentration-time histories of the dye tracer.

Determination of Concentration - Time Histories

and Residence Time Data From Dye Injections

In order to obtain residence time measurements of a fluid flow through a combustor configuration, it was necessary to determine the concentration - time histories at both inlet and exit points. Using a laser light source and photomultiplier detector, the concentration and quantity of an injected dye pulse was determined at the inlet entry and nozzle exit points of the side-dump combustor configuration. The photomultiplier detector outputs, which varied due to light absorption of dye concentration, was recorded using a high speed data acquisition system. Detector outputs were sampled at 0.010 second intervals and stored in computer memory. The data was then processed to obtain the concentration-time history information necessary to determine residence time of each individual data trace.

Knowing the fluid flow rate through the combustor; the time interval between samples; and the mean dye concentration of the fluid stream, the concentration-time and quantity histories could be determined. Figure 2 shows a concentration-time history distribution ($E(t)$ plot) for a typical dye injection. Because of the variations and uncertainty of uniform dye injections, a series of tests were conducted at the same conditions for each test case. In most cases twenty (20) test samples were taken and then examined on the computer to check for proper time registering and the step characteristics of the inlet pulse. If the inlet pulse timing was not within 0.02 to 0.03 seconds of the mean value for the group or if the output characteristics showed a poor quality input pulse the sample was not used in the averaging of the test

Typical Concentration - Time Distribution Plot

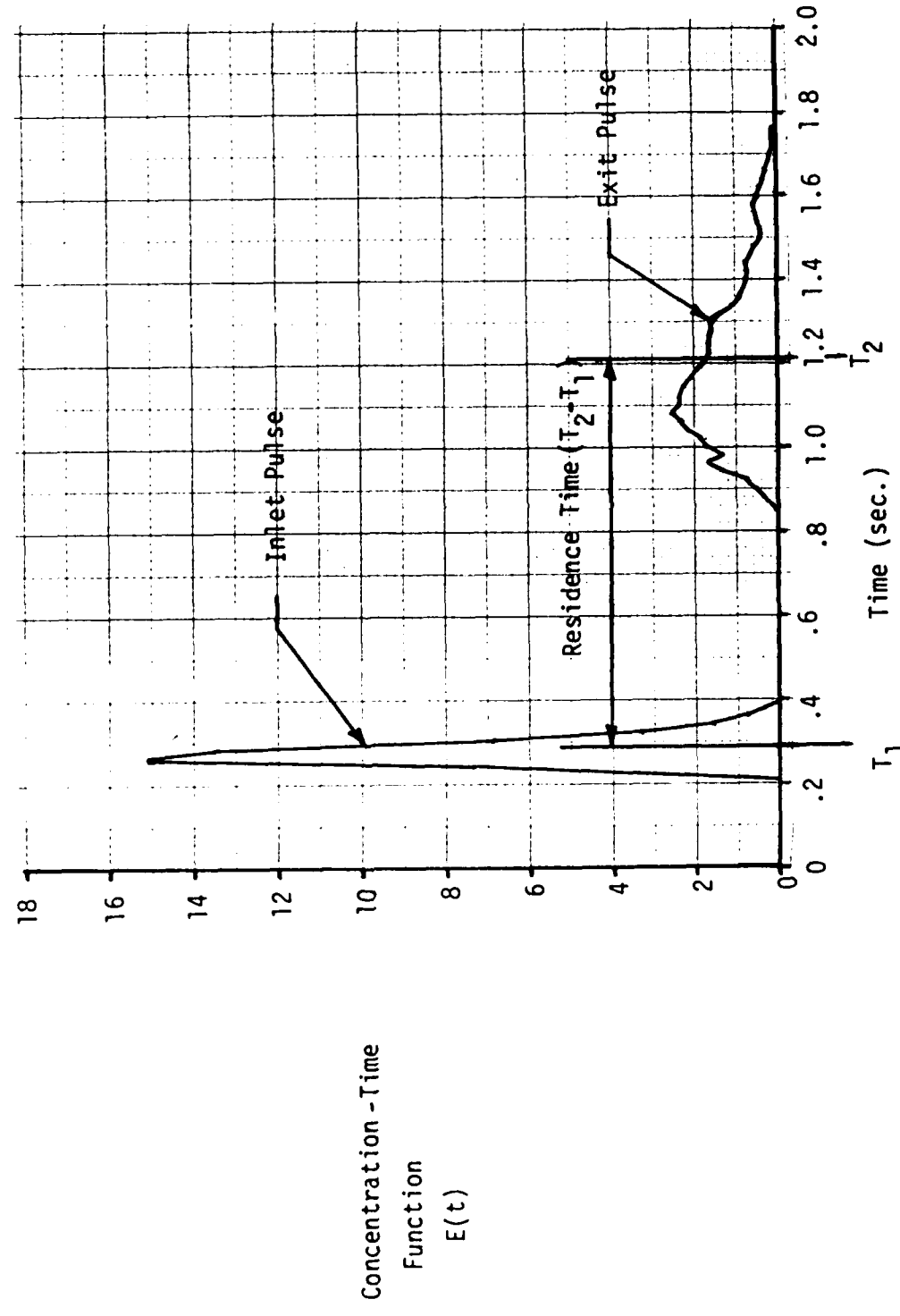


Figure 2 Concentration - Time Function Distribution Plot

samples. Then the inlet and exit residence times were evaluated using "Chauvenet's Criterion." "Chauvenet's Criterion" are acceptable values of the ratio of maximum deviation to the standard deviation. Data that are outside the criterion were eliminated from the test samples.

"Chauvenet's Criterion"

<u>Number of Readings</u>	<u>Max. Deviation</u>
<u>Acceptable Standard Deviation</u>	
10	1.96
15	2.13
25	2.33

After test data were examined and evaluated the results were averaged together to yield a composite data set. The composite data represents a mean value of the input pulse and the systems response. Composite data results were then used for determination of residence times, standard deviations, variance, and skewness of the concentration - time history distributions.

From the composite data set several statistical properties were determined for both the inlet and exit pulses. The mean residence time, standard deviation, variance, and moment of skewness were calculated. The following equations show how each were determined.

Mean Residence Time:

Inlet Pulse Residence Time

$$T_1 = \frac{\sum_{i=1}^N t_i c_{1i}}{\sum_{i=1}^N c_{1i}}$$

c_{1i} - Dye Concentration at time interval i at inlet

t_i - Time at interval i

T_1 - Inlet Residence Time

Exit Pulse Residence Time

$$T_2 = \frac{\sum_{i=1}^N t_i c_{2i}}{\sum_{i=1}^N c_{2i}}$$

c_{2i} - Dye Concentration at time interval i at Exit
 t_i - Time at interval i
 T_2 - Exit Residence Time

Combustor Residence Time equals the difference between the Inlet and Exit Mean Residence Times

$$T_R = (T_2 - T_1)$$

Variance of Concentration Distribution:

Inlet Variance

$$\sigma_1^2 = \frac{\sum t_i^2 c_{1i} (t_i - t_{i-1})}{\sum c_{1i} (t_i - t_{i-1})} - T_1^2 \quad \sigma_1^2 - \text{Inlet Variance}$$

Exit Variance

$$\sigma_2^2 = \frac{\sum t_i^2 c_{2i} (t_i - t_{i-1})}{\sum c_{2i} (t_i - t_{i-1})} - T_2^2 \quad \sigma_2^2 - \text{Exit Variance}$$

Skewness of Concentration Distributions:

Inlet Skewness

$$\gamma_1^3 = \frac{\sum t_i^3 c_{1i} (t_i - t_{i-1})}{\sum c_{1i} (t_i - t_{i-1})} - T_1^3 \quad \gamma_1^3 - \text{Inlet Skewness}$$

Exit Skewness

$$\gamma_2^3 = \frac{\sum t_i^3 c_{2i} (t_i - t_{i-1})}{\sum c_{2i} (t_i - t_{i-1})} - T_2^3 \quad \gamma_2^3 - \text{Exit Skewness}$$

Standard Deviation of Concentration Distributions:

$$\text{Inlet } S_1 = \sqrt{\sigma_1^2}$$

S_1 - Inlet Standard Deviation

$$\text{Exit } S_2 = \sqrt{\sigma_2^2}$$

S_2 - Exit Standard Deviation

The Dispersion Coefficient is defined, for a "One-Shot" tracer input, as the difference in variances of the concentration distribution curves for the inlet and exit points of the reactor.

Dispersion Coefficient:

$$D/uL = \left(\frac{1}{2}\right) \frac{(\sigma_2^2 - \sigma_1^2)}{(T_2 - T_1)^2} = \frac{\Delta\sigma^2}{2} \quad (\text{Open Vessel})$$

For Open-Closed or Closed Vessels:

$$\Delta\sigma^2 = 2\frac{D}{uL} + \left(\frac{D}{uL}\right)^2 \left(e^{-2uL/D} + 4e^{-uL/D} + 4\frac{uL}{D} \cdot e^{-uL/D} - 5\right)$$

$$\text{For } \frac{D}{uL} \ll 1 \quad \frac{D}{uL} \approx \frac{\Delta\sigma^2}{2}$$

The following is a sample calculation for an inlet dye tracer pulse. Shown are the equations for determination of residence time, variance, and standard deviation.

INLET DYE TRACER SAMPLE CALCULATIONS

TIME T (SEC.)	DELTA TIME (SEC.)	INLET DETECTOR OUTPUT VOLTAGE (V)	DYE CONC. $C = (\ln(V/V_i))/B$	$(T) \times (C)$	$(C) \times (\Delta T)$	$E(T) = \frac{\text{SUM}((C) \times (\Delta T))}{2}$	CONC.-TIME FUNCTION	2	$(T) \times (C) \times (\Delta T)$	3
							(C)	$(T) \times (C) \times (\Delta T)$		
.2	.01	-5.33	0	0	0	0	0	0	0	0
.21	.01	-5.025	5.71E-7	1.20E-7	5.711E-9	.4775893	2.52E-10	5.29E-11		
.22	.01	-4.06	2.64E-6	5.80E-7	2.638E-8	2.205904	1.277E-9	2.81E-10		
.23	.01	-3.485	4.12E-6	9.47E-7	4.118E-8	3.443648	2.178E-9	5.01E-10		
.24	.01	-2.206	8.55E-6	2.05E-6	8.550E-8	7.149928	4.925E-9	1.182E-9		
.25	.01	-1.281	1.38E-5	3.45E-6	1.382E-7	11.55528	8.636E-9	2.159E-9		
.26	.01	-.872	1.75E-5	4.56E-6	1.755E-7	14.67249	1.186E-8	3.084E-9		
.27	.01	-.712	1.95E-5	5.27E-6	1.951E-7	16.31545	1.422E-8	3.840E-9		
.28	.01	-1.069	1.56E-5	4.36E-6	1.557E-7	13.02160	1.221E-8	3.418E-9		
.29	.01	-1.552	1.20E-5	3.47E-6	1.196E-7	9.999917	1.006E-8	2.916E-9		
.3	.01	-2.352	7.93E-6	2.38E-6	7.929E-8	6.630523	7.136E-9	2.141E-9		
.31	.01	-3.022	5.50E-6	1.70E-6	5.499E-8	4.598999	5.285E-9	1.638E-9		
.32	.01	-3.617	3.76E-6	1.20E-6	3.758E-8	3.142332	3.848E-9	1.231E-9		
.33	.01	-4.075	2.60E-6	8.59E-7	2.602E-8	2.176015	2.834E-9	9.35E-10		
.34	.01	-4.412	1.83E-6	6.23E-7	1.832E-8	1.532019	2.118E-9	7.20E-10		
.35	.01	-4.645	1.33E-6	4.67E-7	1.333E-8	1.114913	1.633E-9	5.72E-10		
.36	.01	-4.865	8.85E-7	3.18E-7	8.847E-9	.7398546	1.147E-9	4.13E-10		
.37	.01	-4.975	6.68E-7	2.47E-7	6.680E-9	.5586393	9.15E-10	3.38E-10		
.38	.01	-5.1	4.28E-7	1.62E-7	4.275E-9	.3575141	6.17E-10	2.35E-10		
.39	.01	-5.195	2.49E-7	9.70E-8	2.486E-9	.2079288	3.78E-10	1.47E-10		
.4	.01	-5.265	1.19E-7	4.76E-8	1.189E-9	.0994482	1.90E-10	7.61E-11		
							2			
			SUM OF (C) = 1.20E-4			SUM OF (T)X(C)X(DEL. T) = 9.172E-8				
							3			
			SUM OF (T)X(C) = 3.29E-5			SUM OF (T)X(C)X(DEL.T) = 2.588E-8				
						SUM OF (C)X(DEL. T) = 1.196E-6				

$$\text{RESIDENCE TIME (T1)} = \frac{\text{SUM OF (T)X(C)}}{\text{SUM OF (C)}} = .2752783 \text{ SEC.}$$

$$\text{VARIANCE OF DISTRIBUTION} = \frac{\text{SUM OF (T)X(C)X(DEL.T)} - T1^2}{\text{SUM OF (C)X(DEL.T)}^2} = 9.202E-4$$

$$\text{STANDARD DEVIATION} = \text{SQR(VARIANCE)} = .0303351$$

$$\text{THIRD MOMENT ABOUT DIST.} = \frac{\text{SUM OF (T)X(C)X(DEL.T)} - T1^3}{\text{SUM OF (C)X(DEL.T)}^3} = 7.830E-4$$

$$\text{SKEWNESS OF DISTRIBUTION} = (\text{THIRD MOMENT})/(\text{VARIANCE}) = 28.04974$$

$$\text{INITIAL INLET DETECTOR VOLTAGE (V1)} = -5.33 \text{ VOLTS}$$

$$\text{DYE CONCENTRATION CALIBRATION COEFFICIENT (B)} = -103180$$

Equating Water Tunnel Measured Residence Times
to Actual Combustor Residence Times

Let Re_1 be Inlet Reynolds Number of Actual Flight Vehicle.

Then

$$\frac{Re_1 = x_1 u_1}{v_1}$$

Let Re_2 be inlet Reynolds Number of Water Simulation Model.

Then

$$\frac{Re_2 = x_2 u_2}{v_2}$$

For Simularity of Inlet Flows, Reynolds Numbers must be equal.

$$Re_1 = Re_2$$

$$\frac{x_1 u_1}{v_1} = \frac{x_2 u_2}{v_2}$$

Residence Time is Defined as the ratio of Combustor Volume to Volume Flow Rate of Fluid into the Combustor.

Therefore: $T_{R_1} = \frac{V_1}{\dot{V}_1}$ for Actual Flight Vehicle

and $T_{R_2} = \frac{V_2}{\dot{V}_2}$ for Water Simulation

For Incompressible Flows we have the Volume Flow Rates are given by

$$\dot{V}_1 = A_1 U_1 ; \dot{V}_2 = A_2 U_2$$

A_1 = Cross Sectional Area of Actual Inlet

A_2 = Cross Sectional Area of Simulation Model

U_1 = Flow Velocity of Actual Inlet

U_2 = Flow Velocity of Simulation Model

Then $U_1 = \frac{\dot{V}_1}{A_1}$ and $U_2 = \frac{\dot{V}_2}{A_2}$

Put these in Reynolds Number Simularity Equations to get

$$\frac{x_1 \dot{V}_1}{v_1 A_1} = \frac{x_2 \dot{V}_2}{v_2 A_2}$$

From Residence Time Equations solve for Volume Flow Rates

$$\dot{V}_1 = \frac{v_1}{T_{R_1}} \quad \dot{V}_2 = \frac{v_2}{T_{R_2}}$$

Solve for T_{R_1}

$$T_{R_1} = \frac{x_1}{x_2} \cdot \frac{v_2}{v_1} \cdot \frac{A_2}{A_1} \cdot T_{R_2}$$

$\frac{x_1}{x_2}$ - Ratio of Characteristic Lengths of Actual Vehicle and Simulation Model.

$\frac{v_2}{v_1}$ - Ratio of Kinematic Viscosities of actual fluid and simulation fluid

$\frac{v_1}{v_2}$ - Ratio of Actual and Simulation Combustor Volumes

$\frac{A_2}{A_1}$ - Ratio of Inlet Cross Sectional Areas

For Full Scale Simulation of Combustor Flows the following equations would apply.

$$\frac{x_1}{x_2} = 1; \quad \frac{v_1}{v_2} = 1; \quad \frac{A_2}{A_1} = 1$$

Then $T_{R_1} = \frac{v_2}{v_1} T_{R_2}$

The actual residence time is the ratio of kinematic viscosities times the measured residence for incompressible flows. The following example equates a typical measured residence time to actual residence time for a full scale water simulation.

For $T_{R_2} = 1.025$ sec. (45 Degree Configuration, 300 GPM, Water Simulation)

Water Kinematic Viscosity

$$\nu_2 = 1.083 \times 10^{-5} \text{ ft.}^2/\text{sec.} @ 68 \text{ Deg. F}$$

Air Kinematic Viscosity

$$\nu_1 = 100 \times 10^{-5} \text{ ft.}^2/\text{sec.} \text{ High Altitude and High Temperature}$$

Result $T_R = \frac{1.083 \times 10^{-5} (1.025 \text{ sec.})}{100 \times 10^{-5}}$

$T_{R_1} = 0.0108 \text{ sec.} \quad (\text{Should be Actual Residence Time})$

0306a

Apparent Stagnate Combustor Volume

$$T_M = \frac{V_A}{\dot{V}}$$

$$T_C = \frac{V}{\dot{V}}$$

For a constant \dot{V}

$V = V_S + V_A$ = Total Combustor Volume

V_S = Apparent Stagnate Volume

V_A = Active Volume

T_M = Measured Residence Time

T_C = Calculated Residence Time

V = Fluid Flow Rate

$$\frac{V}{T_C} = \frac{V_A}{T_M}$$

$$\frac{T_M}{T_C} = \frac{V_A}{V} = \text{Percent of Combustor Volume Active}$$

$$\text{or } \frac{T_M}{T_C} = \frac{V - V_S}{V} ; \frac{T_M}{T_C} = \frac{1 - V_S}{V}$$

$$\text{then } \frac{V_S}{V} = \frac{1 - T_M}{T_C} = \text{Percent of Combustor Volume Stagnate}$$

REFERENCES

1. S. P. Vanka, Analytical Characterization of Flowfield in Combustor Configurations, UES Number UES-TR-82-728-01, Universal Energy Systems, Inc., Dayton, Ohio, October, 1982.
2. James E. Craig, Holography Diagnostic Techniques for Ramjet Flows, SDL Number 83-2239-01F, Spectron Development Laboratories, Inc., Costa Mesa, California, March, 1983.
3. O. Levenspiel, Chemical Reaction Engineering, John Wiley and Sons, 1962.

END

FILMED

6-85

DTIC